DOCTOR OF PHILOSOPHY

Effect of composite action on the dynamic behaviour of space structures

Elabd, Maher Mostafa Abdel-Hakeem

Award date:
2010

DOCTOR OF PHILOSOPHY

Effect of composite action on the dynamic behaviour of space structures

Maher Mostafa Abdel-Hakeem Elabd

2010

University of Dundee

EFFECT OF COMPOSITE ACTION ON THE DYNAMIC BEHAVIOUR OF SPACE STRUCTURES

By

Maher Mostafa Abdel-Hakeem Elabd

A thesis submitted to the University of Dundee
for the degree of Doctor of Philosophy

DIVISION OF CIVIL ENGINEERING
UNIVERSITY OF DUNDEE
UK

June, 2010

TABLE OF CONTENTS

CHAPTER 3: RESEARCH METHODOLGY

CHAPTER 4: DESIGN AND MANUFACTURING OF SHAKING TABLE

CHAPTER 5: RESULTS OF EXPERIMENTAL TESTS

CHAPTER 6: ANALYSIS AND DISCUSSION OF EXPERIMENTAL RESUTLS

CHAPTER 7: NUMERICAL ANALYSIS RESULTS

LIST OF TABLES

CHAPTER 3: RESEARCH METHODOLOGY

CHAPTER 5: RESULTS OF EXPERIMENTAL TESTS

CHAPTER 6: ANALYSIS AND DISCUSSION OF EXPERIMENTAL RESUTLS

CHAPTER 7: NUMERICAL ANALYSIS RESULTS

LIST OF FIGURES

CHAPTER 1: INTRODUCTION

CHAPTER 2: LITERATURE REVIEW

CHAPTER 3: RESEARCH METHODOLGY

CHAPTER 4: DESIGN AND MANUFACTURE OF SHAKING TABLE

CHAPTER 5: RESULTS OF EXPERIMENTAL TESTS

CHAPTER 6: ANALYSIS AND DISCUSSION OF EXPERIMENTAL RESUTLS

CHAPTER 7: NUMERICAL ANALYSIS RESULTS

ACKNOWLEDGMENTS

I would like to express my sincere gratitude and indebtedness to my supervisor Dr. A. I. El-Sheikh for his guidance, supervision and encouragement throughout the progress of this work. I also want to thank Dr. R. I. Mackie for his patience, guidance and helping me through all work stages in this thesis.

I want to take the chance to thank my beloved country Egypt and Ministry of Higher Education for awarding me this scholarship to study PhD. Thanks are specially due to all Egyptian Cultural Centre and Educational Bureau in London for their taking care of me and all my colleagues through all the period of conducting this research.

I would like also to thank my professors, colleagues and friends here in UK and in my home country for their continuous encouragement.

I would like to thank all the technical staff of the Structures Laboratory of the University of Dundee for their help during experimental work and tests preparations. Thanks are especially due to Mr. E. Kuperus for his help in preparing all material and apparatus for testing. Thanks are also due to Mr. M. Mckernie for his help and assistance in preparing the data logger for work.

Last but not least, thanks and sincere gratitude is due to my wife and daughter for their continuous support and patience besides all support from other family members through all work period in this project.

DECLARATION

I, the undersigned, declare that I am the author of this thesis and, unless otherwise stated, all references cited have been consulted by me. I wish also to declare that, except for commonly understood ideas, or where a specified reference is made to work of others, the work of which this thesis is a record has been done by me and it has not been previously presented in any application for a higher degree.

Maher Elabd

June, 2010

CERTIFICATION

This is to certify that Maher Elabd has done this research under my supervision and that he has fulfilled the conditions of Ordinance 14 of the University of Dundee, so that he is qualified to submit the following thesis in application for the degree of Doctor of Philosophy.

Dr A. I. EI-Sheikh
Department of Civil Engineering
University of Dundee
June, 2010

NOTATIONS

a	The acceleration of point P moving along the vertical axis.
A_I	Effective shear area of the driving pin at section I-I.
a_i	Acceleration of shaking platform at time t
A_{II}	Effective shear area of the driving pin at section II-II.
a_{max}	Maximum wave amplitude from actual centre.
b_{max}	Minimum wave amplitude from actual centre.
C	Damping value
C_{cr}	Critical damping value
d	The distance from the projection point P to the centre of rotation of the flywheel.
d_I	Diameter driving pin at section I-I.
d_{II}	Diameter driving pin at section II-II.
e_{max}	The maximum shift between theoretical and actual centre.
f	Cyclic frequency of vibration.
FS	Factor of safety.
g	Gravitational acceleration 9.81 m/sec^2.
I_I	Second moment of area of driving pin at section I-I.
I_{II}	Second moment of area of driving pin at section II-II.
K	Stiffness of the models in the assigned direction.
K_a	Surface finishing factor of the driving pin.
K_c	Stress concentration factor due to changes in driving pin section.
M	Overall structure mass.
M_I	Bending moment at section I-I of the driving pin.
M_{II}	Bending moment at section II-II of the driving pin.
P	The projection of eccentric point P_1 on vertical axis.
P_1	The eccentric point at flywheel where eccentric arm is connected.
P_2	Point at the end of eccentric arm at the connection with horizontal actuator.
P_d	Factored design load of the driving pin.
P_e	Effective design force for the driving pin.
Q_I	Statical moment of area at section I-I.
Q_{II}	Statical moment of area at section II-II.
R	The radius of eccentric point P_1.
r	Eccentric arm length.

r_I	Radius of driving pin at section I-I.
r_{II}	Radius of driving pin at section II-II.
t	Time.
u	Horizontal movement output of shaking table platform.
v	Velocity of point P along the vertical axis.
V_I	Shear stress at section I-I of the driving pin.
v_i	Velocity of shaking platform at time t
V_{II}	Shear stress at section II-II of the driving pin.
W	Total weight of the shaking table platform.
x_i	Displacement of shaking platform at time t
ω	Circular frequency.
α	Rotation angle taken from horizontal axis in clockwise direction.
μ	Coefficient of friction.
ξ	Damping ratio
σ_e	Actual endurance stress limit of material.
σ_I	Normal stress in driving pin at section I-I.
σ_{II}	Normal stress in driving pin at section II-II.
σ_m	Mean stress of the alternating stresses.
σ_{max}	Maximum stress at the section under the applied load.
σ_{min}	Minimum stress at the section under the applied load.
σ_u	Ultimate strength of material used in manufacturing the driving pin.
σ_y	Yield strength of material used in manufacturing the driving pin.
τ	Allowable shear stress of material used in manufacturing the driving pin.
τ_I	Shear stresses in driving pin at section I-I.
τ_{II}	Shear stresses in driving pin at section II-II.

ABSTRACT

The application of composite action ushered a new era in the use of double-layer space frames as efficient floor systems in addition to their competitiveness as roof covering structural systems. Earlier research on space frames demonstrated large improvements in their static behaviour caused by the introduction of composite action. These improvements included an increase in ductility to avoid progressive collapse, a large increase in load-carrying capacity and a considerable reduction in material consumption.

In this work, the effect of introducing composite action in changing the dynamic characteristics of space frames, in particular the natural frequencies and damping ratios was presented. The study was expanded to determine the effect of composite action in changing the response to dynamic excitations. The measured responses included the lateral displacements and changes in the internal member force distribution under shaking table vibrations.

Three aluminium space frame models of the square on square (SOS) configuration were manufactured. The first model was non-composite, while composite action was applied to the other two models with a top aluminium deck and a timber deck, respectively. Two common cases of support conditions were used in connecting the models to the loading frame, which was the platform of the shaking table.

Initial displacement method (snap test) was used to determine the frequency of vibration and the damping ratio of test models in the vertical and horizontal directions using logarithmic decrement method. All models were then exposed to shaking table vibrations to determine the changes in dynamic responses between different models. These tests were repeated for the three models after the successive removal of panels from one direction to identify the changes to their characteristics and behaviour with different aspect ratios.

The second part of the study was carried out numerically by using the finite element package ABAQUS. It started by selecting a valid finite element model from nine proposed models using experimental test results on physical structures. A parametric study was conducted using the validated finite element model to expand the study to include two common space frame configurations; the square on large square (SOLS) and square on diagonal (SOD), and two other cases of support configurations, namely, fully edge-supported and supports at corners and middle edges of models.

Based on the work done in this study, it can be concluded that composite action changed the dynamic characteristics of space frames, which was clear in the increase of their vibration frequencies in all directions as a result of the increase in stiffness. Furthermore, the increase in stiffness resulted in a general reduction in the damping ratio of space frames covered with aluminium deck, while the high friction with top joints and the nature of timber as a good energy absorbent material resulted in a variable effect on the damping ratio associated with the increase in aspect ratio.

The effect of composite action was clear in reducing the lateral displacement of composite models by more than 50% compared to the non-composite case. Moreover, composite action resulted in changing the distribution of internal forces in diagonal and lower chord members such that forces became more concentrated at corners and edges parallel to the direction of vibrations in both cases of corner and edge-supported models.

CHAPTER 1

INTRODUCTION

1.1 General background

The increasing architectural demands to cover large areas without any intermediate supports encouraged the use of space structures as an excellent competitive structural system compared to other more conventional systems. Double-layer space frame system is considered one of the most important forms of space structures, suitable where large unobstructed spaces are required. They are used in aircraft hangars, stadiums, exhibition centres, sports halls and other large buildings. The competitiveness of the double-layer space frames as a structural system arises from their high degree of indeterminacy, high stiffness/weight ratio, the ease of assembly and erection, lower fabrication costs, light weight, ability to create multipurpose architectural spaces, and aesthetic appeal. Another interesting feature is their capacity to incorporate cladding and finishing surfaces easily. The empty spaces between chords in these structures can be used to accommodate services such as air-conditioning ducts and electricity cables.

Other factors further contributed to the wide use of space frames, including an improved understanding of their behaviour due to the extensive research carried out in this field. In addition, the development in computer science stands as an important factor for the nowadays considerable use of space frames since the analysis of complicated systems and shapes of space structures became possible and can be carried out easily with current advanced computer software packages.

However, space structures have a number of disadvantages including their tendency to collapse in a sudden and progressive manner which may occur even at load levels below the design load mainly due to lack of fit (Schmidt *et al.* 1980 and 1982). The collapse of the 2.4 acre space structure roof of the Hartford Coliseum, Connecticut USA in 1978, is an example of this type of sudden behaviour (Smith and Epstein, 1980). The truss collapsed at nearly half design load due to the initial internal forces created by member lack of fit (Figure 1.1).

Figure 1.1 Collapse of Hartford Coliseum, Connecticut USA, 1978

1.2 Definition

Space structure can be defined as a three-dimensional structural system assembled of linear elements, which, in turn, are arranged to ensure a three-dimensional force transfer from the load application points to the supports. This formation enables easy expansion, and, if required, dismantling and reassembly in another site. The majority of space structures are composed of slender members that carry axial forces and meet

at frictionless nodes. Space structures can be described as space frames or space trusses according to the flexural stiffness of their joints. The term space frames will be used through out this thesis since the joint stiffness is not specified.

A typical double-layer space frame consists of two layers of chord members, forming rectangular panels and connected together by diagonal and/or vertical members (Figure 1.2).

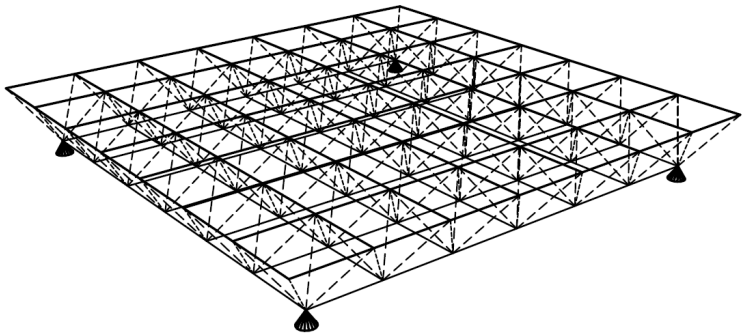

a. Double layer space frame overview

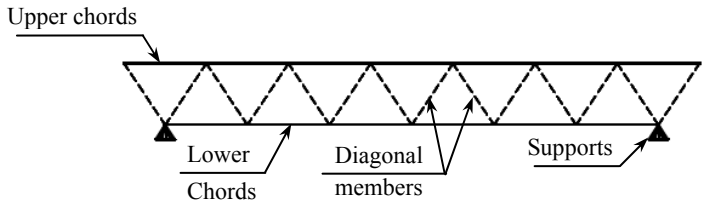

b. Typical double layer space frame components

Figure 1.2 Typical double-layer space frame components

Steel stands as the popular material for manufacturing space frames although other materials are also used such as aluminium, timber and composite materials, including Fibre Reinforced Plastics (FRP).

The most commonly used configurations of double-layer space frames are square on square offset (SOS), square on large square (SOLS), square on diagonal (SOD) and square on square (Figure 1.3).

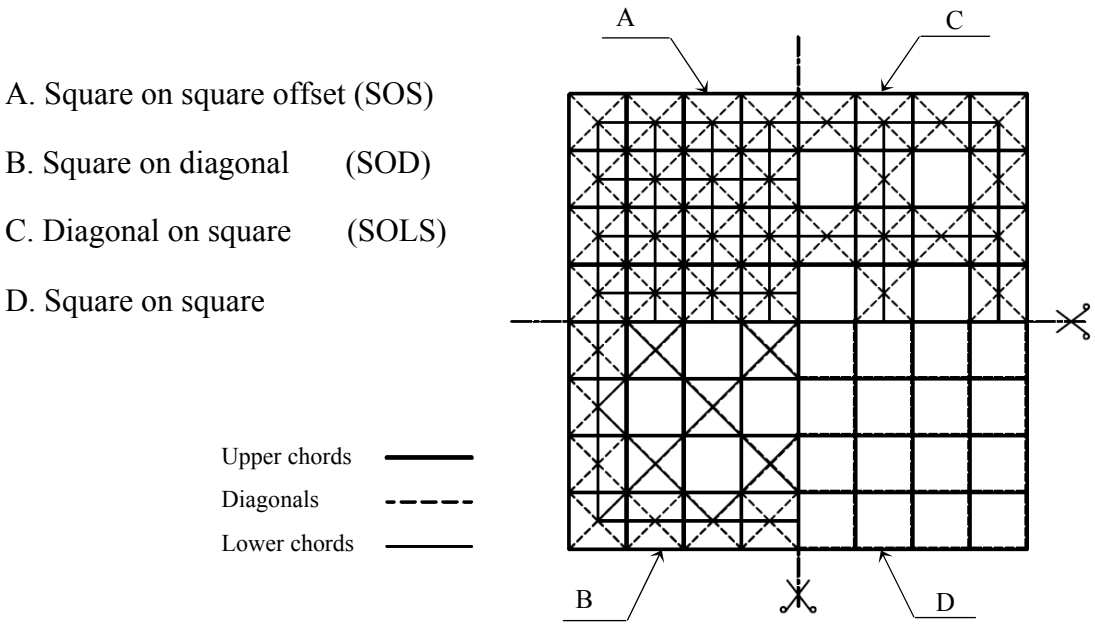

Figure 1.3 Common configurations of flat double-layer space frame

1.3 Common space frame systems

Space frame systems can be divided into two main categories according to the continuity of their chord members. These are:

1. Node connected space frames, which need special node connectors to transfer forces between members; and

2. Continuous chord space frames, which have a direct connection between their chords and web members.

The following is a brief description of the two systems.

1.3.1 Node connected space frames

These structures employ node connectors and member end fittings that have been designed to provide almost frictionless pinned and concentric connections between members so the name of space trusses is more applicable to these structures.

Figure 1.4 presents some commonly used jointing systems. The precise manufacturing of these joints makes them expensive to produce leading to their cost exceeding 60% of the total cost of the structure (El-Bakry, 1995). This affects the cost-competitiveness of the whole system.

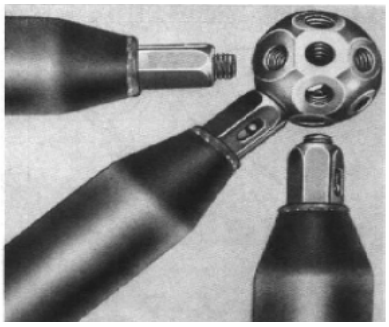

MERO system (Chilton, 2000)

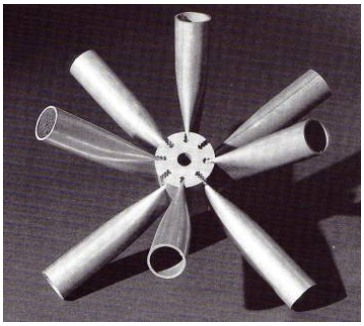

Triodetic system (Chilton, 2000)

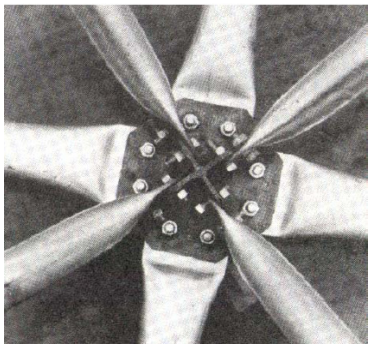

Octatube system (Souza, 2008)

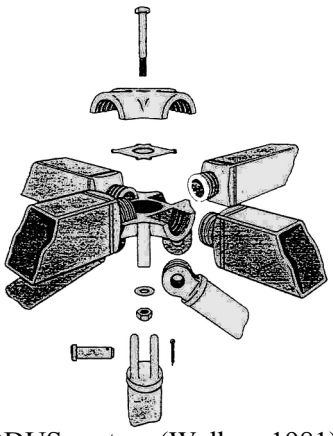

NODUS system (Walker, 1981)

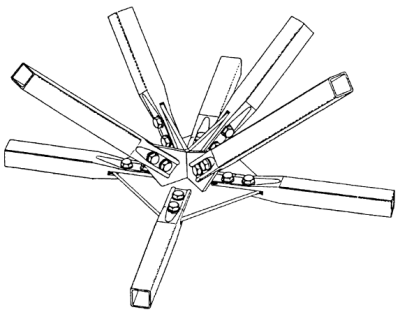

TOP-SYSTEM space frame
(Fulop *et al*, 2004)

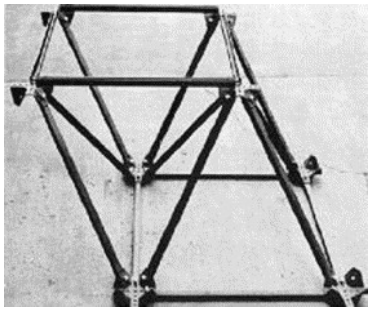

Power-strut system
(Gebhardt, 1984)

Figure 1.4 Joints used for node jointed space frame systems

1.3.2 Space frames with continuous chords

Due to the high cost of node connectors, space frame systems with continuous chords, and therefore no node connectors, have been developed. In these systems, members are bolted directly together in a simple fashion.

Figure 1.5 presents the oldest continuous chord system, the Schmidt system, which was first presented and tested by Schmidt *et al* (1975, 1977 and 1981). This system is based on using continuous chord members with pairs of tubular web members flattened, bent and drilled to be fastened to the sides of these chords.

Later in 1983, another space frame system called Conder-Harley system was presented by an Australian engineer (Codd, 1983 and 1984). The system uses cold formed channels in the chords and circular hollow section in diagonal members such that these webs were flattened and bent to fit between the two chords meeting at joints (Figure 1.6).

The CATRUS space frame system was more recently developed at the University of Dundee by El-Bakry (1995). This system uses rectangular hollow sections in the chords and circular hollow sections in diagonals with stamped ends (Figure 1.7). The system demonstrated better structural behaviour under static loading conditions over the commonly used high cost MERO system (El-Sheikh, 1999).

The most recent example is the W-Truss presented in Japan by Suzuki (2005). The system uses archiform (curved) steel node block welded to the surface of the chord member at both sides of the curved plate (Figure 1.8). Diagonals with stamped ends are then connected to this arc plate by bolting.

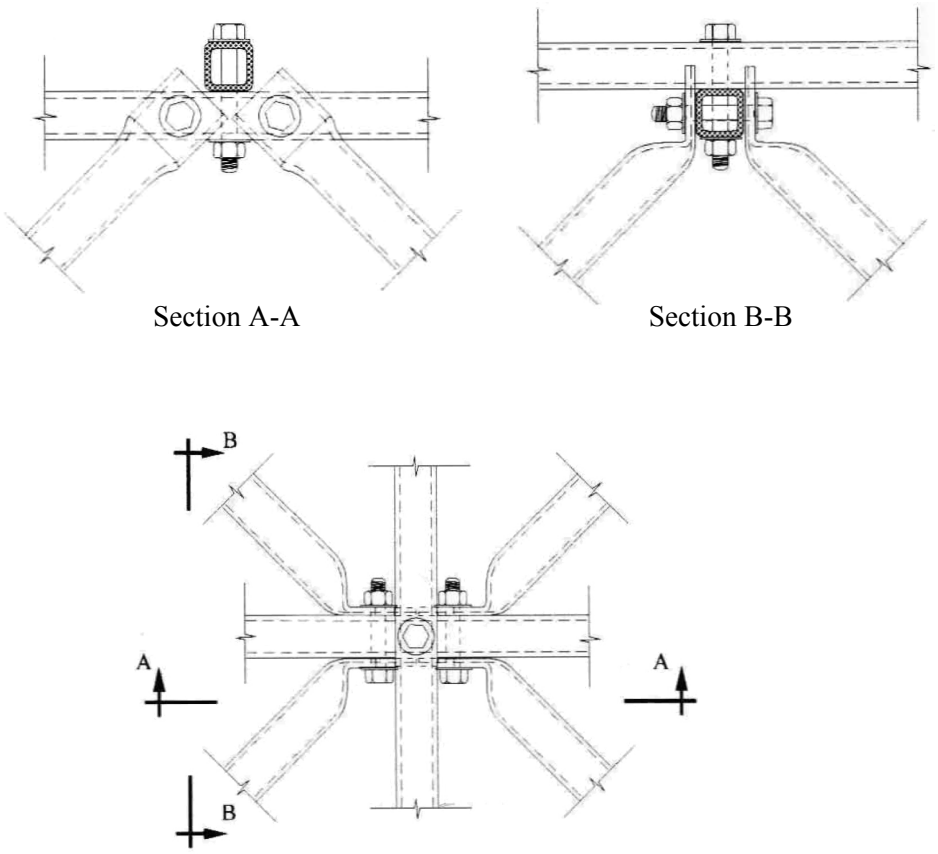

Figure 1.5 Schmidt's continuous chord system

Figure 1.6 Conder-Harley space frame system

a. Lower joint connection b. Upper joint connection

Figure 1.7 CATRUS space frame with upper and lower connections

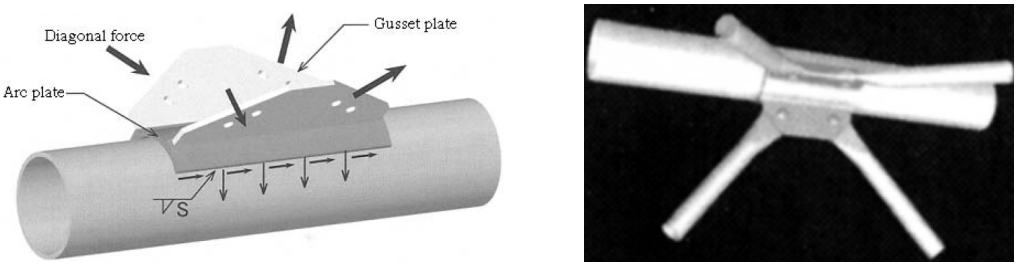

Figure 1.8 W-Truss system (Suzuki, 2005)

Several methods were proposed to improve the brittle behaviour of space frames, most of which showed real improvement in overall behaviour. Providing composite action by connecting the upper chord of the structure with the cladding or the decking material was one of these methods that showed promising results. This method offered an evident ductility, a large increase in load-carrying capacity and large savings in material consumption. Moreover, this technique ushered a new era in the use of space-frame structures as efficient floor systems instead of being used only as roof covering systems.

However, the lack of information about the dynamic behaviour of composite space frame structures affects the popularity of this technique. The study presented in this work is an experimental and numerical investigation into the changes in dynamic characteristics of double-layer space frame structures caused by the introduction of composite action. Additionally, the study extends to include changes to their lateral displacement responses and internal force distribution under external support excitations such as shaking table histories.

1.4 Aims and objectives of the present work

The present work had been designed to achieve the following aims:

1. Achieve a better understanding of the changes brought to conventional double-layer space frame structures by the application of composite action with emphasis on dynamic characteristics and behaviour.
2. Identify the effects of using different structure configurations, boundary conditions and aspect ratios with composite and non-composite double-layer space frame structures in altering the behaviour under dynamic excitations.

The study involved an experimental study, which tested three double-layer space frame models of the SOS configuration. The test models included one non-composite and two composite space frames with a top aluminium deck and a timber deck, respectively. Two common support conditions were used with the test models including supports at the lower corners and along the two edges parallel to the direction of excitation (X-direction). All supports were hinged allowing rotational displacements but preventing all translational movements.

Snap (Initial displacement) tests were carried out on the test models in the vertical (Z-direction) and the horizontal (X-direction) to evaluate the changes in their

dynamic characteristics caused by the introduction of composite action.

The research programme included building a mechanical uni-axial shaking table capable of applying a simple vibration history on the test models. The table uses a servo-motor to drive a rotating flywheel using a timing toothed belt. A horizontally guided actuator linked to the rotating flywheel through another arm connected eccentrically at different positions relative to the flywheel centre to obtain different vibration amplitudes. The shaking platform (slipping deck) is connected to the actuator and supported on three pairs of low friction linear-guide bearings with guides connected to a stiff frame fixed to the floor of the laboratory. Calibration tests were carried out on the shaking table to check the theoretical calculations' accuracy in determining the platform location and the servo-motor's efficiency in controlling the frequency. Operation charts were obtained to allow the table to be used for different applications.

Test models were fixed on the platform of the shaking table and a vibration time history was applied. The response of the models were recorded including the lateral displacements in the direction of vibration (X-direction), and the axial strains in a number of members to check the changes in internal member forces caused by composite action.

Complete panels were removed from the test models, one at a time, to change the models' aspect ratios (AR) from 1:1 to 1:1.2, 1:1.5, 1:2 and 1:3. These changes enabled extending the study to include the effects of models' dimension changes.

The experimental results were used to validate a finite element model built using the finite element package ABAQUS. Following validation, the model was used to carry out a parametric study to assess the effect of composite action on the dynamic

characteristics and behaviour of test structures with different boundary conditions (i.e., corner-supported, edge-supported, and models supported at corners and mid-edges) as well as different configurations (i.e., SOS, SOLS and SOD), and aspect ratios (AR) (i.e., 1:1, 1:1.2, 1:1.5, 1:2 and 1:3).

Modal analysis was carried out using ABAQUS on numerical models to obtain their vibration mode shapes and natural frequencies. In addition, time history analysis was carried out by applying a vibration history similar to that applied on physical models in laboratory conditions to determine the dynamic behaviour of numerical models.

The main objectives of this work were to determine:

1. The effect of composite action on changing the vibration frequencies and damping ratios of double-layer space frames in vertical and horizontal vibration modes.
2. The influence of composite action on the lateral displacements of double-layer space frames under dynamic loads.
3. The internal member forces under dynamic loads in structures with and without composite action.
4. The design impact of using different cladding materials to work compositely with space frames with particular emphasis on the dynamic characteristics and behaviour.
5. The changes in dynamic characteristics and behaviour of composite and non-composite double-layer space frames resulting from altering their aspect ratios and support conditions.

1.5 Outline of thesis

Following a general discussion of main features of the space structures and the scope

of the present study in Chapter 1, earlier research on the static and dynamic behaviour of space structures and the methods used to improve their behaviour is introduced in Chapter 2.

In Chapter 3, a description of the methodology followed in this research is presented. It includes details of the experimental test programme, manufacturing and assembly process of experimental models, test rig setup, theoretical methods used in the analysis of experimental results and finally the development of predictive finite element models of the dynamic behaviour of space structures.

Chapter 4 describes the steps taken to design, construct and calibrate the shaking table. The calibration and the control curves used to analyse the output of the table are also presented.

Chapter 5 presents the results of the experimental test programme on composite and non-composite space frame models. The results covered models with different support conditions, aspect ratios and deck materials used

A detailed discussion of the test results is introduced in Chapter 6 with emphasis on the test parameters noted above.

Chapter 7 presents a numerical parametric study, which can be considered as an extension to the experimental test programme but involving wider parameter ranges of support conditions and space frame configurations.

A summary of the present study, main findings and a number of recommendations for further research are presented in Chapter 8.

CHAPTER 2

LITERATURE REVIEW

2.1 Introduction

In this chapter, a brief discussion of static and dynamic behaviour of composite and non-composite space frame structures is presented. The discussion also covers the methods and techniques developed to improve their behaviour under both static and dynamic loading conditions. Due to the lack of research to improve the dynamic behaviour of space frame structures, a general discussion of techniques used to protect different structural systems is introduced.

2.2 Static behaviour of double-layer space structures

2.2.1 General behaviour

To assess the behaviour of space trusses under static loads, studies carried out by Schmidt *et al* (1975, 1976) and Schmidt (1976) included experimental tests on three identical aluminium small-scale space trusses of SOS configuration. The trusses were edge-supported with 6×6 panels and overall size of 1.83m×1.83m×0.216m (Figure 2.1). The studies reported that tested trusses showed linear behaviour until the failure of the first few compression members, which occurred nearly at the same load level in all tests. The initial linear behaviour was followed by considerable reduction in load-carrying capacity that continued until the formation of two complete perpendicular lines of collapsed compression members. The strength values obtained from the experimental tests were less than those obtained from analytical analysis that was based on finite element modelling, which involved the use of idealised compression member behaviour shown in Figure 2.2a. This difference was thought to be due to

geometrical imperfections in the truss models (Figure 2.2b). The imperfections caused unsymmetrical load distribution in truss members. The fast deterioration in strength as presented in the sudden drop of the load-deflection curve obtained from analytical analysis proved the high sensitivity of this type of structures to member imperfections.

The studies also concluded that the tested trusses had almost no reserve of strength after the initial buckling of critical compression members. The studies suggested that a reserve of strength would have been exhibited by the truss beyond the initial buckling if the members were to have a ductile stage of behaviour.

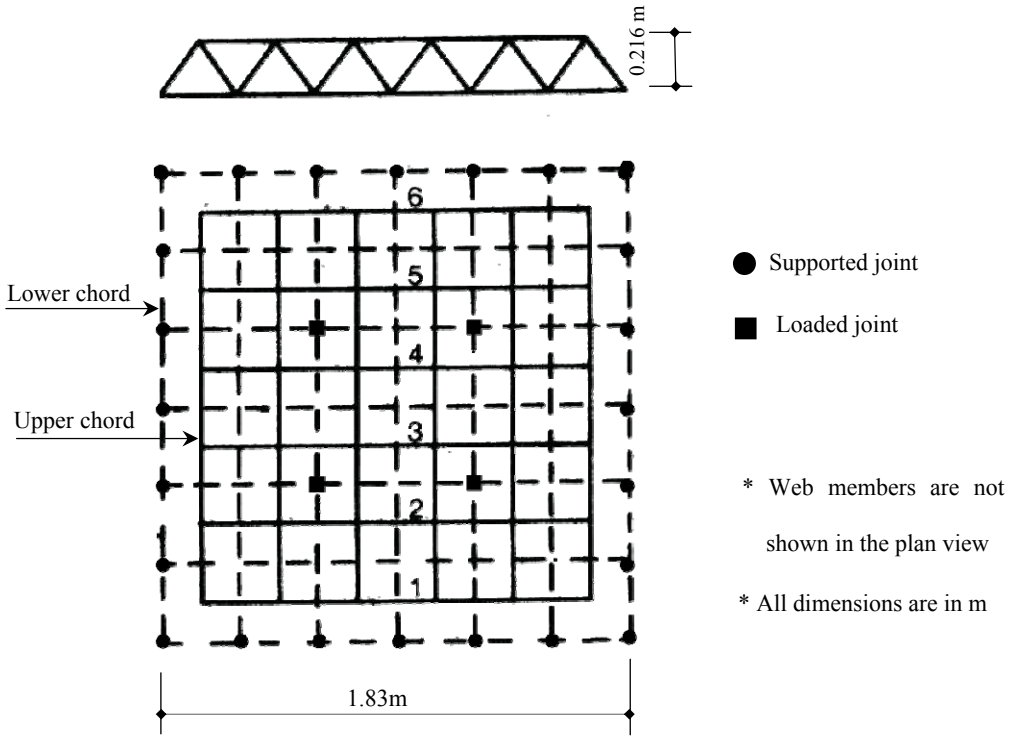

Figure 2.1 Layout and collapse line of test models (Schmidt *et al*, 1976)

In the same work, the effect of strut characteristics on the overall behaviour of double-layer space trusses was included. Numerical analysis was carried out on space trusses with different idealisations of compression members having the same material properties and buckling load but had different levels of residual load after buckling

(Figure 2.3a). The study concluded that changes in compression member characteristics had noticeable effect in increasing the ductility of trusses after the buckling of compression members as shown in Figure 2.3b. Only members with lower slenderness ratios (stocky members), which were rarely used in space structures, were able to offer a reserve of strength after buckling of compression members which was uneconomic leaving these structures to have a little reserve of strength after the first case of buckling.

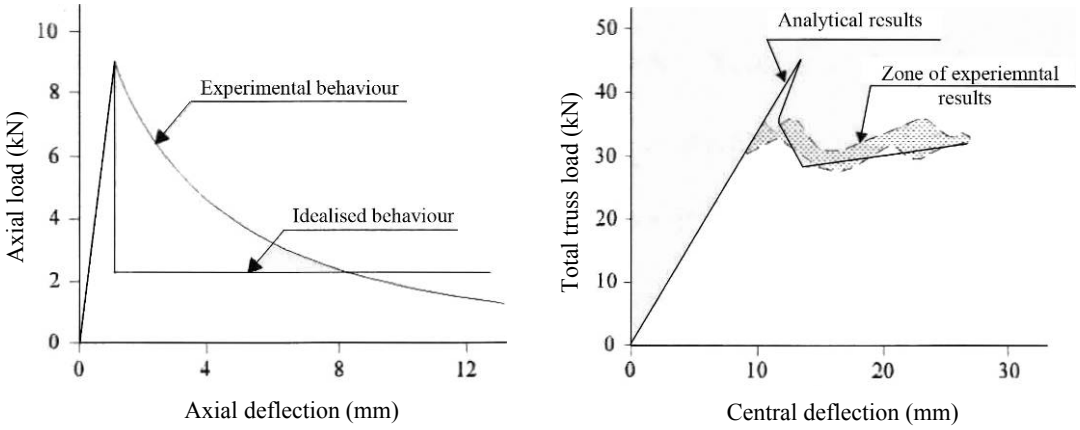

a. Actual and idealised strut models b. Experimental and analytical results

Figure 2.2 Analytical and experimental results for tested space trusses and model strut behaviour (Schmidt *et al.* 1975, 1976)

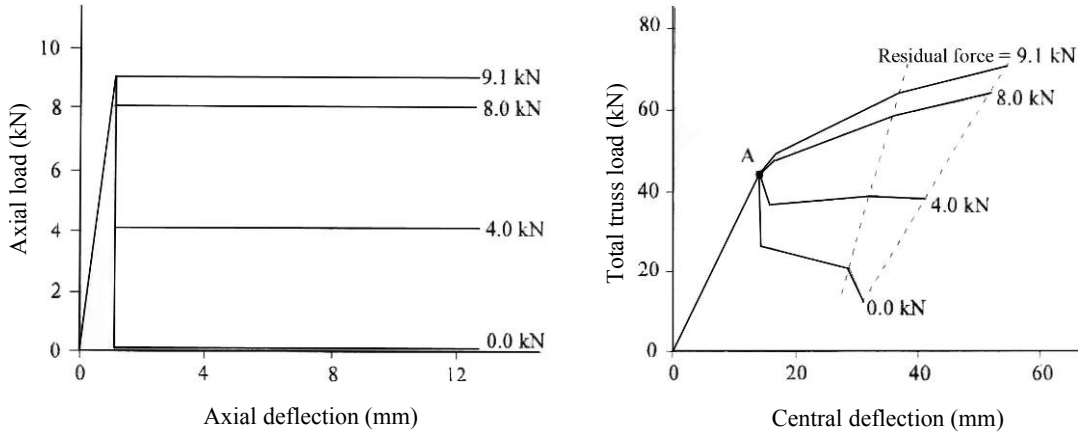

a. Actual and idealised strut models b. Experimental and analytical results

Figure 2.3 Analytical results of space truss with different compression member idealisations (Schmidt *et al,* 1975)

In 1982, Schmidt *et al* introduced the results of experimental tests on 12 double-layer space structures with spans that ranged from 0.914m to 9.60m and two configurations of SOS and SOD (Figure 2.4). The study concluded that the experimental ultimate loads were always less than the predicted results by 3% to 37%. This trend was observed in all trusses even in cases where tension yielding occurred well before the buckling of compression members. The study also discussed the relationship between the degrees of redundancy and the natures of failure loads. It concluded that the load-carrying capacities of trusses were 13% to 37% below the numerically predicted values for trusses with high degrees of redundancy, which was taken to indicate the high sensitivity of space trusses to member imperfections.

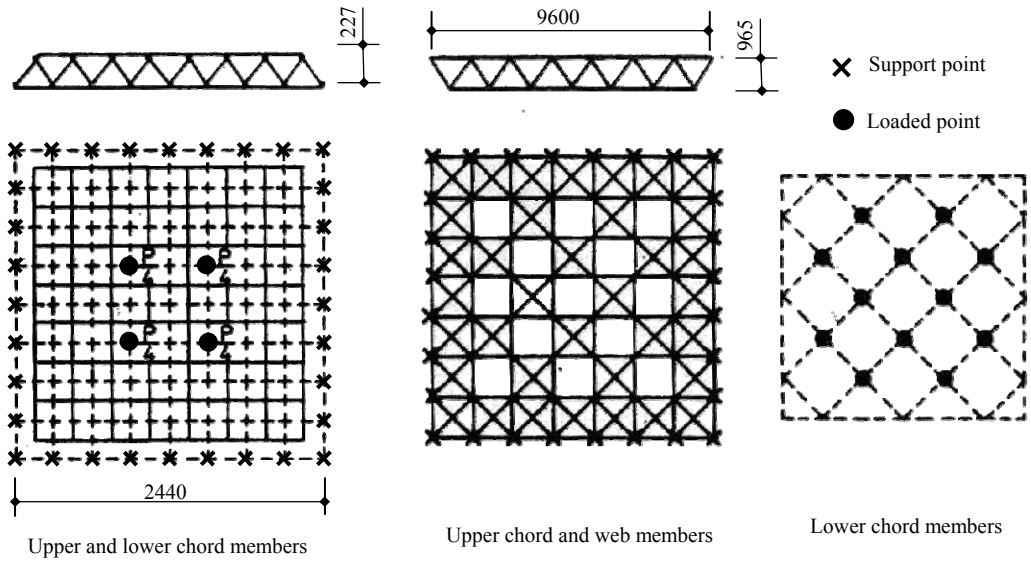

Figure 2.4 Space truss layouts and loading conditions

2.2.2 Sensitivity of space structures to member loss

The sensitivity of space trusses to member loss gained much interest due to its expected effect in overall progressive collapse. A numerical study presented by Hanaor

and Ong (1988) studied the relationship between structural redundancy and the ability of the structure to tolerate member loss. The study was conducted on edge-supported SOS trusses. They concluded that with the typically high redundancy of space trusses, the structures were vulnerable to a loss of strength between 20% and 30% upon the removal of only one member. This behaviour opposed the traditional belief of having more stable structure by the increase in its degrees of redundancy. By adding above reduction in strength to other causes of strength losses such as imperfections, the lack of fit, joint slippage and initial member curvature, the reduction in strength of space trusses could reach about 50% of their strength (Hanaor and Ong, 1988).

To investigate the effect of sudden member loss on the strength of composite and non-composite space trusses, a study was presented by Elsheikh (1996a). The study included the numerical analysis of 12 composite and non-composite SOS space trusses with different aspect ratios and support conditions. Comparison between the behaviour of trusses with gradual (static) and sudden (dynamic) loss of critical members was held. The study concluded that with higher redundancy of space trusses, high sensitivity to member loss was experienced, which was more serious than the gradual member loss. In addition, strength of space trusses supported at corners was seriously reduced by the loss of a critical member compared to edge-supported trusses with the most notably for the loss of diagonal members at supports. However, the composite action with top concrete slab had a positive effect in reducing the sensitivity of space trusses to sudden or gradual loss of critical members.

2.2.3 Sensitivity of space structures to member and support imperfections

In the study presented by Schmidt *et al* (1980) on a full-scale edge-supported space truss of SOS layout, the initial stresses due to member imperfections had a peak of 8% of the member buckling stress while the peak tension in lower chord members reached

9% of the material yield stress. These stresses reduced the strength of the truss below the design value predicted analytically.

In another study presented by Tada and Wakiyama (1993), a loss of space truss strength that ranged from 10% to 15% due to geometric imperfections as errors in setting the level of supports and/or errors in member lengths of up to 3mm, which was the maximum specified according to the Japanese Architectural Standard Specifications 1970, was reported. These results were produced by an analytical study on SOS edge supported space truss of 14m×14m×1.414m dimensions. Imperfections were introduced to the space truss in 2 different ways including an over-length of critical upper chord member of 3mm and a support set at a level 3mm higher than the other supports.

Later, a numerical study was introduced by Elsheikh (1995) on the effect of member imperfection on the behaviour of composite and non-composite space trusses. The truss used in the study was of SOS layout and dimensions as shown in Figure 2.5a. The member imperfections took the form of a lack of fit of ± 0.1% of the original member length of the selected members shown in Figure 2.5b. The study showed a high sensitivity of space trusses to member imperfection resulting in up to 32% reduction in overall strength (Figures 2.6a and 2.6b).

Another study was presented by Elsheikh (1996b), which paid attention to investigate the effect of supports settlement on the strength of space trusses. The study included twelve space trusses with different aspect ratios and two cases of corner and edge supported conditions. For the case of corner-supported trusses, only one of the supports was allowed settlements that ranged between 0.05% and 0.50% of the long span while a settlement of 0.2% of the long span was allowed at one corner or number

of supports adjacent to corners in case of edge-supported trusses. As a result of applied settlements, corner supported space trusses showed low sensitivity due to their lower torsional stiffness, while edge-supported trusses showed high sensitivity for settlement of supports at mid-edge points and low sensitivity to settlement of corner supports.

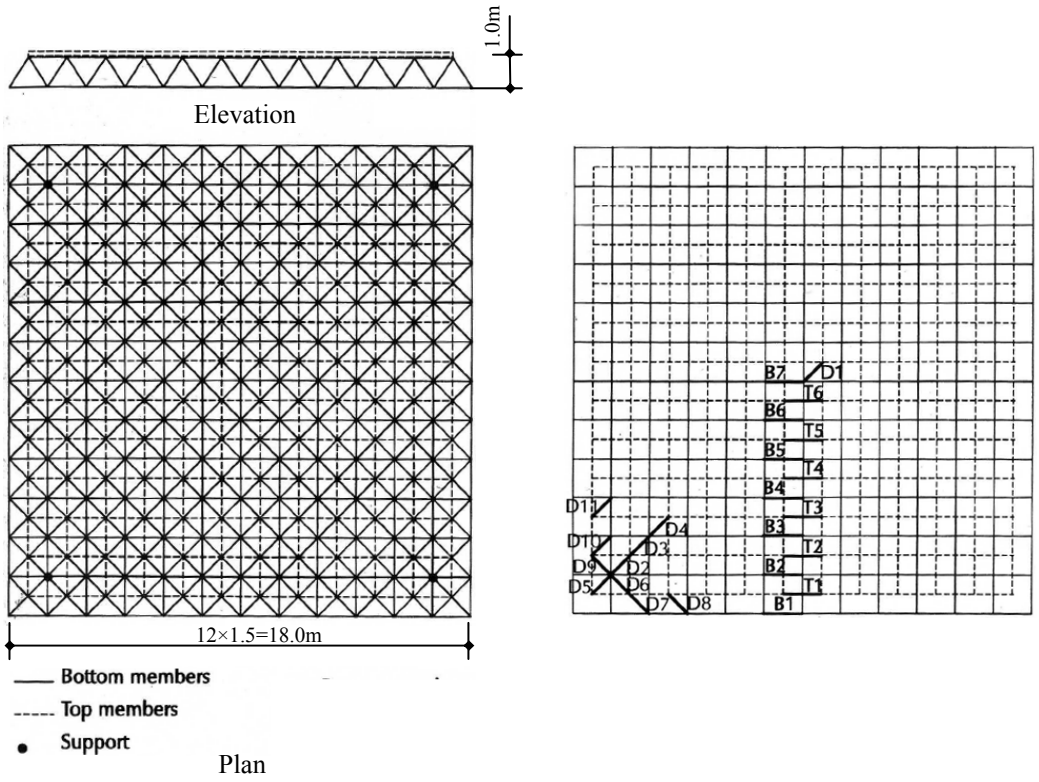

a. Layout of studied space b. Members with imperfections

Figure 2.5 Space truss layout and members having imperfections (Elsheikh, 1995)

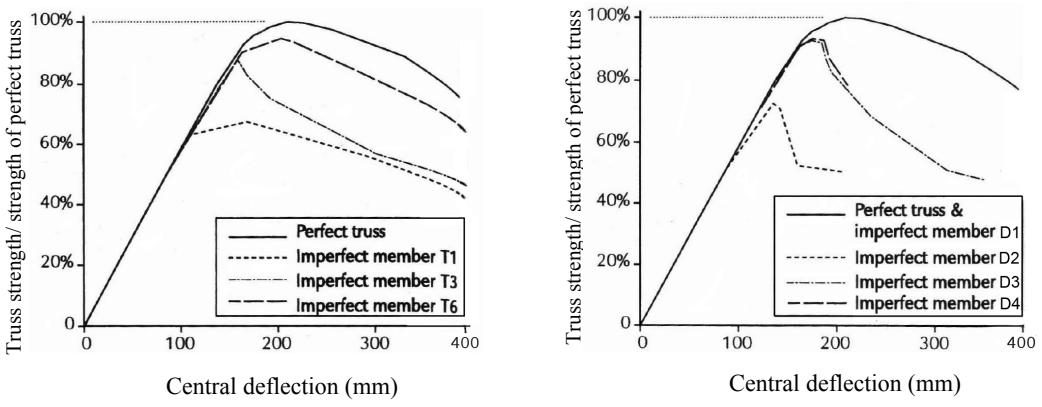

a. Top member imperfection b. Diagonal member imperfection

Figure 2.6 Effect of member imperfection on space trusses behaviour (Elsheikh, 1995)

2.3 Improvement of space truss behaviour under static load

The behaviour of space trusses under static loads as described above encouraged research into methods to improve this behaviour and make it tolerant to individual member imperfection or complete loss. The following discussion covers research into the development of these methods.

2.3.1 Over/under design of chord members

Over and under design of chord members is a technique that was recommended by Schmidt *et al* (1980) as a method to increase the capacity of space trusses. The technique depends on over-designing the upper chord members and under-designing the lower chord members, which make the overall behaviour dependent on the ductile properties of lower chord members during yield and delay the buckling of upper chord members. The study reported results of a full-scale (9.60m×9.60m×0.97m) SOD edge-supported space truss with over-designed upper chords. Test results showed an increase in loading capacity of 18% after the first yield in tension members occurred. At the same time, a 73% increase in compression force in the most heavily loaded compression member was experienced. The study concluded that under high loads the rate of force development in compression chord members escalated and the truss failed once the first member buckling occurred.

Further, Smith (1984) and Parke *et al* (1984) introduced their studies on the technique as a method to improve the ductile behaviour of space structures. As a result of the technique, the structure integrity against sudden collapse was improved, but at the same time the sensitivity for member imperfection was reduced through a much improved load redistribution capability (Smith, 1988). However, due to the progress of yield in the lower chord members, the rate of force development in the upper chord members increased, leading eventually to cases of member buckling as was also found

by Elsheikh and McConnel (1993).

2.3.2 Pre-stressing by lack of fit

Hanaor and Levy (1985) proposed pre-stressing by lack of fit as a method to improve the behaviour of space trusses and to increase their ability to sustain applied loads. The proposed technique depended mainly on controlling the member lengths during manufacturing by introducing a slight length decrease in compression members and a slight length increase in tension members. As a result, initial tension forces were developed in compression members and compression forces in tension members. The resulting truss strength improvement ranged from 40% to 58%. The complexities in applying this technique arise from the need for a precise manufacturing process and a laborious and complicated design process (Levy *et al*, 1994).

2.3.3 Diagonal removal technique

This technique depends on removing a number of selected diagonal members to divert the flow of forces towards less stressed areas. This would be expected to result in a more uniform distribution of forces in the truss chord members. A study introduced by Tabatabaei and March (1993) on a 60m×60m space truss reported that by using this technique there was an improvement in strength to weight ratio of about 56% but the truss deflection also increased as a consequence of diagonal member removal. However, the main disadvantages of this method were the long effort to select the members to be removed, and the resulting high sensitivity of the structure to load changes.

2.3.4 Using force limiting device

To overcome the brittle behaviour of space trusses due to the sudden buckling of compression members, new devices called Force Limiting Devices (FLD) were introduced by Schmidt and Hanaor (1979). The main purpose of adding these devices

to compression members was to increase their ductility through providing a ductile plastic behaviour at the ultimate load (Figure 2.7). Intensive research was carried out to determine their effect on the capacity and behaviour of space trusses and included several space truss configurations with different jointing types and confirmed the high efficiency of FLD in reducing the brittle and progressive collapse behaviour of space truss besides the noticeable increase in the capacity of space trusses of different layouts, support conditions and aspect ratios (Collins (1981), Parke (1993), Imai *et al* (1993), Elsheikh (1999)).

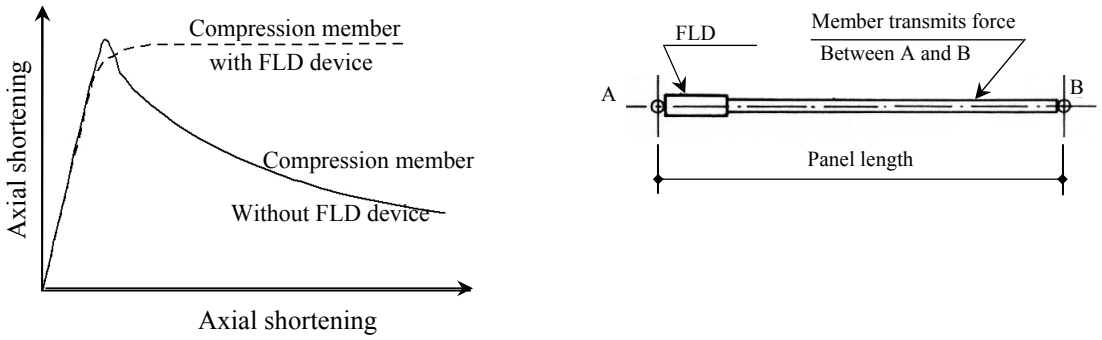

a. Compression member with/without FLD b. Layout of compression member with FLD

Figure 2.7 Effect of FLD device on behaviour of compression member (Schmidt *et al*, 1979)

2.3.5 Eccentric diagonals

The use of eccentric diagonals was another technique introduced by Marsh and Fard (1984) that proved to be successful in improving space truss behaviour through achieving a more uniform distribution of forces in top members. It was found that members eccentrically loaded exhibited nonlinear force-shortening relationships and became less stiff near their ultimate load although still elastic. While forces in chord members were a direct result of the horizontal components of the forces in diagonal members, the use of eccentric diagonals at selected locations limited the contribution

of forces in these diagonals to the highly compressed chord members near the ultimate load. Member eccentricity can be achieved by using unsymmetrical sections such as T-sections resulting in a more uniform distribution of chord forces and high strength. Experimental results recorded an increase in the load carrying capacity of 30% in addition to improvements in overall ductility and warnings to impending failure in the form of curvature in the eccentric diagonal members.

It should be noted that this technique is only applicable for the case when truss connections allow the use of eccentric diagonal members, which limits the use of this method to only specific types of space truss.

2.3.6 Composite action with a top continuum

Previous research showed clearly that the collapse of space trusses commonly arises from the buckling of one or more critical top chord members, spreading rapidly to other members and causing the overall progressive collapse. The above mentioned methods to improve this behaviour suffer from various disadvantages such as sensitivity to changes in load pattern and the considerable effort required in design and manufacturing. The need for a more ductile system encouraged research to use cladding material acting compositely with the upper chord members. Because of the high in-plane stiffness of cladding, it carries most of the upper chord forces and hence reduces significantly the forces in these members. This technique introduces large savings in the use of truss material and makes the behaviour more ductile as it becomes dependent on the behaviour of bottom chord members, which normally carry tension in most cases. By using these fundamental concepts, the behaviour of space trusses would be expected to become more ductile compared to the non-composite space trusses. Figure 2.8 shows the effect of composite action in improving both the ductility and strength of the space trusses as found in an experimental study conducted

by Elsheikh and McConnel (1993) on pin-jointed space trusses of SOS layout with a concrete deck. The tests demonstrated 250% enhancement in the load carrying capacity in addition to the clear effect on ductility.

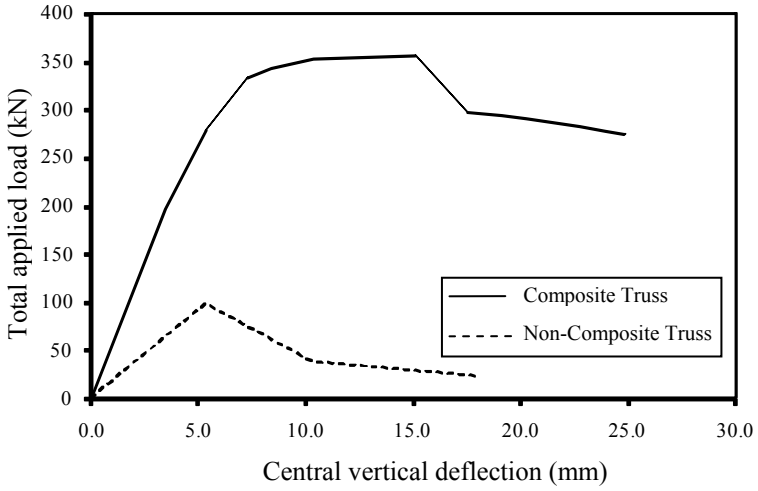

Figure 2.8 Behaviour of composite and non-composite pin-jointed space trusses (Elsheikh and McConnel, 1993)

To develop composite action with upper chord members, a number of techniques were developed. One of the first techniques was introduced by Castillo (1967) by which composite action was achieved by using pre-cast concrete blocks rested on the diagonal members as shown in Figure 2.9. In situ concrete was then cast on top to cover the blocks.

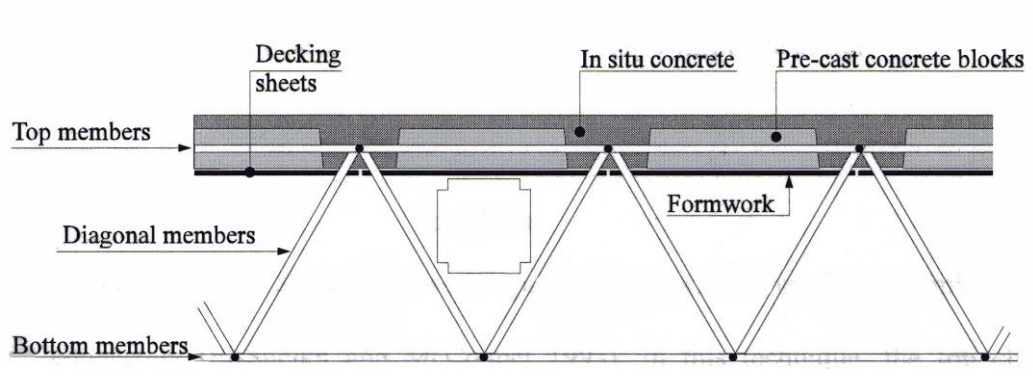

Figure 2.9 Details of Castillo technique for composite space truss (Castillo, 1967)

This system suffers from deficiencies due to the need for sealants to stop leakage of fresh concrete during casting and may require temporary formwork in larger span applications.

Another technique introduced by Al-Bazzaz (1976) and Hong (1984). This technique was based on removing all upper chord members and adding plates welded to top joints as shown in Figure 2.10. A headed stud was welded to each top plate.

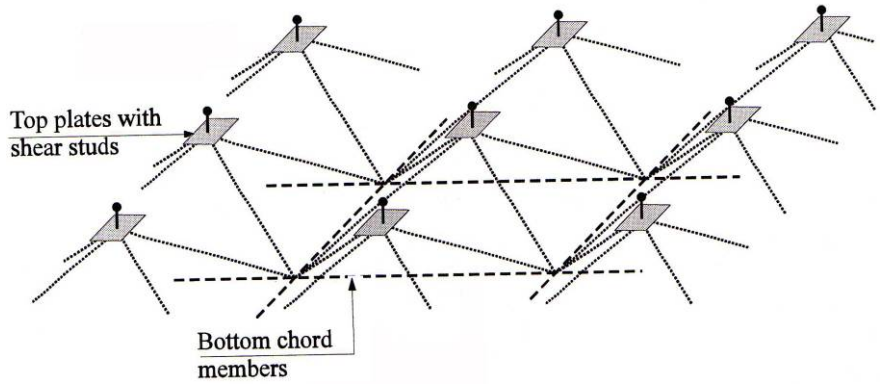

Figure 2.10 Typical components of the second technique (Al-Bazzaz, 1976)

Although this technique introduced an efficient use of steel and concrete in addition to large savings in steel by removing all upper chord members, it suffered the need for temporary formwork from the beginning of construction even for small spans.

A later technique was introduced by Kuleib (1989) in which profiled steel sheets running over the upper chord members were used as a permanent formwork for the fresh concrete. Self drilling shear studs or headed studs welded directly on to the top joints and in the middle of top chord members were used as shown in Figure 2.11. The possibility of using the technique in building composite space truss bridges was introduced by Sebastian and McConnel (1993). This technique has many advantages since it does not need any formwork or steel sheet stiffeners, in addition to its ease of application. However, it suffers a number of disadvantages due to the need for a thick

concrete slab due to the presence of ribs, and that the level of composite action achieved is not as high as in the above techniques.

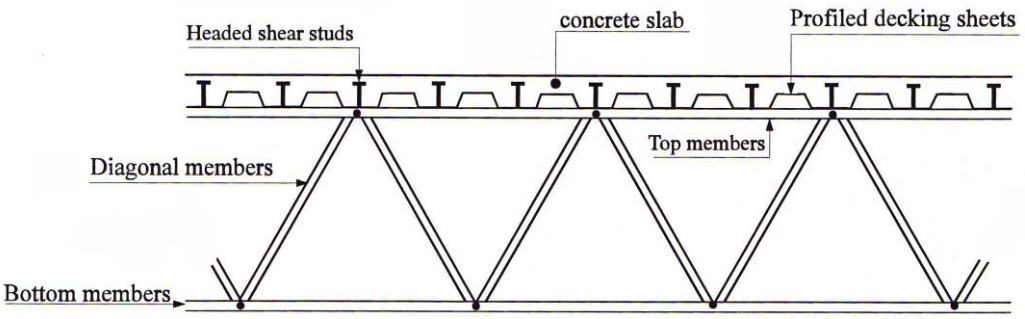

Figure 2.11 Details of composite action by using decking sheets (Sebastian and McConnel, 1993)

Elsheikh and McConnel (1993) developed another technique to be used with short chord members. This technique was based on using channel sections with horizontal web and vertical flanges as upper chord members as shown in Figure 2.12. A shear stud was connected to each top ball joint and another at the middle of each member to achieve a reasonable interaction between the concrete and the steel sections. A thin steel sheet with cut corners and folded edges was prepared to rest on the channels and act as formwork for the concrete slab (Figure 2.12).

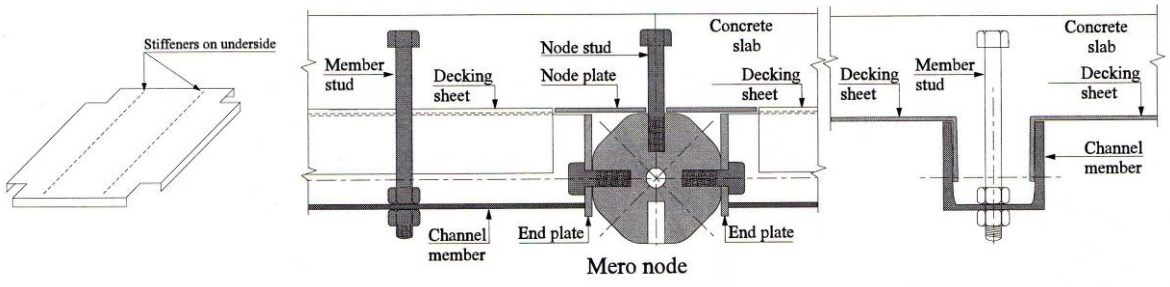

Figure 2.12 Details of Elsheikh and McConnel composite space truss system (Elsheikh and McConnel, 1993)

A development for the CATRUS space truss system was introduced by Shabaan (1997) to enable using the system compositely with a top concrete slab. The technique depended on fixing flat decking sheets between the two layers of the top chord to act as formwork for the wet concrete. Composite action in this system was achieved by the embedded group of top chord members and the bolts connecting the upper member groups (Figure 2.13).

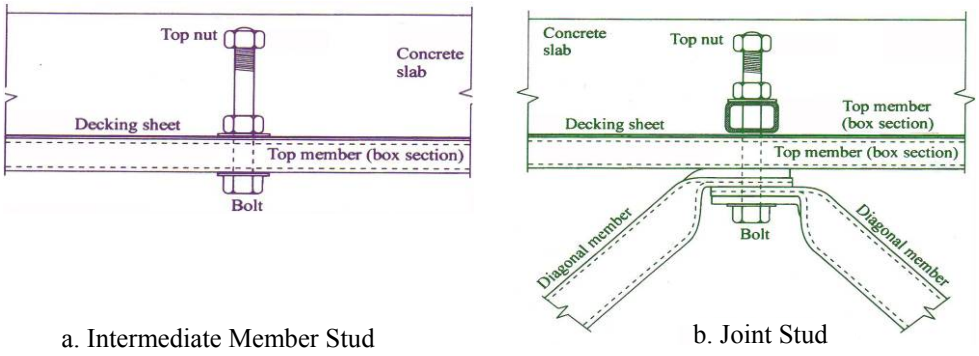

a. Intermediate Member Stud b. Joint Stud

Figure 2.13 Composite deck for CATRUS double-layer space grid (Shabaan, 1997)

Timber boards can also be used instead of concrete to achieve the benefits of composite action (Elsheikh and Shabaan, 1999). The technique was based on a simple shear interaction device fixed between the two layers of upper chord members as shown in Figure 2.14, to connect up to four timber boards to each truss joint. Tests on trusses acting compositely with timber boards showed reasonable improvements in their behaviour. The improvement in load carrying capacity achieved with timber boards was less than that with a concrete deck but the ease of application and the light weight of timber boards could make the boards an attractive solution. However, timber boards still have a number of disadvantages including anisotropy, variation in behaviour in different timber types, low durability compared to concrete and the risks of wear and fire.

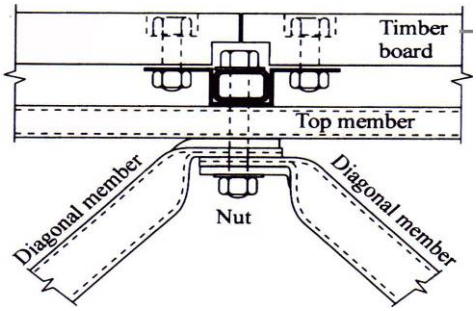

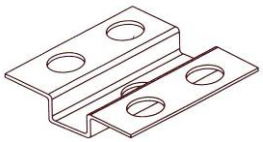

Shear interaction device

Figure 2.14 Composite action by using timber boards (Elsheikh and Shabaan, 1999)

2.4 Behaviour of space structures under dynamic loads

While static analysis is important in determining the strength and stiffness of structures, dynamic analysis is also important since dynamic vibrations add considerable forces and stresses to the structural elements. The resulting stresses may lead to dynamic instability, fatigue cracks or increase in plastic deformations causing members to fail. Several text books covered dynamic analysis of structures from basic principles to advanced analysis techniques; see for example Chopra (1995) and Clough and Penzien (1993).

Due to the high sensitivity of space structures to load changes and the high probability of progressive collapse under small load increases, the study of the dynamic behaviour of space structures has become an important part of the design process to this type of structures. A review of earlier research conducted in this field is presented in the following sections.

2.4.1 Dynamic behaviour of non-composite space structures

A computational procedure to predict the dynamic response of space trusses with both geometric and material nonlinearities was introduced by Noor and Peters (1980). It used a mixed system of algebraic and differential equations to derive values for member forces, nodal velocities and nodal displacements.

To check the accuracy of the proposed technique in predicting the dynamic responses of structures, numerical examples were introduced which included plane and space structure models. Analysis was carried out, for example, on a ten-bay space truss shown in Figure 2.15a, which included linear analysis (L), nonlinear analysis with material nonlinearity (MN) and nonlinear analysis with both geometric and material nonlinearity (GMN). The study reported the importance of considering the material nonlinearity during the prediction of dynamic behaviour of space structures, since it had a more pronounced effect on responses than geometric nonlinearity (Figure 2.15b).

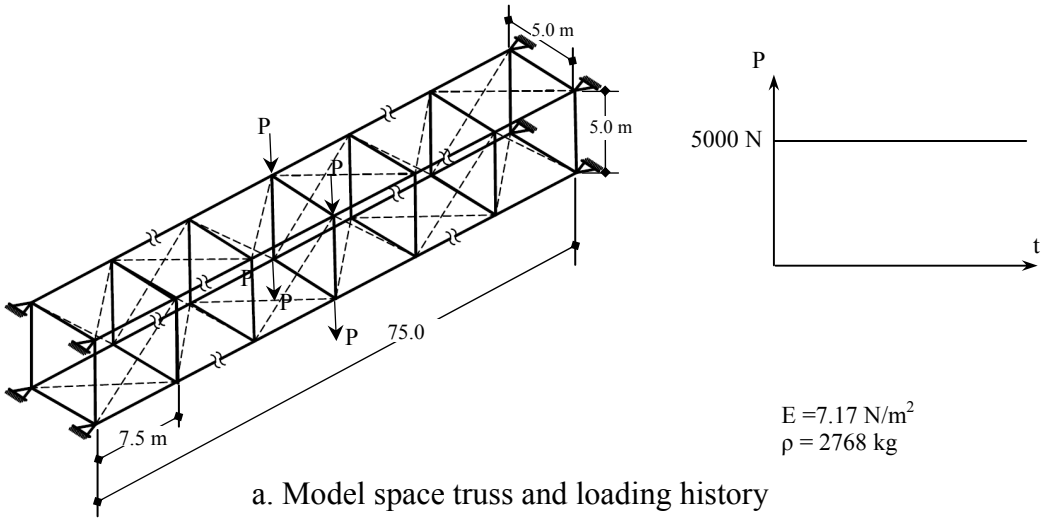

a. Model space truss and loading history

Designation	Type of nonlinearity
GMN	Geometric and material
MN	Material
L	Linear response

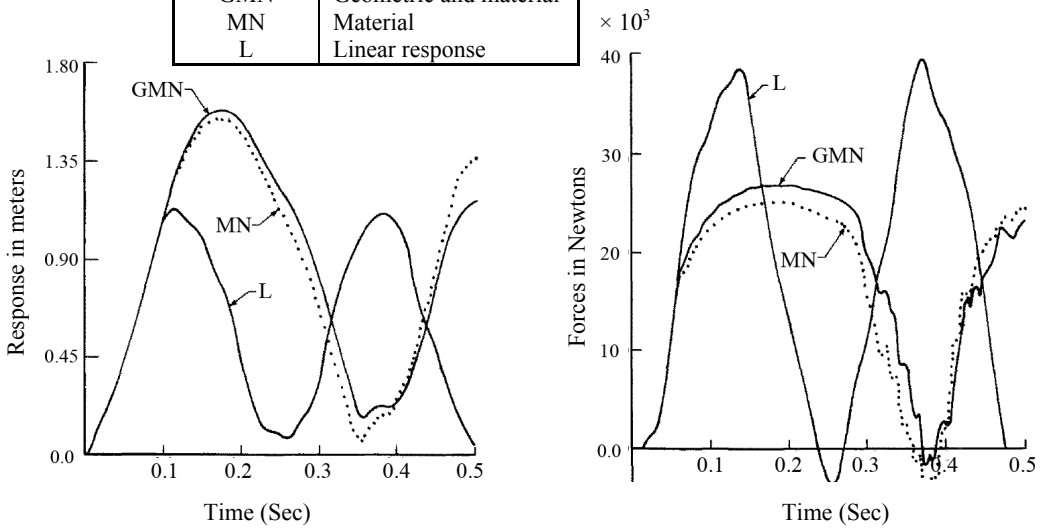

b. Displacement and force responses

Figure 2.15 Dynamic response of a ten-bay space truss using the proposed technique (Noor and Peter, 1980)

Furthermore, the proposed procedure could be considered as an efficient tool for designers capable of predicting the dynamic behaviour of structures.

To study the effect of joint stiffness on the non-linear dynamic behaviour of truss structures, a numerical study was presented by Chan and Chui (1993). The study arose from a previous study carried out by the first author, which reported 18% underestimation of static load carrying capacity of space trusses by considering all joints as pinned. A non-linear simple efficient displacement based computer program was applied, in the 1993 study, to predict the large deformation and dynamic response of trusses with different types of connection stiffness. Numerical examples were presented, which included a 68.58m span truss with 20 kN amplitude sinusoidal load. The load was applied at the op middle joints and had with a frequency equal to the natural frequency of the test truss for each case of joint stiffness (Figure 2.16). Three joint idealizations were used including rigid, pinned and semi-rigid The study concluded that the maximum displacement was mainly affected by the changes in the overall stiffness of the structure, which dominantly affected by both the axial stiffness and the arch effects leading to a minimal effect of joint stiffness on the analysis (Figure 2.17).

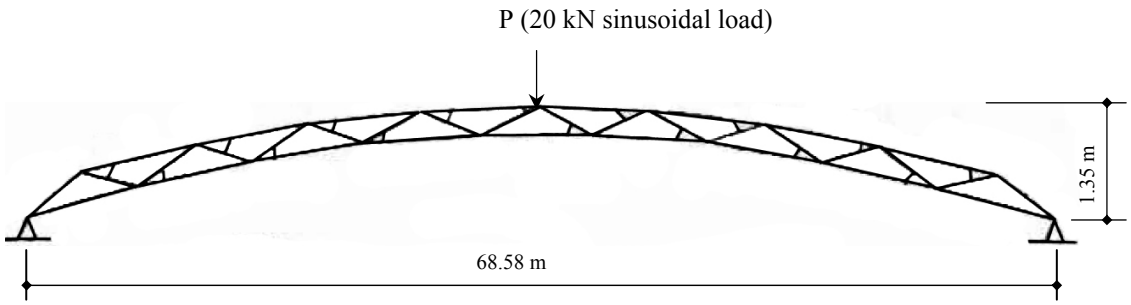

Figure 2.16 Truss layout showing dynamic loads and dimensions

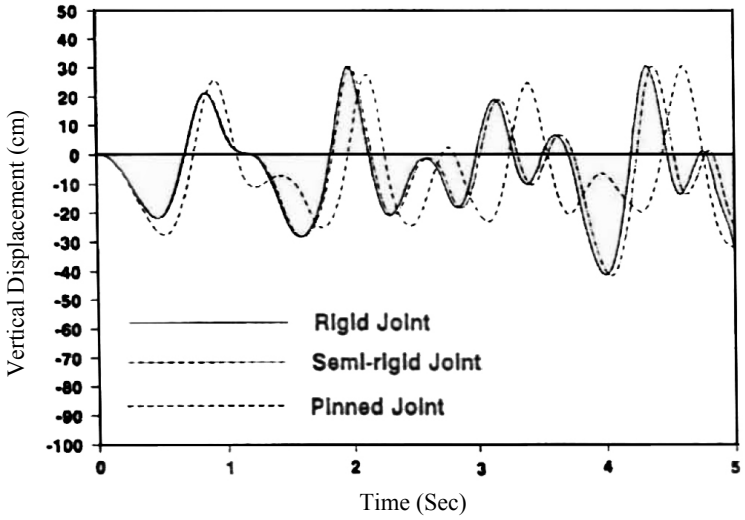

Figure 2.17 Transient response of the arch truss with different joint rigidity (Chan and Chui, 1993)

Although the study was not directed to space trusses, it reflected the possibility of ignoring the effect of joint stiffness on the dynamic behaviour of truss structures. However, the study focused on curved trusses and did not investigate this effect for both plane or space truss structures, which may need further research.

The dynamic response of truss structures during the sudden successive failure of individual members was the subject of another study by Malla and Wang (1993). In this study, the dynamic member failure was represented by replacing the member by its internal forces applied at the end joints and abruptly dropping the force to zero or a reduced value to enable tracing the resulting dynamic response of the truss structure. The proposed method was applied to a cantilever planar truss with the dimensions shown in Figure 2.18a and subjected to a sudden damage to one or more of its critical diagonals. Static, modal and dynamic analyses were carried out on the structure to determine the changes in displacement, member stresses and structure natural frequencies. The analysis results demonstrated the localised effects of static member failure, while the dynamic member failure had a widespread effect on the whole structure (Figure 2.18b). The results proved the suitability of the proposed technique to

represent the dynamic effects caused by the snap-through (sudden) failure of truss members.

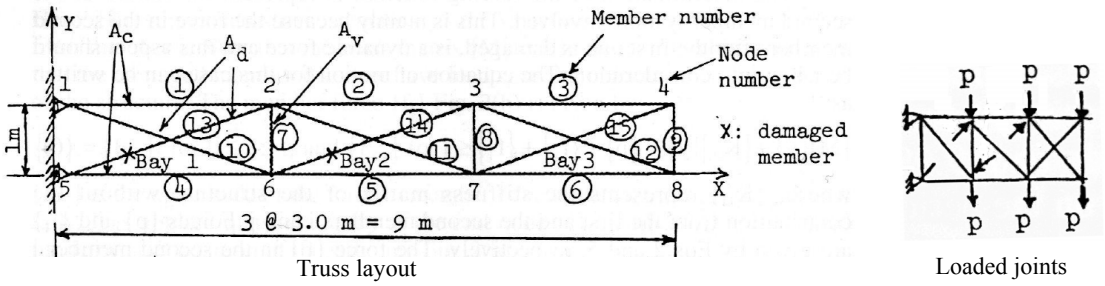

a. Planner cantilever truss layout and loaded joints

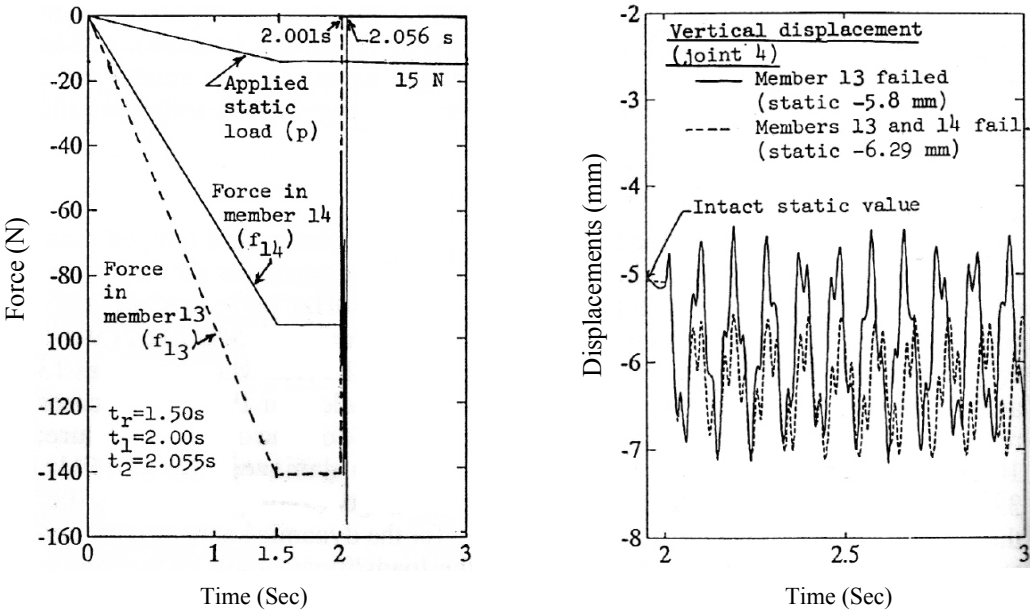

b. Dynamic forcing function and critical displacement results

Figure 2.18 Response of truss due to sudden member failure (Mala and Wang, 1993)

Zhu *et al* (1994) presented a computational procedure for predicting the geometric and material nonlinear dynamic response of space trusses. The technique employed the application of an updated Lagrangian method based on the incremental formulation of the equation of motion. The proposed technique was used to predict the effect of considering the geometric and material non-linearities on the dynamic behaviour of a two-bay cantilever truss shown in Figure 2.19. The tested truss was exposed to a

sinusoidal forcing function with an amplitude of 4.5×10-4 N and t=0.01 sec. The displacement responses accounting for different nonlinearities were compared together. The study recorded an increase in the displacements and a reduction in member forces by the inclusion of the material and geometric non-linearties in the dynamic analysis. This behaviour concluded the significance of the inclusion of both material and geometric nonlinearity during the dynamic analysis of truss structures besides the high efficiency of the proposed technique in tracking the behaviour of different types of structures (Figure 2.19).

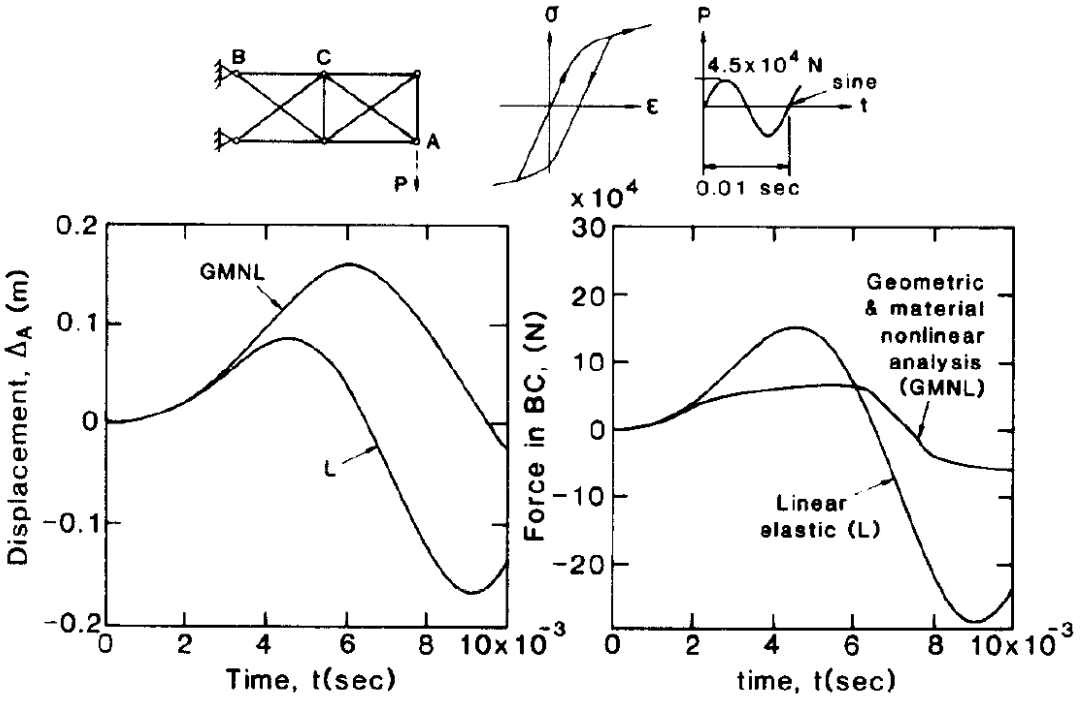

Figure 2.19 Linear and non-linear response of two-bay cantilever under a sinusoidal forcing function (Zhu *et al*, 1994)

A study carried out by Elsheikh (2000) introduced two new methods for the approximate analysis of SOS space trusses. These methods were based on beam and plate analogy techniques and were aimed to be suitable for hand calculations. The methods were intended to provide the designer with easy and accurate predictions within 0 to 15% accuracy of the dynamic behaviour of space trusses and in particular

their fundamental natural frequencies. In the beam analogy method, the truss was modelled as a beam running in the main direction with the same depth and boundary conditions as the original truss. The structural resistance to dynamic loads was assumed to depend on the contribution of chord members in the main direction only as top and bottom flanges. On the other hand, the plate analogy method was based on modelling the two-way truss as a plate for which the equation of motion could be applied.

Both methods were assessed through a parametric study involving 144 space trusses covering a wide range of aspect ratios, span/depth ratios, number of chord panels and type and location of supports (Figure 2.20). The study concluded that beam method was suitable for one-way space trusses such as those used in bridges or where the structure's aspect ratio was greater than 2.0, while plate analogy was suitable for space trusses supported on their edges and with aspect ratio below 2.0.

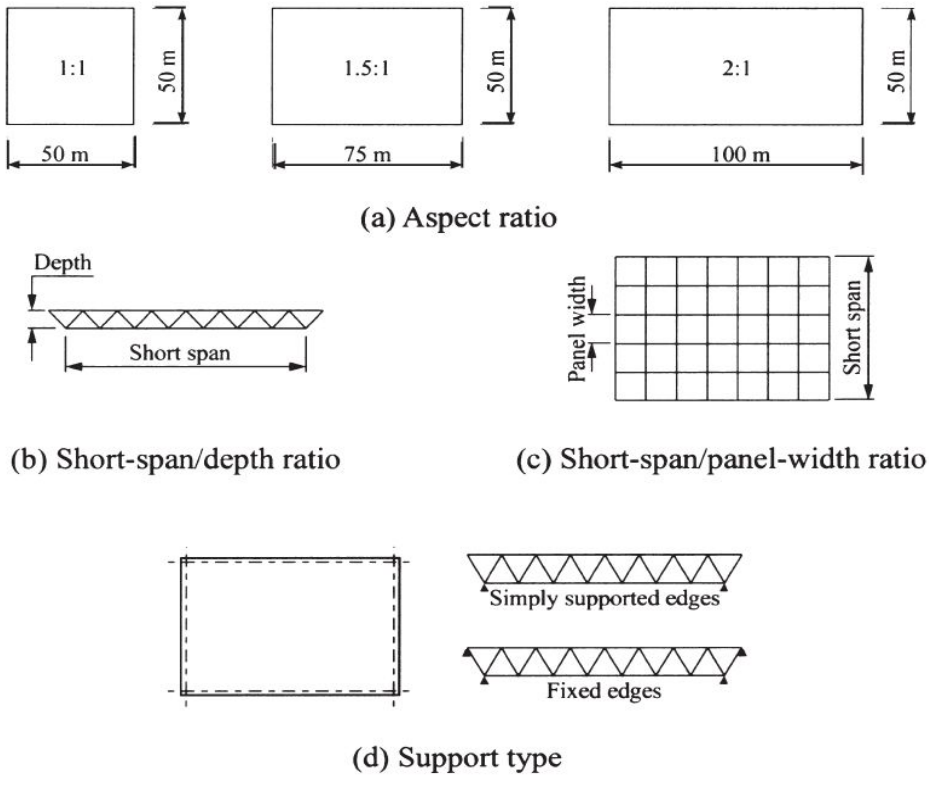

Figure 2.20 Parameters included in Elsheikh (2000) study

A recent experimental study dealing with determining the effects of tightness of bolts on the damping of a MERO-type double-layer space truss was introduced by Pashaei *et al* (2006). Experiments were conducted on a 10m×10m space truss with a MERO jointing system supported at corners and with 12 supports as shown in Figure 2.21. Initial displacement (Snap) tests were carried out by instantly releasing a load applied vertically at the middle top joint of truss and recording the resulted vibrations using high precession accelerometers. Damping ratios were extracted from test results using the logarithmic decrement method.

The study reported that the highest damping ratio corresponded to the case with loose joints, due to the high values of Coulomb damping by internal friction between joint components. A considerable reduction in Coulomb damping was recorded by the increase of bolt tightening to 60Nm, which led to a noticeable reduction in the overall damping. With further increases in the bolt tightening the rate of reduction in Coulomb damping decreased (Figure 2.22a), and the material damping (hystersis damping) caused by the increase of lack-of-fit strains was increasing resulting in increases in the overall damping with maximum at 120Nm. However, further increases in joint tightening led to a reduction in the overall damping caused by the increase of critical damping caused by the increase of structural stiffness (Figure 2.22b).

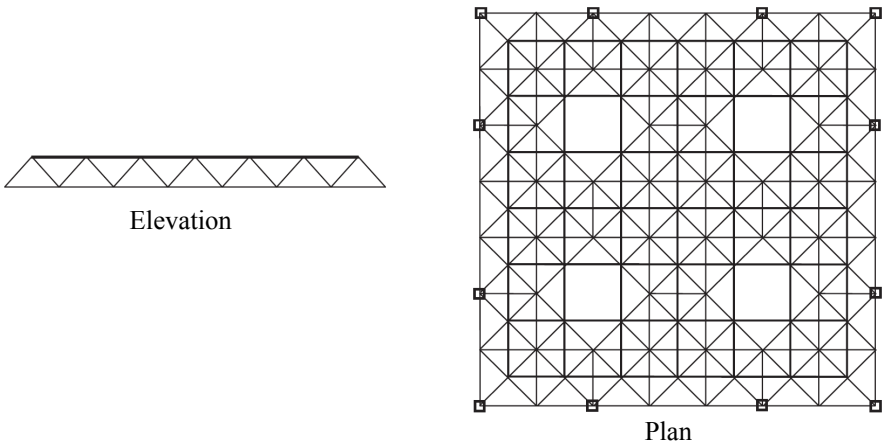

Figure 2.21 Layout of space truss used in Pashaei *et al* (2006) study

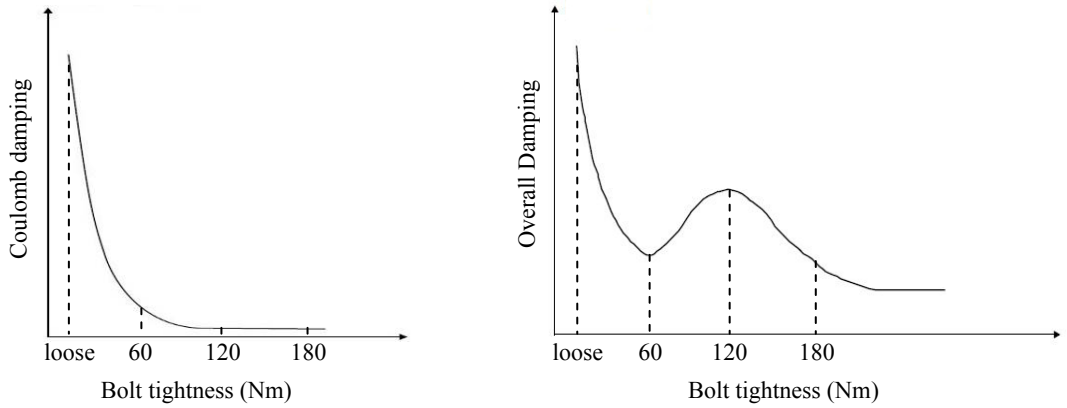

a. Effect of bolt tightness on Coulomb damping b. Effect of bolt tightness on overall damping

Figure 2.22 Effect of bolt tightness on the damping of space trusses (Pashaei *et al,* 2006)

The presented results showed higher accuracy in tracking the effect of bolt tightening on the vibration behaviour of space trusses under only the first mode of frequency; however, the effect of bolt tightening of higher vibration modes was not presented as these would vary according to their higher values of frequency in addition to having different mode shapes which may affect the damping values.

In 2006, Wang *et al* developed a simple formulation, VFIFE or V-5 (Vector Form Intrinsic Finite Element), which can be used to predict the nonlinear dynamic behaviour of reticulated space structures. The analysis method, which was associated with explicit time integration, could effectively simulate the dynamic behaviour of space truss structures using a non-interactive process.

Several examples were presented including different types of static and dynamic problems under various types of excitation. Figure 2.23a presents one of the examples used to check the accuracy of the proposed V-5 technique involving a reticulated latticed dome exposed to a variable dynamic load, P, at the apex (joint 1). The resulting vertical displacement at joint 1 can be seen in Figure 2.23b proving the close

match of results of the V-5 technique to those obtained by earlier research. The study concluded that the proposed technique compared well, in terms of accuracy and stability relative to previous research, which could encourage the use of this method as an effective structural analysis tool for engineers.

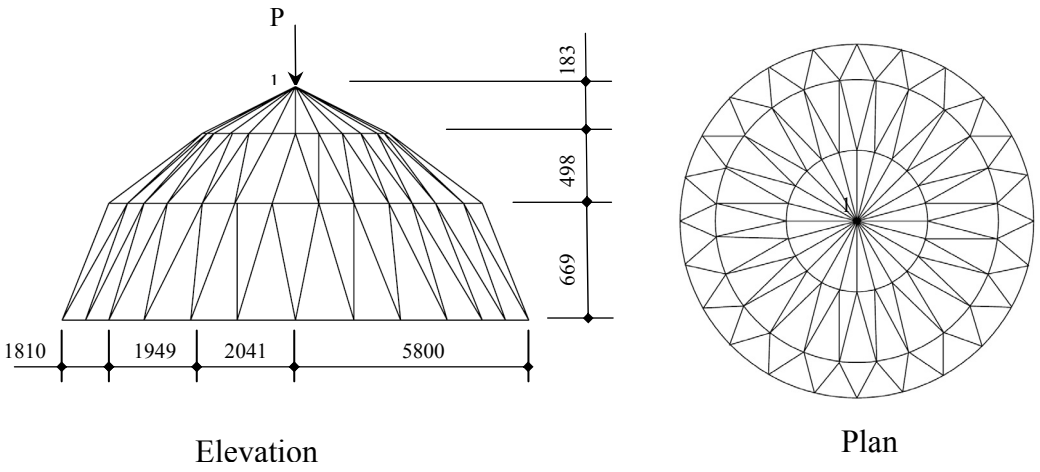

a. Layout of reticulated space truss composed of 168 members

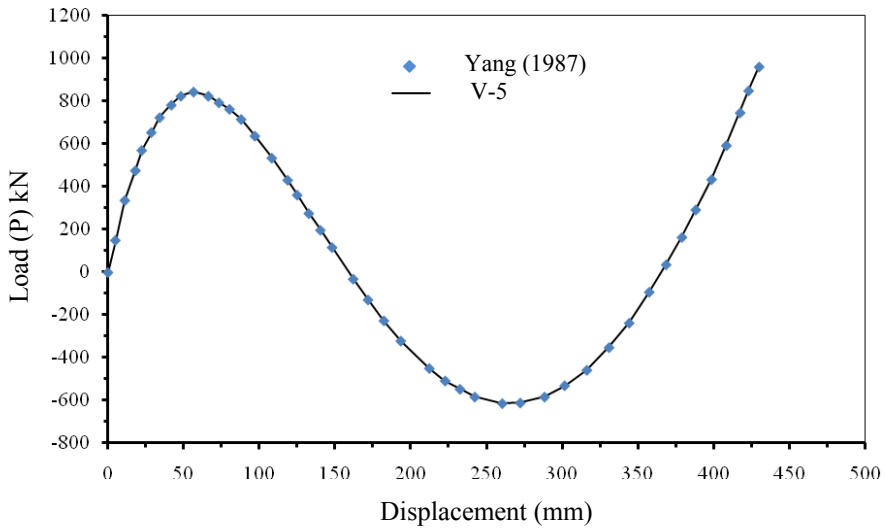

b. Response of joint 1 in vertical direction under dynamic load (P)

Figure 2.23 Layout and vertical response of reticulated latticed dome used in Wang *et al* (2006) study

While the introduction of composite action to space structures showed promising results under static loads, to the author's knowledge, no previous research has been

carried out on the effect of composite action in changing space structures' dynamic characteristics or behaviour, which is the main objective of this research.

The following sections introduce the techniques used to improve the dynamic performance of non-composite space trusses and other, more traditional, types of structures.

2.5 Techniques used to improve the dynamic behaviour of structures

2.5.1 Introduction

Due to the sensitivity of space trusses to dynamic loads, especially the vertical components of earthquake vibrations, several methods have been suggested to enhance the trusses' dynamic behaviour. Moghaddam (2000) reported that space structures' response to severe earthquakes differs from other ordinary structures in many ways;

- The ratio of snow and wind loads to dead loads is noticeably large in space structures compared to ordinary systems. This makes space structures have reserve strength, in case of the absence of these loads, to earthquake loads making them more safe during severe earthquakes.

- Snow loads can reach 2 or 3 times the self weight of the space structure itself leading to the necessity of combing the snow loads and earthquake loads during the design process.

- For ordinary buildings, the horizontal response is dominant governed by the first mode of vibration and the vertical earthquake component is usually ignored in the design. On the other hand, the vertical earthquake component has the dominant effect on space structures and should be considered in the analysis.

- Space structures should be designed to withstand much higher seismic forces

due to their lack of ductility compared to more traditional structures which rely on inelastic deformation to absorb seismic forces.

For these reasons, several techniques are currently being used to improve the behaviour of space structures under seismic loads. These techniques will be discussed in the following sections.

2.5.2 Vibration suppression by adding member dampers

I. Active vibration control using a lead Zirconate-Titanate stack actuator

Analytical and experimental results for the use of the piezoelectric ceramic stack actuator to control active vibration of space truss were presented by Song *et al* (2001). The study was carried out on a space truss with 12 cubic bays shown in Figure 2.24a. The T-shape truss was 3.76m long, 0.35 m wide and 0.7 m tall and included 161 aluminium struts with 52 aluminium node balls and was supported at the lower 4 nodes (01, 02, 27 and 28). A PZT (Piezoceramic Zirconate Titanate) stack actuator strut, shown in Figure 2.24b, was used. The actuator replaced the last diagonal strut at the base between the two nodes (27 and 35), which had the highest modal strain energy according to finite element. The actuator was used to suppress the vibrations induced by a proof mass actuator (LPACT) fixed at the last panel diagonal of the space truss between the two nodes (14 and 52) to simulate the effects of spacecraft disturbance (Figure 2.25). The PZT actuator was made of piezoceramic material, which can generate mechanical strain in response to an applied electric field and known by its high efficiency, fast response, no moving parts and compact size. To suppress the vibration of the truss, an integral plus double integral force controller was designed based on the presence of the PZT actuator and a force transducer as a sensor.

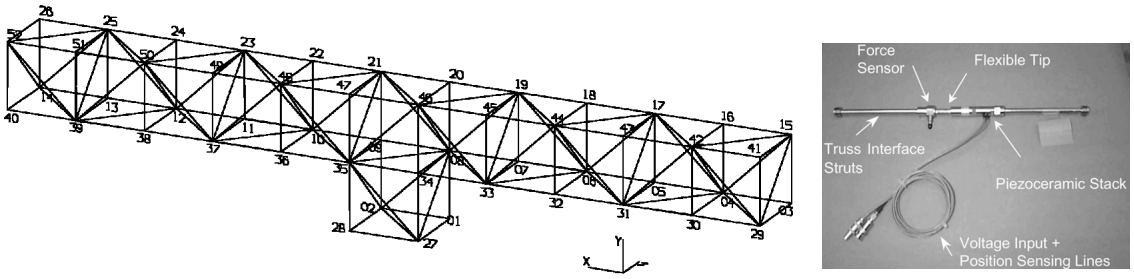

a. Tested space truss b. Details of PZT actuator

Figure 2.24 Layout of NPS space truss and PZT actuator details (Song *et al*, 2001)

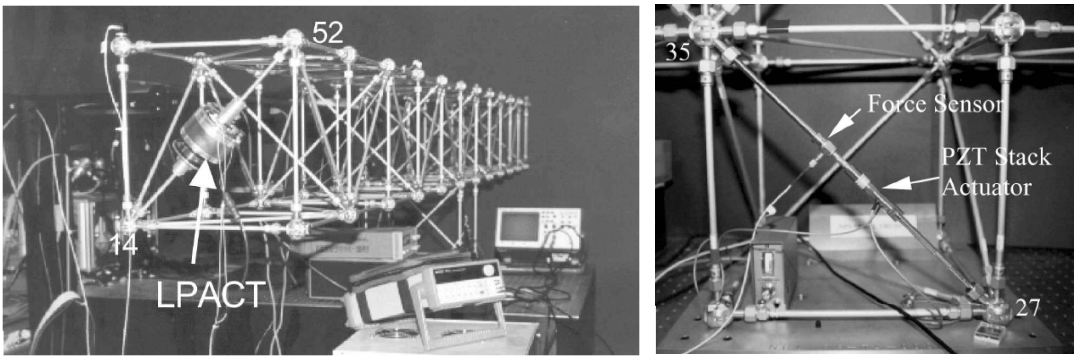

Figure 2.25 Test arrangements for tested space truss (Song *et al*, 2001)

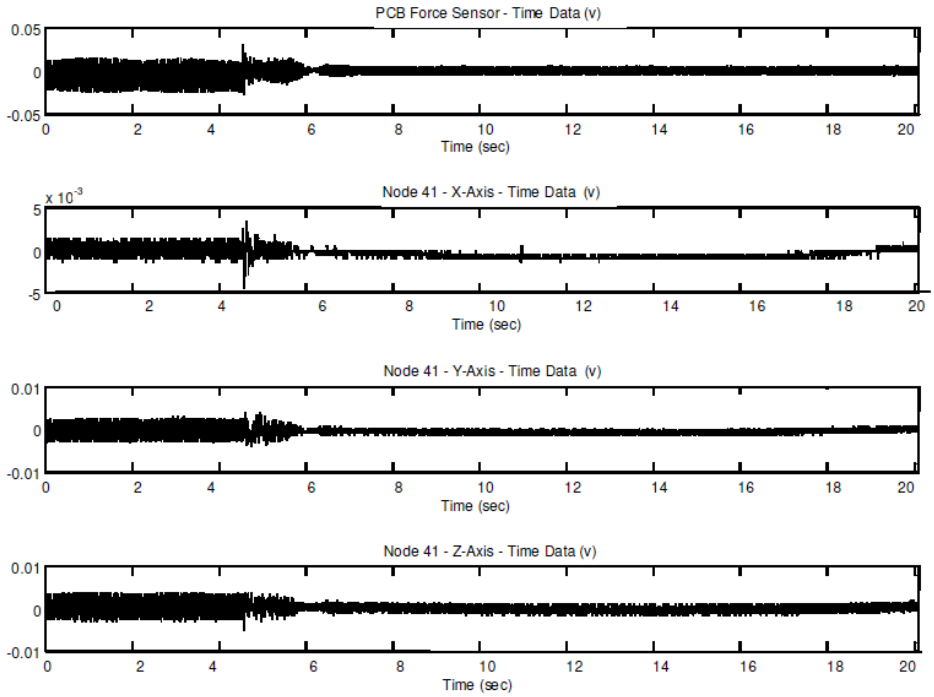

Figure 2.26 Response of space truss before and after the use of the PZT actuator which applied after 5 sec from the start (Song *et al*, 2001)

The study reported the high efficiency of using PZT dampers in suppressing the vibrations in the space trusses under dynamic vibrations as shown in Figure 2.26. It should be mentioned here that this method is mainly used for outer space application, especially for structures that carry highly vibration-sensitive instruments.

II. Using a semi-active Magneto-Rheological fluid variable damper

To mitigate the effects of structural vibrations caused by earthquake motions or strong winds, several methods have been used which can be classified as passive, active, semi-active or hybrid, which include combinations of the previous types. Semi-active systems offer a good alternative to other systems since they possess the adaptability of active control systems in addition to their stability and lower power needed consumption. These systems employ a wide variety of devices such as variable orifice dampers, variable friction devices, controllable fluid dampers and adjustable tuned liquid dampers. A semi-active control system can be defined as a system that has properties which can vary dynamically without increasing the mechanical energy in the controlled system (including the device). Magnetorheological (MR) damper is one of the semi-active devices that use MR fluids to produce controllable dampers. MR fluids can be defined as those fluids that are able to change reversibly their viscosity from linear viscous state to semi-solid state in milliseconds by exposing the fluid to a magnetic field produced by electricity and some coils. Details of an MR damper are shown in Figure 2.27a.

Dyke *et al* (1998) carried out experimental work aimed to investigate the superiority of semi-active MR dampers in reducing the seismic response of structures. Shaking table tests were carried out on a three story steel frame structure using a single 215 mm MR damper with $\pm$ 25 mm stroke in conjunction with a clipped-optimal control algorithm to control the responses of the structure (Figure 2.27b).

The technique demonstrated its high efficiency in reducing the structural responses for a wide range of loading conditions, and this was particularly clear in reducing both the peak responses as shown in Figure 2.28.

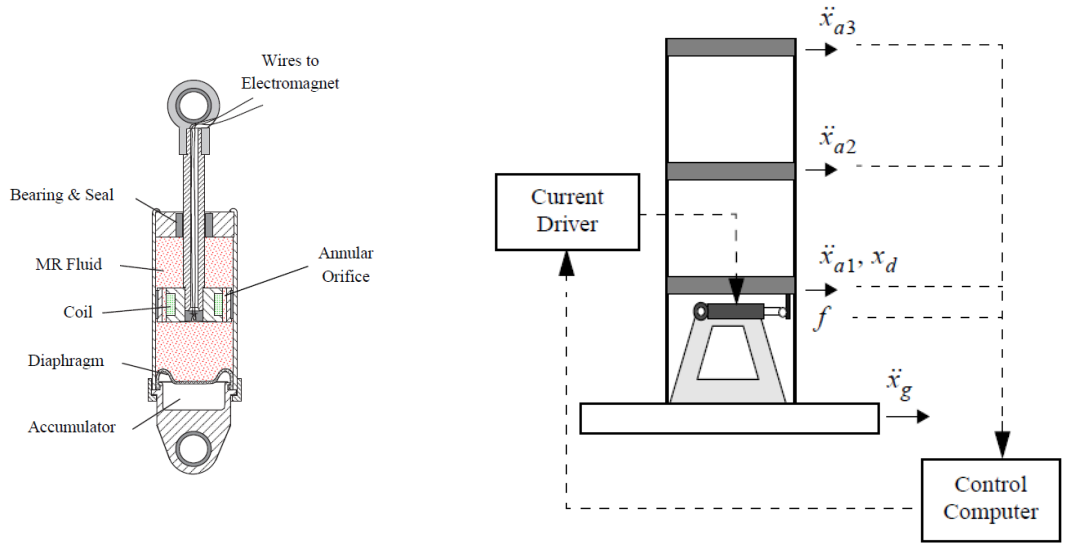

a. Details of MR damper b. MR damper implementation

Figure 2.27 Details and implementation of MR damper system (Dyke *et al*, 1998)

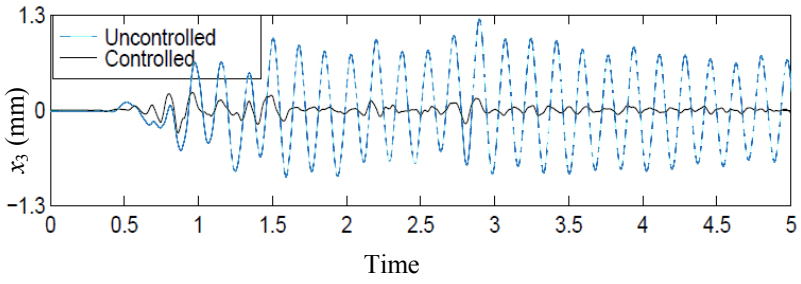

Figure 2.28 Efficiency of MR damper system (Dyke *et al*, 1998)

In another study by Oh and Onoda (2002), the efficiency of using a Magneto-Rheological (MR) fluid damper for the semi-active vibration suppression was demonstrated by using a variable MR damper in their experimental study on the space truss shown in Figure 2.29a. In this study, a high response MR damper (3 millisecond), with the section shown in Figure 2.29b, was fixed at the base of the truss with a lumped mass at the tip. The tip mass was displaced in the x-direction by a certain

amount then released to free vibrate. The control of the MR damper started after 5 seconds after the start of vibration and the results were as shown in Figure 2.29c.

Tests were repeated using different excitation functions and damper types. The results showed a high performance of MR dampers in suppressing vibrations of different excitation functions compared with other types of semi-active damping systems.

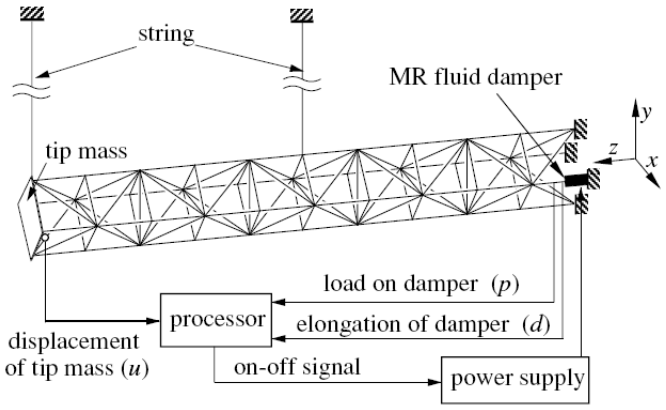

a. Experimental test setup for MR damper

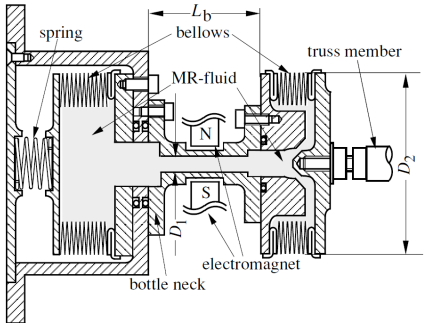

b. Details of MR fluid damper used at the base of tested truss

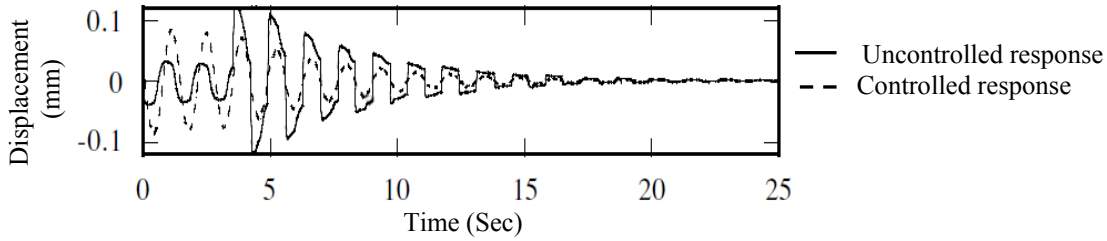

c. Space truss response with and without MR damper

Figure 2.29 Experimental work setup and results (Oh and Onda, 2002)

2.5.3 Dynamic isolation of supports

I. Isolation of supports using Steel Hysteresis Damper system

The Steel Hysteresis Damper (SHD) system was introduced by Kato *et al* (2002). This system was developed for installation at the supports of space structures to absorb the seismic energy transferred into the structure. The SHD damper takes the shape of the

letter J, so it is sometimes called the J-Damper (Figure 2.30). The plastic deformation of the J-plates accompanied with their relative displacement generates a restoring force and makes the J-damper to absorb the seismic energy effectively. The system is made up of four J-shaped steel plates connected to the upper structure (UC) as shown in Figure 2.30a. The damper is assumed to be active against the horizontal displacement perpendicular to the J-plates (PD). A slide plate, lies at the middle between the four J-plates, attached from both ends to rollers connected with stoppers attached to the substructure which allow the whole system to move in the horizontal direction (ND)(Figure 2.30b). The system in this case is considered to be able to move in the ND direction with resistance from a friction damper.

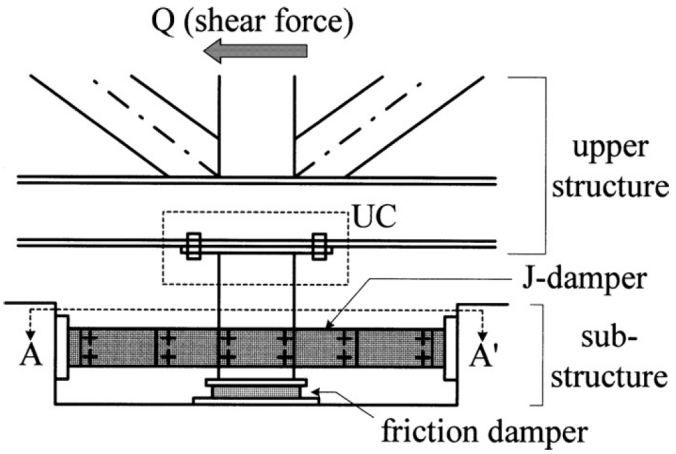

a. Side view of the Hysteretic and friction damper

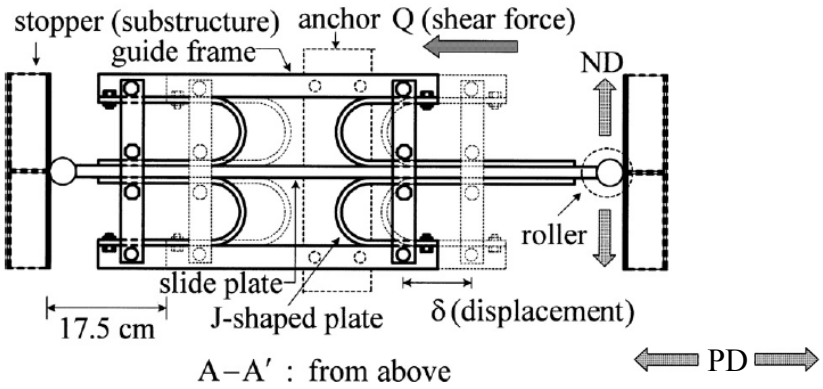

b. Top view of a set of J-dampers

Figure 2.30 Steel hysteresis damper base isolation system (Kato *et al*, 2005)

The system was used in a numerical study carried out by Kato *et al* (2002) to protect a spherical dome supported on a reinforced concrete substructure. The dome has a span of 100m, rise of 18.2m and radius of curvature of 77.8m (Figure 2.31). The substructure consisted of a RC ring girder of 2.50m×0.6 m resting on sixty pairs of RC columns of 1.0m diameter. The columns rested on a RC foundation beam with 2.5m×1.0m dimensions. The foundation ring beam was supported on 60 pairs of piles of 20m length and 0.45m diameters. The whole structure was exposed to Elcentro (1940) earthquake at the ground surface in the X-direction with a maximum acceleration of 500 cm/Sec^2.

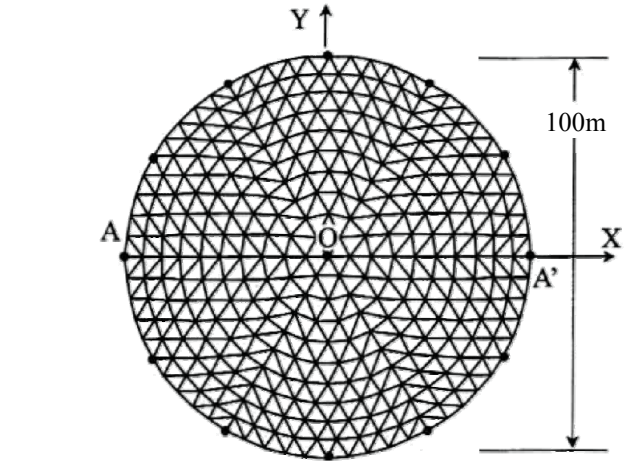

Plan view

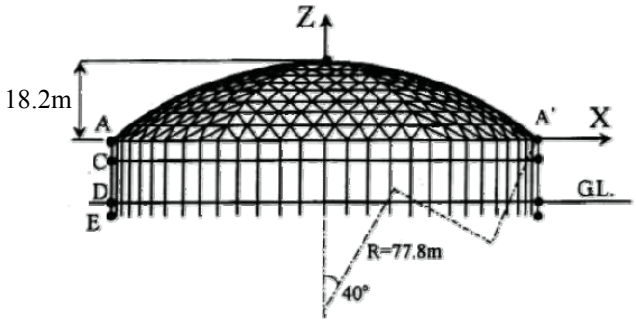

Elevation view

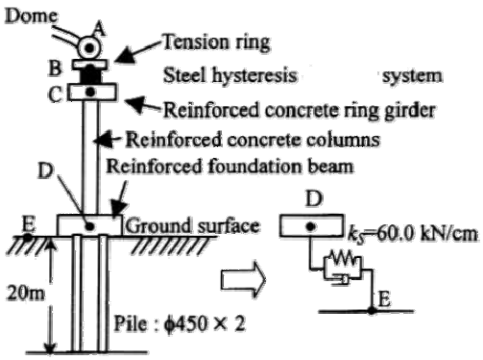

Details of connection with sub structure

Figure 2.31 J-damper used in seismic isolation of dome structure (Kato *et al*, 2002)

The study confirmed the high efficiency of the J-damper system in suppressing the earthquake responses of studied structure. This efficiency was revealed by the large reduction in the maximum vertical and horizontal accelerations of all points on the ridge line AOA'. In addition, the use of SHD damper system participated in reducing the axial forces induced in both the hoop and ridge members of the dome by the earthquake loads.

Later, a finite element model was developed by Kato *et al* (2005) to predict the cyclic behaviour of the J-damper with both geometric and material non-linearity. The efficiency of the system was checked through dynamic analysis of simple mass-spring models. The output of the finite element models showed good agreement with experimental results carried out on corresponding physical models. In addition, results of the dynamic response analysis of a mass-spring model using the proposed models showed high efficiency of the J-damper in reducing the earthquake induced forces by absorbing seismic energy.

The studies discussed above show clearly the possibility of using SHD (J-damper) system in protecting space structure in earthquake-prone regions leading to economical solutions and more safe structures.

II. Adaptive sliding base isolation system

An adaptive seismic isolation system to control the vibration of a simple building frame subjected to disparate earthquake ground motions was introduced by Madden *et al* (2000). The base isolation system used in the study was of the type Friction Pendulum System (FPS), shown in Figure 2.32, combined with an adaptive controllable fluid damper. Several shaking table tests were carried out on a one-bay by one bay three floors welded steel frame shown in Figure 2.33a. The top two floors

were rigidly braced so that the structure behaved as a one-story building frame. The frame was tested as a fixed base structure connected directly to the shaking table platform. The frame was also tested as base isolated structure with FPS only and as base isolated structure with both FPS and supplemental fluid dampers at the level of isolation. In the two cases of base isolated configurations, the frame was connected to a rigid plate resting on four FPS isolation bearings under each column without fluid damper for the first case and with controllable fluid damper for the other case as shown in Figure 2.33b.

The study concluded that the supplemental damping within a base isolation system was useful in controlling the displacement responses of the frame under different earthquakes. In addition, the study recommended that for near field, pulse-like ground motions, the use of high level of damping may be detrimental for the superstructure's response. Furthermore, the numerical simulations showed that the adaptive isolation system was capable of limiting the displacement response of the isolation system and the superstructure simultaneously for both cases of near-field and far-field ground motions. The validity of the analytical models of the adaptive isolation system was achieved by comparisons between the numerical simulations and the experimental test data.

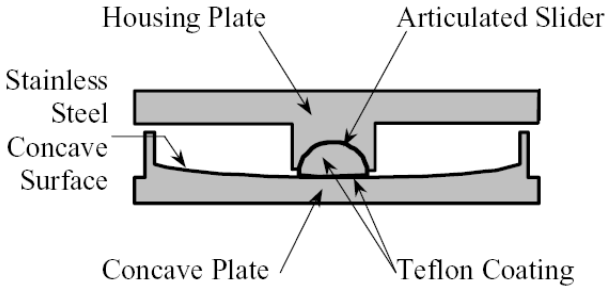

Figure 2.32 Cross section of Friction Pendulum System (FPS) bearing

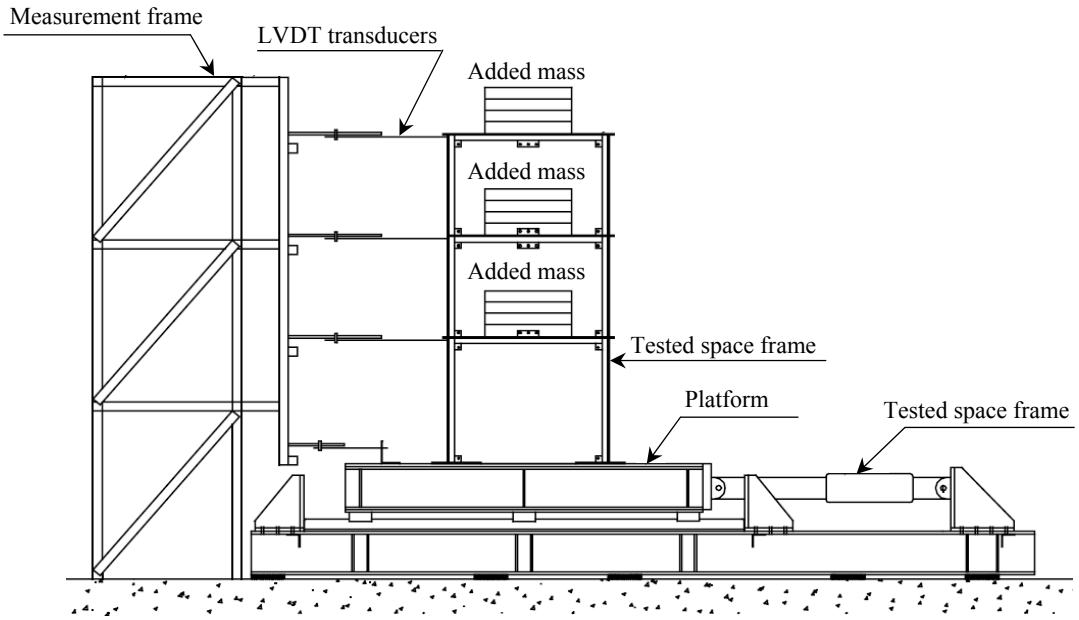

a. Experimental test setup of shaking table and tested frame space frame

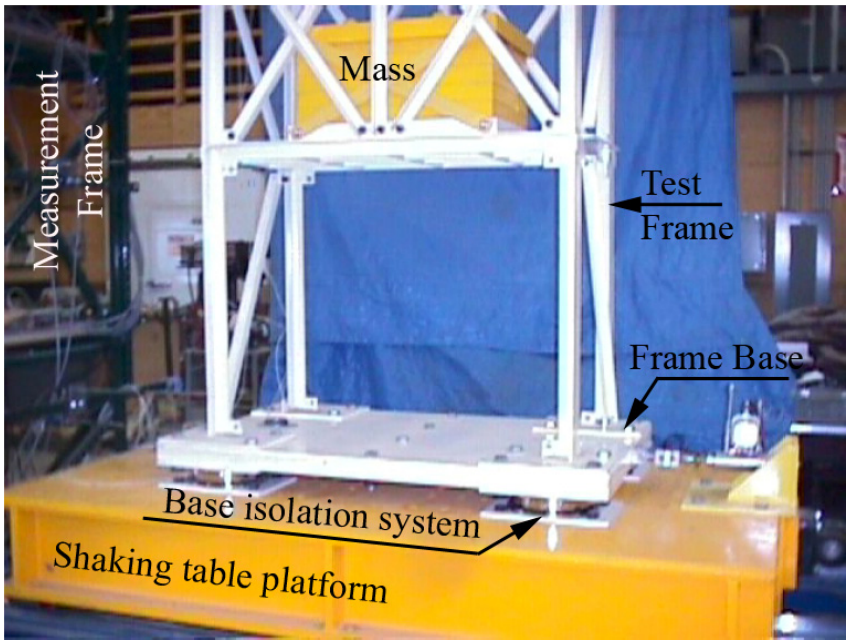

b. Tested frame connected to rigid basemat resting on base isolation bearings

Figure 2.33 Experimental test setup with base isolation system (Madden *et al*, 2000)

2.6 Summary

This chapter presented a brief discussion for the behaviour of space structures under both static and dynamic loading conditions. The discussion on static behaviour concentrated on the common points of weakness of space structures such as the progressive collapse behaviour due to buckling of one or more critical members, sensitivity of space structures to member loss, sensitivity to member and support imperfections and the sensitivity to lack of fit. The review also covered the common techniques proposed by previous research to improve the static behaviour of space structures such as over/under design of chord members, pre-stressing by lack of fit, diagonal removal, the use of eccentric diagonals and the use of force limiting device (FLD) to control maximum force in members. Composite action with a top continuum was also covered as the most important technique to improve space structure behaviour and reliability.

The dynamic behaviour of space structures was introduced including the latest techniques proposed to predict the dynamic response in addition to the effect of joint stiffness on structural behaviour. The effects of sudden member failure and geometric and material non-linearities on the dynamic response of space structures were also discussed.

The discussion further included the techniques used to improve the dynamic behaviour of space structures. The main aim of the techniques was to reduce the sensitivity of this type of structure to dynamic excitations such as those induced by working vibrations, wind pressure or earthquake ground motions. The techniques included the use of special dampers, implemented in the structures as additional elements or replacing one of the structure's elements. The other technique introduced was by using base isolation systems to isolate the structure from earthquake ground motions and keep the response

of the structure within an acceptable level for economical design purposes.

While the use of a deck to work compositely with upper chord members was highly efficient in improving the static behaviour of space structures, the dynamic behaviour of composite space structures received little attention. The increases in the overall structural stiffness and mass caused by the introduction of composite action are significant. These changes in structural characteristics are associated by an increase in friction between the deck and the joints of space frames leading to changes in overall damping and frequencies of the structure.

To the author's knowledge, no previous work considered the effect of composite action on the dynamic characteristics of space structures or the changes brought to their behaviour under dynamic loads. This gap in knowledge will be addressed in this research.

CHAPTER 3

RESEARCH METHODOLOGY

3.1 Introduction

This chapter presents the procedures applied to achieve the aims of current study. It focuses on the steps followed to study the effect of composite action on the dynamic characteristics and behaviour of double-layer space frame structures. Description of the experimental programme and the test procedures are introduced in addition to details of instrumentation used and the manufacturing steps of models. The chapter also presents an introduction to the numerical models used in a finite element parametric study carried out later to develop a valid model capable of predicting the behaviour of composite and non-composite space structures.

3.2 Experimental programme

An experimental programme was planned to achieve the goals of current study. The programme included manufacturing and testing three double-layer space frame models. The first model, Truss A, was a non-composite model that did not have upper deck. Concentrated load masses were added to this model by connecting lead masses to upper joints. The main purpose of the lumped masses was to make up for dead loads in large scale structures concentrated at top joints. On the other hand, composite models Truss B and Truss C had aluminium and timber decks, respectively, connected to the models in such a way to achieve full composite action. Decks were connected to the upper joints where the lead masses were also attached. Two support configurations were adopted including those with corner and two-edge supports at the lower chord level. Several experiments were carried out to determine the dynamic characteristics of the three

models.

The programme also included the design and construction of a shaking table that was used to study the dynamic behaviour of models under shaking table time history, see Chapter 4.

3.3 Manufacturing of physical models

All models were double-layer square on square offset (SOS) with overall dimensions of 1400× 1400×150 mm as shown in Figure 3.1. All models were made of solid aluminium round bars of diameter 4.0 mm for diagonal and lower chord members and 5.0 mm for upper chord members. These sizes were chosen according to many factors such as the design requirements, the availability of material and to ease the manufacturing process. The use of aluminium material made it easier to manufacture the components and assemble the truss models. The manufacturing steps for every component type are presented briefly in the following sections.

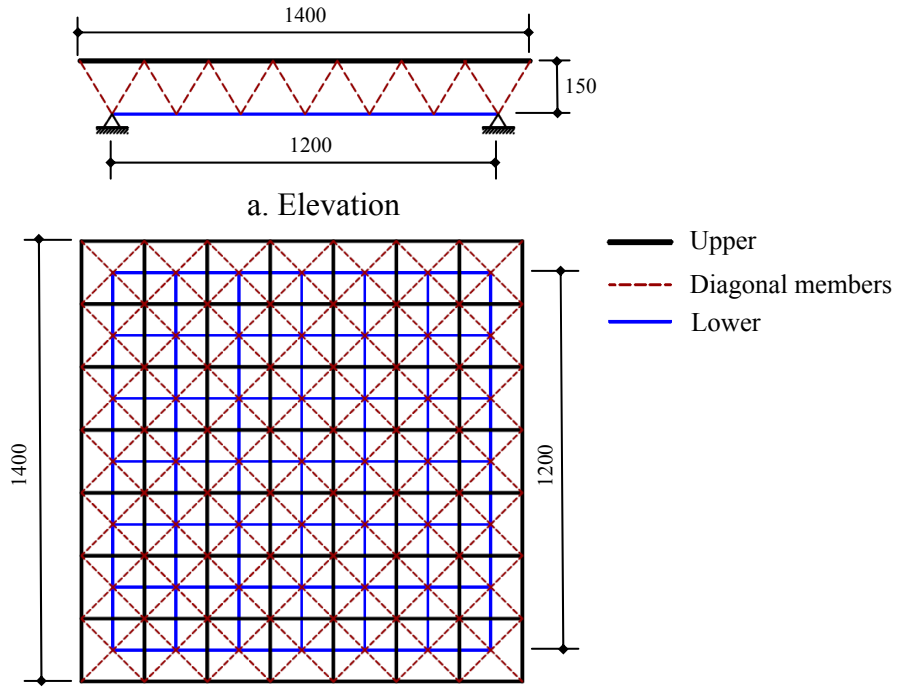

Figure 3.1 Layout of test model without deck

3.3.1 Manufacturing of upper and lower chords

The upper chord members formed a group of round aluminium bars intersecting to form a 7×7 square grid of 200×200 mm square units. The lower chord had a smaller grid with 6×6 panels with the same dimension as upper. Upper chord members were continuous with diameter of 5mm and total length of 1500mm leaving 50mm at each end for attachment of measurement devices. Similarly the lower chord members had a 4 mm diameter and total length of 1300mm. Both sets of members were flattened and punched at each point of intersection to allow for connection with other chord and diagonal members. A special tool was designed to stamp the bars every 200mm (Figure 3.2). This tool consisted of 2 parts; one to be put above the member at the point of the stamp and the other under the member. The tool was designed to be fixed in a manual compressing machine (Flightpress machine) that can apply high pressure on the bar to be stamped. The upper part was designed to allow a smooth section transformation from circular section with diameter of 5 or 4mm to flat section with 2mm thickness. The angle of transformation used was 15 degrees beyond the 10mm flat part. For upper members, the stamping was carried out from one side so that the composite deck can be fixed without having direct contact with either the members or the concentrated joint masses to simulate the connection with cladding in full scale structures.

After stamping the chord members, locations of connection holes were marked and centred precisely using a punching tool. The members were then moved to a stand drill with 3.0 mm bit to drill holes at the marked points. The final shape of a chord member at a typical joint is shown in Figure 3.3.

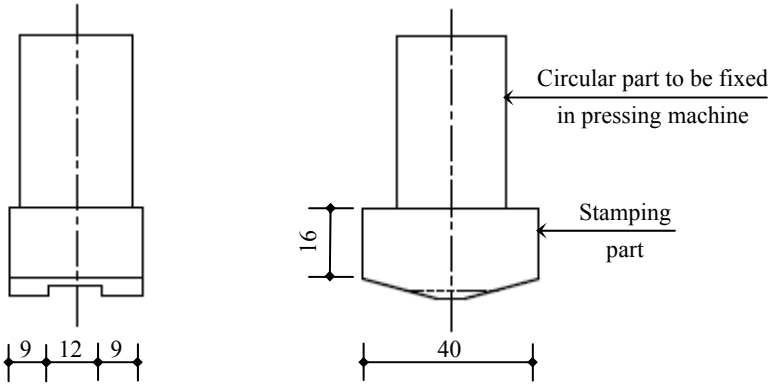

a. Upper part of stamping tool to be fitted in pressing machine jaws

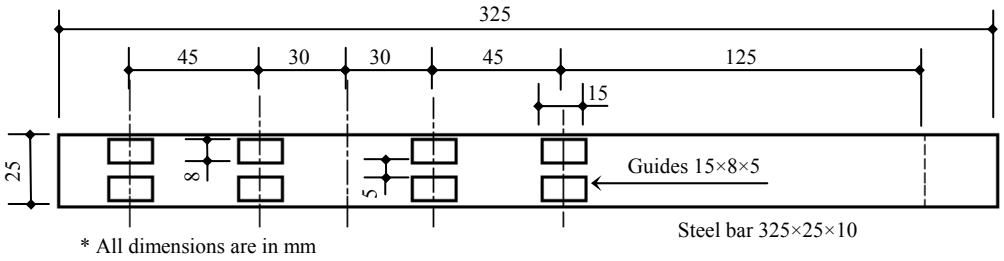

b. Plan of lower piece of the tool used for chord member stamping

Figure 3.2 Details of the tool used in stamping chord members

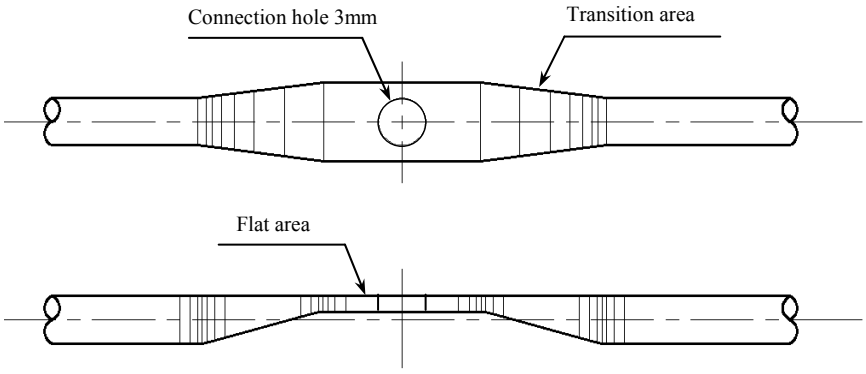

Figure 3.3 A chord member after stamping

3.3.2 Manufacturing of diagonal members

Manufacturing of diagonal members was a laborious process as they involved several steps. It started with cutting the members to length and bending their ends at marked points while allowing enough space for stamping the ends and making connection holes. For this purpose, a special tool to bend the member to a specific angle was designed and manufactured (Figure 3.4). The tool had a space for holding the member in place between two fixed pieces of metal (guides). A lever hinged at its end was moved manually to bend a member around one of the filleted corners of the fixed pieces while clamping the member end to stop the member from sliding. The member manufacturing steps can be summarised as follows:

1. Cutting member to length.
2. Marking the points of bending.
3. Bending the members using the bespoke bending tool seen in Figure 3.4.
4. Stamping the member ends with another tool made of two steel components, each having a 1mm thick groove. The groove ended with an inclined surface to allow for a smooth transition of the section from a round bar to a flat part (Figure 3.5).
5. Points were marked to identify the hole centre at one end using a punching tool.
6. Holes were drilled at the pre-marked points using a stand drill.
7. Members were fixed to a special right angle with a bolt fixed to the angle at one end. The main purpose of the angle was to ensure the accurate marking of the hole location at the other end of member (Figure 3.6).
8. An overhead drill was used to drill holes at the marked locations.

Steps 1 through 8 are demonstrated in Figure 3.7 from a to f, respectively.

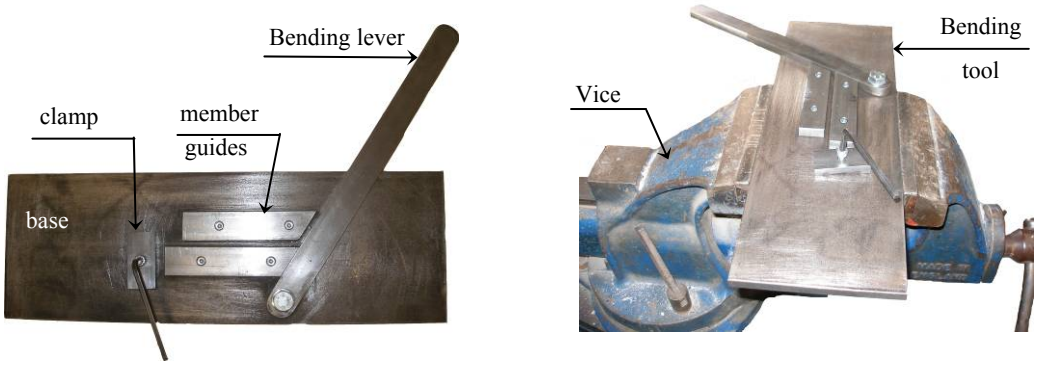

a. Details of bending tool b. Bending tool fixed to a vice

Figure 3.4 Tool used to bend the ends of diagonal members to a predetermined angle

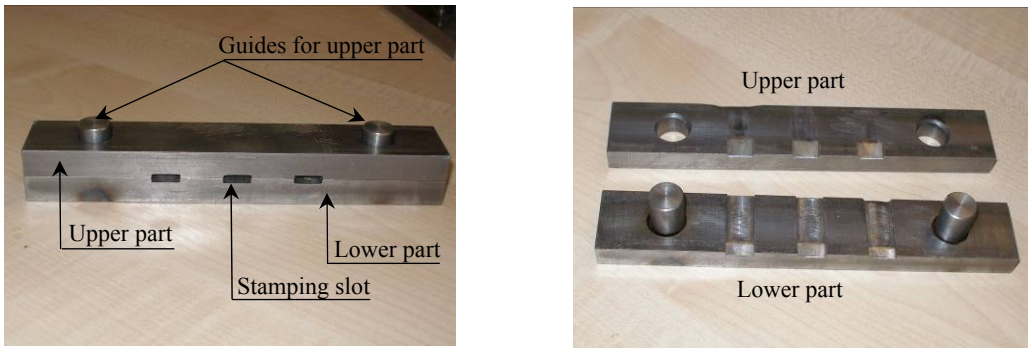

a. Complete overview of stamping tool b. Details of the diagonal stamping tool

Figure 3.5 Stamping tool used to stamp the ends of diagonal members

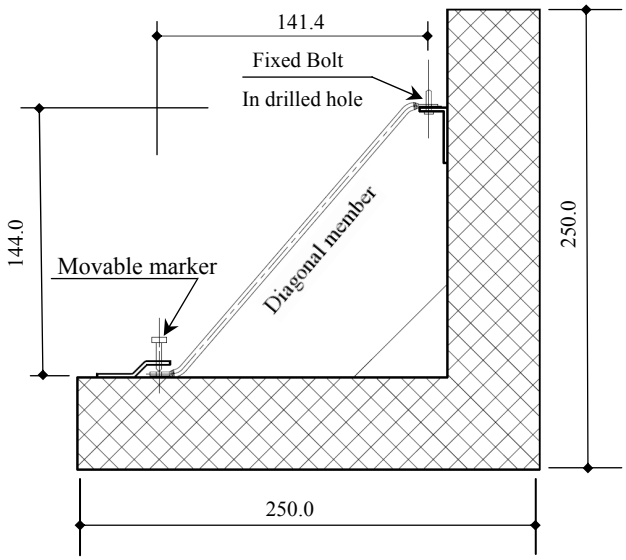

Figure 3.6 Angle frame used to mark hole locations at the ends of diagonal members

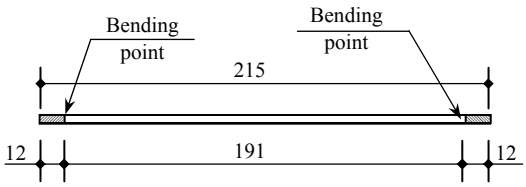

a. Marking the bending points

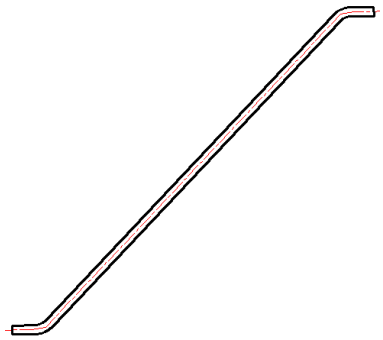

b. Bending the member ends

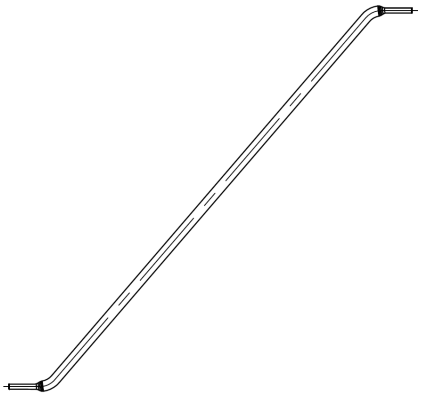

c. Stamping both ends of the member

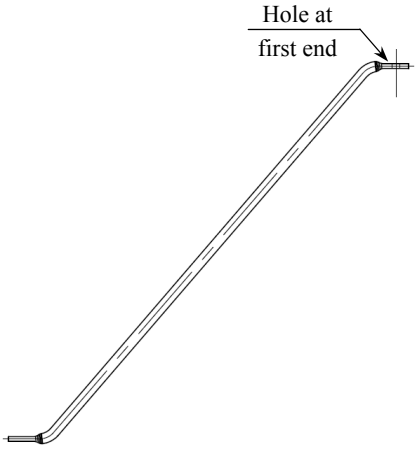

d. Drilling a hole at one end

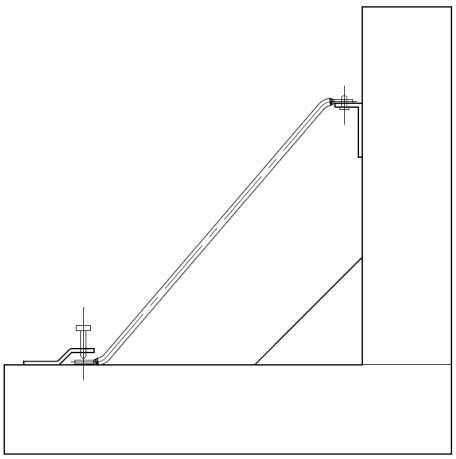

e. Marking the centre of hole at the other end

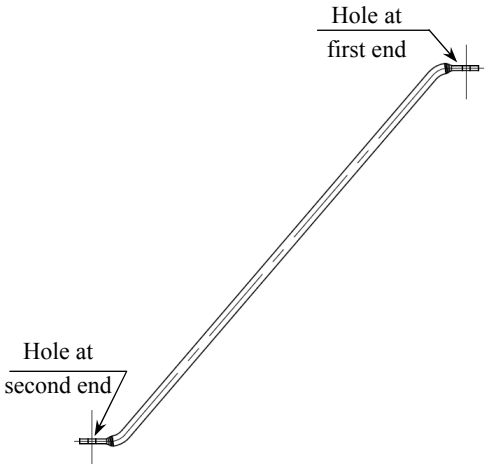

f. Drilling a hole in the other end

Figure 3.7 Manufacturing steps for diagonal members

3.3.3 Preparation and manufacturing of upper decks

To achieve composite action, two different deck types were prepared for both Trusses B and C. One of the decks, used in Truss B, was an aluminium sheet of 1.2mm thickness represented the aluminium sandwich panels commonly used in covering roof structures. The other deck was a timber plywood sheet with 4mm thickness to cover Truss C and represented the use of timber decks as floor systems in space structures. Aluminium and timber were used in the current research for the following purposes;

1. Both materials were commonly used in real structures. Aluminium deck exemplifies the aluminium sandwich panels while plywood deck exemplifies timber decks widely used as floor decks.

2. Each material had its unique static and dynamic characterises so that using them provided a reasonable range of material properties.

3. Both materials were widely used in previous research and showed promising results under static load conditions (Shabaan, 1997).

Each deck had an overall size of 1450×1450 mm, leaving 25mm at the edges to allow for bolts and masses fixation. Holes of 3mm diameter were drilled in the deck sheets at a spacing of 200 mm in each direction to enable connection to upper chord joints.

3.3.4 Concentrated lead masses

To simulate dead loads in actual structures, lead masses were fixed at every upper joint. Lead was selected due to its high specific weight (113.89 kN/m^3), which allowed the use of small mass sizes. Masses were made of 60mm diameter cylinders of lead 42mm thickness and a mass of 1.35 kg.

Grooves were stamped in masses using the stamping tool shown in Figure 3.8. The

grooves were required to enable a concentric connection with upper joints, a feature that simplified the numerical simulation of models as will be discussed later in this chapter.

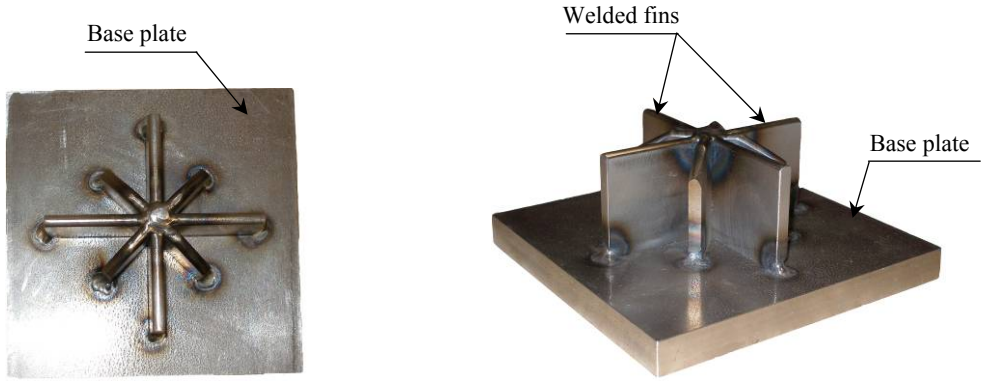

a. Top view b. Isometric view

Figure 3.8 Stamping tool used for having grooves in lead masses

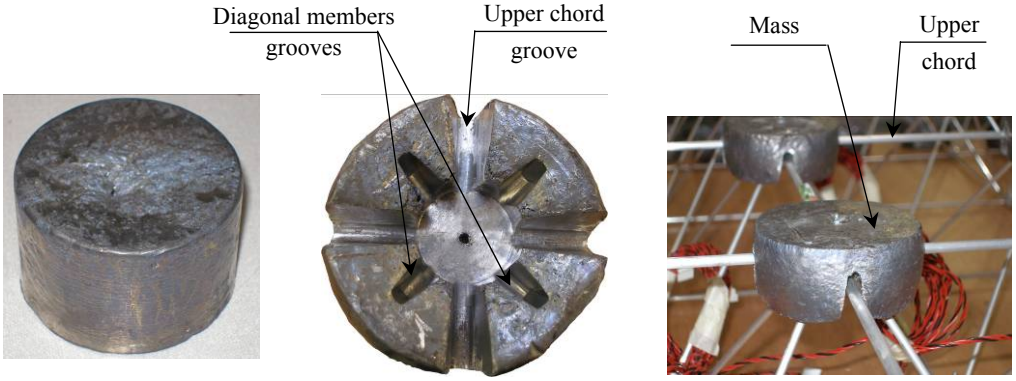

a. Mass before stamping b. Mass after stamping c. Mass fixed at top joint

Figure 3.9 Lead masses before and after stamping

3.4 Assembly of space frame models

Each joint contained four diagonal members and two continuous chord members. One bolt of diameter 2.8mm was used to go through all members meeting at the joint. Bolts in upper joints had extra length over the lower layer to connect both the deck and the lead masses. The nuts were fixed above the connection in upper joints to keep the lead

masses or decks apart from the upper chord members and to avoid direct contact. Another nut was used above the masses to fix them to upper joints. Figures 3.10 and 3.11 show typical views of lower and upper joints of Truss A with and without lead masses in addition to an overall view of the model.

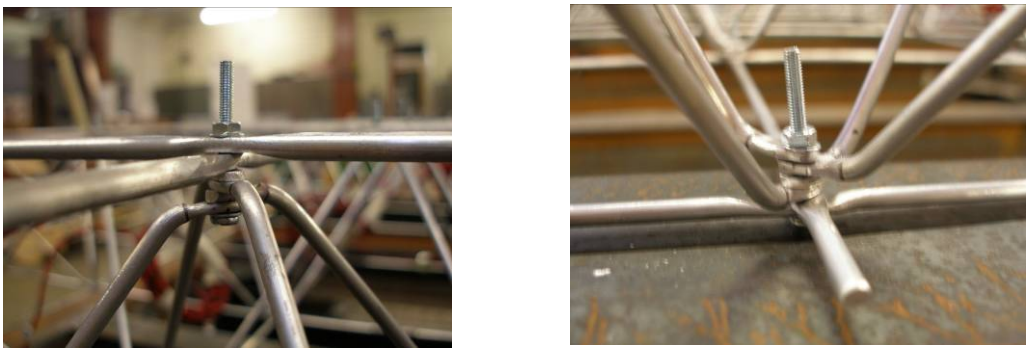

a. Typical view of upper joint b. Typical view of lower joint

Figure 3.10 Typical views for assembled model joints

Figure 3.11 Overall view of Truss A with masses

3.5 Setup of test rig

3.5.1 Support frame

The shaking table platform (described in detail in chapter 4) was used as a support frame in addition to two beams fixed over the platform in all tests. The two beams were

fixed over the platform to give a space for connections, testing tools and measuring devices. Models were fixed to this frame using 4 bolts in case of corner-supported models and multiple bolts spaced at 200mm along the two edges in case of two-edge-supported models.

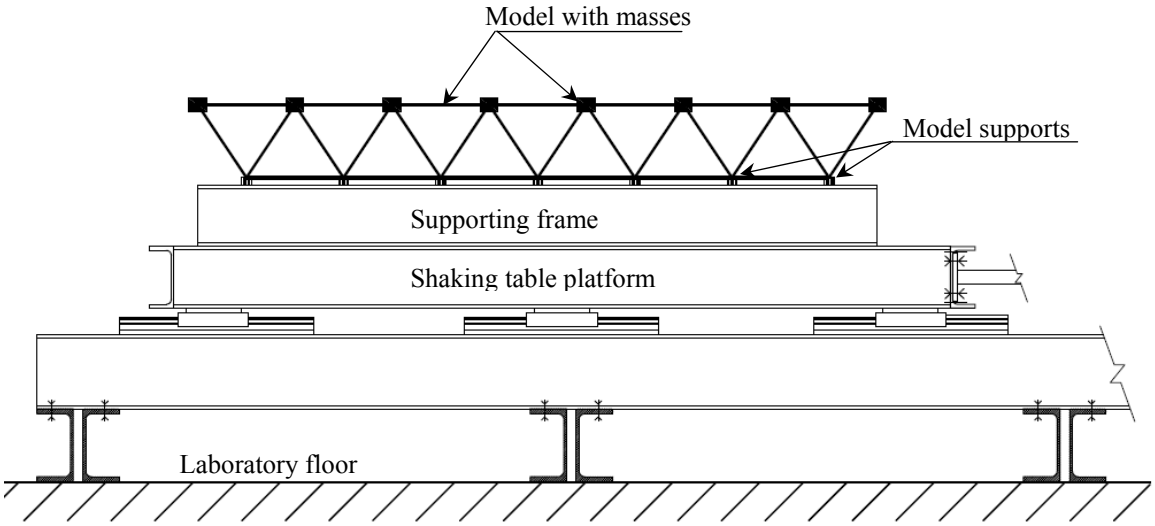

Figure 3.12 One of the physical models fixed on supporting frame

3.5.2 Loading arrangements

All models were loaded by lead masses at the upper joints. When a deck was part of the upper chord, the masses were inverted and fixed over the deck using the same bolts connecting the upper joints (Figure 3.13).

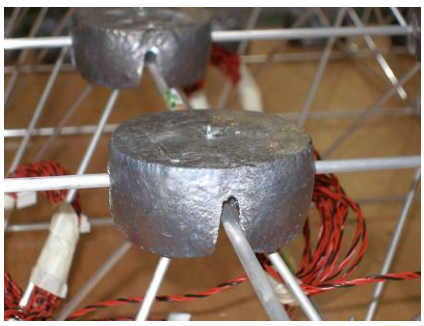

a. Concentric masses at upper joints

b. Mass fixed over aluminium deck

Figure 3.13 Upper joint loads in case of composite and non-composite models

3.5.3 Model supports

Special cylinders were used at model supports. The cylinders had a hole of 3mm diameter so edge joint bolts could go through them to connect the truss to the supporting beams (Figure 3.14).

Figure 3.14 Model support on test rig

3.6 Instrumentation

The models' response to initial displacement tests and base motion excitation loads was measured to determine the natural frequencies in the vertical and horizontal vibration modes (and other aspects of behaviour) of models. The response included the vertical and horizontal joint displacement and member strains. Three LVDT (Linear Variable Differential Transformer) transducers of 10mm stroke were used to monitor the horizontal responses. Two of these transducers were fixed at the two middle edge joints of the upper chord (Figure 3.15). The third transducer was fixed at one of the supports to monitor any support movements or slippage during tests. All transducers were of self rebound types and were also glued to measurement points to keep well contact during the tests. All three transducers were fixed to a rigid frame which was firmly fixed to the shaking table platform (Figure 3.15). Another LVDT transducer of the same specifications was fixed vertically at the middle joint of the lower chords grid to

monitor the vertical vibration of models during the vertical snap test.

It is worth mentioning herein that the natural vibration frequencies in vertical and horizontal vibration modes will be briefly described as vertical and horizontal vibration frequencies in the rest of the thesis.

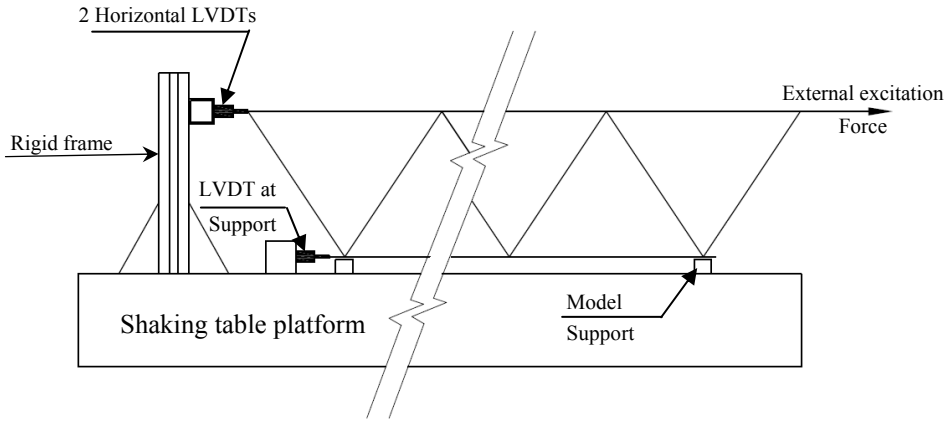

Figure 3.15 Test setup for monitoring the horizontal displacement at three model joints

Due to the limitation of the number of channels available in the data acquisition system, only 12 channels were chosen for strain gauges and 4 channels for LVDT transducers. Longitudinal, transverse and diagonal symmetry of models allowed concentration on one eighth of the members as shown in Fig.3.16. Two further members in other model locations were equipped with strain gauges to assess the assumption of symmetry. Another group of strain gauges were glued to other members waiting to be used when changing the truss aspect ratio specially those used to check symmetry of behaviour (Figure 3.16).

A 16 channel data acquisition system (Microlink 770 + Microlink 594 Unit) was used. This system was connected to a computer through USB port with a high sampling rate of 100 kSample/sec. The system was originally designed to measure strains only in a quarter bridge arrangements. Two modifications were carried out by the author to the system. The first modification was necessary to make at least 4 channels capable of

monitoring LVDT transducers output, which was achieved by removing resistors forming the quarter bridge and connecting the output of LVDT directly to the input of the system where measurements ranged between ± 10.25 volts. The other modification aimed to increase the accuracy of the system in reading strains, because of the low accuracy of the system in measuring strains, which was ± 80 μ strains in quarter bridge connectivity. The accuracy was obtained by recording the average strain readings for the system under no external changes in loading conditions for the models. The second modification was achieved by removing one of the resistors for each channel and changing resistors connectivity arrangement to work in half bridge style. Removed resistors were replaced by dummy strain gauges, similar to those used with the model, glued to bars of aluminium with the same size of model members. The modified system was able to reduce noise caused by the difference in temperature and electrical waves in the laboratory from other devices.

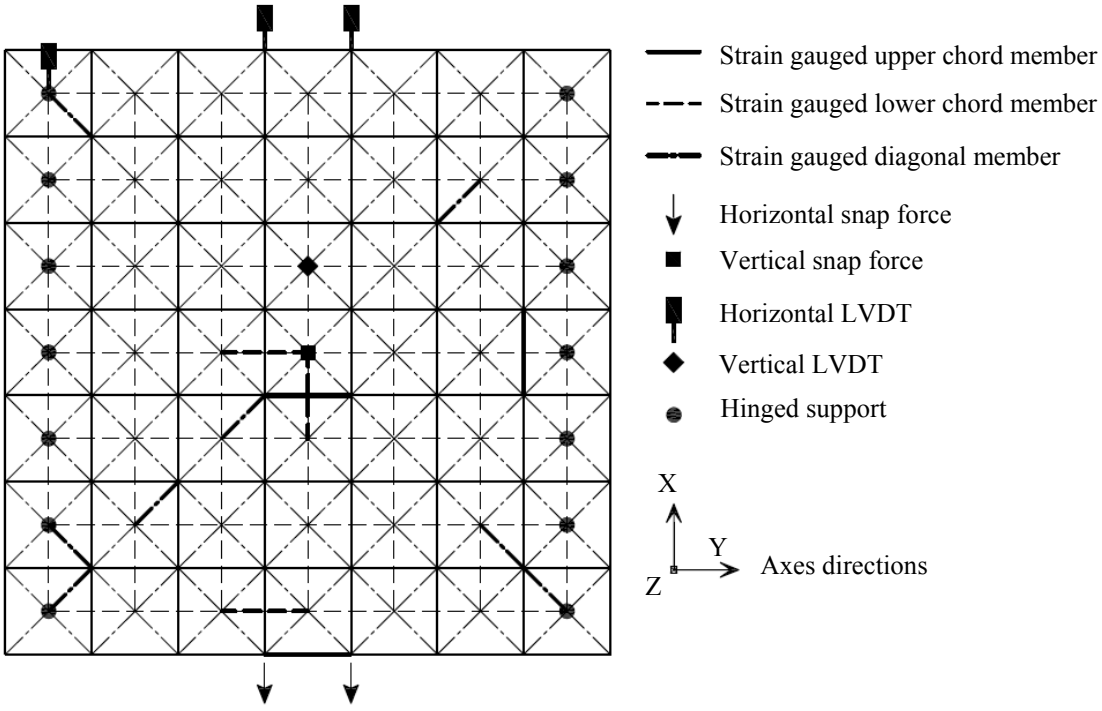

Figure 3.16 Layout of a model showing locations of strain gauges and LVDT transducers

The accuracy of the system after modification was ± 6 μstrain, which was competitive to other commercial systems. Furthermore, the accuracy of the system in measuring displacements reached ± 3 mV, which meant reducing the error margin to ± 0.003 mm when using LVDT with 10 mm range.

3.7 Data filtering and noise reduction

3.7.1 Precautions taken to avoid measurement noise

Responses of models were quite small, so special care was necessary to reduce the noise during sampling. All wires were shielded from external magnetic fields. Thermal effects due to continuous current passing through strain gauges were avoided by using a half bridge technique involving dummy strain gauge glued to a bar of aluminium with the same size as that of members.

To avoid the noise caused by the inertia force of LVDT transducers' cores, rebound transducers were used. The measurement ends of the transducers were glued to the points of interest on the models to avoid any separation during vibration or snap tests.

3.7.2 Techniques used after tests to filter noise in data

To have a higher sensitivity of responses, the sampling rate during all tests was selected to be 1000 Sample/sec. This high rate gave the opportunity to use two techniques to filter the output signals to reduce the noise in recorded data. The unavailability of automatic filtering in the used data acquisition system pushed the need to use separate filtering techniques.

I. Data filtering by an averaging technique

An averaging technique for a number of successive data samples was used over a period of 0.009 sec. This meant that the step average included 9 samples of successive

readings. This technique was found to be sufficient when assessing the operation of the shaking table displacement responses as the readings in this case were relatively high compared to the noise level. The filtering technique was considered a simple FIR (Finite Impulse Response) system of the ninth order and can be called a Nine-Term Average Filter, Equation 3.1.

$$y_n = \frac{x_{n-4} + x_{n-3} + x_{n-2} + x_{n-1} + x_n + x_{n+1} + x_{n+2} + x_{n+3} + x_{n+4}}{9} \qquad (3.1)$$

where y_n is the average reading after 9 samples, x_n is the reading at time t_n.

II. Data filtering using Fast Fourier Transformation technique

This technique depended on the Fast Fourier Transformation (FFT) method to filter the recorded strain signals. A MATLAB program developed by the author to read the strain signals and to remove the noise caused by the laboratory electric waves due to nearby electric wires and power supplies to all connected devices. The vibration of the sliding table platform was another noise source. This vibration resulted in local vibrations in models' elements producing a noticeable noise in readings specially that this vibration was mainly bending in nature creating larger strains compared to those due to axial forces. This filter was considered a low pass filter as it allowed signals with low frequency to pass, while high-frequency signals were eliminated.

The basic theory behind this technique depends on converting recorded strain signals from time domain to frequency domain using FFT. Frequencies higher than 45 Hz, which was just below the frequency of electric supply with 50 Hz, were truncated. After the completion of noise removal, inversed FFT technique was used to covert data back from frequency domain to time domain for comparison purposes. The MATLAB computer code for filtering data using FFT technique is listed below:

```
**********************************************************************
% Reading the original data from file and plotting it [Time-Domain]
%**********************************************************************
clc
clear all
File=input('Enter Data File Name     :','s')
data=load (File);                          % Copy Data from file to a temp. Matrix data
time=data(:,1);                            % Reading time vector data
T=time(5)-time(4);                         % Periodic Time
strs=data(:,[2:end]);                      % Response vector (Strain [Data from 10 strain
Gauges]) )
[r c]=size (strs)                           % Finding Data matrix size [rows columns]
%D=length (time)                           % Finding the length of data vector
hold on
subplot(2,1,1);
plot(2,1,time,strs(:,1),'r');              % Plotting original data
Ulimit=max(strs(:,1))+5
Mlimit=-1*max(strs(:,1))-5
axis([0 time(r) Mlimit Ulimit])
grid
title('Vibration Test Strains')
xlabel('Time')
ylabel('Mico-Strain')

%% ************************************************************
% Carry out FFT for Data Obtained from Input File
%** ************************************************************
Z=2^nextpow2(r)            % Next power of 2 from length of DATA
Y = fft(strs,Z);               % Carry out FFT for a Z number of vector [delta] data
%% ************************************************************
% Selecting the unwanted noise frequencies to be filtered [Frequency-Domain]
%************************************************************
rmin= input('Enter lower range of frequencies to be Omitted      :')
```

```
rmax=input('Enter upper range of frequencies to be Omitted      :')
R=zeros(Z,c);
xmin=floor(rmin*Z*T+1.5);
xmax=floor(rmax*Z*T);
for i=1:(Z/2 )
for j=1:c
   if i< xmin || i> xmax
      R(i,j)=Y(i,j);
   else
      R(i,j)=0;
   end
end
end
%Second part of Data (inversed as it is the second half (negative part)
xmin2=floor(Z-(rmin*Z*T+1.5)+2);
for i=((Z/2)+1 ):Z;
   for j=1:c
      if i<xmin2;
      R(i,j)=0;
      else
      R(i,j)=Y(i,j);
      end
   end
end
%% ************************************************************
% Carrying out Inverse FFT on the rest of filtered frequencies → time domain
%************************************************************
FR=ifft(R);                %Inverse on filtered(R)
fin=real(FR);              %find the real values of inversed(R) at it is in imaginary case
%%************************************************************
% plotting the final results Time-Domain
%************************************************************
hold on
```

```
subplot(2,1,2);plot(2,2,time(1:r),fin(1:r))
%plot(time(1:D),fin(1:D))
axis([0 time(r) Mlimit Ulimit])
grid
title('Filtered Vibration Test Strains ')
xlabel('Time')
ylabel('Mico-Strain')
dd=[time(1:r),fin(1:r,1:c)];
%%
g=13-(c+1);
if g>0;
   df=zeros(r,g);
   ds=[dd df];
else
   ds=dd;
end;
%% ************************************************************
% Saving output results to file (Time-Domain).
%************************************************************
Outf=input('Enter Output File Name   :','s')
fid = fopen(Outf, 'wt');
fprintf(fid,'%6.4f  %12.4f %12.4f %12.4f %12.4f %12.4f %12.4f %12.4f %12.4f %12.4f
%12.4f %12.4f\n',ds');
fclose(fid);
hold off
```

The developed program could efficiently remove noise of any frequency within any favourable limit which can be fed to the program as input during program execution.

Figure 3.17 shows one of the channel readings of strain gauge before and after filtering process.

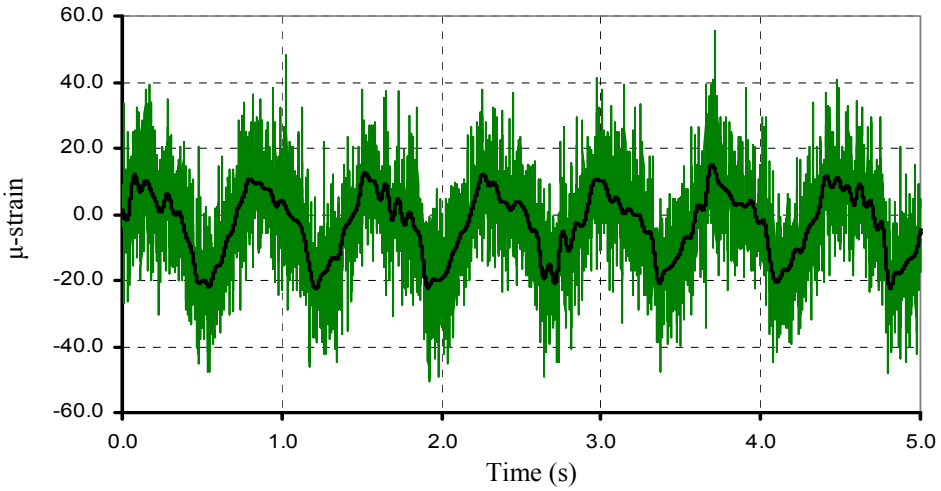

Figure 3.17 Strain readings before and after applying the FFT filter

As shown from the Figure 3.17, the filtering process was successful in eliminating noise coming from different sources.

3.8 Test procedure

A large number of tests were carried out on models to determine their vertical and horizontal natural frequencies. Measurements included the lateral displacement and strain at several model locations. The models included one non-composite and two composite space frames; all tested with different aspect ratios and boundary conditions. Layout and details of testing programme is shown in Figure 3.18. The test procedures are presented in the following sections.

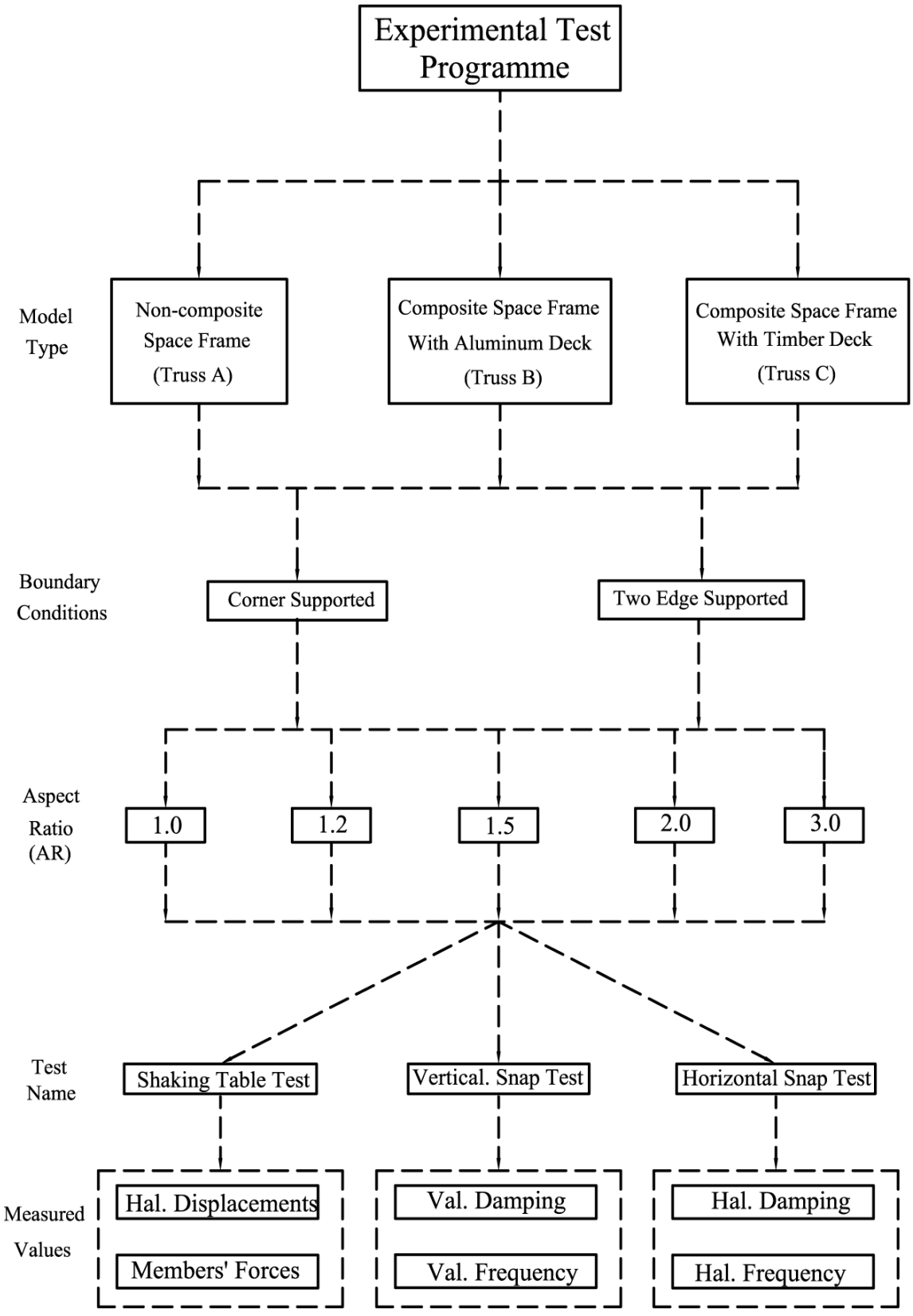

Hal. : Horizontal Val.: Vertical

Figure 3. 18 Details of experimental programme

3.8.1 Vertical snap test

This test was conducted to measure the vertical natural frequency of models by initial displacement method (Snap test). The test involved applying a vertical load to the middle joint of the lower grid and releasing this load suddenly. To apply the load, a special load arrangement and release mechanism was as shown in Figure 3.19. A wire with high tensile capacity was used to transfer a horizontal load through guides fixed to the platform to the middle point of the model. Another wire was connected to a steel hanger carrying variable weights. Each one of the two wires ended with a ring. A piece of rope was used to join the two rings. To snap the load instantly, a sharp blade was used to cut the rope. The resulting model vibrations were recorded using a high resolution vertical transducer connected to the data acquisition system and a high sampling rate of 1000 Sample/sec was used.

All tests were repeated four times and the average of the closest three frequencies were obtained. This test was repeated for all models to study the changes in vertical frequency and damping ratio caused by the introduction of composite action.

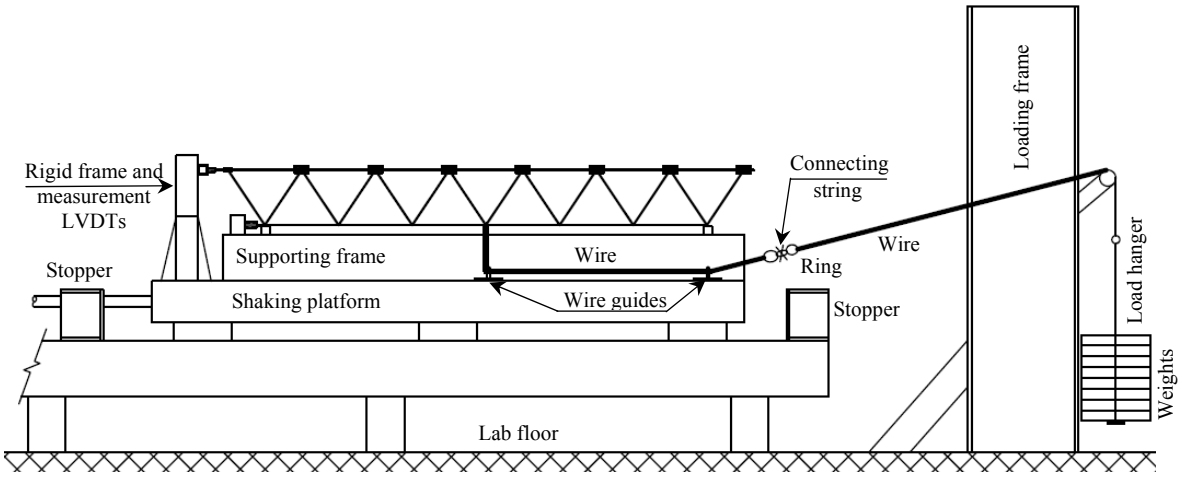

Figure 3.19 Test arrangements for vertical snaps tests

3.8.2 Horizontal snap test

This test was carried out to measure the natural frequency of the structure by applying a horizontal excitation load and removing it suddenly using test arrangements shown in Figure 3.20. The system was almost the same as that used for vertical snap tests except that there was a specially designed steel plate connected to the two longitudinal middle upper chords, Figure 3.20. The ends of the two middle members were stamped and two holes were drilled for connection to the steel plates. Bolts of 2.8 mm diameter were used to connect the members to the steel plate. These bolts worked in double shear to allow a large snap force to develop without shearing off.

A short piece of rope was used as before to connect between a hole in the loading steel plate and the ring at the end of the loading wire. A sharp blade was used to cut the rope to release the load suddenly. Two transducers were used at the other side of the model at the upper chord level. The aim of using two transducers was to check the symmetry of recorded data and to increase the accuracy of readings.

This test was repeated four times for every case, and the average of the closest three readings was determined. High sampling rate of 1000 Sample/sec was selected to capture the lateral vibration of the models.

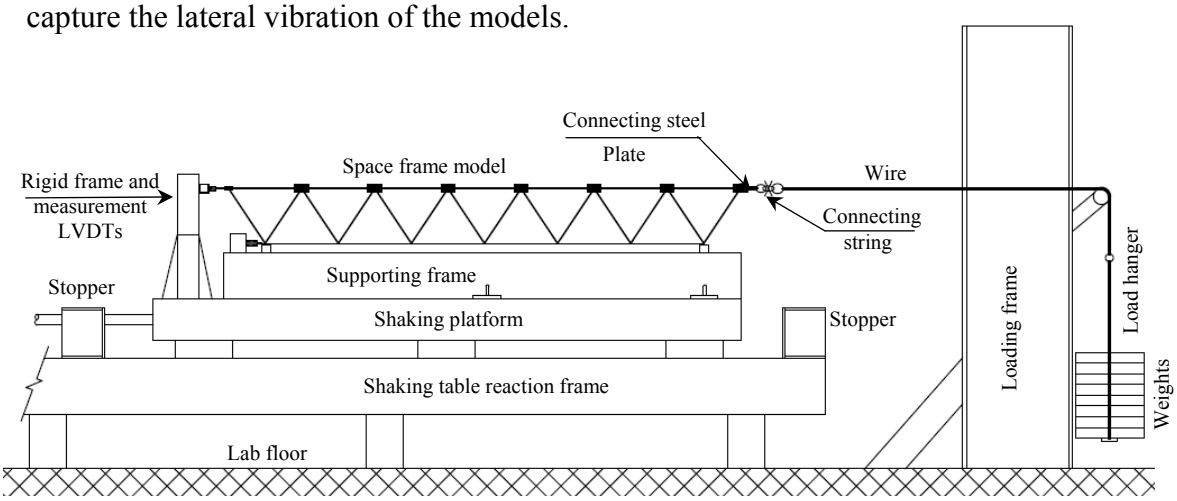

Figure 3.20 Test arrangements for horizontal snap test

3.8.3 Shaking table tests

The vibration tests were carried out on models using a specially designed shaking table (discussed in detail in Chapter 4). Readings were taken after 10 seconds of the steady the steady state vibrations.

The acceleration applied on tested models was 0.65 G which was strong enough to produce a clear deformation in models offering a chance for clear response comparisons. Vibration tests were repeated for all tested models and for different cases of aspect ratios and boundary conditions.

3.9 Tests of material and models' components

3.9.1 Introduction

Tests were carried out to determine the material properties of models' components. Special emphasis was given to the behaviour of members. The tests attempted to represent the actual member connectivity. They included upper chord members with different end connectivity and diagonal members with special devices designed to simulate the members' connection in the structure.

The results of these tests were used in simulating member behaviour in later finite element analyses, which used to extend the experimental study to include more parameters. The test procedures and the specimen details were selected according to ASTM A370-08A (standard test methods and definitions for mechanical testing of steel products, 2004)

3.9.2 Material tests

To find the modulus of elasticity, E, the yield strength, $F_{y,}$ and the ultimate strength, F_u, of aluminium, tension tests were carried out on 3 specimens. The net specimen length was 100 mm long. An extra length of 50 mm was added at each end to allow for the

testing machine grips. Details of specimen and the results obtained from the tension tests are presented in Figure 3.21.

On the other hand, three groups of tension tests were conducted on the two deck materials. The tests included those on the aluminium deck sheet and plywood timber sheet in both longitudinal and perpendicular fibre directions. Each group included three specimens and the average results are shown in Figures 3.22 and 3.23.

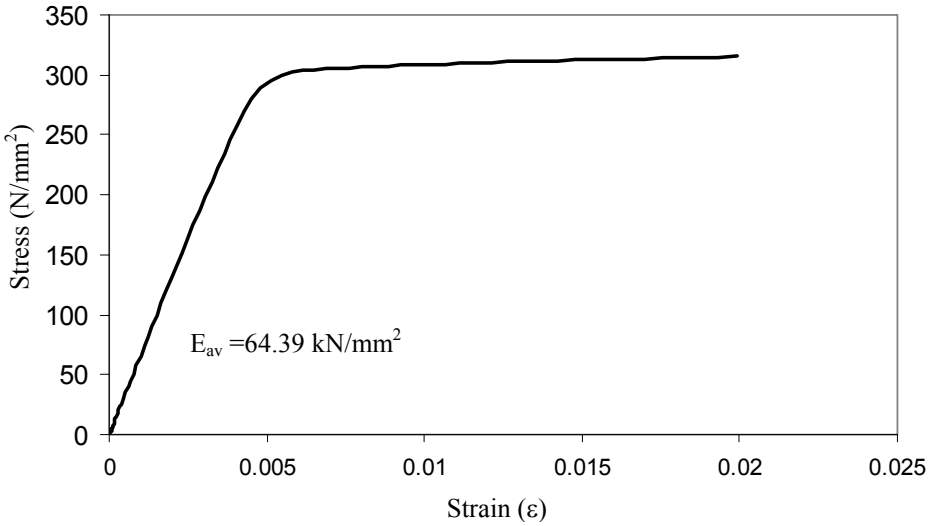

Figure 3.21 Stress-strain behaviour of the material used in models' members

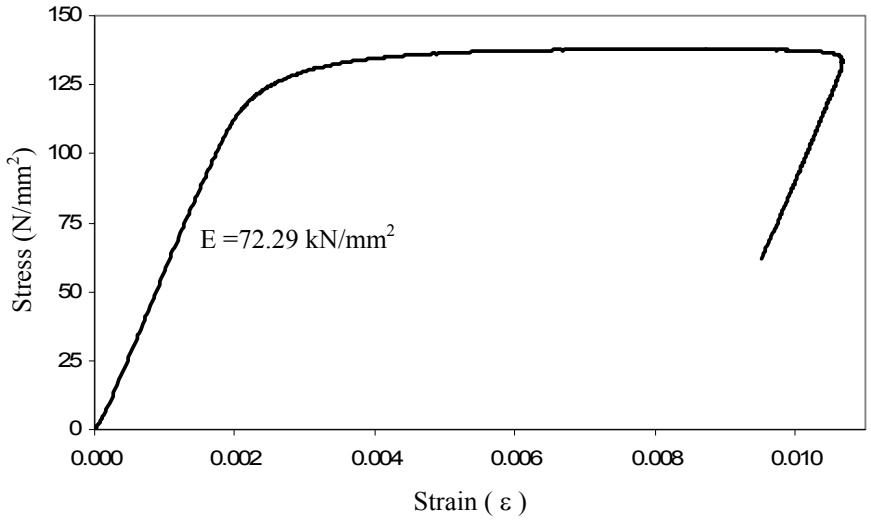

Figure 3.22 Stress-strain behaviour of aluminium deck

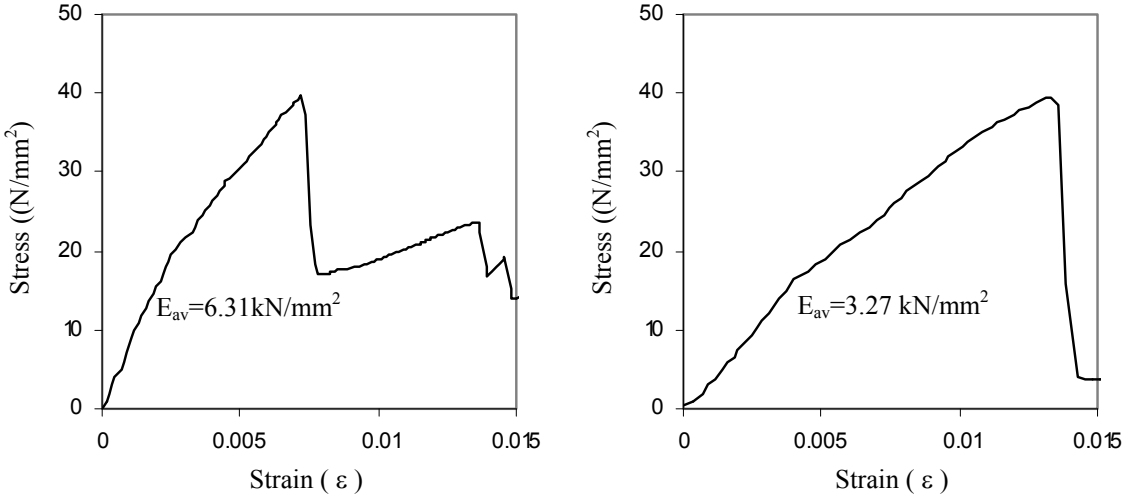

a. Longitudinal direction b. Cross direction

Figure 3.23 Stress-strain behaviour of timber

3.9.3 Top chord compression tests

The form of connection of upper chord members within the models meant that their ends were neither purely pinned nor fixed. The two extremes of members' boundary conditions were tested to obtain their behaviour and capacity in both cases, Figure 3.24.

Two sets of tests were conducted on three members with 5 mm diameter. Specimens were held between the testing machine grips while applying a compression load to simulate the fixed-fixed case with a net free length of 200 mm (Figure 3.24a). The other set of members were 200mm long and were prepared with spherical ends. Special parts were designed to hold the spherical ends by the testing machine grips (Figure 3.24b). Grease was used to reduce the friction at the member spherical ends. Figure 3.25 shows the average behaviour of both groups with the two end conditions considered.

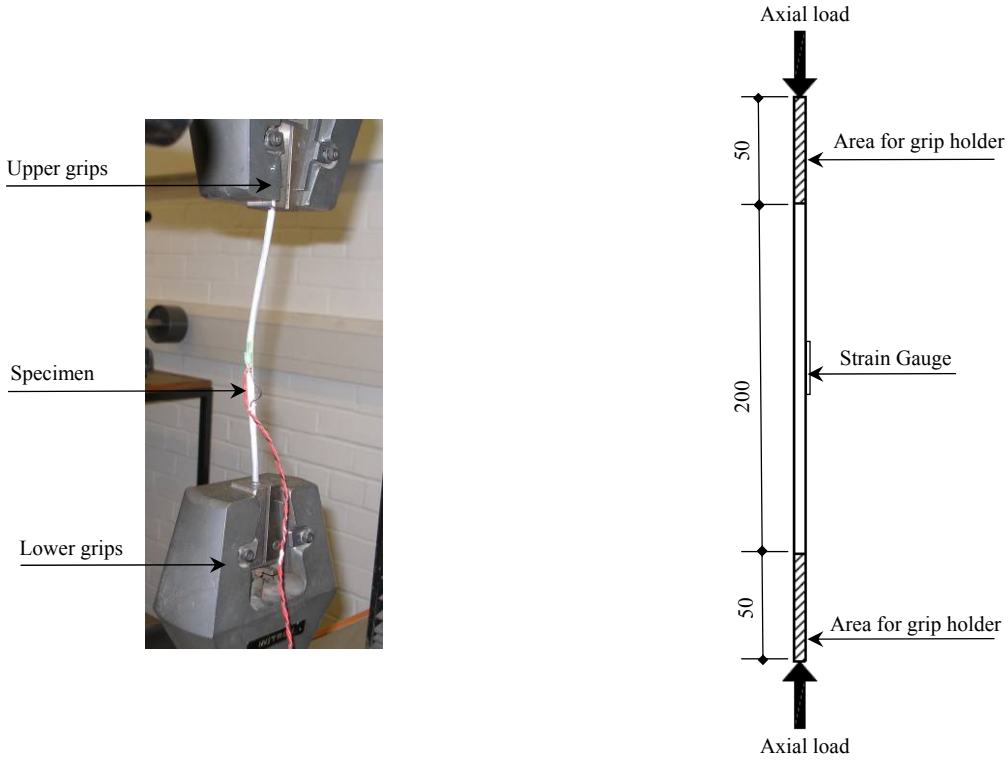

a. Fixed-ended member

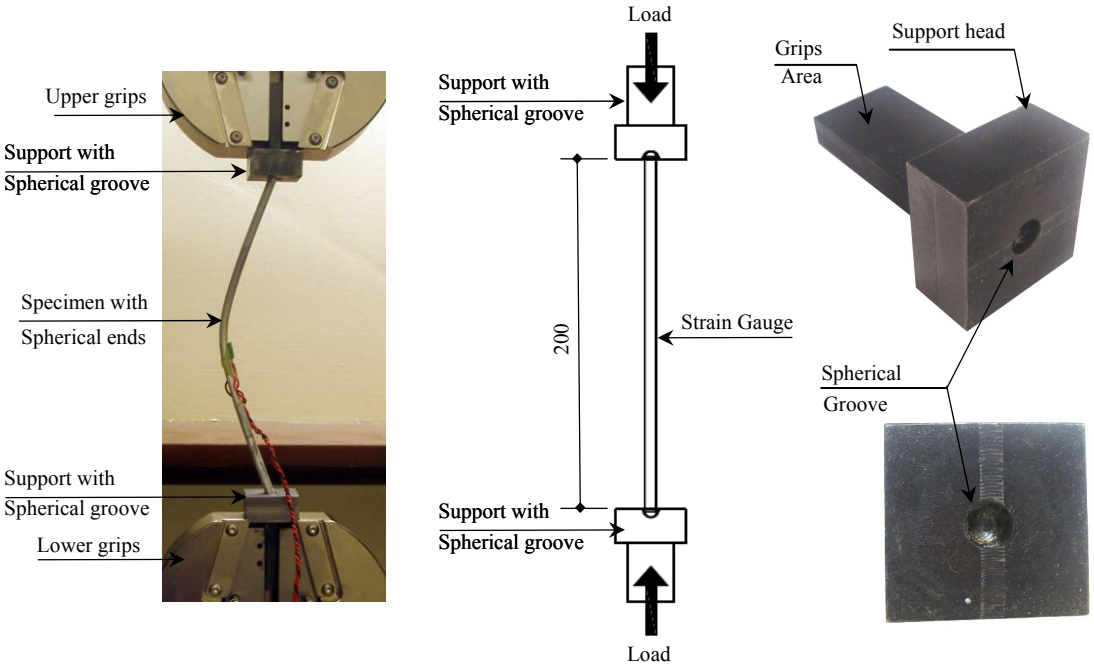

b. Pin-ended member

Figure 3.24 Compression tests of chord member

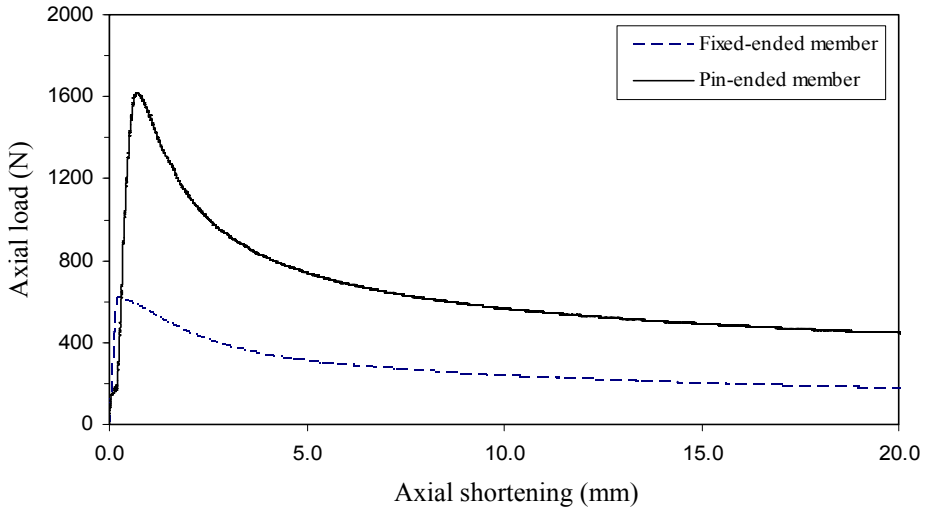

Figure 3.25 Results of axial compression tests on chord members

3.9.4 Diagonal member compression tests

Compression tests for a group of three specimens of diagonal members were conducted to determine the load carrying capacity and failure mode of these members. The specimens were taken from diagonal members similar to those used in building the models. A special support was manufactured to simulate the connection type at the ends of actual members (Figure 3.26).

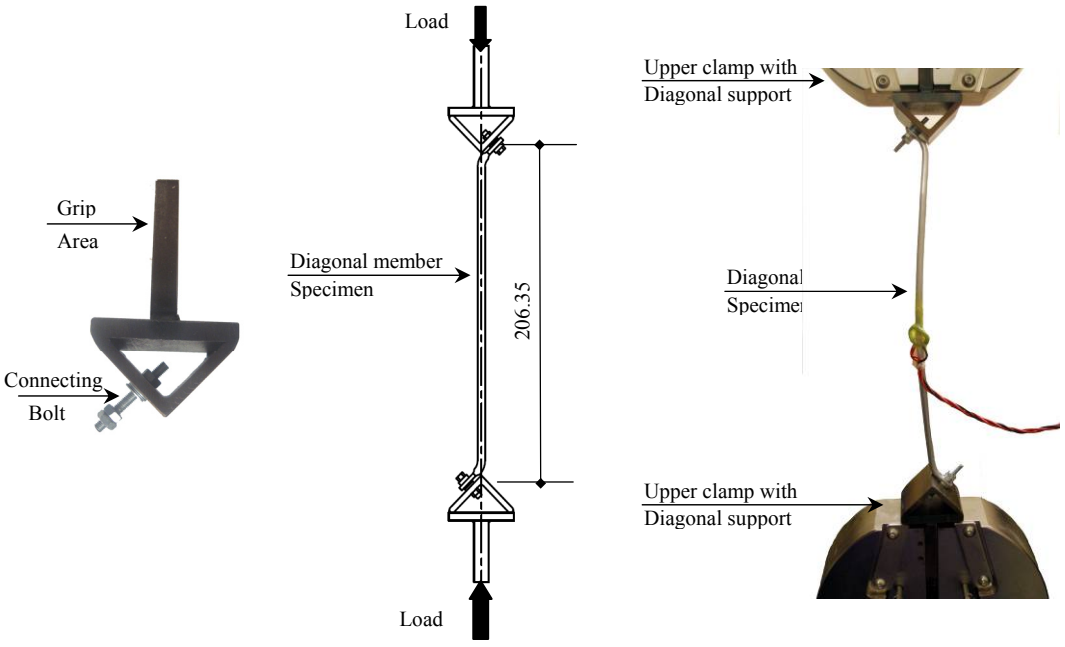

Figure 3.26 Test setup used to subject diagonal members to axial compression

Members underwent little deformation and showed linear behaviour until buckling took place as shown in Figure 3.27. The average critical load obtained from tests was 401.5 N which lies between the theoretical (Euler) buckling load for the two extreme cases of pin-ended and fixed-ended members with values of 187.5 N for the first and 750.2 N for the second.

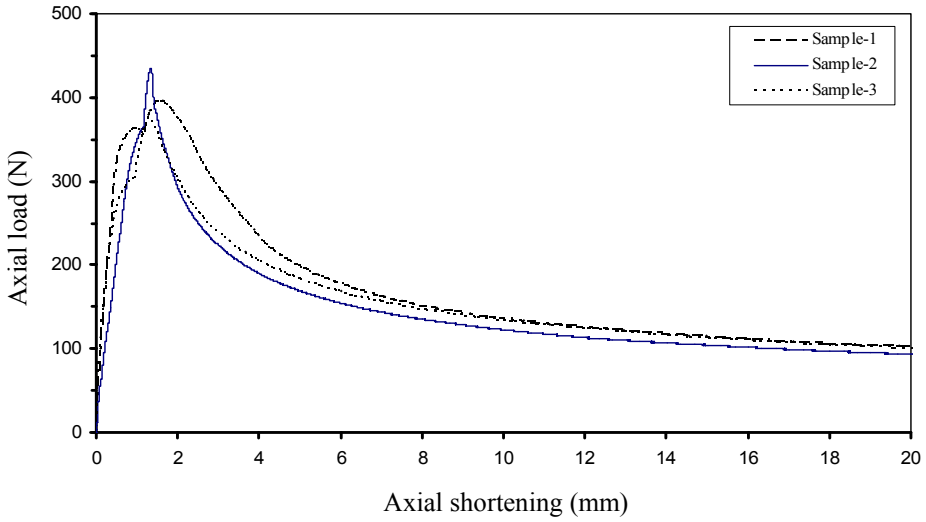

Figure 3.27 Axial compression test results for diagonal members

3.10 Finite element modelling

3.10.1 Introduction

Finite element analysis provides (FEA) an efficient tool to model structures' behaviour and their response to mechanical actions. Although it does not have the same accuracy as experimental testing, FEA provides good approximations suitable for describing structural behaviour.

In the following sections the use of numerical analysis is presented to develop an accurate and reliable model to predict behaviour of the experimental models. Commercial software package, ABAQUS, was used in this numerical simulation. The

program included a wide library of elements and analysis techniques which helped in simulating the experimentally tested models with high accuracy.

Different simulation approaches with different degrees of sophistication were introduced to describe the elements of the models. The shaking table displacement output was applied to the numerical models to help in simulating the actual boundary conditions in the laboratory.

Modal analysis was carried out on the proposed models to obtain their natural frequencies and vibration mode shapes, while nonlinear time history analysis was carried out to determine the lateral displacements and member forces. Nonlinear time history analysis was used to account for any geometric or material nonlinearly under loading conditions.

3.10.2 Damping considerations

In general, it was difficult to quantify the source of damping in the tested models as it was caused by several sources including energy loss during hysteretic loading, viscoelastic material properties and friction at joints.

Joint friction was one of the most effective damping sources in the system arising from the sliding between member surfaces' interfaces. This type of damping was extended to increase in composite models, Truss B and C, since the addition of upper decks increased friction between the top continuum and the upper supporting joints.

Material damping was another source of damping in tested models due to the members' deformations resulting in an internal energy loss caused by the internal behaviour of the material particles.

Due to the complexity of measuring these values experimentally, damping was taken in

numerical analysis as a global composite damping (ABAQUS analysis user's manual, 2007). In this system, damping is supplied as a global viscous property that is proportional to the mass, M, and stiffness, K, of the structure so the amount of damping changes with the natural frequency of the structure according to Equations 3.3 and 3.4:

$$c = \alpha \, \mathrm{M} + \beta \, \mathrm{K} \tag{3.3}$$

$$\zeta_i = \frac{\alpha}{2\omega_i} + \frac{\beta\omega_i}{2} \tag{3.4}$$

where c denotes the damping in the system, α represents the mass factor and β represents the stiffness factor. The values of α and β were varied during the dynamic analysis of each case to make for the damping values obtained during the experimental tests at measured modes of vibration frequencies.

3.10.3 Numerical modelling of elements

Several element models were attempted in the analysis. The models started with simple truss elements and increased in sophistication gradually to complicated models that included all variations in cross-section along the members' length. Furthermore, material properties were taken from the experimental tests carried out on material specimens and presented in section 3.9.

3.10.4 Material idealisation for FE analysis

To introduce the material used in building the test models into the finite element analyses, a linear idealisation of the tests' results was adopted as shown in Figures 3.29 to 3.32. These idealisations enabled the analysis to consider the material nonlinearities.

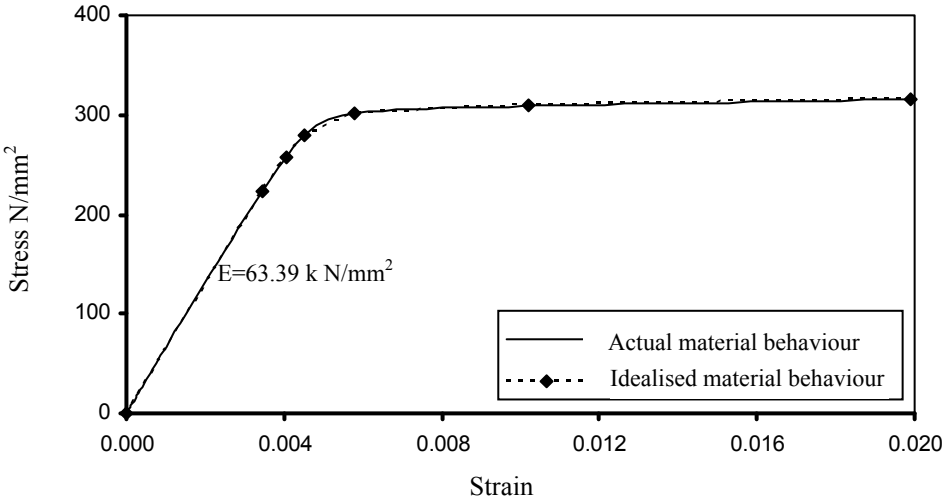

Figure 3. 28 Actual and idealised behaviour of Aluminium material used in space frame members

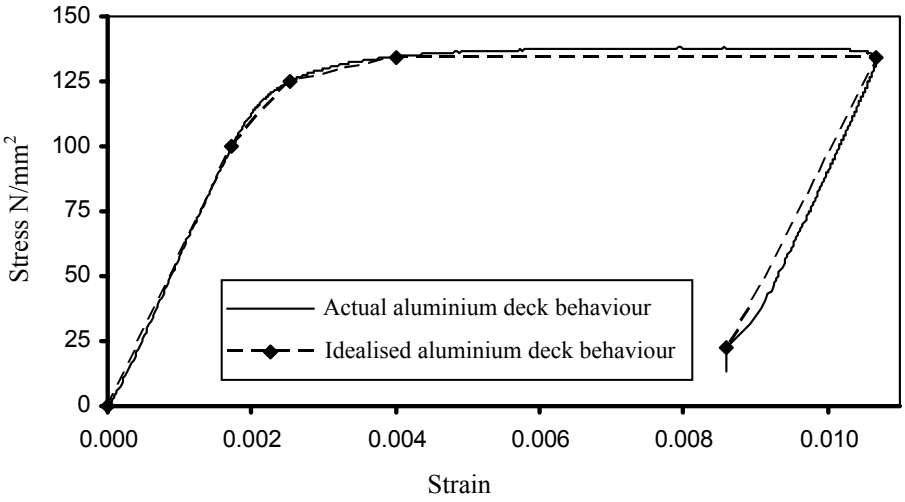

Figure 3.29 Actual and idealised material properties for Aluminium deck

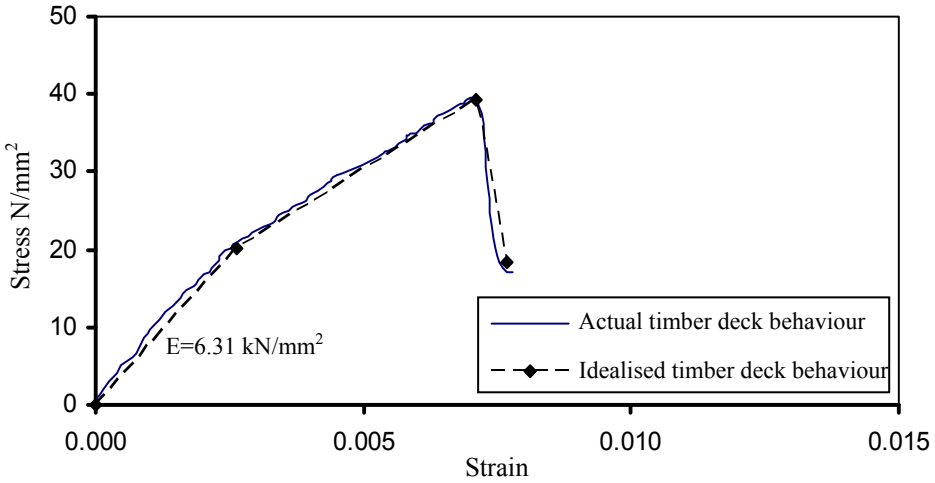

Figure 3. 30 Actual and idealised material properties of Timber deck (Longitudinal direction)

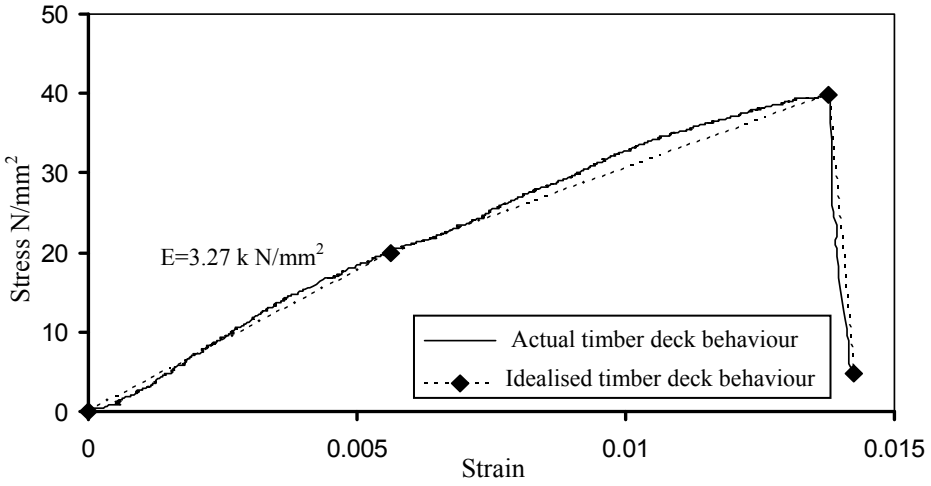

Figure 3.31 Actual and idealised material properties for Timber deck (Cross direction)

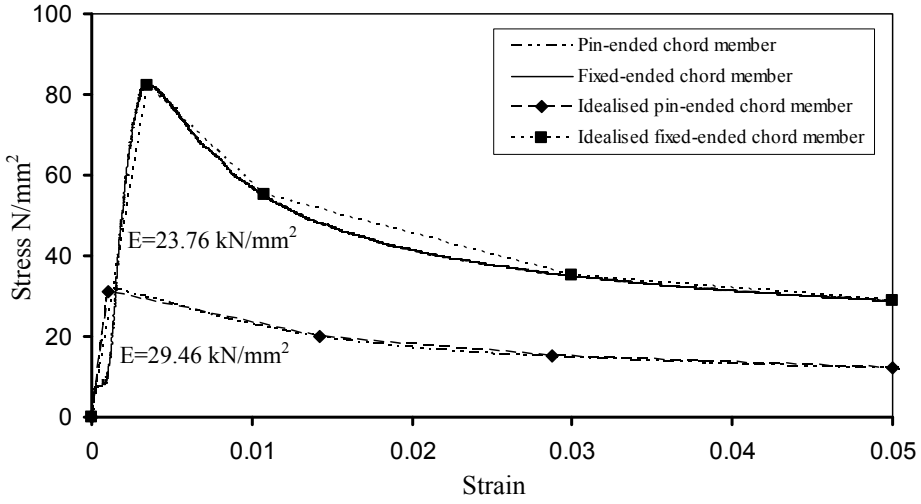

Figure 3.32 Actual and idealised material properties for upper chords

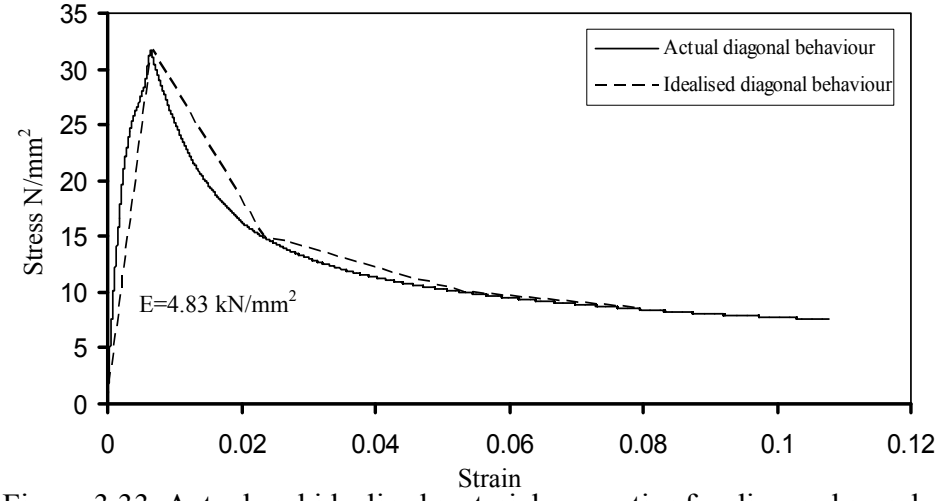

Figure 3.33 Actual and idealised material properties for diagonal members

Figures 3.32 and 3.33 present the actual and idealised behaviour of upper chord and diagonal members. Both were used in the static analysis of test models before applying any dynamic excitations. Table 3.1 presents a summary for the idealised material properties for different element groups made of aluminium, while Table 3.2 shows the idealised material properties for the timber deck sheet used in building Truss C. These values were those used as an input for material properties during finite element analysis.

Table 3.1 Summary of idealised material properties of aluminium components

	Modulus of elasticity E (N/mm^2)	Yield strength f_y (N/mm^2)	Non-linear Idealisation	
			Stress (σ)	Strain (ε)
General Properties	63.92E+03	259.2	259.2	0.000000
			281.3	0.000114
			303.6	0.001044
			311.9	0.005247
			321.5	0.014683
Continuous upper chord member in compression	23.756E+3	82.69	82.69	0.00000
			55.59	0.00885
			36.09	0.02878
			30.27	0.04897
Pin-ended upper chord member in compression	29.464E+3	30.97	30.97	0.00000
			20.3	0.01352
			15.5	0.02827
			12.7	0.04958
Diagonal member in compression	8.835E+03	30.85	30.85	0.00000
			15.35	0.01968
			10.53	0.04968
			9.17	0.07416
Aluminium deck sheet	57.98E+03	100.51	100.51	0.00000
			125.40	0.00037
			135.08	0.00167
			138.52	0.00783

Table 3.2 Summary of idealised material properties of timber deck sheet

	Modulus of elasticity E (N/mm^2)	Yield strength f_y (N/mm^2)	Non-linear Idealisation	
			Stress (σ)	Strain (ε)
Timber deck sheet (Longitudinal direction)	6.82E+03	20.2275	20.3	000000
			39.5	0.00403
			18.4	0.00249
Timber deck sheet (transverse direction)	3.55E+03	20.12682265	20.13	000000
			40.28	0.00759
			4.83	0.01351

3.10.5 Geometric modelling of test space frames

The numerical study included simulations to model the experimentally tested Trusses A, B and C. All models had 7×7 panels and SOS configuration and had the same dimensions and element sizes. Truss A was a non-composite space frame, while Trusses B and C were composite space frames formed by adding a 1.2mm thick of aluminium deck connected to the top joints of Truss A and timber deck with 4mm thick Truss B. All models were supported on their lower corners or along the two lower edges parallel to X-direction. Support joints were not allowed to displace but free to rotate.

A group of 9 finite element models were introduced with gradually increasing complexity to model the changes in the members' cross-sections along their length. The models also included some end releases for specific members to allow rotations in specific directions to occur. Figure 3.34 shows typical upper and lower joints and shows clearly the eccentricity of the diagonals and the stacking arrangements of diagonal members at joints. The actual and idealised upper chord members, diagonal members and lower chord members are shown in Figures 3.35 to 3.37, respectively, for different FE simulations.

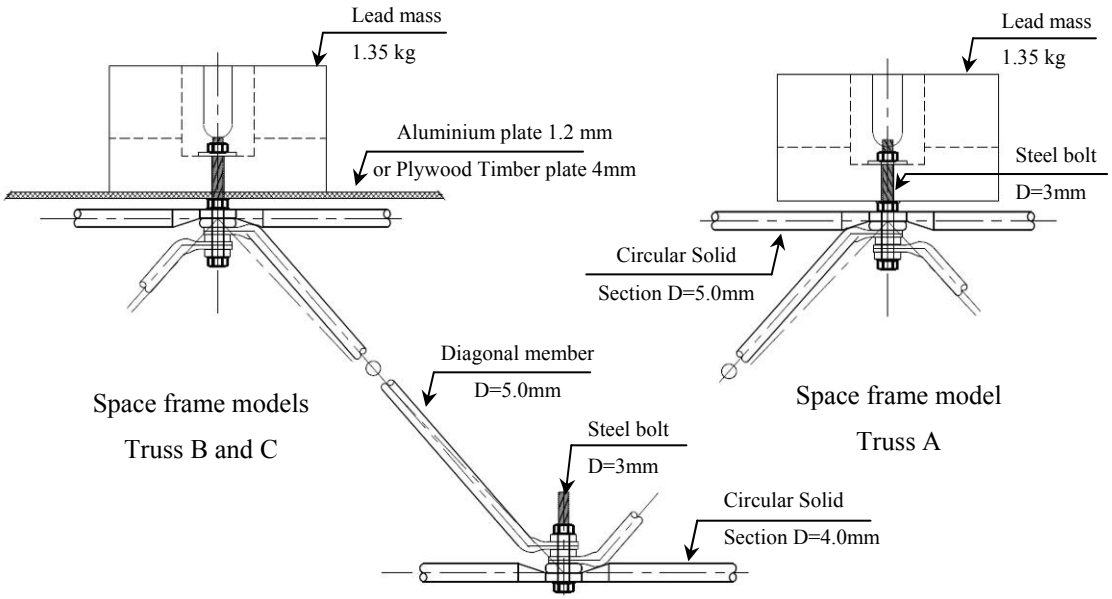

Figure 3.34 Typical upper and lower joints of space frame models

The accuracy of numerical analysis for the three models was assessed by comparing the analysis output with the experimental results. For composite Trusses B and C, the deck sheet was simulated as a series of shell elements at the same level as the upper chord members due to the small eccentricity of the deck above the upper chords in the test models. The shell elements were connected at the top joints without any intermediate connections with the upper chord.

The above mentioned models were introduced for the two cases of corner and edge-supports. Furthermore, two extreme aspect ratios, AR= 1.0 and 2.0, were considered in the test programme to help validate the finite element models. The validation against the experimentally obtained dynamic properties concentrated on the values of the first five natural frequencies and their associated vibration mode shapes. Comparisons between the maximum horizontal displacement at the upper middle joints as obtained from the finite element analysis and the experimental tests were used to further evaluate the accuracy of finite element models. Details of the validation process and results can be found in Chapter 7.

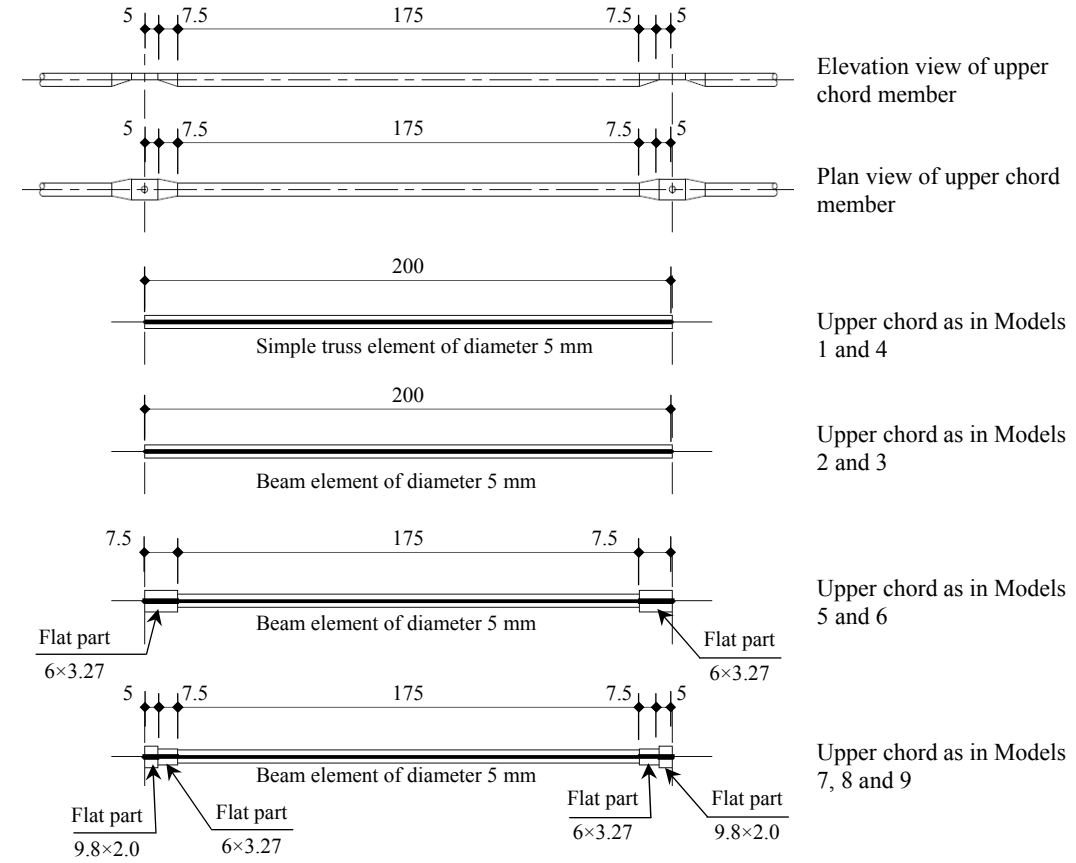

Figure 3.35 Actual and idealised upper chord member for FE models

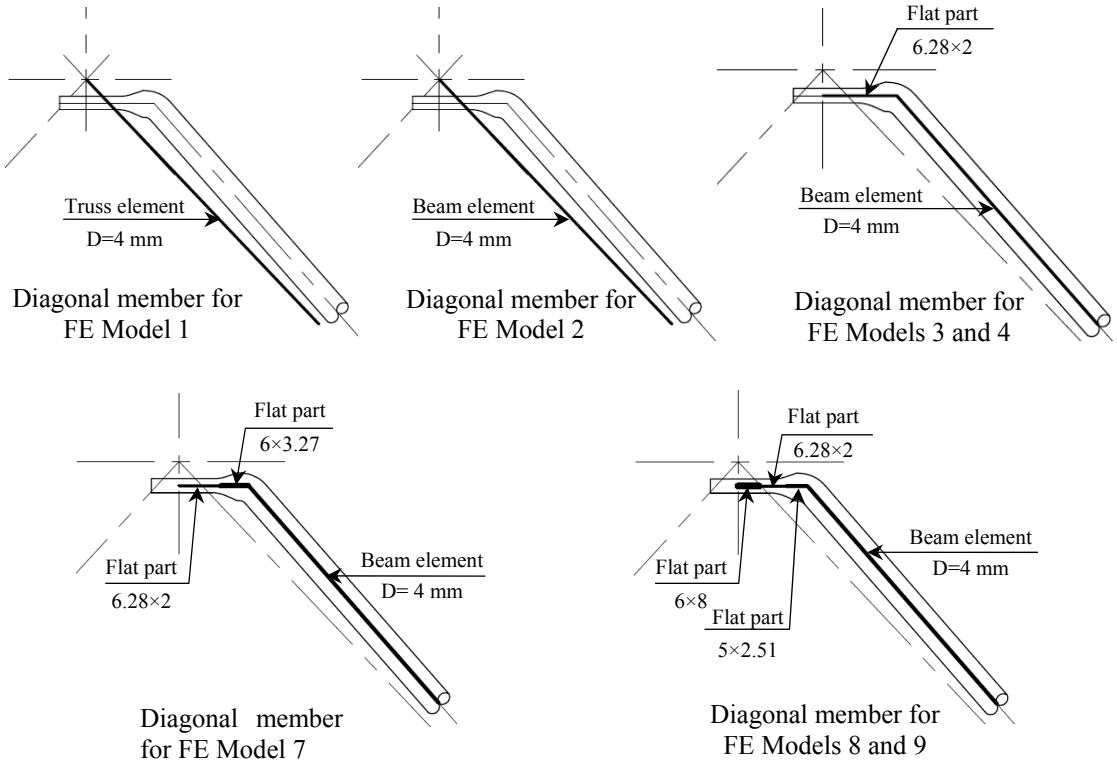

Figure 3.36 Actual and idealised diagonal member for FE models

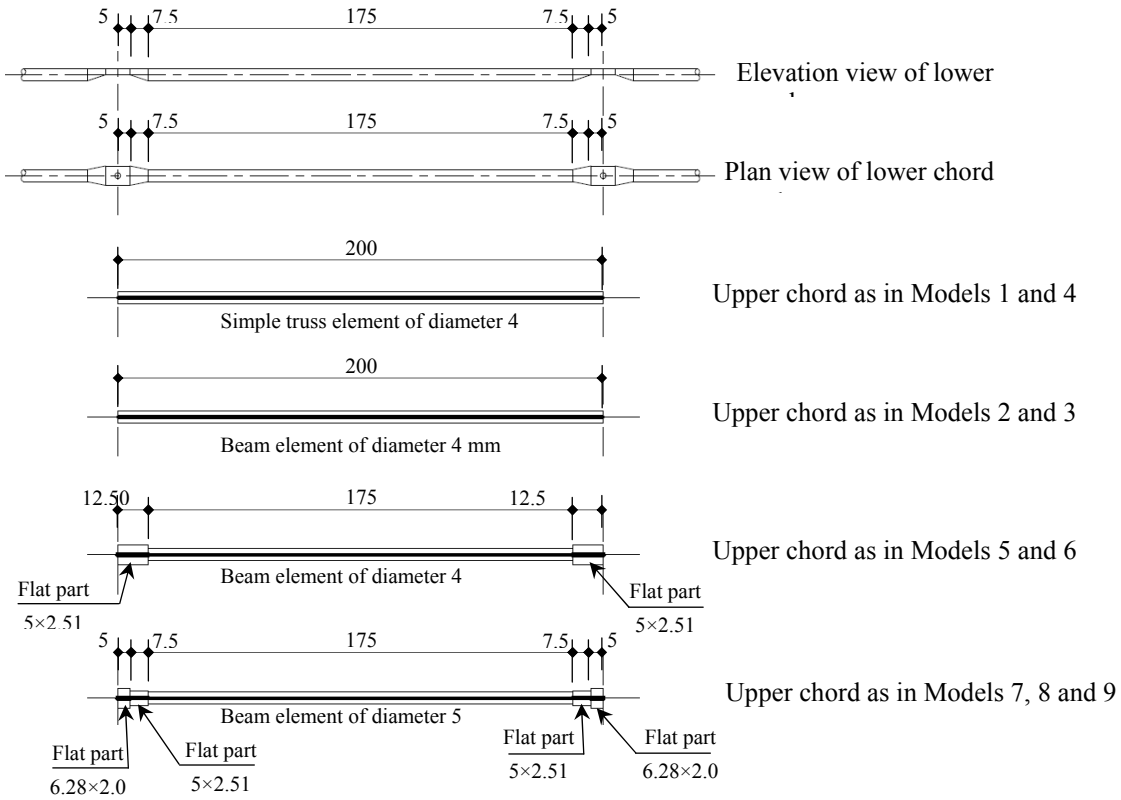

Figure 3.37 Actual and idealised lower chord member for FE models

Model 1

In this model, all members were represented as simple truss elements. This model was considered the simplest model as it did not take into consideration any eccentricity, cross-section changes or joint stiffness (Figure 3.38a). Mass elements were located at the upper joints without considering any mass eccentricity. Member continuity in the top and bottom chords was also ignored.

Model 2

Due to the continuity of upper and lower chord members and the stiffness of members at joints, all members in this model were introduced as linear beam elements. Members were divided into four segments to enable tracing the buckling behaviour and any intermediate deformations. No joint or mass eccentricities were considered (Figure

3.38b).

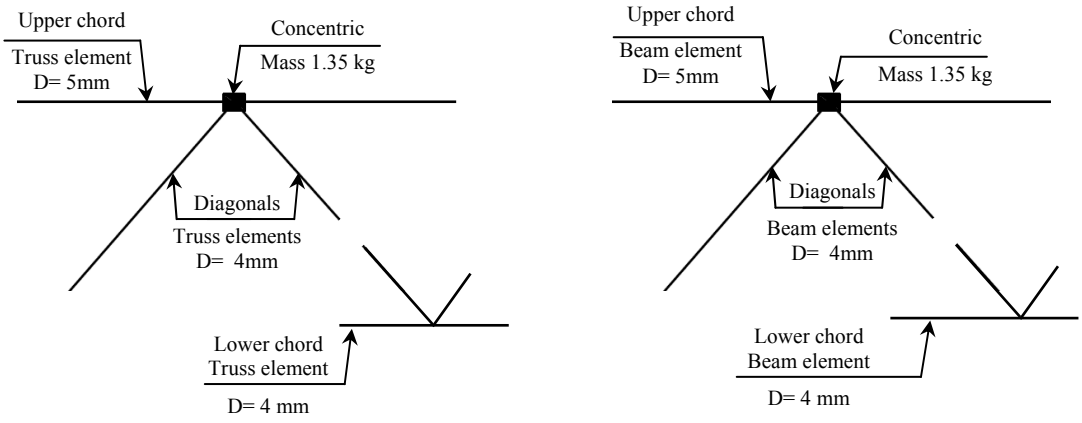

a. Model 2 b. Model 2

Figure 3.38 Modelling of top joints and elements of Models 1 and 2

Model 3 and 4

The eccentricity of diagonal members was introduced in these models by using horizontal beam elements at both ends of diagonal members. The cross-section of these flat ends was rectangular with dimensions 6.28×2.0mm, and 10 mm length. The flat rectangular section simulated the squashed circular section at the connection with the top chord and diagonal members. Top and bottom members were circular solid sections with diameters of 5.0mm and 4.0mm, respectively. Chord members in Model 3 were considered truss elements to consider the high reduction of element stiffness caused by stamping of ends (Figure 3.39a). However, the chord members in Model 4 were modelled as beam elements released for rotation in the out of plan direction only while considered continuous in the other direction (Figure 3.39b). No attention was given for any section changes along upper or lower members for both models. Masses were considered to be concentric with top joints.

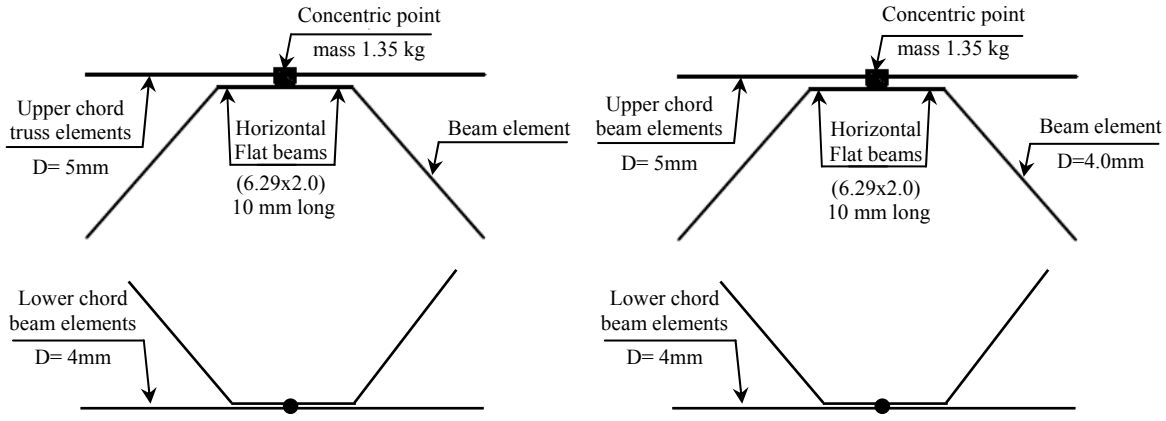

a. Model 3 b. Model 4

Figure 3.39 Representation of top and lower joints of Models 3 and 4

Model 5

Figures 3.35 and 3.37 show that the upper and lower chord members were stamped at the joints to enable connection to other members. To incorporate these changes in upper chord elements, an average rectangular section 6×3.27mm was introduced at both ends of each member with 12.5mm length. Stamped ends of the lower chord members were substituted with elements with an equivalent rectangular section 5.03×2.50mm with 12.5 mm length. No end releases were allowed for chords or diagonal members.

In this model, diagonal members had the same modelling components as in Models 3 and 4. Masses were considered concentric with the top chord joints. For models with a top aluminium sheet or a timber board, the deck was simulated as thin shell elements sharing the same level as the top chord members and connected to them only at the main joints.

Model 6

The components of this model were the same as Model 5 but end releases at the ends of diagonal members were included. Diagonal members were released to allow for rotation

around the vertical axis representing the jointing bolts while they still rigid in all other directions.

Trials were also made to release the upper and lower chords members to allow for rotation around their horizontal axis in conjunction with the previously mentioned release for diagonal members. This change led to the structure losing much of its stiffness and demonstrating significant reductions in the frequencies obtained by modal analysis.

Model 7

A further sophistication to what was considered in Model 5 was adopted in this model. The changes in the upper and lower chords were more fully considered. Each member was divided into 5 parts. Transition from a circular to a rectangular cross-section by stamping was modelled as 2 separate elements, each with a different cross-section size as shown in Figure 3.35 and 3.37.

On the other hand, cross-section variations in diagonal members were modelled by dividing the flat parts at their ends into 2 elements to make the diagonal member composed of 5 beam elements with 3 different cross-sections (Figure 3.36). Lead masses were considered concentric at the top joints where all members were connected.

Model 8

In this model, the flat part of the diagonal member was divided into 3 segments. The first segment was 3 mm long with cross-section of 6×8mm to express the flat part bounded by other diagonal member ends and chord members meeting at the connection. The second segment, which was the free segment, was fully squashed and had no contact with other elements. This segment measured 4.0 mm long with a rectangular section 6.254×2.0mm. The last segment was 3mm long and 5.0×2.51mm section size to

represent a transition from a circular cross-section to a flat cross-section. The total number of segments in a diagonal member was 7 representing all changes in the member along its length.

The upper and lower chord members kept their number of segments and cross-sections the same as in Model 7. The eccentric connection of masses with the top joints was considered by adding beam elements with 10mm length and 2.8 mm diameter joining the masses to the centres of the top joints (Figure 3.40).

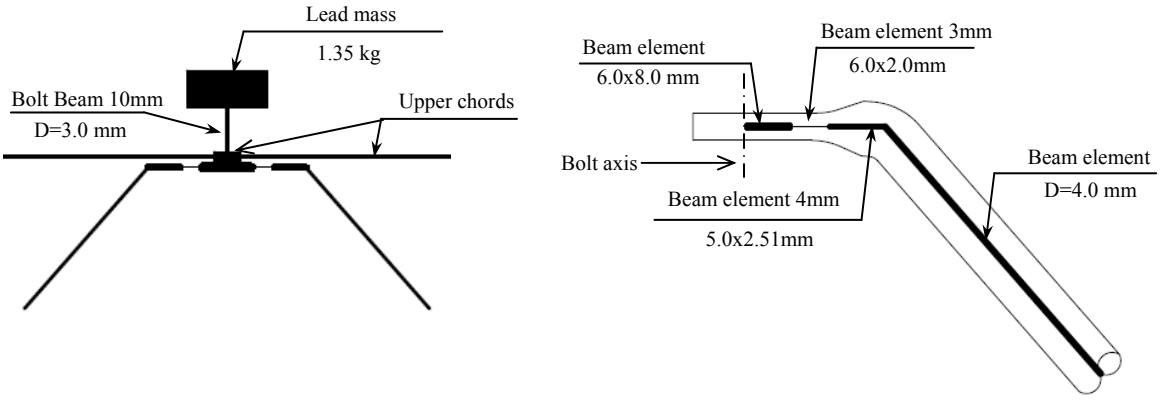

a. Full connection details b. Diagonal details

Figure 3.40 Finite element model details of Model 8

Model 9

This model was considered the most sophisticated model due to the large number of elements used to account for eccentricity of diagonal members from the upper and lower chord members and to consider mass eccentricity. The flat ends of diagonal members were considered as one block with the ability of members to have rotation around their vertical axes. Beam elements with bolt diameter of 2.8 mm and length 5.25mm connected this block with the nearest chord joint. Another beam element with the same diameter connected the two perpendicular members of the same chord to allow for simulating any relative rotations between the two members. Finally, beam elements

with 8.0mm long were used to join the eccentric masses to the top joints (Figures 3.41 and 3.42).

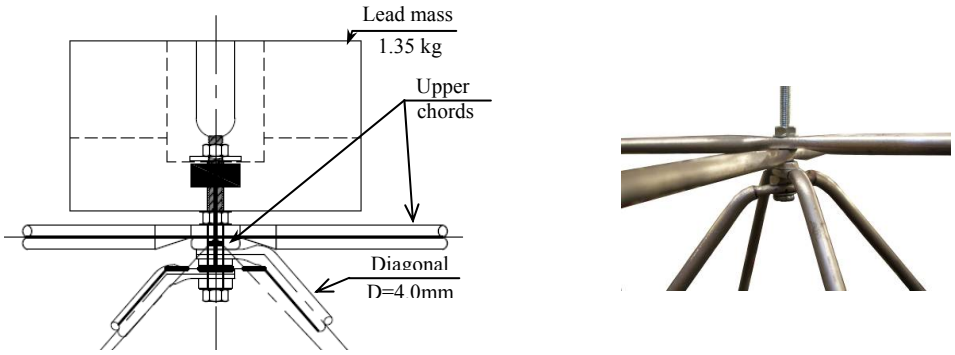

a. Details of top joint as modelled b. Actual truss joint without mass

Figure 3.41 Details of top joints of Model 9

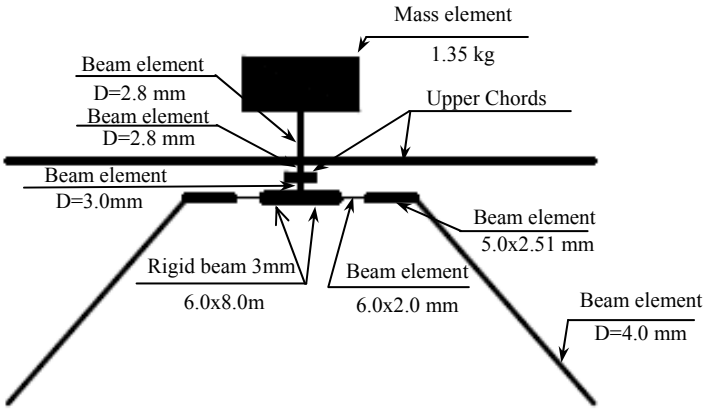

Figure 3.42 Modelled top joints of Model 9

3.11 Summary

This chapter introduced the methodology and tools used to achieve the goals of current study. It included the manufacturing process of the experimental models in addition to the tests carried out to determine their material and member behaviour. A brief description of the test rig used in testing the experimental models was introduced. The test procedures used in the vertical and horizontal snap tests and the shaking table tests

were discussed.

Instrumentation used in monitoring responses and measurements and also precautions taken during tests to avoid noise sources during tests were presented. Furthermore, discussion was introduced for filtration methods used to eliminate noise from recorded data.

An introduction to the finite element analysis used in modelling space frame components was presented and included material modelling idealisations and how they were considered in the analysis. Geometrical modelling of test space frames with different sophistication levels was introduced. In total, nine numerical models were introduced and discussed to simulate the manufactured models. The adequacy of these models and their ability to trace the behaviour of the experimental space frames will be assessed in Chapter 7 before using them to cast further light on the dynamic behaviour of composite and non-composite space frame structures.

CHAPTER 4

DESIGN AND MANUFACTURING OF SHAKING TABLE

4.1 Introduction

Earthquake simulators (shaking tables) are important tools in testing structural models of important buildings. An accurate shaking table can be described as one that can accurately simulate not only the ground motions experienced in earthquakes, but also vibrations from different sources such as machines, explosions and wind excitations in a three dimensional space. The cost of manufacturing and running fully functional shaking tables is very high as they need sophisticated technology and controlling techniques. The need for an inexpensive and simple earthquake simulator encouraged the author to design and manufacture a mechanical shaking table that was able to produce sinusoidal like motion waves on tested structures. This shaking table was considered enough for exposing tested models to simple sinusoidal like acceleration waves. The produced acceleration waves represented an approximate simulation of the ground motions produced by earthquakes. Both wave amplitude and frequency could be controlled either manually or by using a computer control program. The shaking table tests were used to determine the behaviour of both composite and non-composite space frame models in terms of lateral displacements and internal member forces.

4.2 Description and layout of shaking table

The mechanical shaking table was designed to produce a sinusoidal like wave by converting the circular rotations obtained by an electrical motor to linear motion. To

achieve this goal, an eccentric arm was connected, at one end, to a rotating flywheel and to a linearly guided horizontal actuator at the other to transfer linear motion to a sliding deck (Figure 4.1). The flywheel had three points ready for connecting the eccentric arm, positioned at 100mm, 75mm, 50mm from the centre of rotation of the flywheel using the driving pin. Other points could be obtained by adding reinforced threaded holes at different positions as needed. The flywheel was keyed to a polished steel shaft of 50mm diameter going through two block bearings. A toothed pulley of 180.4mm diameter, component 7 in Figure 4.1, was keyed to the same shaft behind the flywheel. A timing belt, component 8 in Figure 4.1, was used to transfer rotational motion from electric motor to the toothed pulley lied behind the flywheel. Full details and shop drawings can be found in Appendix A

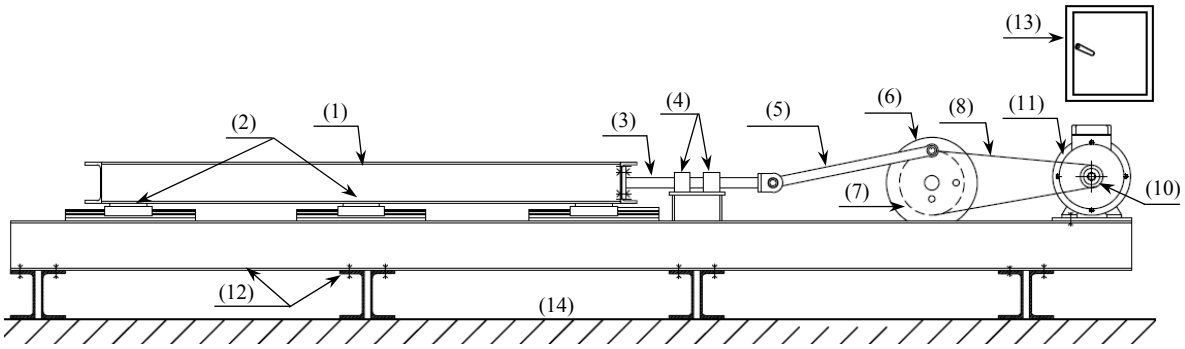

a. Elevation View

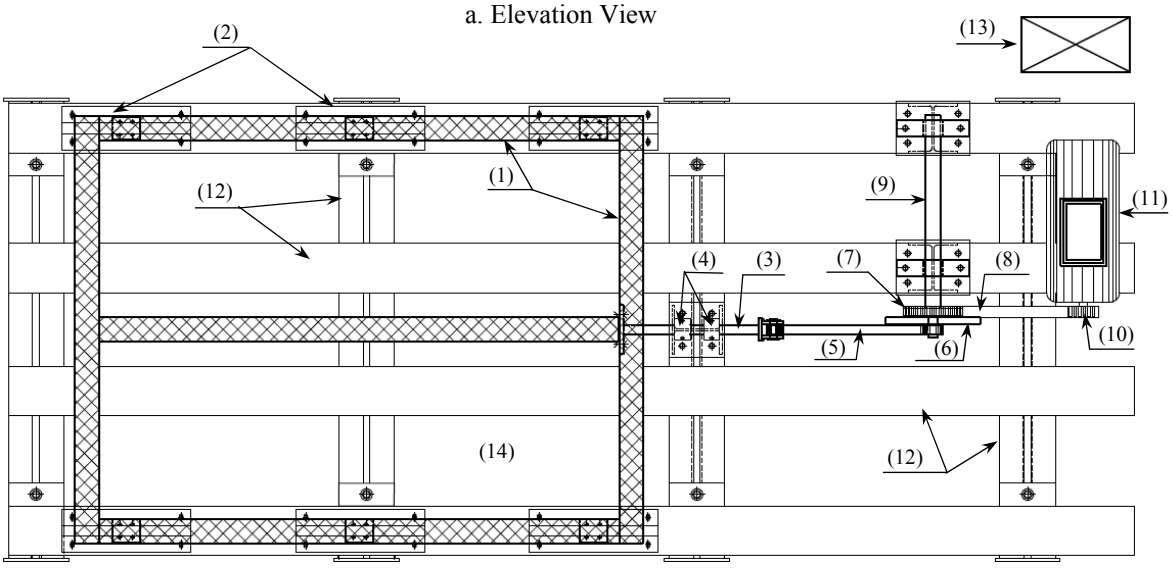

b. Plan View

Figure 4.1 Shaking table layout and components

A shaking platform (component 1 in Figure 4.1) was made from three longitudinal UB127×76×13 steel beams connected at their ends to two C130×13channel members. All platform components were welded together and had holes on the beams every 100 mm to attach the test models. The platform rested on 6 frictionless linear guide bearings, component 2 in Figure 4.1. These guides well designed for not tipping over the shaking platform under any load eccentricity. The carriages of the linear bearings were running on rails connected to a supporting frame, component 12 in Figure 4.1. The supporting frame consisted of four parallel UC157×157×23 steel beams, which rested on four pairs of cross channel BFC150×75×18 sections connected to the lab floor using 8 pre-tensioned anchor bolts. The lab floor was a heavy concrete slab of 600 mm thickness representing a heavy reaction mass to the shaking table. Main shaking table components are shown in Figure 4.1 and a list of the main components is given below:

1. Sliding deck (shaking platform)
2. Linear guide bearings placed between shaking platform (1) and supporting frame (12)
3. Actuator arm (polished stainless steel rod of 30 mm diameter connected from both ends to female rod ends with 16 mm bore hole)
4. Linear bearings of the actuator (to control the movement to be in longitudinal direction only)
5. Eccentric arm connecting actuator to flywheel (flywheel is a steel plate of diameter 280 mm and 25mm thickness keyed to horizontal shaft)
6. Supporting frame connected to a rigid floor
7. Toothed pulley keyed on the same shaft with driving flywheel
8. Polished steel shaft of 50mm diameter supporting the flywheel
9. Timing (toothed) belt

10. Toothed pulley connected to driving motor's shaft
11. Electrical driving motor with speed control
12. Rigid supporting frame
13. Control box contain power switches and motor controllers.
14. Laboratory floor of 600mm high strength reinforced concrete with holes spaced at 1016mm (40in) in two directions

4.3 Calculations of theoretical movement

As mentioned before, the shaking table was designed to provide sinusoidal like waves of displacements, velocities and accelerations as the main output. Shaking table output was variable and depended on the load over the platform (payload or model weight). The design payload target for the shaking table was 200 kg (≈ 2.0 kN) at a maximum acceleration of 0.70g.

The acceleration value could be increased or decreased according to the value of the payload (Figure 4.2). The maximum acceleration which could be obtained by the table was 2.0g (18.62 m/sec^2), which was applicable only for the case with no payload (free platform). However, the maximum acceleration value of 2.0g was independent of the location of the eccentric arm connection on the flywheel. All calculations given in the following sections depended mainly on the load carrying capacity of the driving pin, which was used to connect the eccentric arm to the flywheel. In addition, motor capacity that could be afforded was another limitation for choosing the maximum payload. The design load of the driving pin depended on the available diameters of rod ends, which should be connected at both ends of eccentric arm. Rod ends were chosen to be 16mm bore diameter, the same diameter of the driving pin, connected at both ends of eccentric arm.

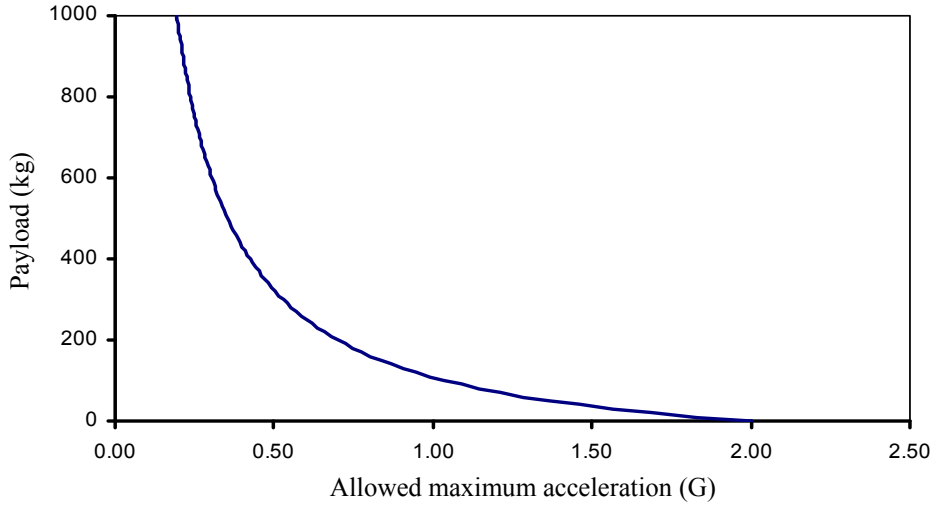

Figure 4.2 Relation between payload and allowed acceleration

In the following discussion, the governing equations controlling the output of the shaking table are briefly introduced.

The basic equation for the vertical projection of a point moving on a circular path can be written as follows:

$$d = R \sin \alpha \qquad (4.1)$$

where d is the distance of projection point, P, from the centre of rotation, R is the radius of eccentric point P_1, and α is the rotation angle. Due to the change of rotation angle with time t and speed of rotation, ω, the symbol α is replaced by ωt (Figure 4.3). The distance d therefore becomes variable with time and Equation 4.1 becomes:

$$d = R \, \mathrm{Sin} \, \omega t \qquad (4.2)$$

Velocity ν of the eccentric point P along the vertical axis can be obtained by differentiating the above equation with respect to time t, and differentiating it again gives the acceleration, a, of this movement around the centre, see Equations 4.3 and 4.4.

$$v = R\omega \mathrm{Cos} \, \omega t \qquad (4.3)$$

$$a = -R\omega^2 \sin \omega t \qquad (4.4)$$

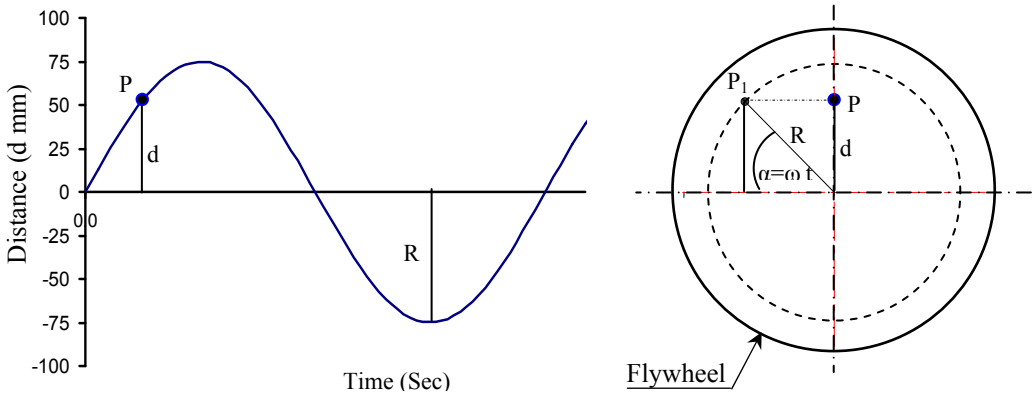

Figure 4.3 Basic sine wave of an eccentric point moving in a circle

Figure 4.3 represents the ideal case when an eccentric point moves around a centre point in a circular path. The actual movement of the sliding platform was slightly different from the above representation due to the existence of the eccentric arm. The arm created a distortion in the sine wave and also a shift in the location of the centre at which the driven point P_2 moves around. Figure 4.4 shows the shift of the centre of movement and also the difference in movement between the driven point P_2 and the horizontal projection of the eccentric point P_1. The distance between these two points changed due to the inclination angle of the eccentric arm θ. This angle varied due to the change in the angle of rotation of the eccentric point that in turn varied with time.

To determine the effect of the eccentric arm on the distortion of the sinusoidal wave, it is important to locate the new centre of the wave. The shift of the wave centre C_2 from the undistorted wave centre C_t can be calculated when the eccentric point P_1 coincides with the centre C_1 (at $\omega t = \pi/2$) and the angle θ becomes maximum (Figure 4.4).

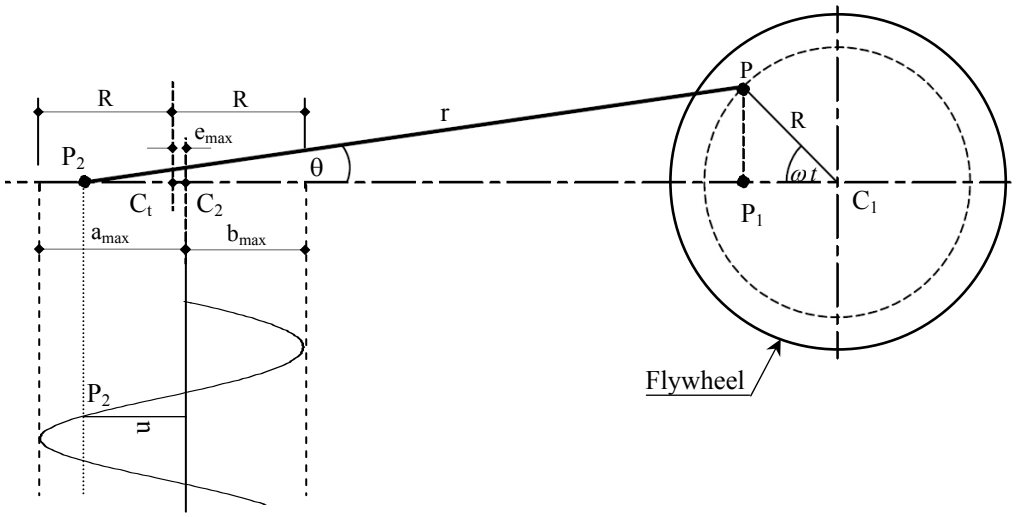

Figure 4.4 Effect of eccentric arm in motion transformation between P_1 and P_2

The maximum shift between theoretical and actual centre, e_{max}, and the maximum and minimum wave amplitudes, a_{max} and b_{max} (Figure 4.4), can be calculated using the following equations;

$$e_{max} = r - r\,\mathrm{Cos}\,\theta \tag{4.5}$$

$$b_{max} = R - e_{max} \tag{4.6}$$

$$a_{max} = R + e_{max} \tag{4.7}$$

The eccentric arm not only had an effect on moving the theoretical centre C_t, but also had an effect on the output displacements due to changes in the inclination angle θ with time t. Equation 4.8 relates the inclination angle θ to the angle of rotation ωt of the eccentric point P_1 around the centre C_1.

$$r \sin\theta = R \sin\omega t \tag{4.8}$$

$$\theta = \sin^{-1}\left(\frac{R \sin\omega t}{r}\right) \tag{4.9}$$

The distance between points P_1 and P_2 should, in perfect case, be constant all the time but changes in the inclination angle of the eccentric arm created a variable distance e,

which could be obtained from the following equation:

$$e = r - r\cos\left[\sin^{-1}\left(\frac{R\sin\omega t}{r}\right)\right] \quad (4.10)$$

This value was the difference in the distance between the two points P_1 and P_2, which varied with time t. The distortion value, e, was maximum, e_{max}, when the eccentric P_1 coincided with the centre point of rotation C_1, and this position further gave the maximum inclination angle θ. In contrast, the value of e diminished when angle θ tended to zero with the eccentric arm taking the horizontal position.

To obtain the final equation that governed the horizontal movement, u, of point P_2 which was linked to the shaking table platform, Equation 4.10 should be added to Equation 4.2 as follows;

$$u = R\cos\omega t - e \quad (4.11)$$

Or

$$u = R\cos\omega t - \left(r - r\cos\left[\sin^{-1}\left(\frac{R\sin\omega t}{r}\right)\right]\right) \quad (4.12)$$

A comparison between the pure sinusoidal and distorted waves is illustrated in Figure 4.5. It appears from the above equations that the distortion, e, of the wave depended mainly on the length of the eccentric arm, r. The distortion decreased with increases in either the eccentric arm length or the eccentricity of the connecting point (Figure 4.5).

The eccentric arm was selected to be 500 mm resulting in a moderate value in wave distortion in addition to giving suitable dimensions of shaking table to fit available space in the laboratory (Figure 4.6).

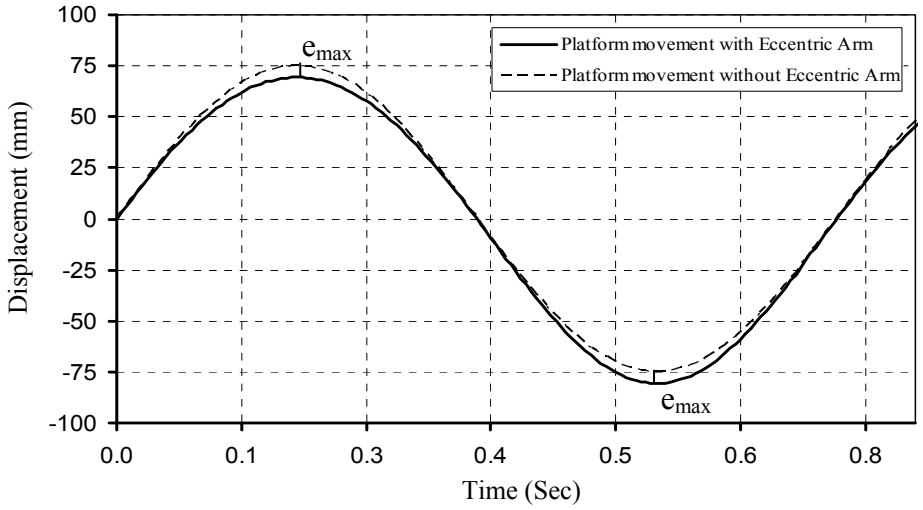

Figure 4.5 Ideal and distorted displacement wave with R= 75 mm

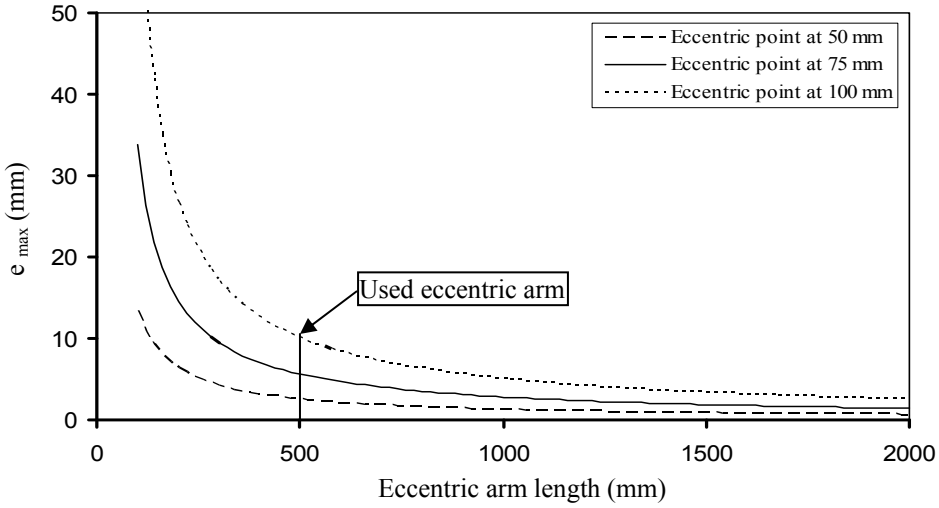

Figure 4.6 Effect of eccentric arm length and connecting point eccentricity on maximum displacement distortion

4.4 Design of shaking table components

4.4.1 Design of sliding platform

The sliding deck was the part of shaking table used to fix the test models. It was driven by a single actuator to move in a uni-axial direction. The sliding deck was made of three parallel beams of section UB127×76×13 with two cross channels of section C130×13

welded from their backs to both ends of UB beams (Figure 4.7). The platform was covered with a cover plate of 3.0 mm thickness to support the measurement devices and to help in fixing the test models, while tested models including their support frame should be connected to main beams only through special holes drilled at 100 mm. The platform was designed to run on 6 linear guide bearings of the type NSK (LAH30AN/ANZ).

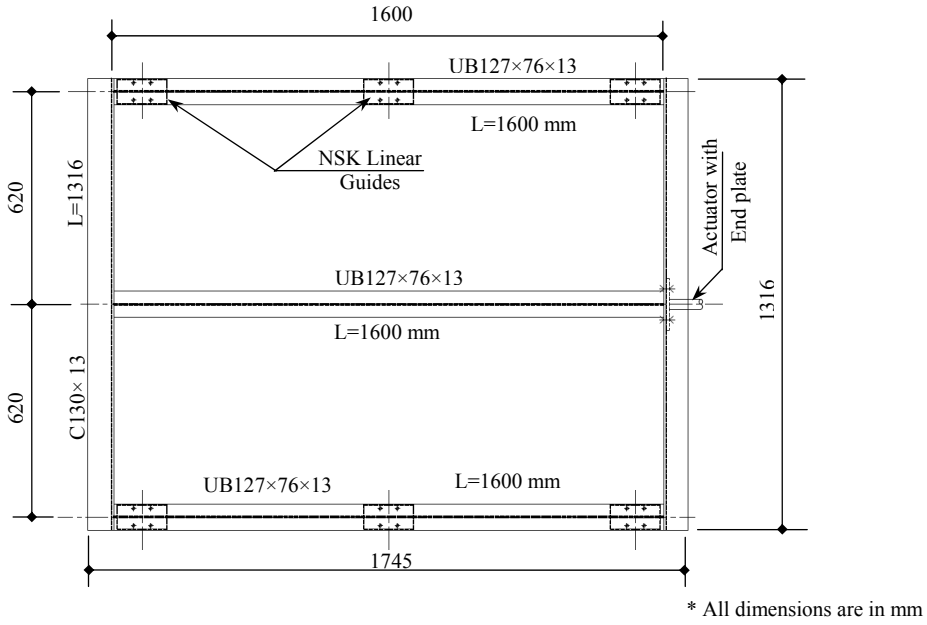

Figure 4.7 Components of simulator platform

A finite element modal analysis was carried out using SAP2000 for different cases of loading to determine the critical natural frequencies of the simulator platform. The platform was simulated as 5 beams resting on 6 supports restrained against translations in Y and Z directions and allowed to move only in the X-direction. The 6 supports were restrained against rotation around all three principal axes (Figure 4.8).

To achieve a stable structure, the platform is considered to be restrained in X-direction at the point of connection with the actuator arm.

According to Muhlenkamp (1997), three constraints control the design of shaking table

platforms:

1. The platform should have enough stiffness to eliminate all significant dynamic table-structure interaction.
2. The platform should have the smallest possible weight to minimise the driving force needed to move it.
3. The lowest natural frequency of the platform must be at least three times the maximum frequency which can be produced by the shaking table. This condition was important to minimise table-structure interaction.

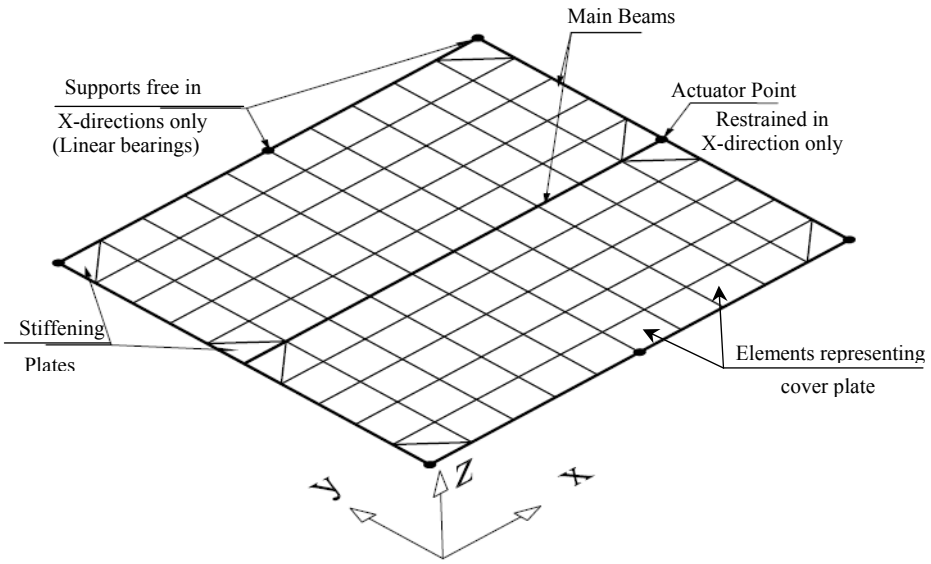

Figure 4.8 Finite element model of sliding platform

The full speed of the motor was 1440 rpm, which reduced by a factor of 3.7 through connection to a gearbox to 389.20 rpm. Rotation was transferred from the motor shaft to the flywheel using toothed pulleys. The toothed pulley connected to the motor had 32 teeth (Pulley A) and the other pulley, which was keyed to the shaft carrying the flywheel, had 72 teeth (Pulley B). A toothed timing belt was used to connect between both pulleys (Figure 4.9).

The maximum shaking table frequency of vibration can be calculated according to the maximum motor speed as follows:

$$f = \frac{\text{Motor speed rpm/min} \times \text{no. of teeth for Pulley A}}{\text{Gear box factor} \times \text{no. of teeth of Pulley B} \times 60 \text{ seconds}} \quad (4.13)$$

$$= \frac{1440 \times 32}{3.7 \times 72 \times 60} = 2.88 \text{ Hz}$$

So, according to Muhlenkamp the minimum platform natural frequency should be more than or equal to 8.64Hz (3×2.88Hz). Modal analysis was carried out to determine the natural frequencies of the platform in different loading cases.

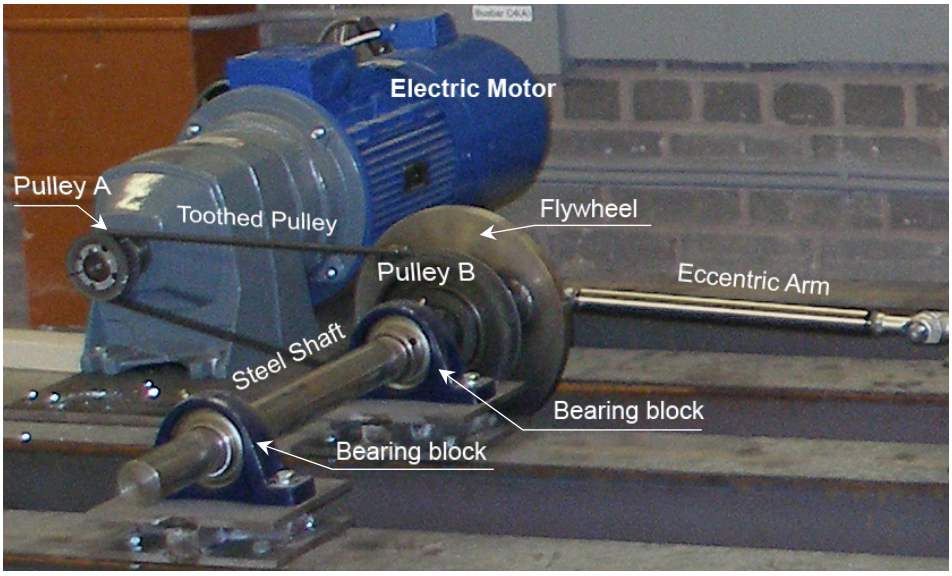

Figure 4.9 Components of shaking table driving system

The main frame of the platform was modelled as beam elements. All beams were divided into 10 elements. The cover plate was represented as shell elements connected to the platform frame at nodes between segments of main frame with thickness of 3mm. The platform was analysed in the loaded and unloaded cases. In addition, it was also analysed for the two cases with and without cover plate. Figures 4.10 and 4.11 show the modal analysis results for different cases of unloaded platform.

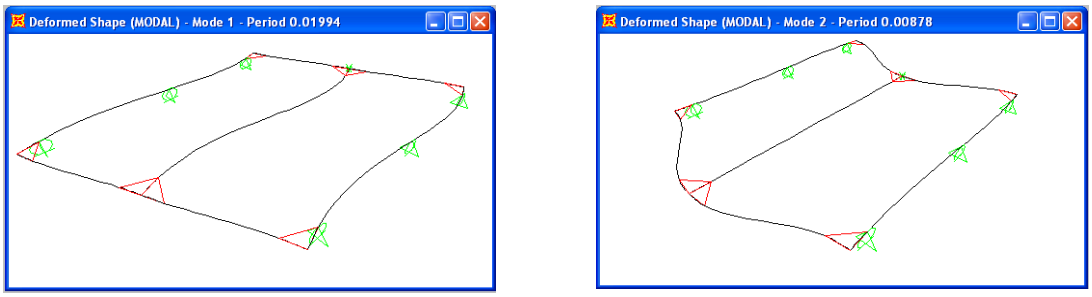

a. First mode of vibration b. Second mode of vibration

Figure 4.10 Vibration mode shapes of the free sliding platform without cover plate

a. First mode of vibration b. Second mode of vibration

Figure 4.11 Vibration mode shapes of the free shaking table platform with cover plate

For the free platform without cover plate, the first and second frequencies of vibrations were 50.15Hz and 113.89Hz, respectively. For the platform with cover plate, the first and second vibration frequencies were 95.97Hz and 125.95Hz, respectively.

From above results, it can be noticed that the fundamental frequencies of the sliding platform with cover plate were higher than those without a cover plate due to the increase in deck stiffness. It should also be noticed that the above frequencies ignored the local frequencies in cover plate which were very low compared to those of the platform's main frame so the test models were allowed to be fixed only to the main frame of the sliding deck. The small values of covering plate frequencies were a direct result of their small thickness.

As can be seen from the above results, the fundamental frequencies for the free shaking table platform with and without cover plate were high compared to the frequency recommended by Muhlenkamp (1997), which should be at least three times more than the maximum frequency that can be produced by the shaking table (2.88Hz).

The case of loaded platform was also important for the following reasons:

1. By connecting the test structure to the platform, the total mass increases which affect noticeably the fundamental vibration frequencies of the platform.

2. The eccentricity of test structure mass increases the vulnerability of platform to have rotational and bending modes of vibrations in platform's main frame.

To load the platform, a 1.0 m high cubic steel frame with masses of 50 kg lumped at its upper corners was used as a case of maximum design payload eccentricity. The steel frame was rigid enough to avoid having local modes of vibrations in the frame before the platform. Modal analysis was performed to find the fundamental frequency of loaded platform with and without the cover plate (Figures 4.12 and 4.13).

For the loaded platform without a cover plate, the first vibration mode had 23.607Hz of vibration frequency, while the frequency of the first vibration mode of the platform with a cover plate was 70.97 Hz; which were still higher than 8.649 Hz.

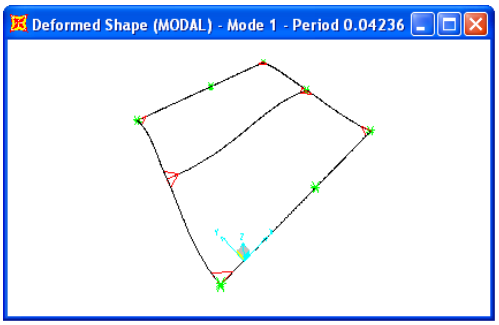

a. First mode of frequency

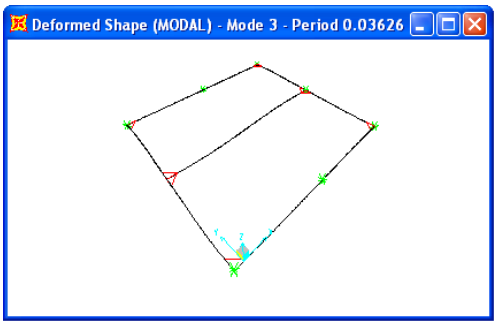

b. Second mode of frequency

Figure 4.12 Vibration mode shapes of the loaded platform without cover plate

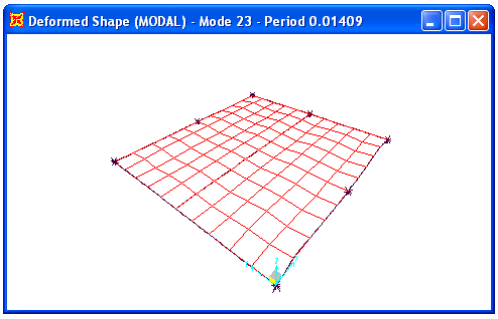

a. First mode of frequency

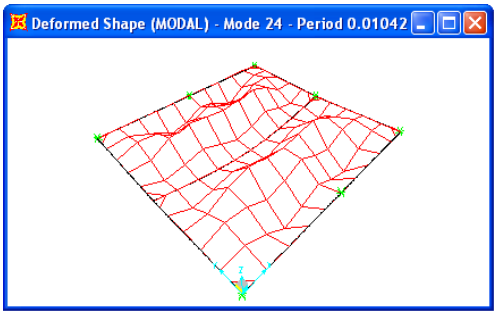

b. Second mode of frequency

Figure 4.13 Vibration mode shapes of the loaded platform with cover plate

From the above modal analysis, it could be concluded that the designed platform could be used with or without cover plate, as needed, safely.

4.4.2 Linear guide bearings

Linear guide bearings were selected to provide the following functions:

1. Smooth running of sliding platform with very low friction
2. Withstand the dynamic forces caused by violent movement of the platform
3. Can carry safely platform in addition to models with masses up to 200 kg
4. The bearings were selected to accommodate any overturning moments due to the eccentricity of loads in all directions with the focus to the direction of platform movements
5. Supporting the sliding platform at many points to keep its fundamental frequencies higher than three times the maximum frequency, which can be produced by the shaking table driving system

Many trials had been made to select the optimum number of bearings, which could offer minimum number of bearings in addition to satisfying the frequency requirements and keeping the weight of the sliding platform to the minimum. The trials started with 4 linear guide bearings at lower corners of platform's main frame, which did not cover the

above requirements. The number of linear guide bearings therefore increased to 6 linear guide bearings, 3 under each external side beam of platform's main frame, which was the optimum choice satisfying the above requirements.

By going through commercially available linear guides, the NSK (LAH30AN/ANZ) were the most suitable linear guides to be used with the shaking table. Full details, dimensions and specifications of linear bearings can be found in Appendix A.

Each bearing included two pieces. The first part was the truck, which connected to the platform facing the supporting frame (Figure 4.14). The other part was the guides, which were fixed to the supporting frame by fixing them first to supporting plates of 10mm thickness and the supporting plates were therefore fixed to the top of supporting frames through 4 slotted holes (Figure 4.15). These slotted holes were giving a chance to adjust the guides to avoid having any stresses on linear bearings during assembly or running of the shaking table.

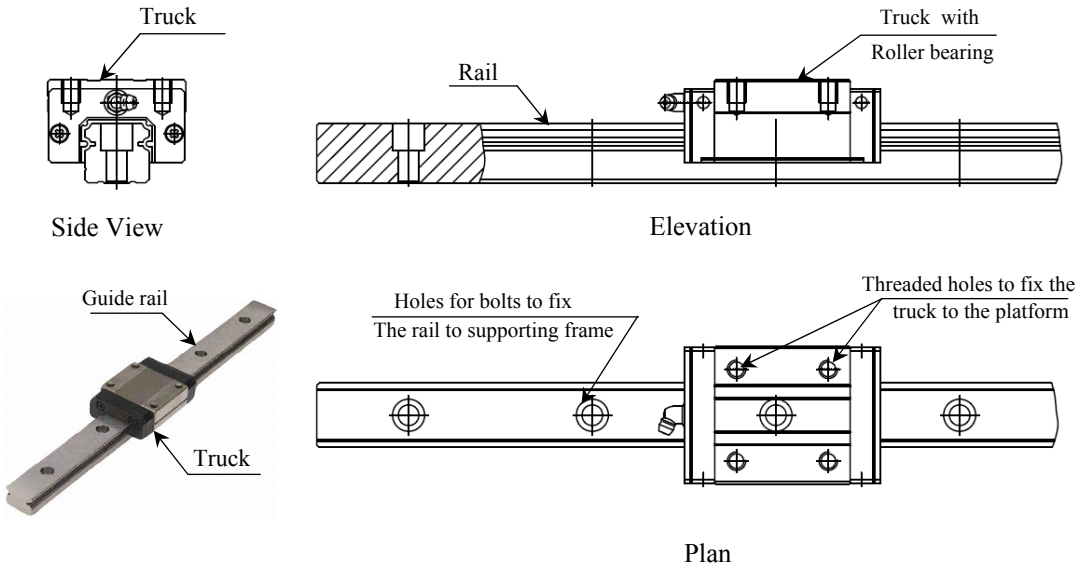

Figure 4.14 Details of LAH30AN/ANZ linear Guide Bearings

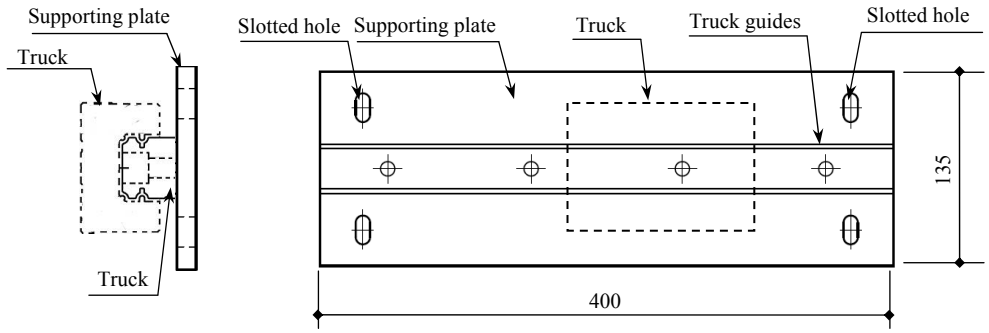

Figure 4.15 Details of supporting plate for linear guide bearings

4.4.3 Supporting frame

The supporting frame was needed as a supporting system for the platform, flywheel and driving motor. The supporting frame should be stiff enough to transmit the sliding platform loads and vibrations to the laboratory floor. Four longitudinal beams of section UC152×152×23 were chosen to support the system (Figure 4.16). These beams were supported on 4 cross beams spaced at 1016mm (40 in). The longitudinal beams were tied to the cross beams using 16mm HSFG bolts at each intersection point. Each cross beams composed of a pair of channels of section BFC170×75×15 tied together using tie plates between the main beams and also by welded plates at their ends leaving a 22mm space to allow for anchor bolts to pass through to the floor. A number of 8 pre-tensioned anchor bolts of 20mm diameter passed through the gap in the cross beams and continued through holes in the laboratory concrete floor. The anchor bolts went through the tie plates rested on the cross beams and also through a hole in the laboratory floor at distances of 1016mm (40in). The floor slab (reaction mass) was of 600mm thickness introducing a very high rigid reaction mass for the shaking table. The complete drawing details of the shaking table can be found in Appendix A.

4.4.4 Flywheel and its supporting system

The flywheel was a circular steel plate of 280mm diameter and 25mm thickness. The flywheel contained 3 threaded holes at different positions from the centre of rotation; 100 mm, 75 mm and 50 mm (Figure 4.18) and other holes can be added as needed. The flywheel was keyed to a solid steel shaft of 50mm diameter. A timing toothed belt pulley with 72 teeth of 8 mm pitch and 20 mm width was also keyed to the shaft just behind the flywheel with a 20 mm distance between them to allow for the nut of the driving pin to move freely (Figure 4.17).

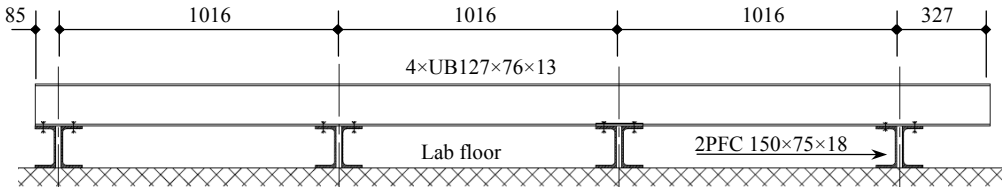

a. Elevation view

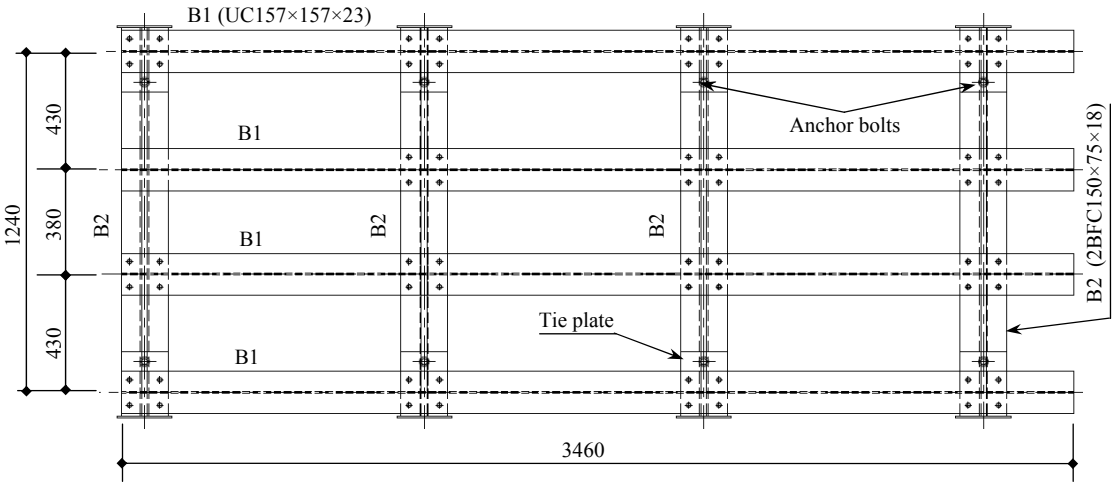

a. Plan view

Figure 4.16 Supporting frame of shaking table

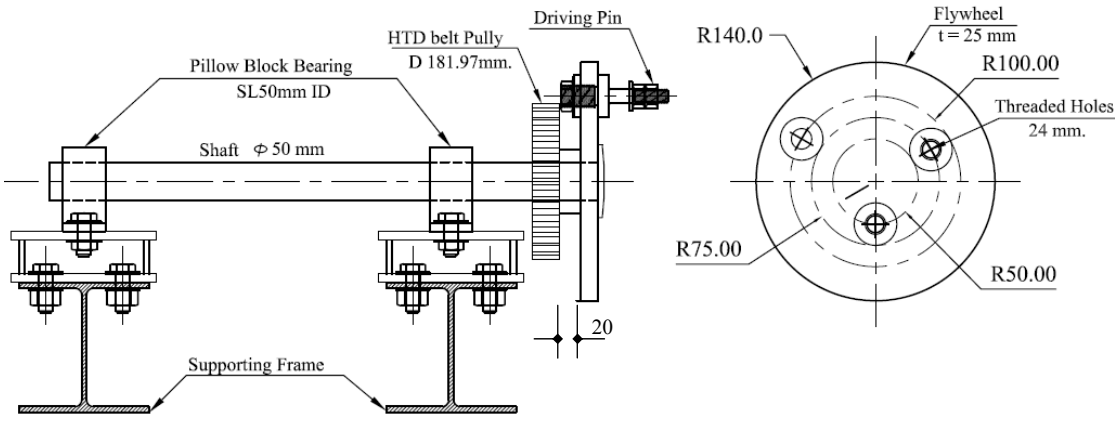

Figure 4.17 Flywheel supporting system and flywheel details

4.4.5 Actuator and eccentric arm

The actuator and the eccentric arm transferred the circular rotations of the flywheel to a linear motion of the sliding platform. The actuator was a bar of high tensile polished steel of 30mm diameter. It ended on one side with plate connected by four high strength bolts to the sliding platform and on the other end to a clevis of bore axis of 16mm diameter. The actuator went through two guide bearings to limit the movement of the actuator to horizontal direction (Figure 4.18).

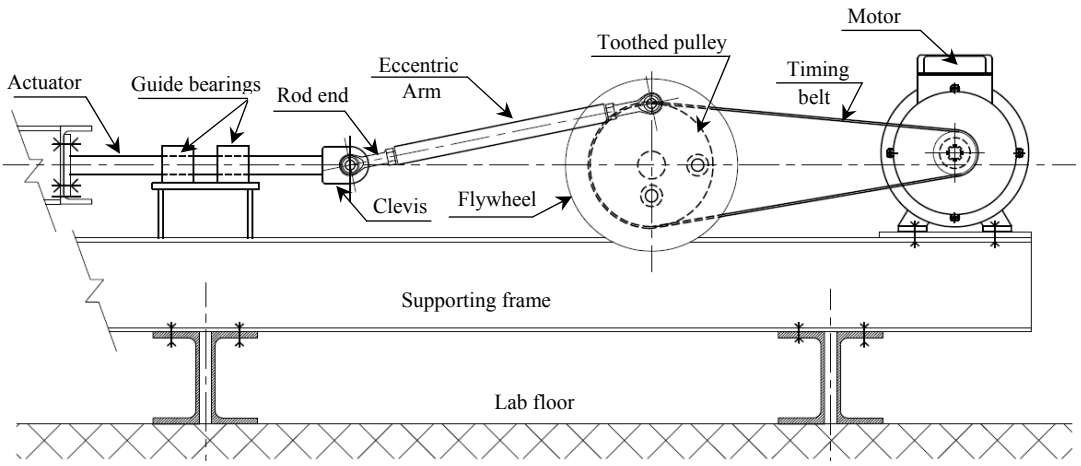

Figure 4.18 Driving system showing eccentric arm and actuator

The eccentric arm was another round bar of high tensile polished steel of 30mm diameter that ended on both sides with female rod end bearing with 16mm bore size. Rod ends had high load capacity compared to that predicted for the shaking table to avoid failure under violent movements.

4.4.6 Driving pin

The driving pin, shown in Figure 4.19, was used to connect the driving system (motor and flywheel) to the sliding platform. Fatigue stresses were the design control for the pin due to the repeated changes in load direction and value. The design of the driving pin is described below:

Maximum payload (mass) over the platform	= 200 kg
Mass of sliding deck including cover plate	= 150 kg
	==========
Total design mass (M)	= 350 kg

Friction test was carried out to determine the value of the coefficient of static friction by measuring the force needed for the platform to start moving. A wire was connected to a load cell at one side while the load cell was connected to the platform from the other side. The actuator was disconnected from the eccentric arm, but remained connected to the platform. By pulling the wire and recording the load at which the platform started to move which was f =115.56 N, the static coefficient of friction μ of the system could be estimated as follows;

$$\mu = \frac{f}{W} = \frac{115.56}{1471.5} = 0.0785 \qquad (4.13)$$

where W was the total weight of the platform. The coefficient of friction in the whole system was found to be 7.85 % of the load. The value of μ decreased noticeably with the start of platform movement and the system shifting to kinetic friction.

The table was designed such that the maximum allowed acceleration was 0.7g at a payload of 200 kg. The effective design force, P_e, of the driving pin was calculated as:

$$P_e = M(a + \mu g) = 350 \times (0.7 \times 9.81 + 0.0785 \times 9.81) = 2672.98 \text{ N} \qquad (4.14)$$

$$P_d = P_e \times \text{Impact factor} = 2672.98 \times 1.50 = 4009.47 \text{ N} \qquad (4.15)$$

where M was the total mass of the deck and payload and P_d was the actual design load. The impact factor was obtained from BS2573 considering the driving pin as a part of heavily used and loaded crane to be 1.50.

From the details of the driving pin shown in Figure 4.20, the critical sections were I-I and II-II.

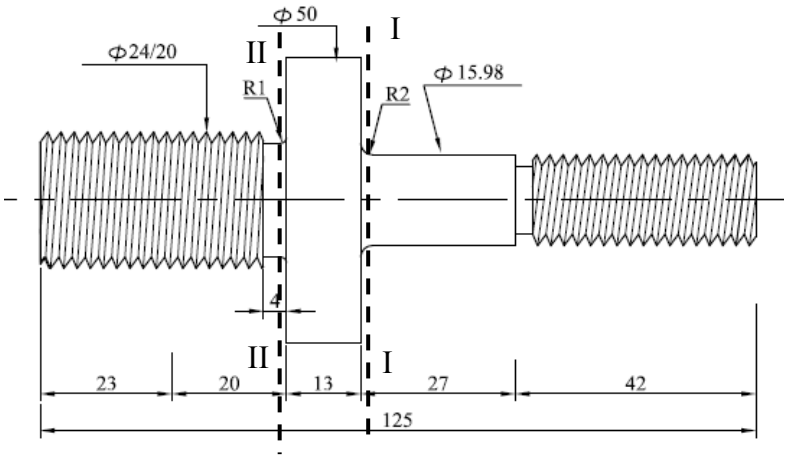

* All dimensions are in mm

Figure 4.19 Driving pin details

I. Straining actions at critical sections of the driving pin

At Section I-I

$$M_I = 4009.47 \times \frac{27}{2} = 54127.85 \text{ N.mm}$$

$$V_I = P_d = 4009.47 \text{ N}$$

$$A_I = \frac{\pi \times 16^2}{4} = 201.06\,\text{mm}^2$$

$$I_I = \frac{\pi \times 16^4}{64} = 3217.00\,\text{mm}^4$$

At Section II-II

$$M_{II} = 4009.47 \times (13 + \frac{27}{2}) = 106250.96\,\text{N.mm}$$

$$V_{II} = P_d = 4009.47\,\text{N}$$

$$A_{II} = \frac{\pi \times 20^2}{4} = 314.16\,\text{mm}^2$$

$$I_{II} = \frac{\pi \times 20^4}{64} = 7853.98\,\text{mm}^4$$

Where

M_I and M_{II} = Maximum bending moment at sections I-I and II-II

V_I and V_{II} = Maximum predicted applied shear force from Equation 4.14

A_I and A_{II} = Area section of driving pin at sections I-I and II-II

I_I and I_{II} = Second moment of inertia at critical sections I-I and II-II

There was no torsion straining action since the used end rods were equipped with a mechanism prohibited the transfer of any torsional moments to the pin.

II. Check of stresses due to bending moment and shear force

Assuming the steel used in manufacturing the driving pin was of S355 grade, then according to BS5950 the tensile yield strength $\sigma_y = 355\,\text{N/mm}^2$ and allowable shear stress $\tau = 0.6 \times \sigma_u = 213\,\text{N/mm}^2$. Both normal and shear stresses at critical sections can be calculated as follows:

At section I-I:

$$\sigma_I = \frac{M_I \times r_I}{I_I} = \frac{54127.85 \times 8}{3217.0} = 134.60 \text{ N/mm}^2 \qquad < 355\text{N/mm}^2 \quad \text{OK}$$

$$\tau_I = \frac{4\,V_I}{3\,A} = \frac{16\,V_I}{3\,\pi\,D_I^{\,2}} = \frac{16 \times 4009.47}{3 \times \pi \times 16^2} = 26.59 \text{ N/mm}^2 \qquad < 213\text{N/mm}^2 \quad \text{OK}$$

At section II-II:

$$\sigma_{II} = \frac{M_{II} \times r_{II}}{I_{II}} = \frac{106250.96 \times 10}{7853.98} = 137.84 \text{ N/mm}^2 \qquad < 355 \text{ N/mm}^2 \quad \text{OK}$$

$$\tau_{II} = \frac{4 \times V_{II}}{3 \times A} = \frac{16 \times 4009.47}{3 \times \pi \times 20^2} = 17.02 \text{ N/mm}^2 \qquad < 213 \text{ N/mm}^2 \quad \text{OK}$$

where;

σ_I and σ_{II} = the maximum normal stress due to bending at sections I-I and II-II

τ_I and τ_{II} = the maximum shear stress due to shear force at both sections

Q_I and Q_{II} = the statical moment of area at both sections

I_I and I_{II} = the moment of inertia at both sections

d_I and d_{II} = the diameter of driving pin at both sections

III. Check for fatigue stresses

From above results, it was clear that the stresses in the pin section were mainly normal stresses due to bending while shear stresses were considerably low. These stresses were fluctuating between tension and compression according to the direction of force applied due to the rotation of the flywheel (Figure 4.18).

To check the safety of driving pin to fatigue, the following equations given by Carvill (1993) were used. In this method, the factor of safety against fatigue failure can be obtained from the following equation;

$$FS = \frac{\sigma_y}{\sigma_m + \left(\frac{\sigma_y}{\sigma_e}\right) \times K_c \times \sigma_a} \qquad (4.14)$$

Where,

FS= factor of safety against fatigue failure

σ_y = the yield stress of the material used

σ_m = mean stress which was the mean of the alternating stresses

σ_e = the actual endurance stress limit of the material

σ_a = the average alternating stress

K_c = stress concentration factor due to changes in pin section

The following steps shed more light on these factors and how they were calculated to check the ability of the driving pin in tolerating fatigue stress.

Since the steel used was S355, the following properties could be obtained:

$$\sigma_y = 355\ \mathrm{N/mm^2} \quad , \sigma_u = 490\ \mathrm{N/mm^2}$$

According to Carvill (1993), the theoretical endurance limit, $\sigma_e^{'}$, for steel material was calculated as follows:

$$\sigma_e^{'} = 0.5 \times \sigma_u = 0.5 \times 490 = 245\ \mathrm{N/mm^2} \qquad (4.13)$$

where $\sigma_e^{'}$ was the theoretical endurance limit of steel when the number of alternating stress cycles approaches infinity.

The actual endurance limit depends on the surface factor, k_a, which was taken to be 0.9 as the surface was properly machined, smoothed and polished.

$$\sigma_e = k_a \times \sigma_e^{'} = 220.5\ \mathrm{N/mm^2} \qquad (4.14)$$

For any system with totally reversible stresses such as shown in Figure 4.20, no steady stress exist so, the mean stress can be calculated as follows;

$$\sigma_m = \frac{\sigma_{max} + \sigma_{min}}{2} = 0.0 \tag{4.15}$$

where σ_m was the mean stress and σ_{max} and σ_{min} were maximum and minimum normal stresses in the driving pin.

The average value of the alternating stresses σ_a occurred in the driving pin was calculated as follows:

$$\sigma_a = \frac{\sigma_{max} - \sigma_{min}}{2} = \frac{134.60 - (-134.60)}{2} = 134.60\ \mathrm{N/mm^2} \tag{4.16}$$

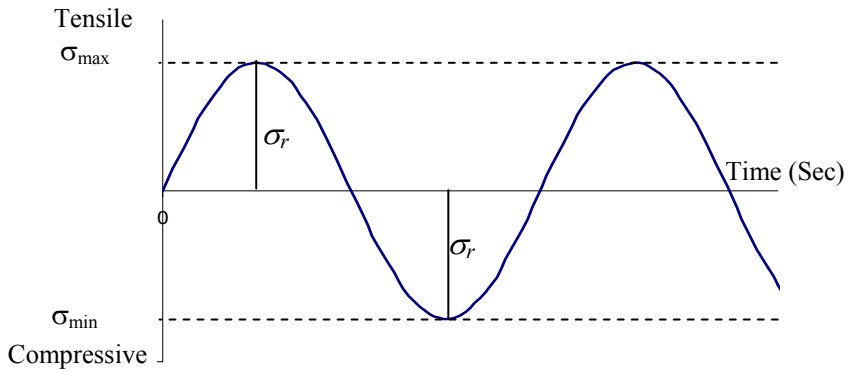

Figure 4.20 Fluctuation of bending stresses in driving pin

Stress concentration factor K_c was another important factor, which negatively affected the ability of the driving pin to tolerate fatigue stresses. For the driving pin, the stress concentration factor according to the section transition from 16 mm diameter to 50mm diameter with a fillet radius r of 2.0 mm was calculated as follows:

$$r/d = \frac{2}{16} = 0.125$$

$$D/d = \frac{50}{16} = 3.125$$

From tables provided by Carvill (1993), the factor K_c was selected to be 1.65.

The factor of safety was then calculated by substituting in Equation 4.14 to check if the section can tolerate the fatigue stresses as follows:

$$FS = \frac{355}{0.0 + \left(\frac{355}{220.5}\right) \times 1.65 \times 134.60} = 0.986 \qquad < 1.0 \qquad \rightarrow \text{unsafe}$$

A material with higher strength should be used such as S460 steel;

$$\sigma_y = 460\ N/mm^2 \quad , \ \sigma_u = 550\ N/mm^2$$

Substituting by the new values of yield and ultimate stresses of the new material in Equations 4.13 and 4.14 the actual endurance limit will be as follows;

$$\sigma_e = 0.5 \times k_a \times \sigma_u = 0.5 \times 0.9 \times 550 = 247.5\ N/mm^2$$

The factor of safety of the driving pin to fatigue stresses will be;

$$FS = \frac{460}{0.0 + \left(\frac{460}{247.50}\right) \times 1.65 \times 134.60} = 1.115 \qquad > 1.0 \qquad \rightarrow \text{safe}$$

It is worth mentioning that the above results showed that the use of S460 as a material for the driving pin was safe. A number of factors were ignored in the above design such as the pretension force produced on the pin shank by tightening it to the flywheel, widening the diameter of the bolt to be 50 mm which in turn rest on the flywheel due to tightening the bolt. These factors provided more strength to the driving pin which, in turn, increased the factor of safety.

4.5 Shaking table output and calibration

Several tests were carried out to check the accuracy of the previously proved equations with the actual output of the shaking table. The tests included measuring the actual centre of the produced wave of motion, which was expected to be the location of the platform when the eccentric point P_1 became over the centre of the flywheel (Figure 4.4). Calibration tests also included measuring the extreme positions of the platform

using a 300 mm long stroke LVDT transducer. These tests were repeated for different positions of the eccentric points on the flywheel.

The results showed high accuracy of calculations compared to shaking table outputs for both the actual centre and extreme positions of the platform. Figure 4.21 presents the actual displacement of the sliding platform and the displacements time history predicted using theoretical calculations. The figure shows close between the actual table output and the theoretical predictions.

Displacement, velocity and acceleration time histories are presented in Figures 4.22 to 4.24 respectively. Both velocity and acceleration time histories were obtained by conducting a numerical differentiation of the shaking table displacement output by using the central difference method presented in Equations 4.17 and 4.18 as follows:

$$\nu_i = \frac{dx}{dt} = \frac{x_{i+1} - x_{i-1}}{t_{i+1} - t_{i-1}} \tag{4.17}$$

$$a_i = \frac{d^2x}{dt^2} = \frac{x_{i+1} - 2x_i + x_{i-1}}{(t_{i-1} - t_i)^2} \tag{4.18}$$

where x, ν and a are the displacement, velocity and acceleration, respectively, at time t.

To use the shaking table for different loads and with different speeds, calculations were conducted to derive practical working charts which can be used the user for the shaking table. The relationships between the percentage motor speed on one hand and the resulting acceleration, the frequency and the maximum allowed payload are shown in Figures 4.25 to 4.28, respectively for different eccentric point P_1 positions on the flywheel.

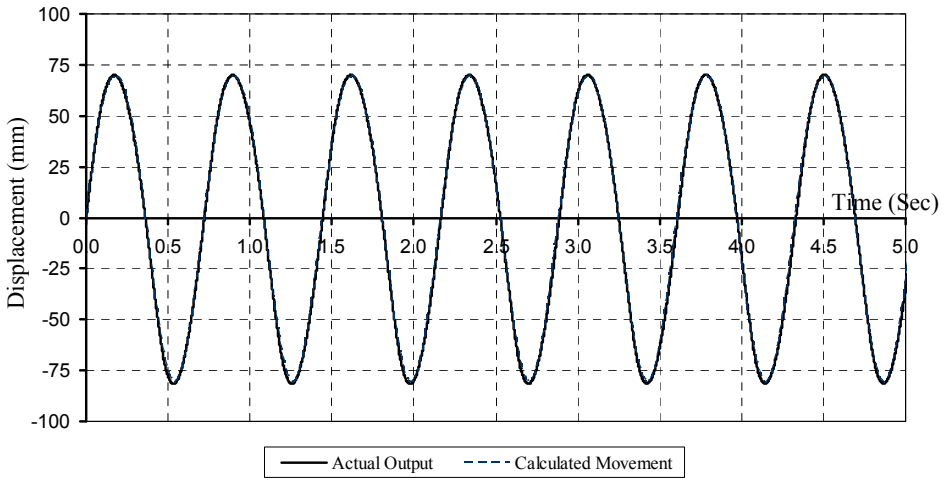

Figure 4.21 Theoretical and actual platform displacement with time

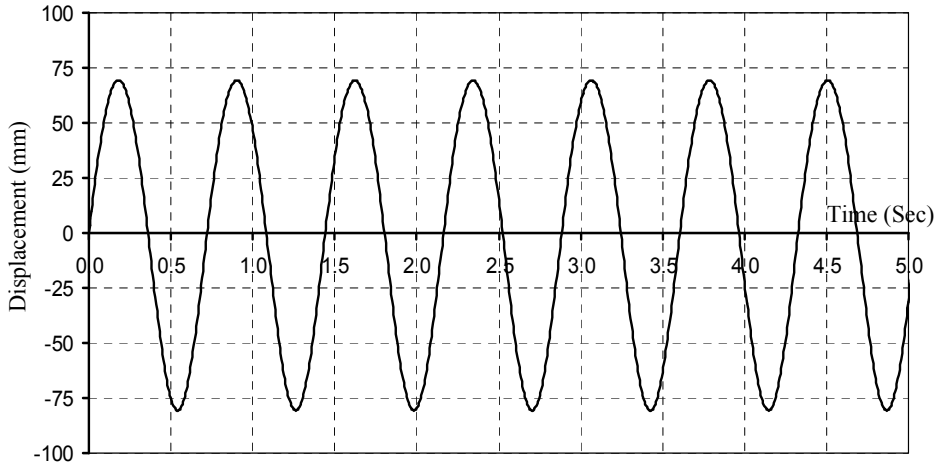

Figure 4.22 Displacement time history output of the shaking table platform

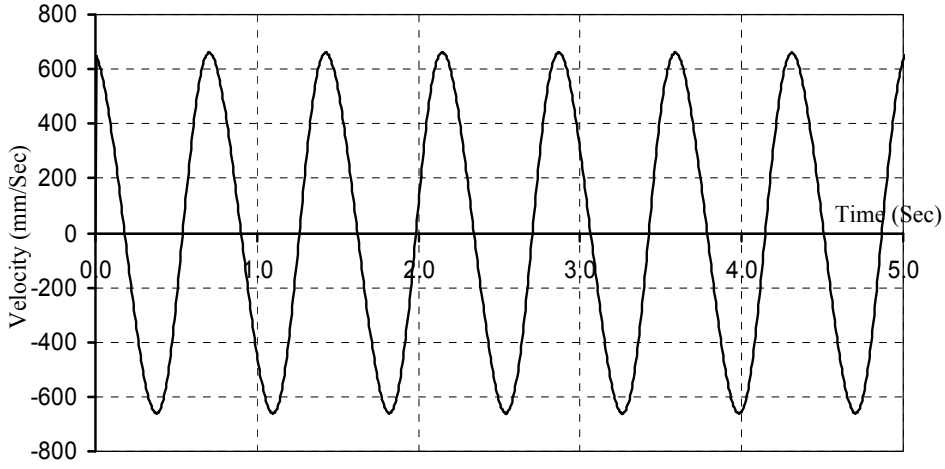

Figure 4.23 Velocity time history output of the shaking table platform

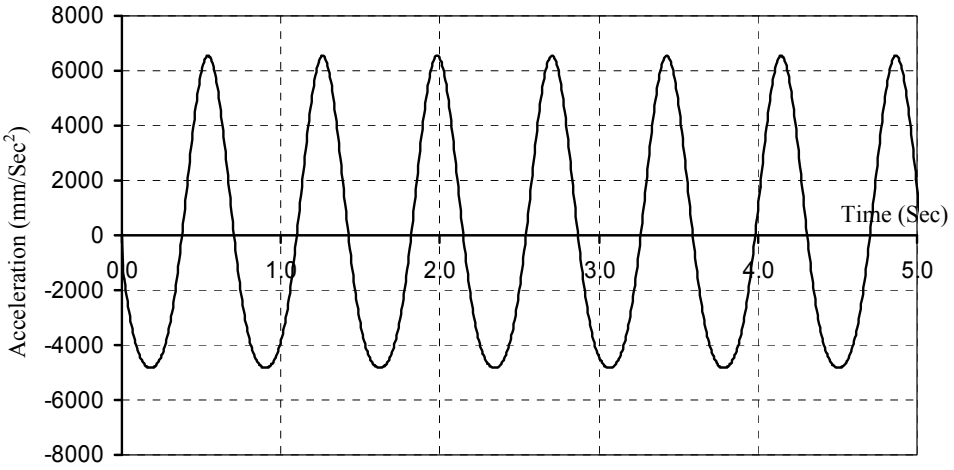

Figure 4.24 Acceleration time history output of the shaking table platform

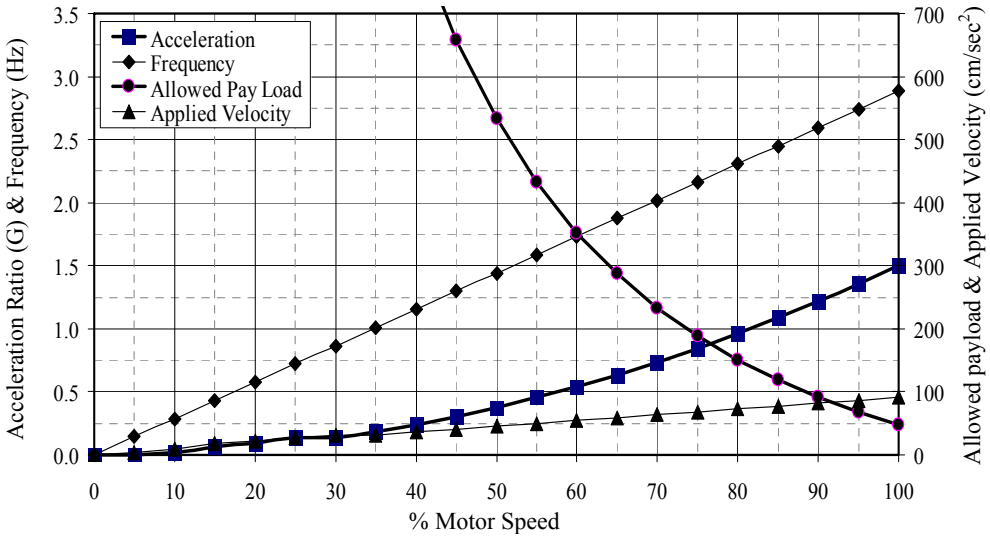

Figure 4.25 Usage chart for shaking table with eccentric arm at 50 mm radius

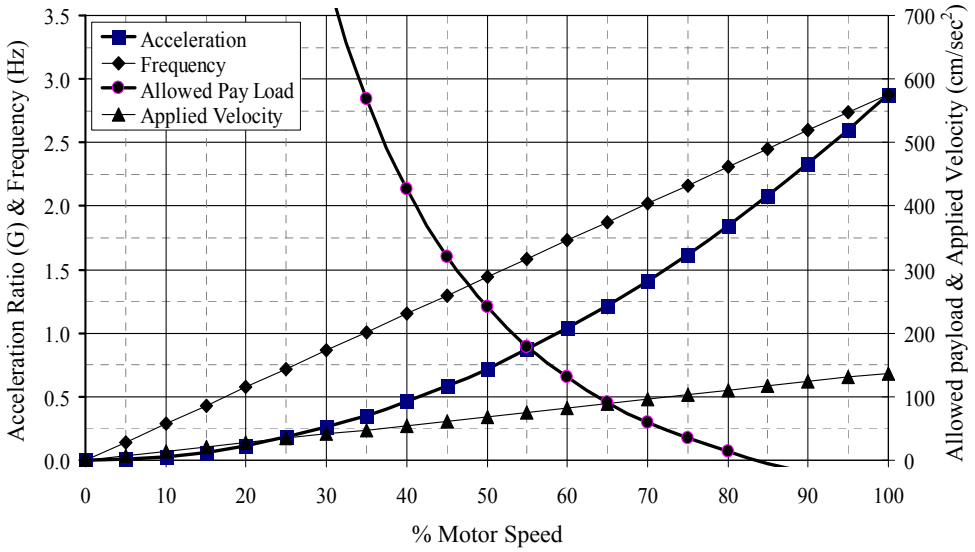

Figure 4.26 Usage chart for shaking table when eccentric arm at 75 mm radius

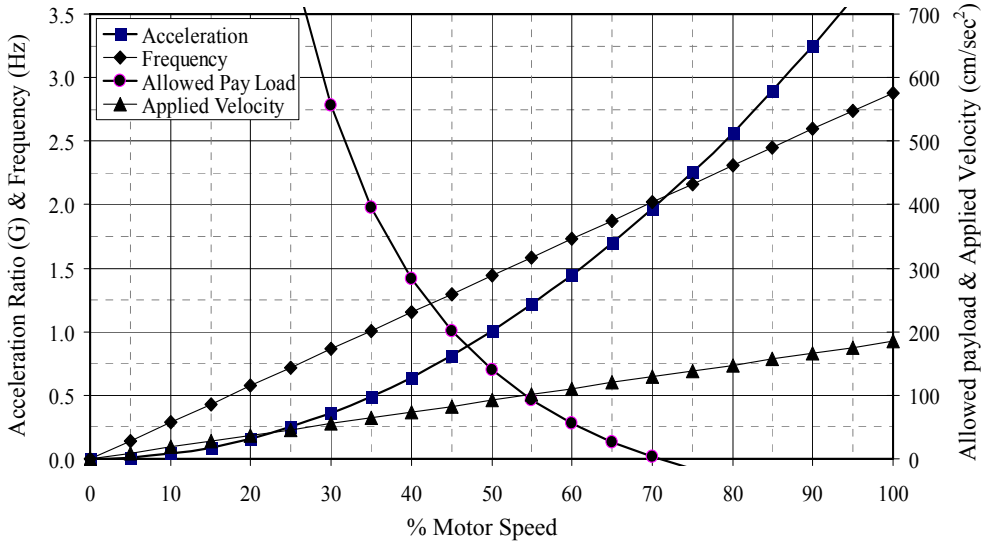

Figure 4.27 Usage chart for shaking table with eccentric arm at 100 mm radius

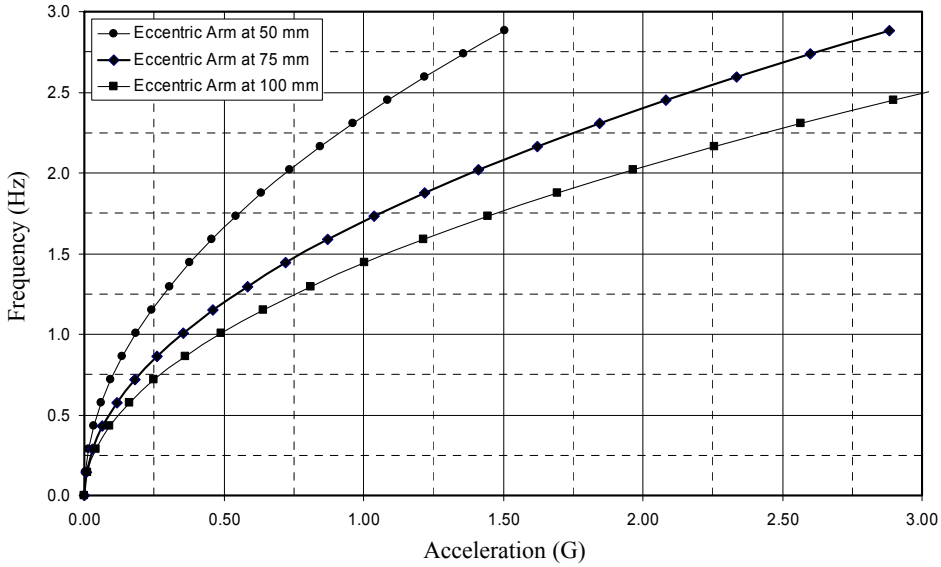

Figure 4.28 Frequency-acceleration relationships for different positions of the driving pin in the flywheel

4.6 Summary

In this chapter, details of the designed shaking table were thoroughly discussed. The shaking table was able to provide sinusoidal like waves, which could be used as an external excitation device for the test models and an approximate simulation of the earthquake waves. The output history of the shaking table depended on the basic principles of transforming circular motion to linear motion through connecting an eccentric arm to a circular flywheel. The eccentric arm was connected at its other end to

a horizontal guided actuator, which then transferred the linear motion to a linearly guided platform. Several checks were made to avoid structure-platform interaction within the shaking table frequency range.

The shaking table output was thoroughly checked and calibrated. Charts were derived to simplify its usage in the current and future projects. These charts related the allowable payload, the maximum acceleration and the frequency to the motor speed which could be controlled manually or by using computer.

CHAPTER 5

RESULTS OF EXPERIMENTAL TESTS

5.1 Introduction

This chapter presents the experimental results of non-destructive tests conducted on non-composite and composite space frame Trusses A, B and C, previously described in Chapter 3. Each test was repeated at least four times, and the average of the nearest three results was considered in the analysis and final discussion. These tests included models with two support conditions, namely, corner supports at the lower chords and two opposite edge-supports parallel to the direction of shaking table vibrations (X-direction). The tests included vertical and horizontal snap tests and shaking table tests to determine the dynamic characteristics of test models including the vertical and horizontal vibration frequencies and the damping ratios in test directions. The tests also investigated the changes in dynamic behaviour, in particular the lateral displacement and axial force responses to shaking table acceleration history. The lateral displacements of models and the strain progression in critical members due to shaking table vibrations were particularly monitored and reported in this chapter. To avoid repetition, representation of results is limited to two extreme cases with Aspect Ratios (AR) of 1.0 and 2.0, respectively. Details of the experimental results of other cases can be found in Appendix C. Full discussion and observations of the test results are presented in Chapter 6.

5.2 Experimental measurements

5.2.1 Calculating dynamic properties from snap tests

The dynamic properties measured experimentally were the frequency of vibration

modes of the test models in horizontal (X) and vertical (Z) directions, and their respective damping ratios. Two methods were used to determine the vibration of frequencies of models in test directions. The first manual method depended on going through the LVDT (displacement) signals recorded by the data acquisition system and recording the times that corresponded to the maximum amplitudes. The difference between any two successive readings at maximum amplitude was taken as the value of the periodic time, τ, for this cycle (Figure 5.1). The average of n successive cycles, at least three, was considered as the periodic time, τ_{av}, of the structure vibration, from which the frequency of the structure, f, can be calculated as;

$$f = \frac{1}{\tau_{av}} \tag{5.1}$$

$$\tau_{av} = \frac{\tau_1 + \tau_2 + \ldots\ldots + \tau_n}{n} \tag{5.2}$$

Where;

f = natural (circular) vibration frequency;

τ_{av} = average period time of number of cycles

$\tau_1, \tau_2, \ldots \tau_n$ = period time of vibrations

n = the average period time of vibrations

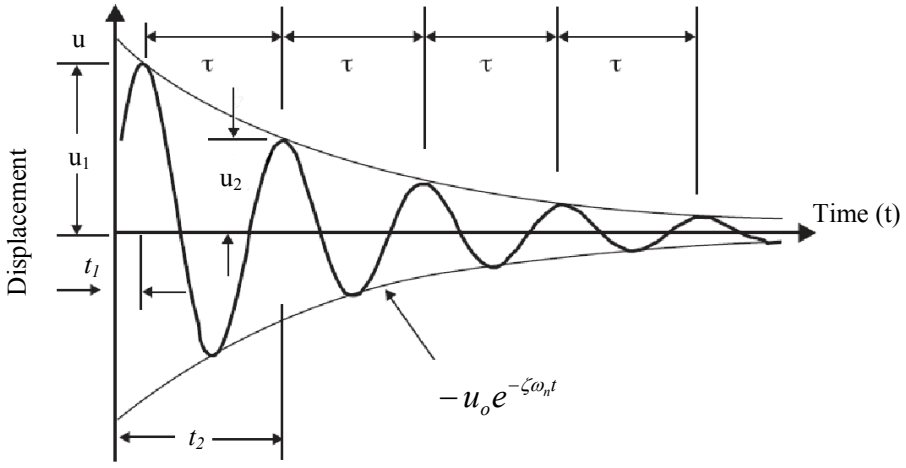

Figure 5. 1 Effect of damping on structure free vibration

The second method used to find the vibration frequencies of models was the power spectrum (PS) method. This method was based on using the Fast Fourier Transformation (FFT) technique to transform the resulted vibration signals from the time domain to the frequency domain using a computer program written by the author using MATLAB, see Appendix B. The FFT produced two pieces of information known as the magnitude (amplitude) and phase in polar coordinates. The square of the amplitude was calculated and the resulted plots were called the power spectrum, which presented the predominant vibration frequency of the model in the test direction.

The PS method was useful in finding frequencies of vibrations especially in cases where the maximum amplitudes were not easy to distinguish due to the interference of two waves or more or because of beating phenomenon, which occurs from the overlap of two waves with the same amplitude and different frequencies. Both manual and PS methods were used to determine the values of frequencies from experimental tests.

To calculate the damping ratio, the logarithmic decrement method was used (Smith, 1988). This method depended on measuring the rate of decay in the structure's free vibration due to the effect of damping as shown in Figure 5.1.

The free displacement vibrations of any structure caused by the snap (initial displacement) test can be predicted at any time, t, using the following equation:

$$u = u_o e^{-\xi\omega_n t} \sin\left(\omega_n \sqrt{1-\xi^2} + \varphi\right) \qquad (5.3)$$

where;

u = the displacement of the structure at any time during vibration

ξ= the damping ratio

ω_n= the natural frequency of the structure

u_o and φ = arbitrary constants, whose values depend on the initial boundary conditions.

In Figure 5.1, decay in any two successive amplitudes can be calculated as follows;

$$\delta = \ln \frac{u_1}{u_2} \tag{5.4}$$

where

δ= the natural logarithmic decrement

u_1 and u_2= Any two successive values of amplitudes which can be determined by substitution in Equation 5.3 at time t_1 and $t_{1+\tau}$.

The values of u_1 and u_2 can be determined from experimental tests by recording the maximum amplitudes of displacement. It is also possible to use any two amplitudes but their rank should be known, so Equation 5.5 can be used to find the value of the logarithmic decay, δ, for any u_i and u_{i+n} amplitudes;

$$\delta = \frac{1}{n} \ln \frac{u_i}{u_{i+n}} \tag{5.5}$$

The damping ratio ζ can be determined according to Smith (1988) by applying Equation 5.6 as follows;

$$\xi = \frac{\delta}{\sqrt{4\pi^2 + \delta^2}} \tag{5.6}$$

However, the value of the structure's damping, C, can be calculated from Equation 5.7 as follows;

$$C = 2m\xi\omega_n \tag{5.7}$$

Where

C= value of damping in test structure

m= mass of the structure

ξ= damping ratio

ω_n= the circular frequency of the structure

The above equation shows that the damping value, C, depends on the damping ratio, ζ,

the total mass of the structure, m, and the circular frequency of the structure, ω_n, measured from experimental tests by applying the following equation;

$$\omega_n = 2\pi f \tag{5.8}$$

5.2.2 Responses under shaking table vibration

Shaking table tests were used to evaluate the lateral displacement response of models in addition to studying the changes in the distribution of forces in space frame members at various locations. Figure 5.2 presents the locations of LVDTs used to measure the displacement response and the members equipped with strain gauges to study the effect of composite action on the distribution of forces in test space frames.

The displacement, velocity and acceleration time history applied by using the manufactured shaking table are shown in Figures 4.22 to 4.24 in Chapter 4.

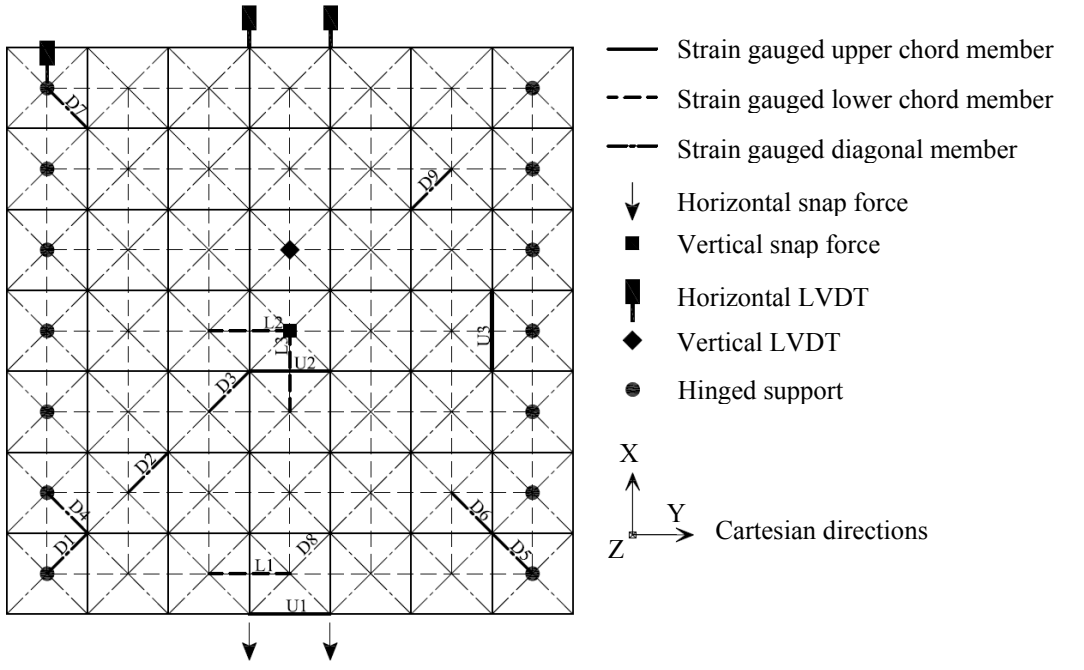

Figure 5.2 Layout of experimental test models and behaviour measurement devices

5.3 Experimental results of space frame models with aspect ratio 1.0

5.3.1 Corner-supported models

The following results are for snap and shaking table tests carried out on corner-supported models, Truss A, B and C, with AR = 1.0.

I. Results of vertical snap tests

Three groups of four vertical snap tests were carried out to determine the vibration frequency of test models in the vertical Z-direction. The tests included the application of a vertical load at the lower central point of models followed by the sudden release of the load and monitoring of the structure's free vibration. This method was used to determine the structural dynamic properties using experimental means.

Two cases were considered, for which the centres of lead masses were concentric and eccentric relative to the centres of upper joints, respectively. The latter case was considered to represent the case with a top composite deck where the deck's mass was at the higher level relative to the top joints. Table 5.1 presents the closest three results of free vibration tests carried out on non-composite model for both cases of concentric and eccentric mass positions. Results of vertical snap tests conducted on non-composite Truss A are shown in Figures 5.3 and 5.4. As can be seen in Figure 5.3, there was a quick reduction in the amplitude in case of concentric masses followed by an increase of the amplitude. This trend was thought to be a result of the interference of two modes of vibrations.

Table 5.1 Results of vertical snap tests on corner-supported Truss A

	Concentric masses		**Eccentric masses**	
	Frequency (f) Hz	Damping ratio (ζ)	Frequency (f)	Damping ratio (ζ)
Test 1	17.99	2.51%	20.00	2.85%
Test 2	18.59	2.42%	18.52	2.37%
Test 3	18.38	2.51%	18.60	2.66%
Average	**18.45**	**2.45%**	**18.85**	**2.68%**

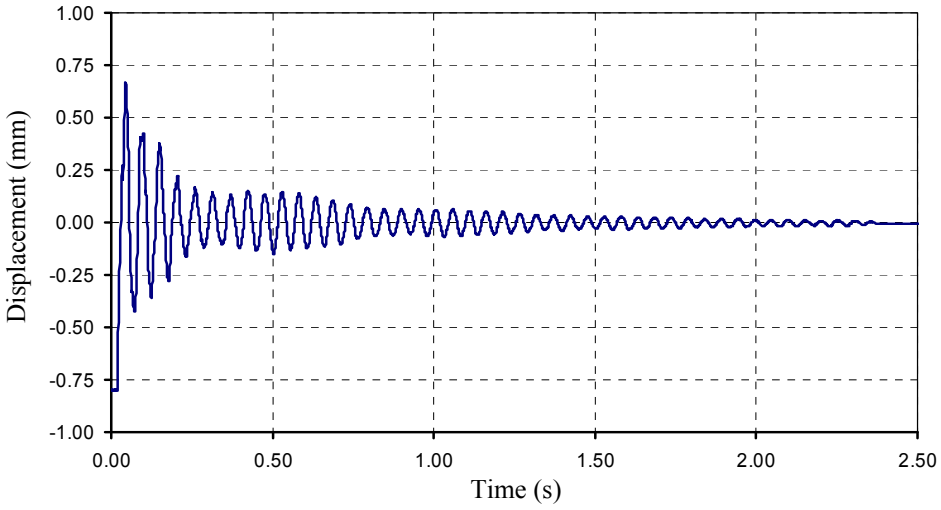

Figure 5.3 Vertical displacement at the middle point of Truss A with concentric masses during the vertical snap test

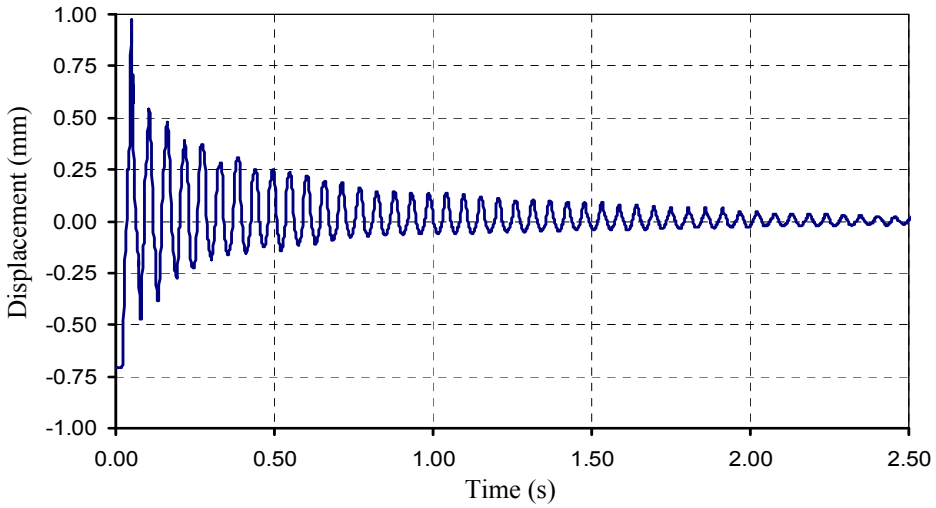

Figure 5.4 Vertical displacement at the middle point of Truss A with eccentric masses during the vertical snap test

The results of the vertical snap test carried out on composite corner-supported Trusses B and C are shown in Table 5.2. Figures 5.5 and 5.6 present the vertical displacement of corner-supported Trusses B and C, respectively, during the test. As observed from Figures 5.5 and 5.6, there was a lower rate of decay in vertical displacement compared to non-composite Truss A, which can be explained by the large increase of models'

stiffness by the introduction of composite action leading to a reduction in the vertical damping of composite models.

Table 5.2 Results of vertical snap tests on corner-supported Trusses B and C

	Truss B		**Truss C**	
	Frequency (f) Hz	Damping ratio (ζ)	Frequency (f)	Damping ratio (ζ)
Test 1	20.24	0.60%	19.29	1.53%
Test 2	20.04	0.70%	19.35	1.50%
Test 3	20.09	0.71%	19.29	1.53%
Average	**20.10**	**0.72%**	**19.29**	**1.52%**

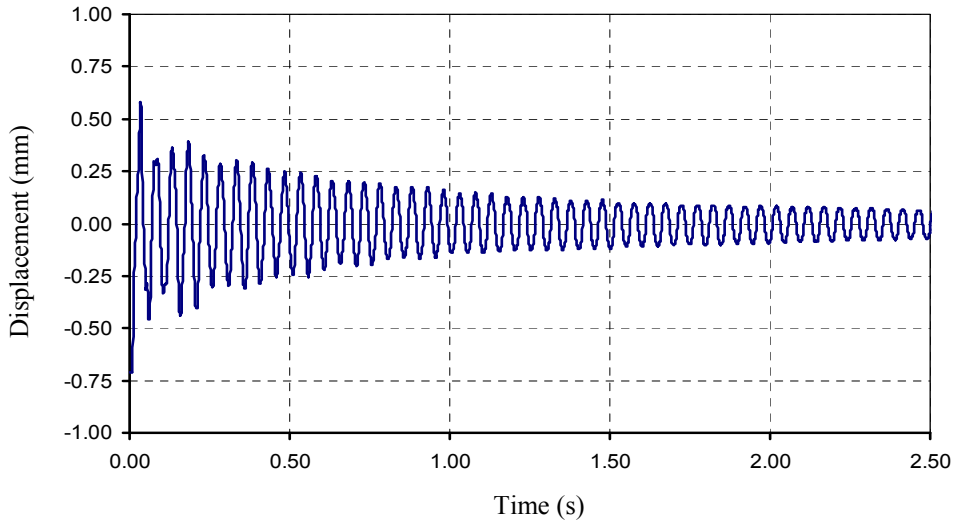

Figure 5.5 Vertical displacement results of Truss B during vertical snap test

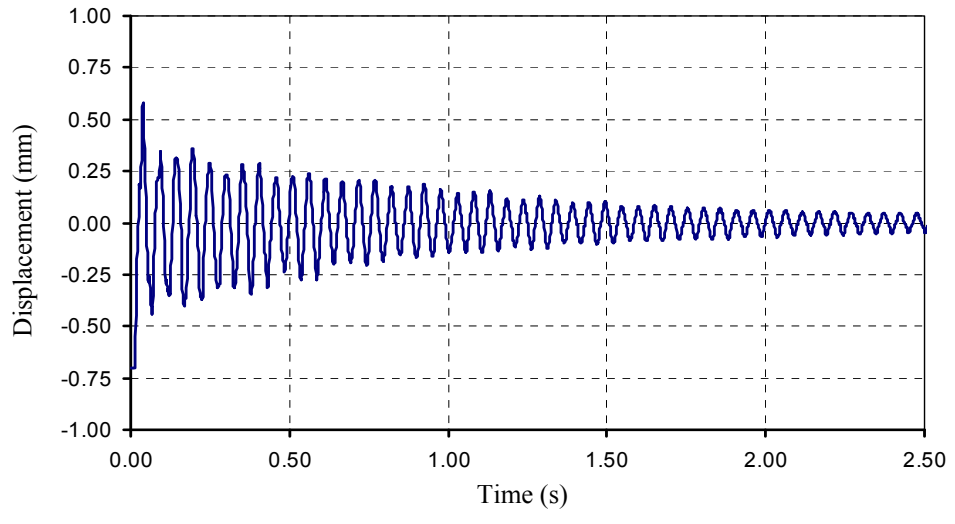

Figure 5.6 Vertical displacement results of model Truss C during vertical snap test

II. Results of horizontal snap tests

Four tests were carried out on non-composite Truss A to measure its frequency of vibration in the horizontal X-direction. The tests were conducted with both eccentric and concentric masses. Average values of displacement response as obtained from the two horizontal transducers were recorded, and results are shown in Table 5.3. The displacement results during the free vibration test results are shown in Figures 5.7 and 5.8. A rapid deterioration of displacement response was noticed with both cases of Truss A followed by an increase in the response, which was thought to be caused by the interference of two vibration modes. Table 5.4 further presents the vibration frequencies and damping ratios of composite space frames, Trusses B and C. The results of the horizontal snap test on both composite Trusses B and C are shown in Figures 5.9 and 5.10, respectively.

Table 5.3 Results of horizontal snap tests on corner-supported Truss A

	Concentric masses		**Eccentric masses**	
	Frequency (f) Hz	Damping ratio (ζ)	Frequency (f)Hz	Damping ratio (ζ)
Test 1	18.38	2.33%	19.80	3.35%
Test 2	17.99	2.51%	18.78	3.18%
Test 3	18.59	2.51%	21.19	4.64%
Average	**18.45**	**2.45%**	**20.93**	**4.24%**

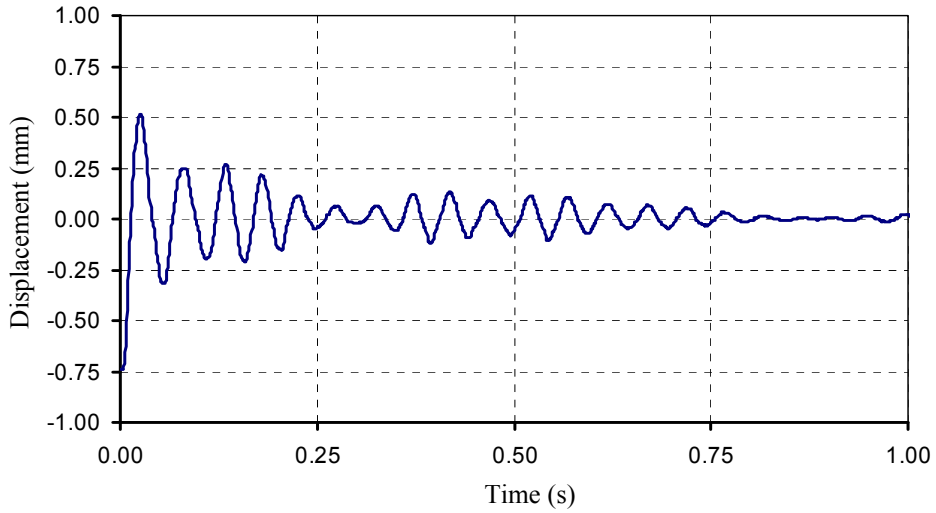

Figure 5.7 Horizontal displacement of Truss A with concentric masses during horizontal snap test

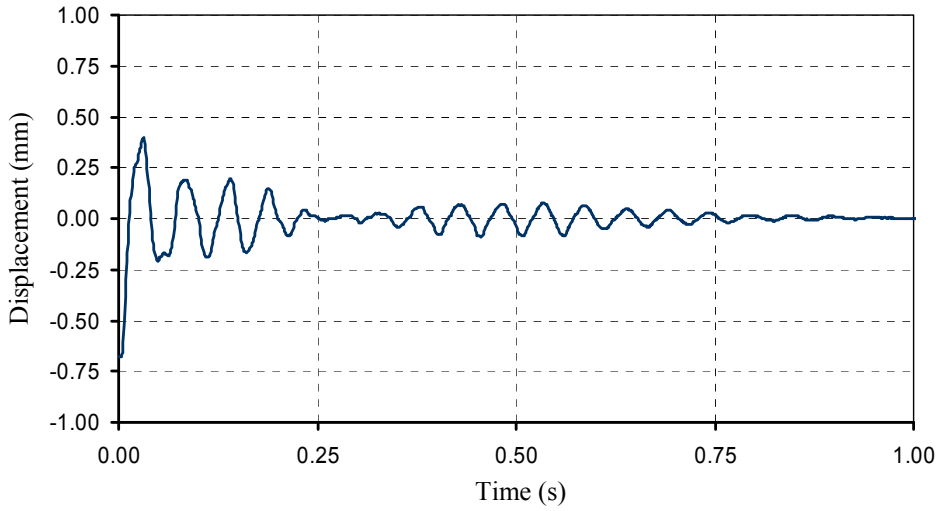

Figure 5.8 Horizontal displacement of Truss A with eccentric masses during horizontal snap test

Table 5.4 Results of horizontal snap tests on corner-supported Trusses B and C

	Truss B		**Truss C**	
	Frequency (f) Hz	Damping ratio (ζ)	Frequency (f)	Damping ratio (ζ)
Test 1	28.57	2.27%	28.59	5.39%
Test 2	29.76	2.46%	28.68	4.59%
Test 3	29.97	2.56%	27.62	5.31%
Average	29.43	2.43%	28.55	5.28%

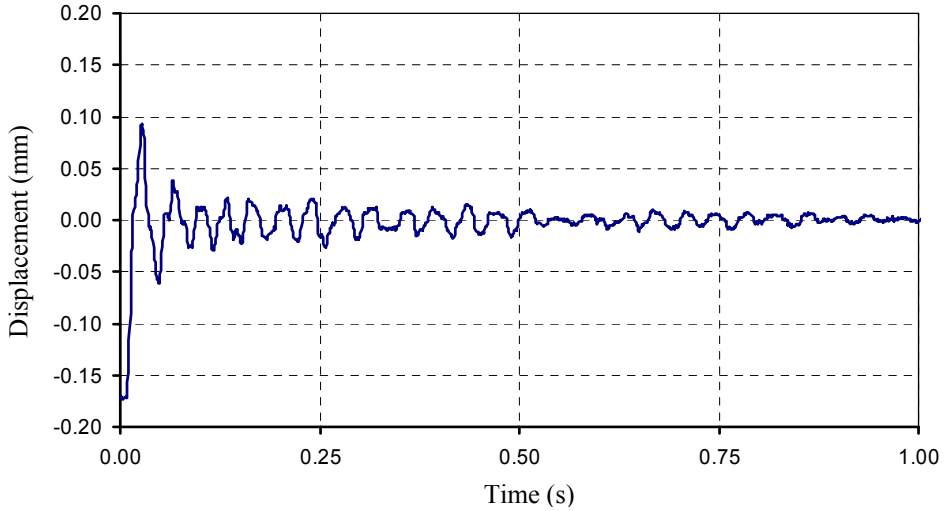

Figure 5.9 Horizontal displacement of Truss B during horizontal snap test

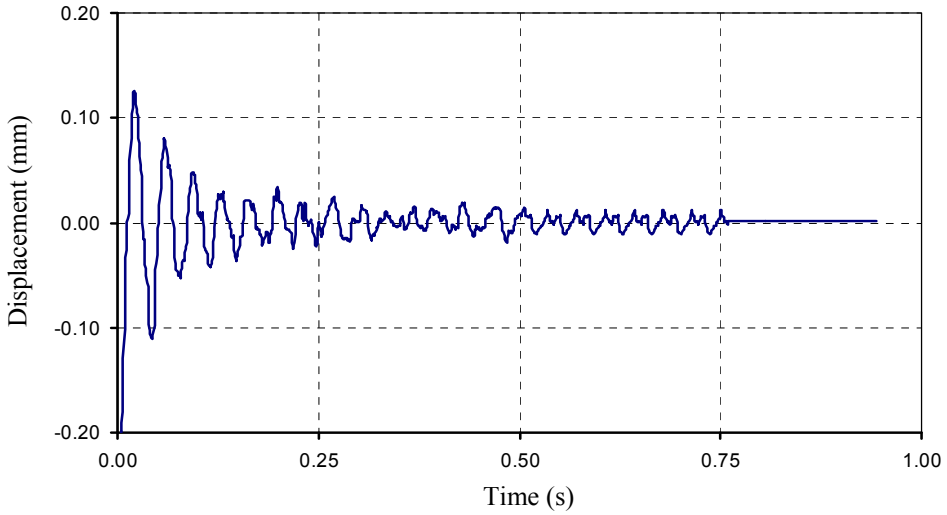

Figure 5.10 Horizontal displacement of Truss C during horizontal snap test

III. Results of shaking table tests

Shaking table tests were carried out on all models to determine their maximum lateral displacements in addition to the changes in the internal forces of a number of selected members. Figure 5.11 shows the horizontal displacement of the non-composite Truss A and the displacements that occurred at supports, which could not be avoided in the test setup due to the need for clearance in support cylinders. The net displacement results are shown in Figure 5.12, while values of the maximum lateral displacements are presented in Table 5.5 for all models.

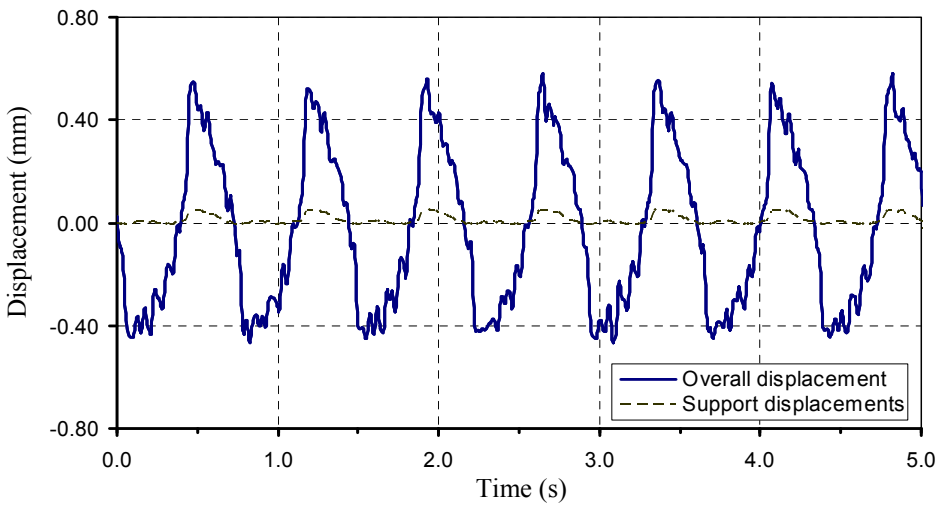

Figure 5.11 The lateral displacement of Truss A with support displacement

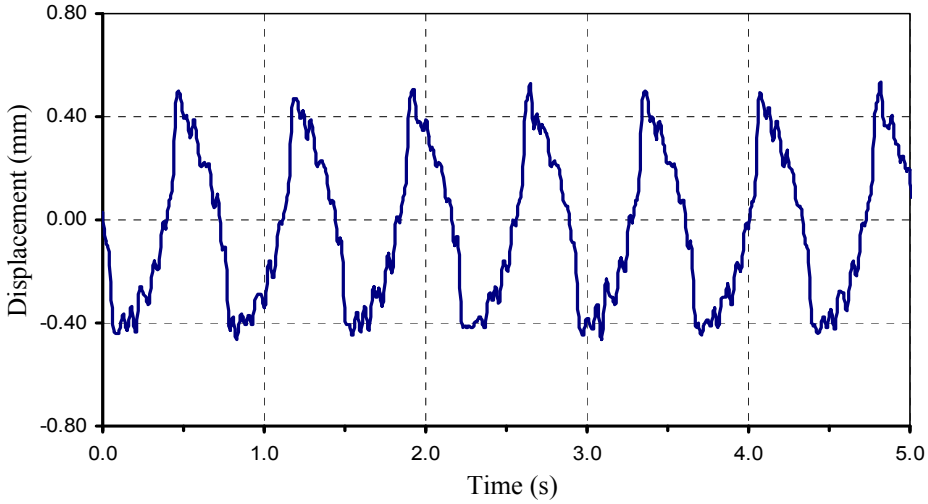

Figure 5.12 Net lateral displacement of Truss A under shaking table vibrations

Shaking table tests were also carried out on composite Trusses B and C and the displacement responses were as shown in Figures 5.13 to 5.16 including Figures.5.14 and 5.16, which present the net displacements of the two models.

The positive sign indicates the displacements occurred in positive X-direction while the negative sign implies the negative X-direction.

Table 5.5 Maximum and minimum displacement of corner-supported models

	Truss A	**Truss B**	**Truss C**
Max. displacement	0.543	0.276	0.281
Min. displacement	-0.439	-0.171	-0.211

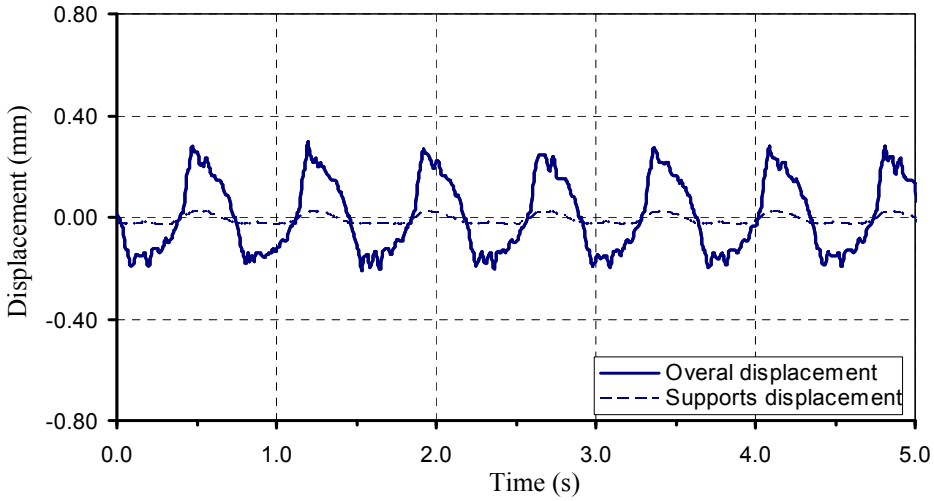

Figure 5.13 The lateral displacement of Truss B with support displacement

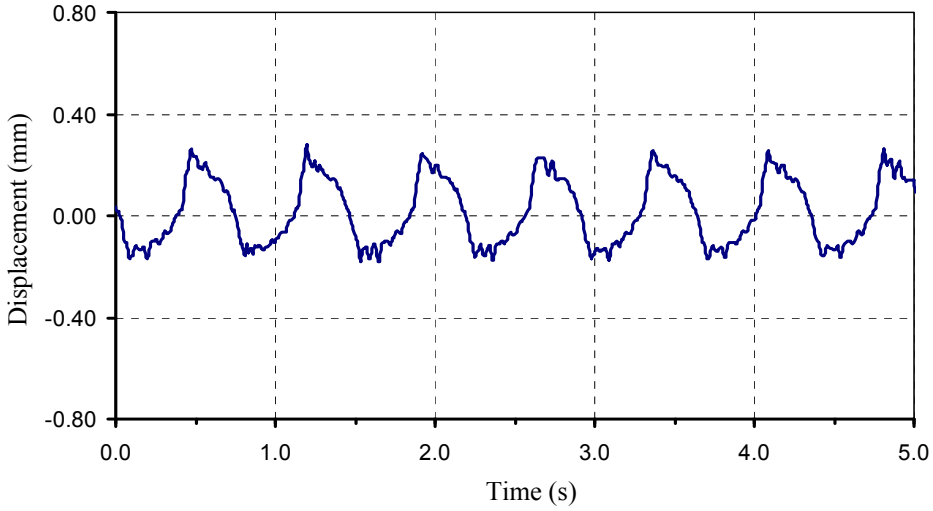

Figure 5.14 Net displacement of Truss B under shaking table vibrations

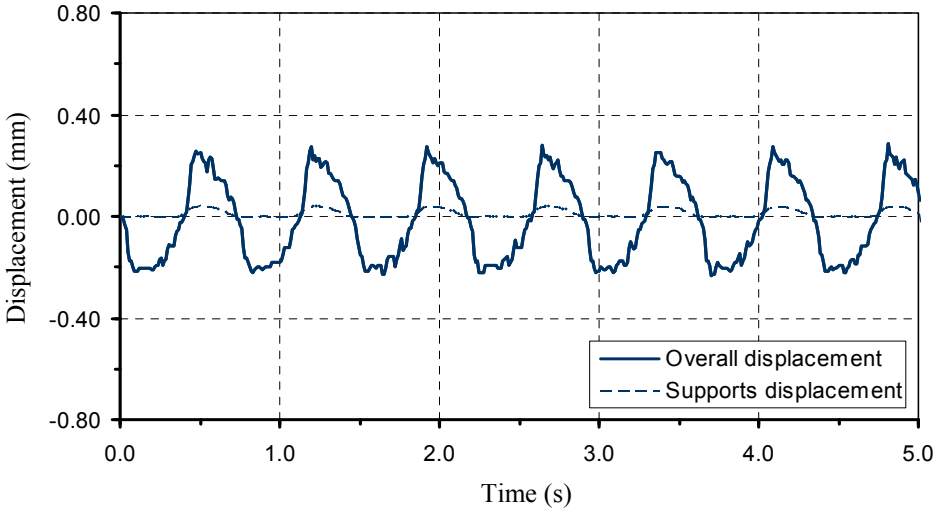

Figure 5.15 The lateral displacement of Truss C with support displacements

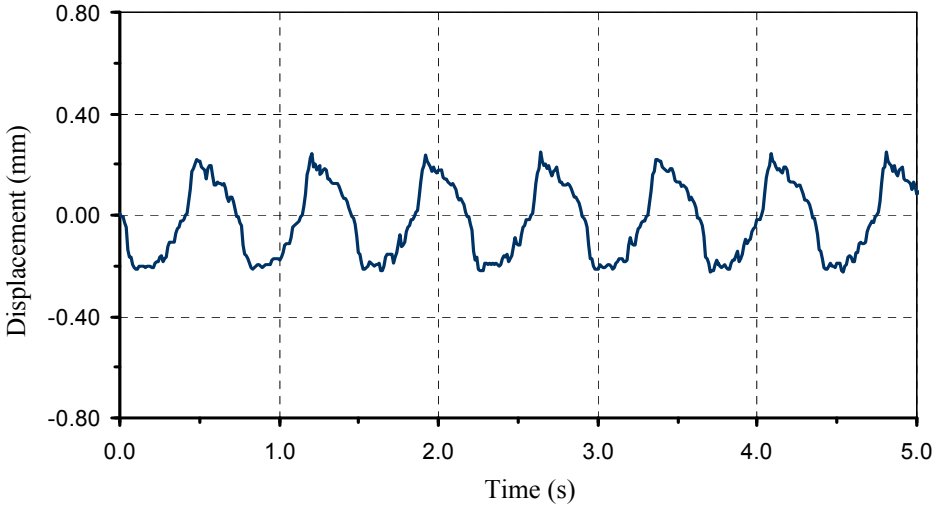

Figure 5.16 Net displacement of composite Truss C under shaking table vibrations

The effect of composite action was clear in reducing the lateral displacement responses of composite Trusses B and C by about 50-55%.

The distribution of internal forces in a number of selected members (presented in Figure 5.2) in the three test models are shown in Figure 5.17 in the form of micro-strains. Only diagonal and lower chord members were selected for comparison since the application of composite action resulted in high reduction of the forces in upper chords, which turned to zero in some members. The values shown in Figure 5.17 were the maximum absolute values of strain produced by the applied shaking table time history.

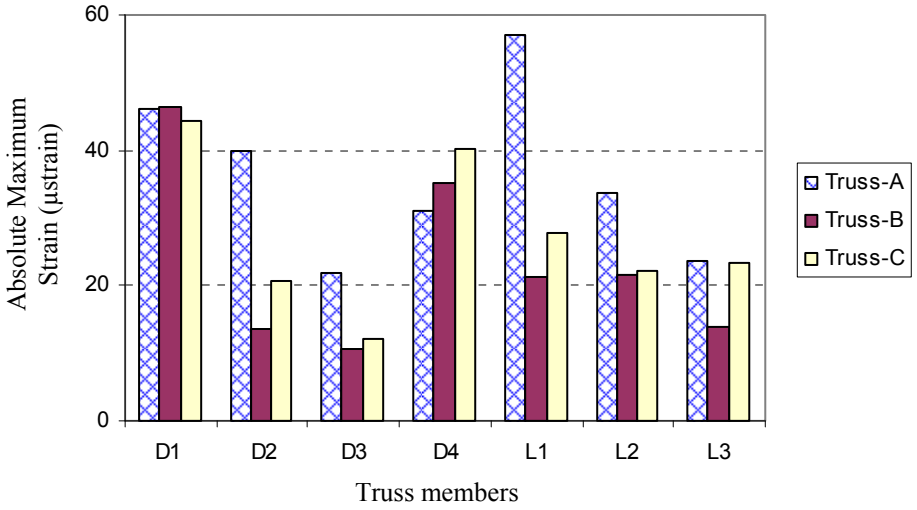

Figure 5.17 Absolute maximum strains in a number of diagonal and lower chord members in Trusses A, B and C

As can be noticed in Figure 5.17, the introduction of composite action resulted in an increase of forces in diagonal members around the corners and along the edges. On the other hand, there was a considerable reduction in the internal forces in diagonal and lower chord members located at the middle region such as D2, D3, and L2 and L3.

5.3.2 Results of two-edge-supported models

A group of tests were carried out on square (AR=1.0) non-composite and composite space frame models supported along the two lower edges parallel to the vibration direction. The results of these tests are introduced in the following sections.

I. Results of vertical snap tests

The average results of the two cases of concentric and eccentric masses connected to the non-composite Truss A are given in Table 5.6. Figures 5.18 and 5.19 show results of the vertical snap tests carried out on the same model with concentric and eccentric masses, respectively. The vertical snap test results of composite Trusses B and C, are shown in Figures 5.20 and 5.21, respectively, while Table 5.7 introduces the vibration frequencies of composite Trusses B and C.

Table 5.6 Results of vertical snap tests on two-edge-supported Truss A

	Concentric masses		**Eccentric (Inverted) masses**	
	Frequency (f) Hz	Damping ratio (ζ)	Frequency (f)	Damping ratio (ζ)
Test 1	25.67	4.97%	25.51	6.34%
Test 2	27.78	5.27%	25.64	6.51%
Test 3	27.78	5.80%	25.64	6.68%
Average	**27.41**	**5.35%**	**25.60**	**6.51%**

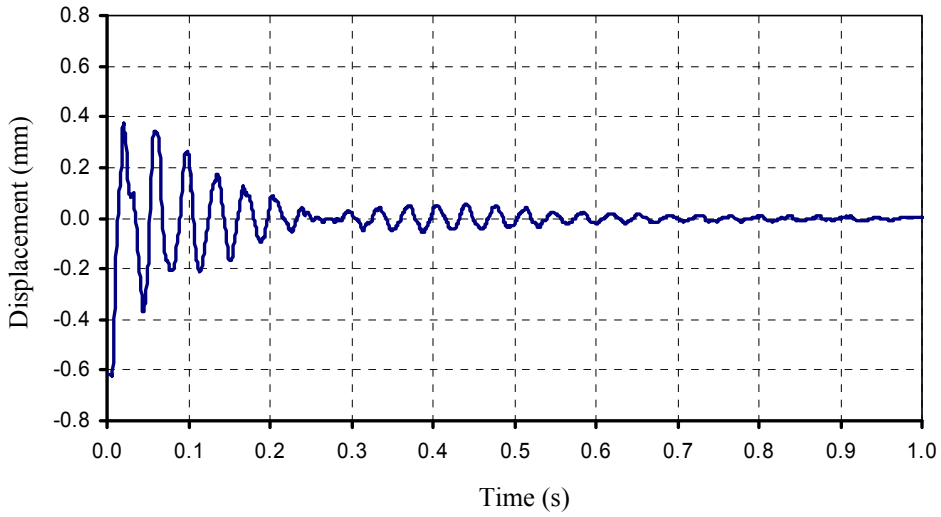

Figure 5.18 Vertical displacement of Truss A with concentric masses during vertical snap test

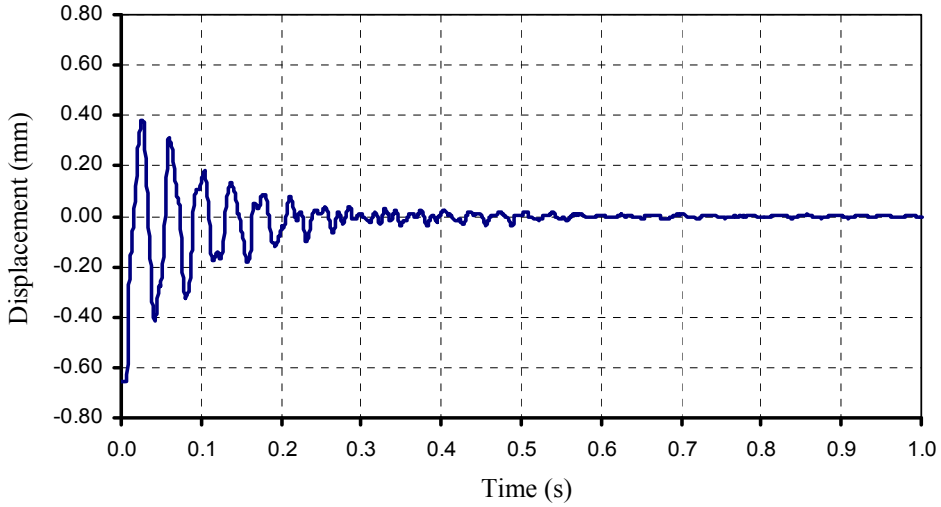

Figure 5.19 Vertical displacement of Truss A with eccentric masses during vertical snap test

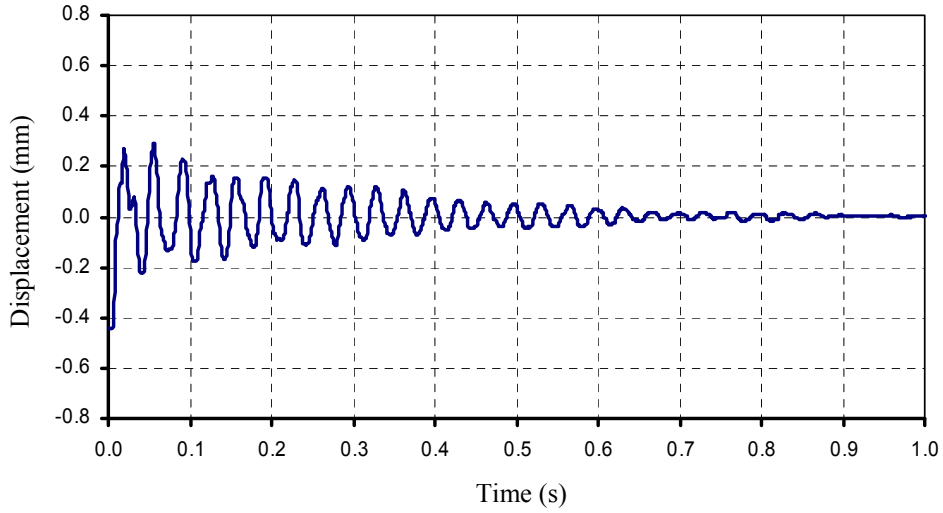

Figure 5.20 Vertical displacement of two-edge-supported Truss B during vertical snap test

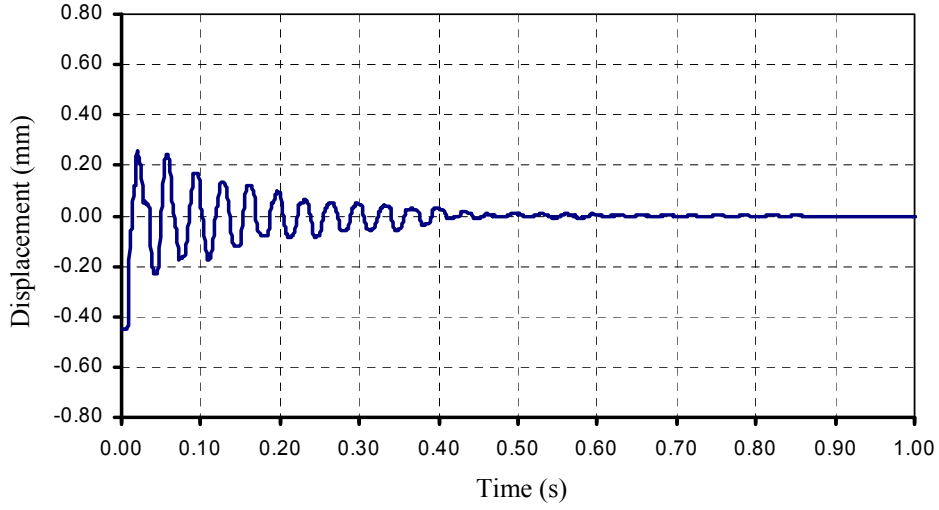

Figure 5.21 Vertical displacement of two-edge-supported Truss C during vertical snap test

Table 5.7 Results of vertical snap tests of two-edge-supported Trusses B and C

	Truss B		Truss C	
	Frequency (f) Hz	Damping ratio (ζ)	Frequency (f)	Damping ratio (ζ)
Test 1	29.13	1.80%	29.13	3.71%
Test 2	29.27	1.70%	29.13	3.70%
Test 3	29.27	1.90%	29.21	3.60%
Average	**29.22**	**1.72%**	**29.20**	**3.63%**

As can be seen from Figures 5.18 and 5.19, fast decay was observed for non-composite Truss A with both cases of eccentric and concentric mass connectivity. On the other hand, the introduction of composite action led to a noticeable reduction in the damping ratio which ranged between 73.6% to 44.2% for Trusses B and C, respectively.

II. Results of horizontal snap tests

Another group of tests were carried out on the three non-composite and composite models to determine their frequencies in the direction parallel to the two supported edges (X-direction). Table 5.8 presents values of horizontal vibration frequencies and damping ratios of Truss A with concentric and eccentric masses. Figures 5.22 and 5.23 present the horizontal snap tests results of non-composite Truss A for both cases, respectively. The results of the horizontal snap tests conducted on composite Trusses B, C are shown in Figures 5.24 and 5.25, respectively, while their vibration frequencies and damping ratios are listed in Table 5.9.

There were difficulties in calculating the horizontal vibration frequencies due to the rapid decay of vibration in composite models. The rapid decay was though to be caused by the high damping ratios due to the high friction between the decks and the top joints. Furthermore, the overlap of vibration modes was thought to be another factor in the rapid decay experienced. The use of the power spectrum (PS) method beside the manual method helped in determining the frequency of vibration in the horizontal direction.

Table 5.8 Results of horizontal snap tests on two-edge-supported Truss A

	Concentric masses		Eccentric (Inverted) masses	
	Frequency (f) Hz	Damping ratio (ζ)	Frequency (f)	Damping ratio (ζ)
Test 1	20.49	6.71%	21.51	18.65 %
Test 2	20.16	6.97%	20.69	21.89 %
Test 3	20.33	6.24%	22.19	13.43 %
Average	**20.33**	**6.64%**	**21.46**	**17.99%**

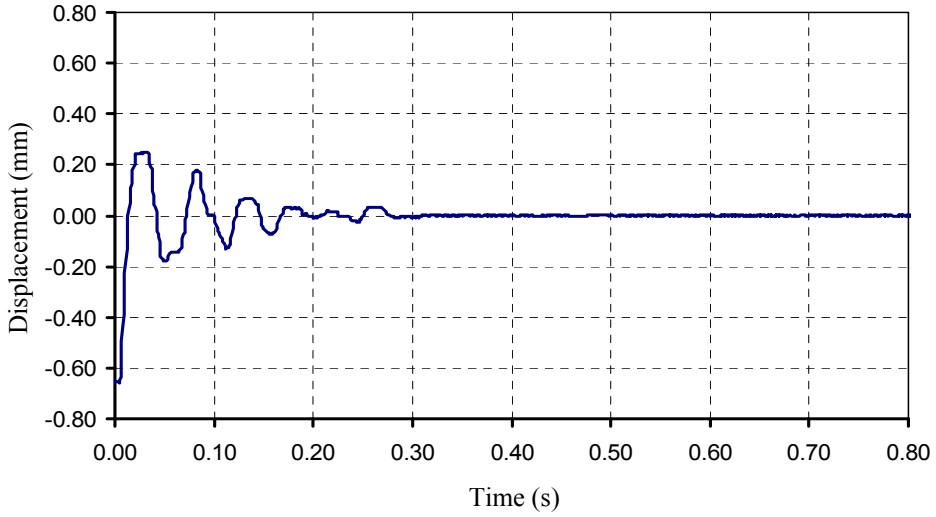

Figure 5.22 Horizontal snap test results of Truss A with concentric masses during horizontal snap test

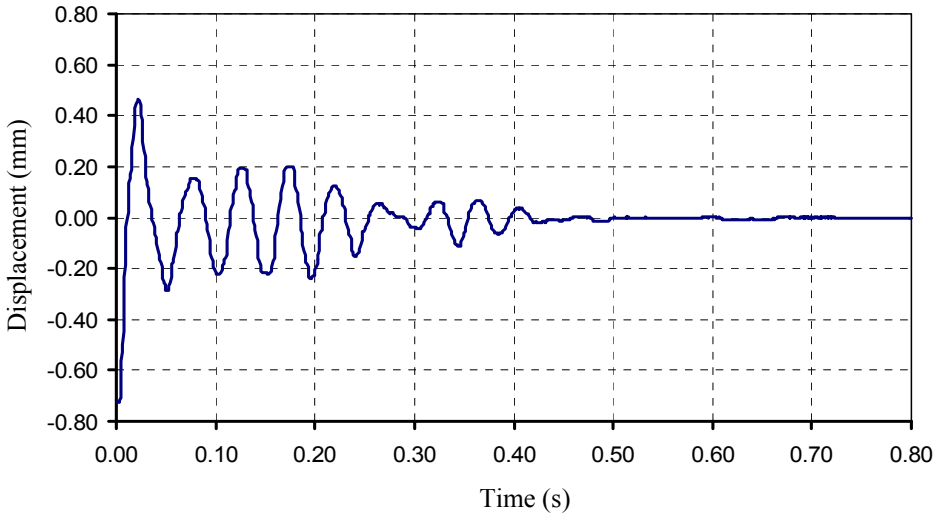

Figure 5.23 Horizontal displacement of Truss A with eccentric masses during horizontal snap test

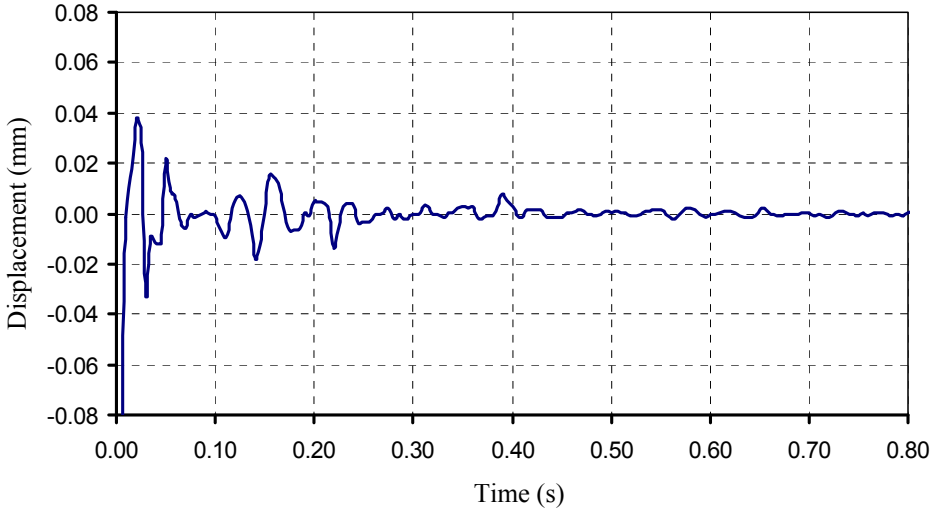

Figure 5.24 Horizontal displacement of Truss B during horizontal snap test

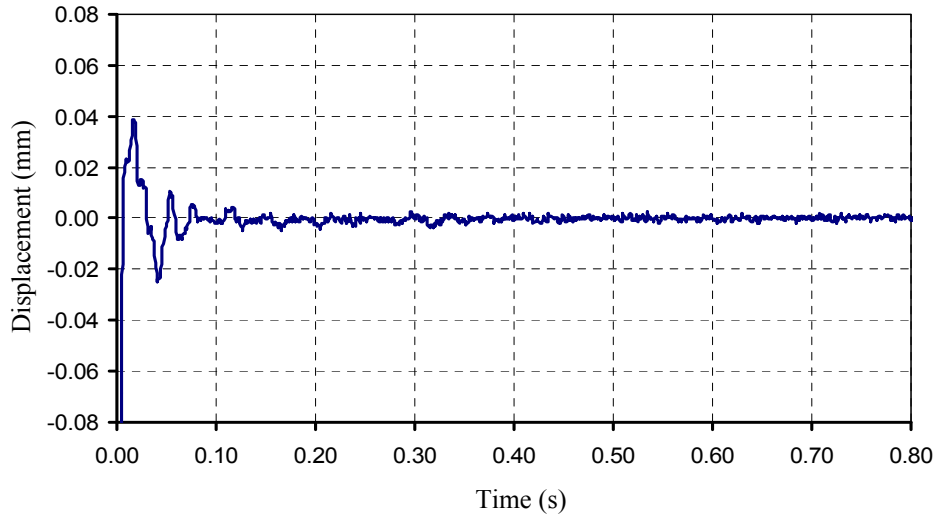

Figure 5.25 Horizontal displacement of Truss C during horizontal snap test

Table 5.9 Results of horizontal snap tests of two-edge-supported Trusses B and C

	Truss B		**Truss C**	
	Frequency (f) Hz	Damping ratio (ζ)	Frequency (f) Hz	Damping ratio (ζ)
Test 1	39.43	2.41%	27.78	6.72%
Test 2	36.04	1.89%	23.81	13.35%
Test 3	36.78	1.54%	25.00	15.18%
Average	**37.42**	**1.95%**	**35.96**	**11.75%**

III. Results of shaking table tests

The horizontal displacement response of non-composite Truss A with two-edge supports is shown in Figure 5.26. It is worth mentioning that support movements were ignored in these tests due to their small values. The values of maximum and minimum displacements recorded in the vibration direction are listed in Table 5.10. Figures 5.27 and 5.28 present the displacement responses of composite Trusses B and C, respectively.

The distribution of internal forces in a number of selected diagonal and lower chord members, shown in Figure 5.2, under shaking table vibrations are presented in Figure 5.29 in the form of micro-strains.

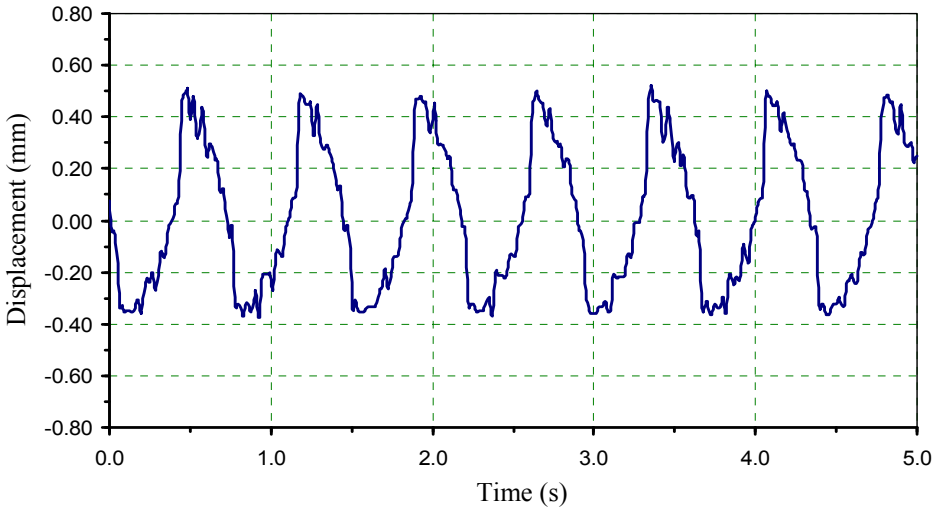

Figure 5.26 Displacement of two-edge-supported Truss A during shaking table tests

Table 5.10 Maximum and minimum displacement of two-edge-supported models

	Truss A	**Truss B**	**Truss C**
Max. displacement (mm)	0.511	0.222	0.229
Min. displacement (mm)	-0.366	-0.126	-0.204

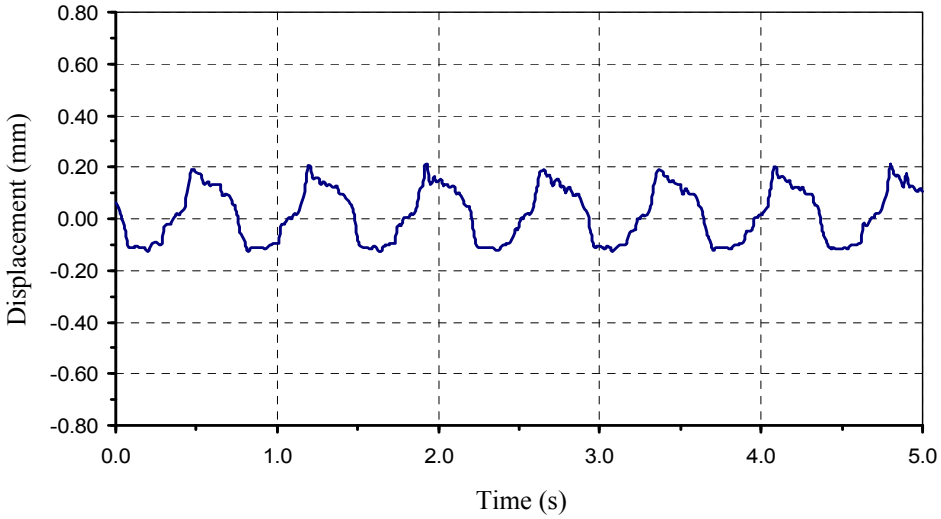

Figure 5.27 Displacement of two-edges supported model Truss B under shaking table vibrations

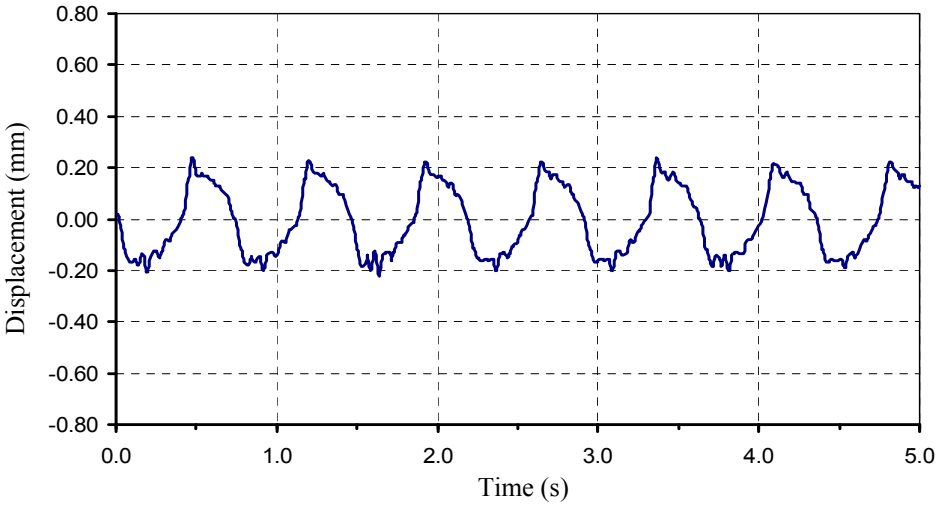

Figure 5.28 Displacement responses of two-edges supported model Truss C under shaking table vibrations

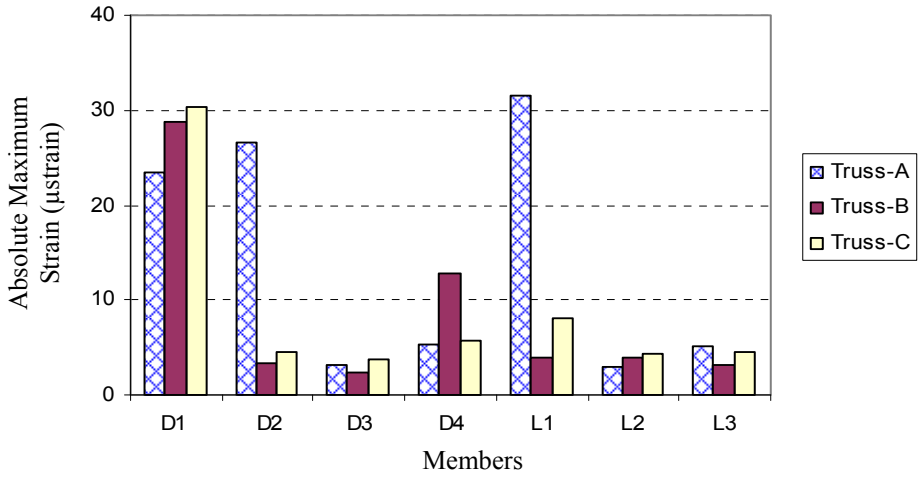

Figure 5.29 Absolute maximum strains in a number of diagonal and lower chord members in two-edge-supported Trusses A, B and C

There was a reduction in the lateral displacements observed by the introduction of composite action to space frames, which reached about 56%. Furthermore, there was an increase of internal forces in diagonal members at corners and edges, while there was a reduction of forces in the diagonal members at the middle regions (Figure 5.29). For lower chord members, there was a considerable reduction of internal forces in the lower chords at the edges perpendicular to the vibration direction while a slight increase was observed in the lower chords at the middle region (Figure 5.29).

5.4 Experimental results of space frame models with aspect ratio of 2.0

Three panels were removed from one side of all three models, Truss A, B and C, to leave only three panels in the X-direction. In the other direction, Y-direction, all models kept the same number of panels. Vertical and horizontal snap tests were carried out on models to determine the values of damping ratios and vibration frequencies in test directions. Shaking table tests were conducted on models to determine the maximum and minimum lateral displacements in addition to the axial forces in previously selected members. Results of tests on all models under the two support conditions, corner and two-edge supports, are presented in the following sections

5.4.1 Results of corner-supported models

This section covers the presentation of experimental results of the corner-supported models with aspect ratio = 2.0.

I. Vertical snap test results

Figure 5.30 presents the vertical snap test results of non-composite Truss A, while Figures 5.31 and 5.32 introduce the vertical snap test results for composite Trusses B and C, respectively. Values of frequencies and damping ratios of each case are listed in Table 5.11.

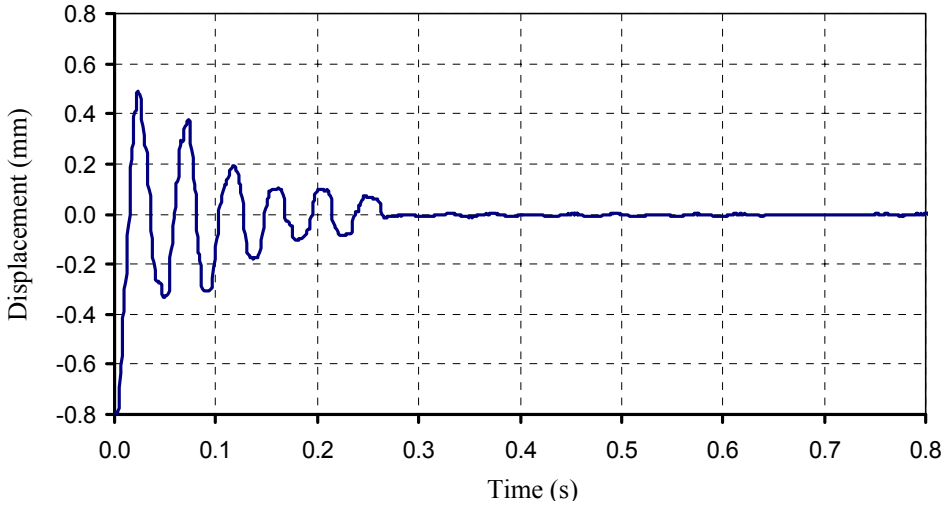

Figure 5.30 Vertical displacement of non-composite Truss A during vertical snap test

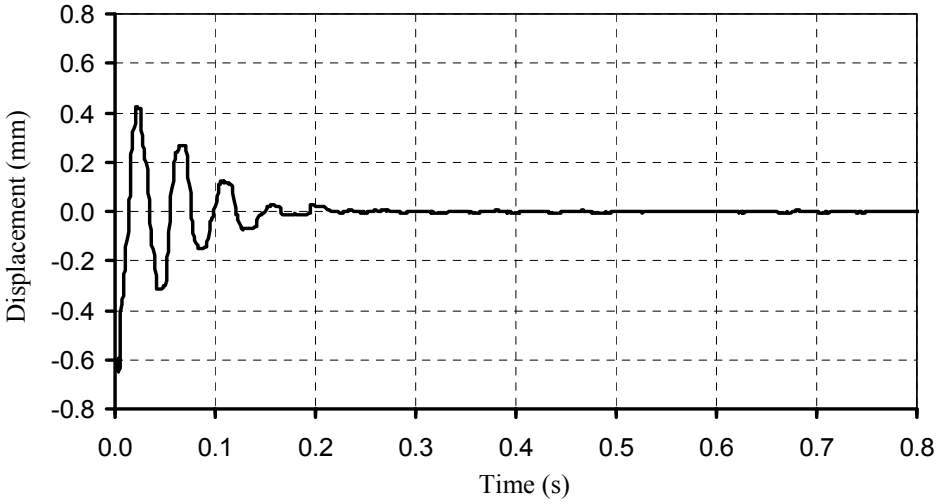

Figure 5.31 Vertical displacement of Truss B during vertical snap test

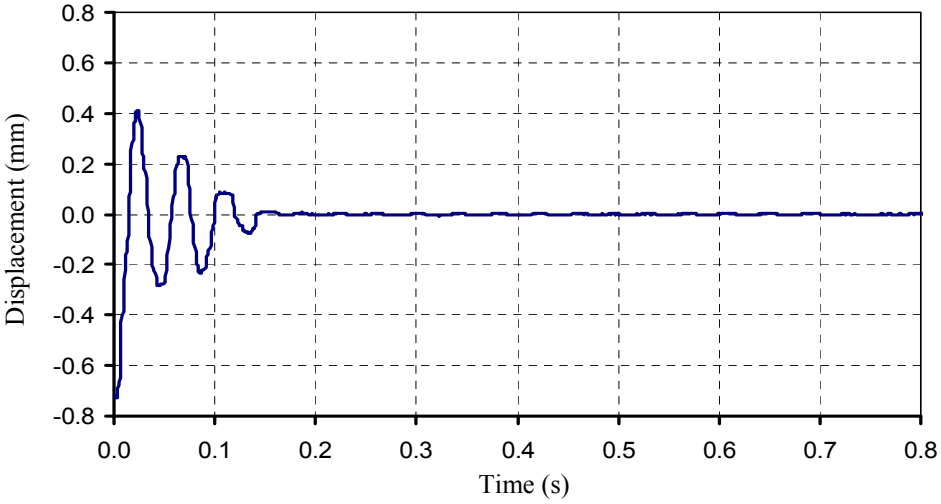

Figure 5.32 Vertical displacement of Truss C during vertical snap test

Table 5.11 Results of vertical snap tests on corner-supported models with AR=2.0

	Truss A		**Truss B**		**Truss C**	
	Freq. (f) Hz	Damping ratio (ζ)	Freq. (f) Hz	Damping ratio (ζ)	Freq. (f) Hz	Damping ratio (ζ)
Test 1	22.22	7.10%	22.06	10.02%	23.26	12.74%
Test 2	22.52	6.54%	22.06	9.43%	24.40	11.90%
Test 3	22.32	7.52%	22.73	9.37%	23.44	12.44%
Average	**22.36**	**7.05%**	**22.28**	**9.61%**	**23.69**	**12.36 %**

As can be seen from above figures and values of vibration frequencies and damping ratios in the above table, there was almost no change in the models' frequencies by the application of composite action. However, there was an increase in the damping ratio, which thought to be coming from the increase of the overall damping in the system.

II. Results of horizontal snap tests

To determine the frequency of vibration of corner-supported models with AR = 2.0 in X-direction, horizontal snap tests were carried out. Figure 5.33 presents displacement results of the non-composite Truss A during the horizontal snap test, however, Figures 5.34 and 5.35 present the results of composite space frames Trusses B and C, respectively. Values determined by horizontal snap tests are presented in Table 5.12.

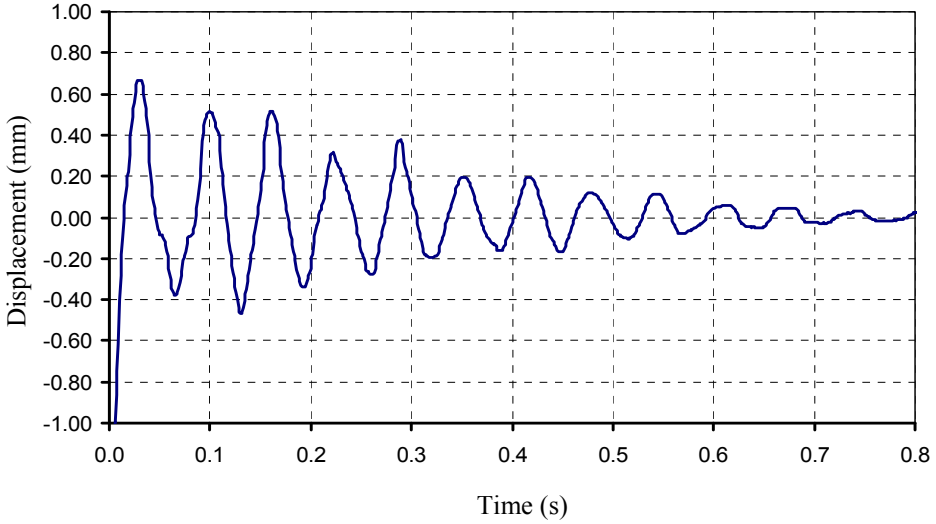

Figure 5.33 Horizontal displacement of Truss A during horizontal snap test

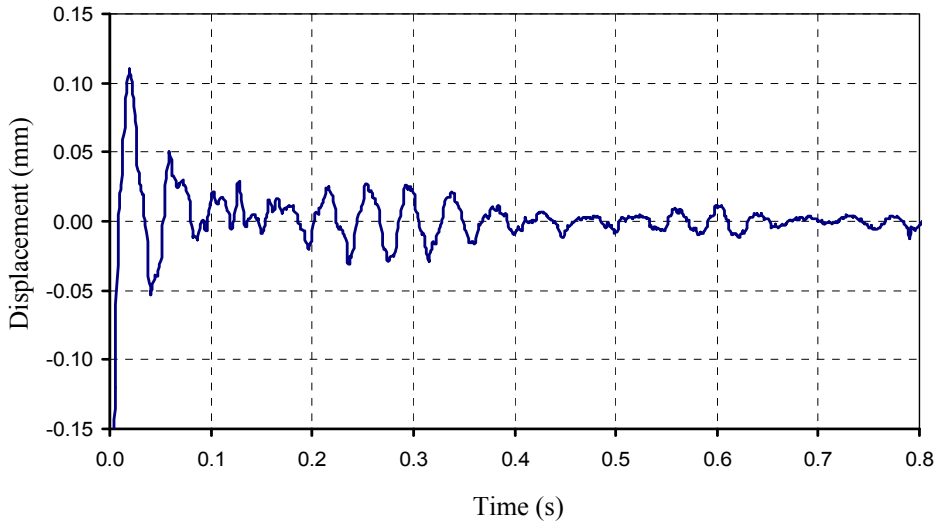

Figure 5.34 Horizontal displacement of composite Truss B during horizontal snap test

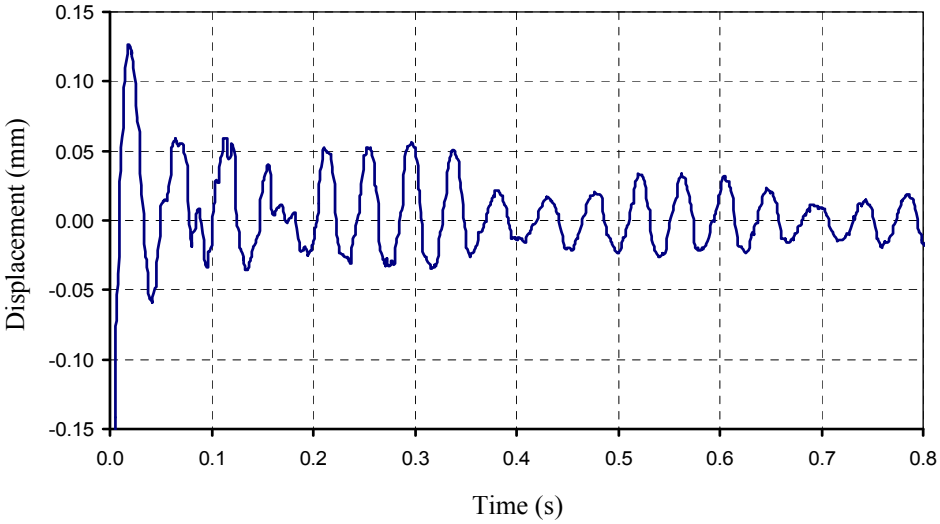

Figure 5.35 Horizontal displacement of composite Truss C during horizontal snap test

Table 5.12 Results of horizontal snap tests on corner-supported models with AR = 2.0

	Truss A		**Truss B**		**Truss C**	
	Freq. (f) Hz	Damping ratio (ζ)	Freq. (f) Hz	Damping ratio (ζ)	Freq. (f) Hz	Damping ratio (ζ)
Test 1	15.50	3.86 %	21.43	0.81 %	21.74	0.85 %
Test 2	15.63	3.90 %	21.82	0.76 %	21.66	0.78 %
Test 3	15.50	3.86 %	21.43	0.70 %	21.66	0.70 %
Average	**15.54**	**3.87%**	**21.56**	**0.76 %**	**21.69**	**0.78%**

III. Results of shaking table tests

Figure 5.36 presents the results of shaking table test conducted on Truss A, while results of the two composite Trusses B and Truss C are shown in Figures 5.37 and 5.38, respectively. The maximum and minimum lateral displacements to shaking table vibrations can be seen in Table 5.13.

A considerable reduction in the lateral displacement to shaking table vibrations was observed with composite models, which was about 60%.

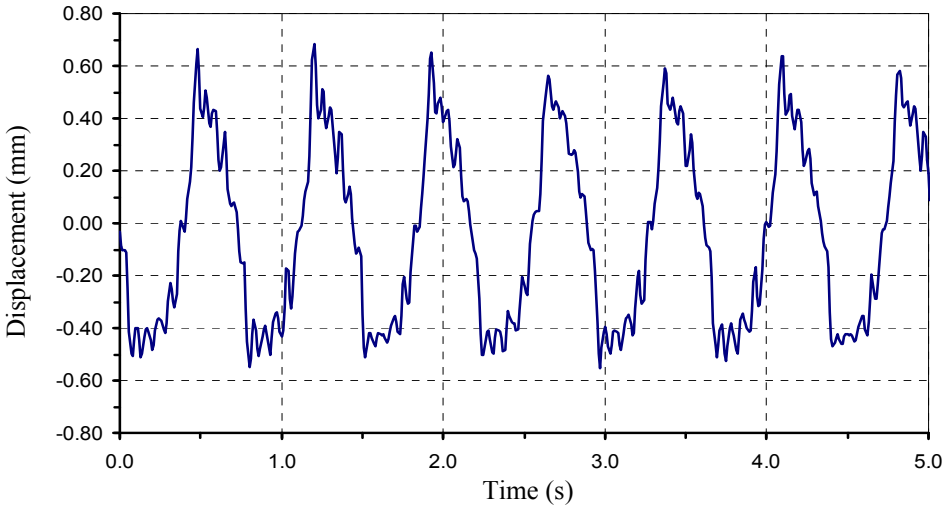

Figure 5.36 Displacement of corner-supported Truss A with AR = 2.0 during vibration test

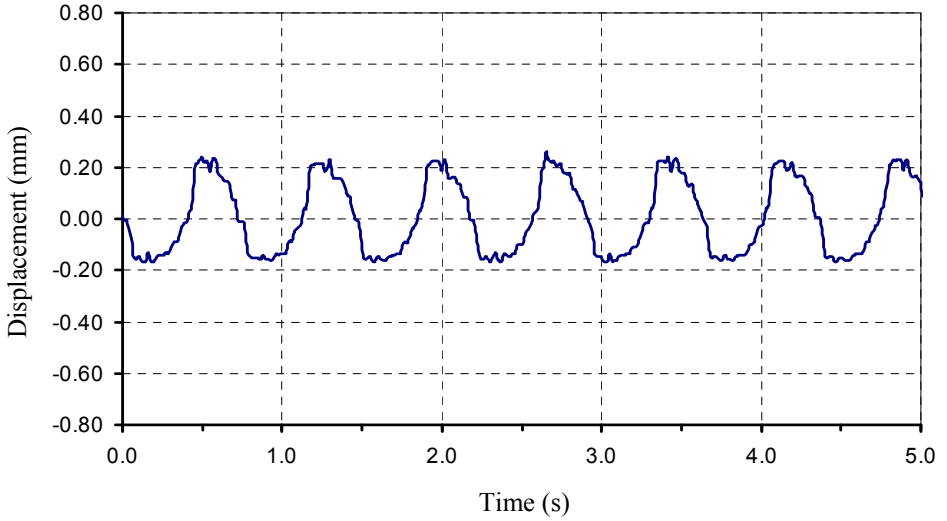

Figure 5.37 Displacement of corner-supported Truss B with AR = 2.0 during vibration test

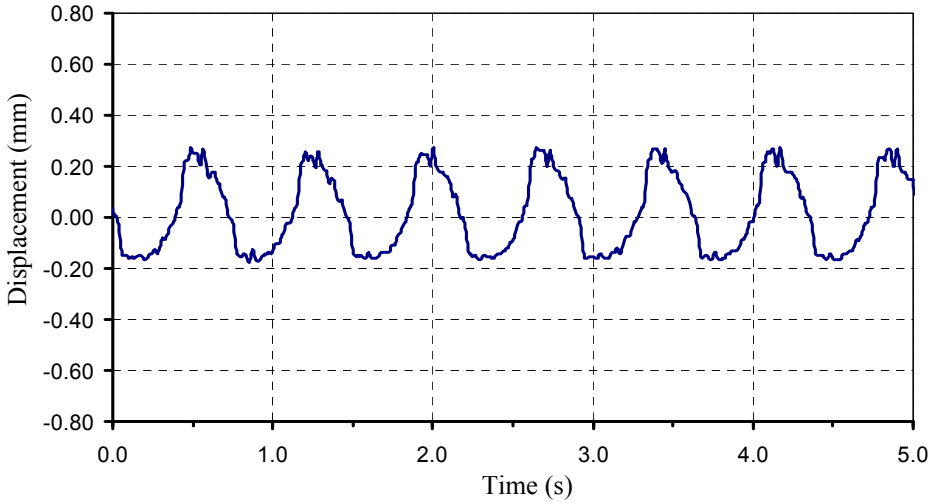

Figure 5.38 Displacement of corner-supported Truss C with AR = 2.0 during vibration test

Table 5.13 Maximum and minimum displacements of corner-supported models with AR = 2.0

	Truss A	**Truss B**	**Truss C**
Max. displacement (mm)	0.684	0.264	0.275
Min. displacement (mm)	-0.553	-0.170	-0.175

The distribution of internal forces in a number of selected diagonal and lower chord members is shown in Figure 5.39, which present the values of the internal forces the form of the absolute maximum strains.

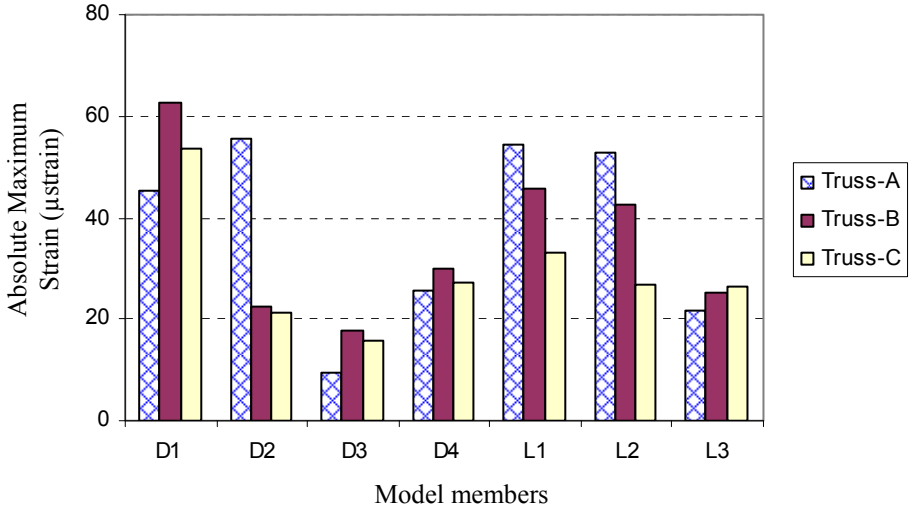

Figure 5.39 Member force distribution in corner-supported models with AR = 2.0 under shaking table vibrations

The effect of composite action was clear in increasing the forces in diagonal members at corners and along the edges parallel to the vibration direction. However, the low values of member forces in the middle regions made it difficult to predict the actual behaviour.

5.4.2 Results of two-edge-supported models

The following section presents results for the experimental tests carried out on models supported along the two lower edges parallel to X direction.

I. Vertical snap test results

Figure 5.40 presents displacement results of vertical snap test on non-composite Truss A, while Figures 5.41 and 5.42 introduce the test results of composite Trusses B and C, respectively. Values of damping ratios and vibration frequencies in vertical and horizontal directions can be found in Table 5.14.

The successive removal of panels from models resulted in reducing the stiffness in all directions, which reflected in the reduction experienced in the vibration frequencies in the vertical and horizontal directions compared to square models.

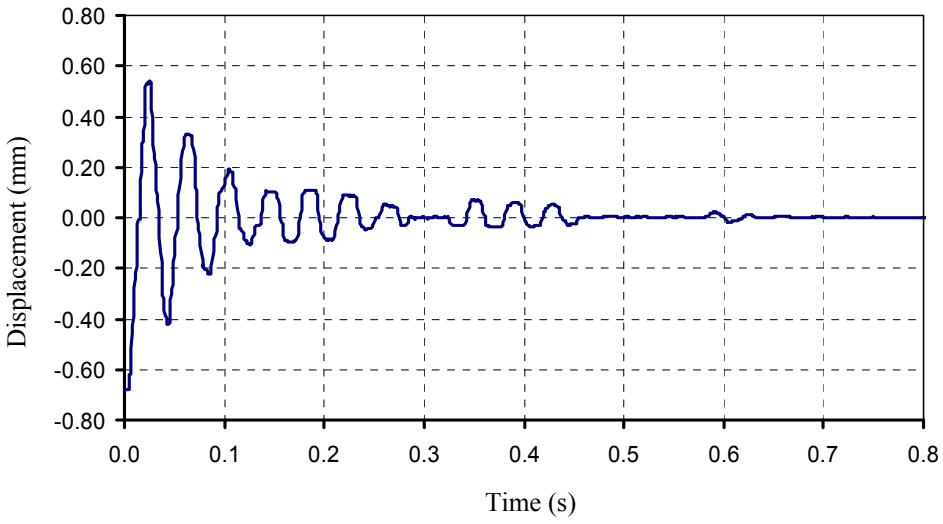

Figure 5.40 Vertical displacement of Truss A with AR = 2.0 during vertical snap test

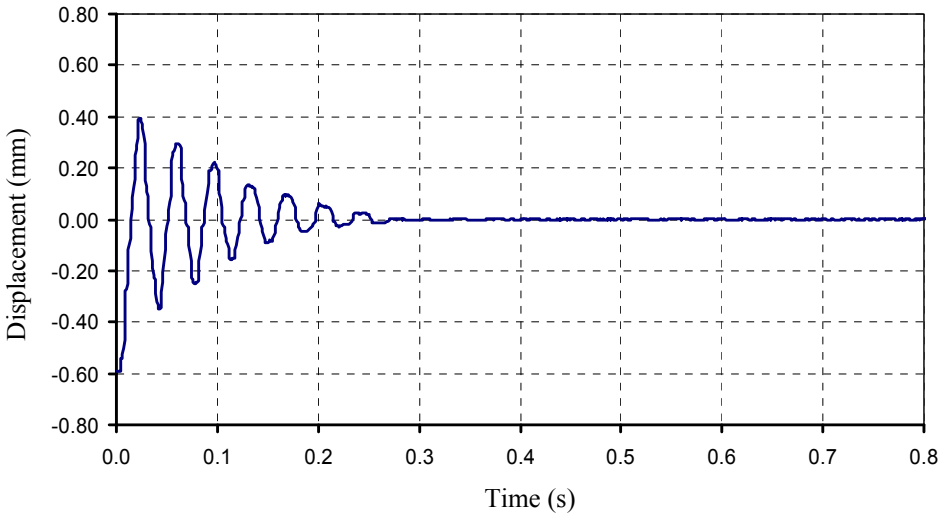

Figure 5.41Vertical displacement of Truss B with AR = 2.0 during vertical snap test

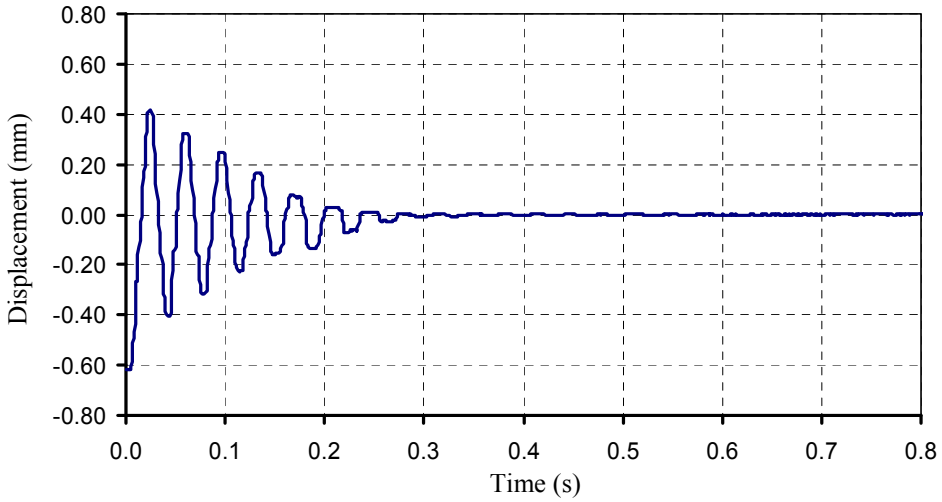

Figure 5.42 Vertical displacement of Truss C with AR = 2.0 during vertical snap test

Table 5.14 Results of vertical snap tests on two-edge-supported models with AR=2.0

	Truss A		**Truss B**		**Truss C**	
	Freq. (f) Hz	Damping ratio (ζ)	Freq. (f) Hz	Damping ratio (ζ)	Freq. (f) Hz	Damping ratio (ζ)
Test 1	24.89	6.46%	27.97	6.01%	28.17	7.92%
Test 2	25.42	5.15%	28.09	5.98%	27.33	7.45%
Test 3	25.32	5.76%	27.78	6.07%	27.59	7.39%
Average	**25.21**	**5.79%**	**27.95**	**6.02%**	**27.69**	**7.59%**

II. Horizontal snap test results

A group of horizontal snap tests were carried out on the two-edge-supported models with AR = 2.0 to determine their dynamic characteristics in the longitudinal X-direction. Figure 5.43 presents snap test results of non-composite Truss A, while results of composite Trusses B and C are presented in Figures 5.44 and 5.45, respectively. The calculated values of vibration frequencies and damping ratios in the horizontal direction are presented in Table 5.15.

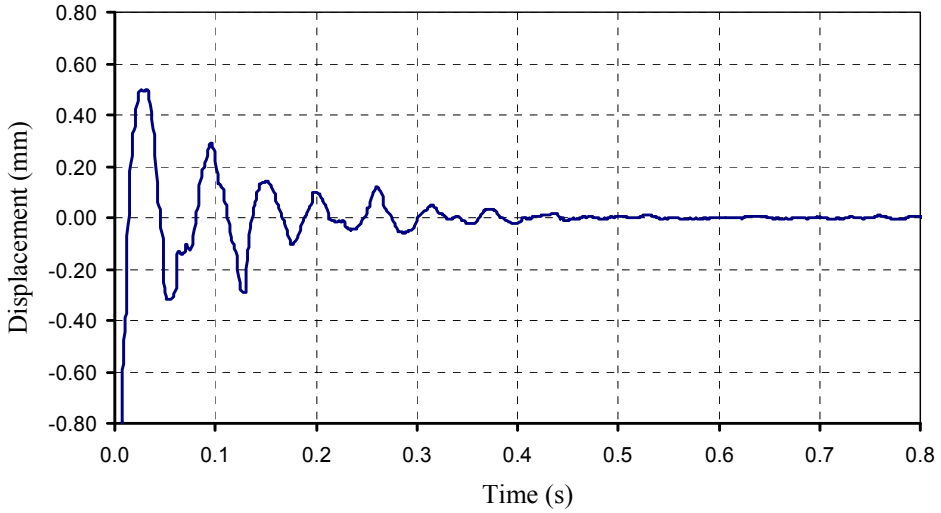

Figure 5.43 Horizontal displacement of Truss A with AR = 2.0 during horizontal snap test

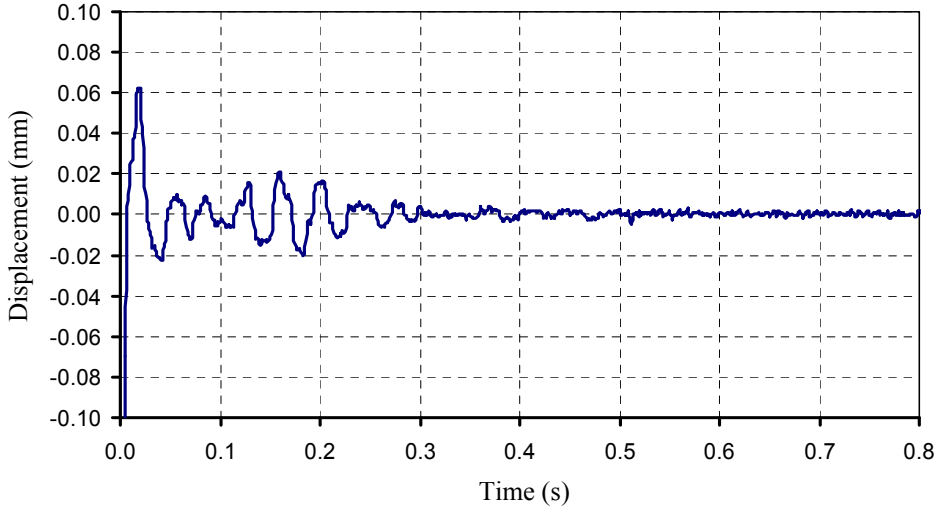

Figure 5.44 Horizontal displacement of Truss B with AR = 2.0 during horizontal snap test

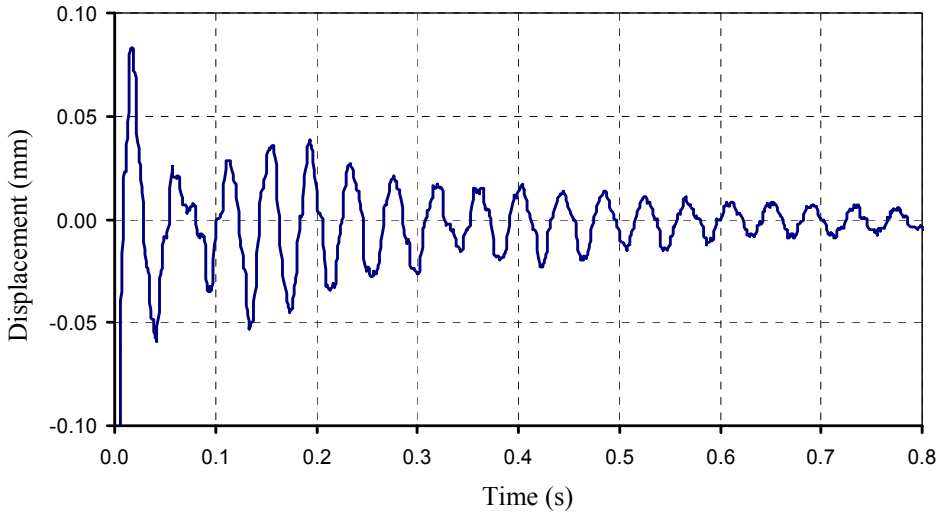

Figure 5.45 Horizontal displacement of Truss C with AR = 2.0 during horizontal snap test

Table 5.15 Results of horizontal snap tests on two-edge-supported models with AR =2.0

	Truss A		**Truss B**		**Truss C**	
	Freq. (f) Hz	Damping ratio (ζ)	Freq. (f) Hz	Damping ratio (ζ)	Freq. (f) Hz	Damping ratio (ζ)
Test 1	18.87	5.37 %	27.52	2.83%	23.15	2.78 %
Test 2	17.20	7.29 %	26.04	2.40%	23.04	2.64 %
Test 3	17.55	4.69 %	27.03	3.02%	23.26	2.94 %
Average	**17.87**	**5.78%**	**26.86**	**2.75%**	**23.15**	**2.79%**

III. Results of shaking table tests of two-edge-supported models with AR=2.0

Net displacement responses for shaking tests carried out on the two-edge-supported Truss A is shown in Figure 5.46, while Figures 5.47 and 5.48 present the results of the two composite Trusses B and C, respectively. A comparison between maximum and minimum responses for all models is presented in Table 5.16.

Changes in the internal forces by the introduction of composite action can be seen in Figure 5.49. All forces are presented in the form of absolute maximum strains.

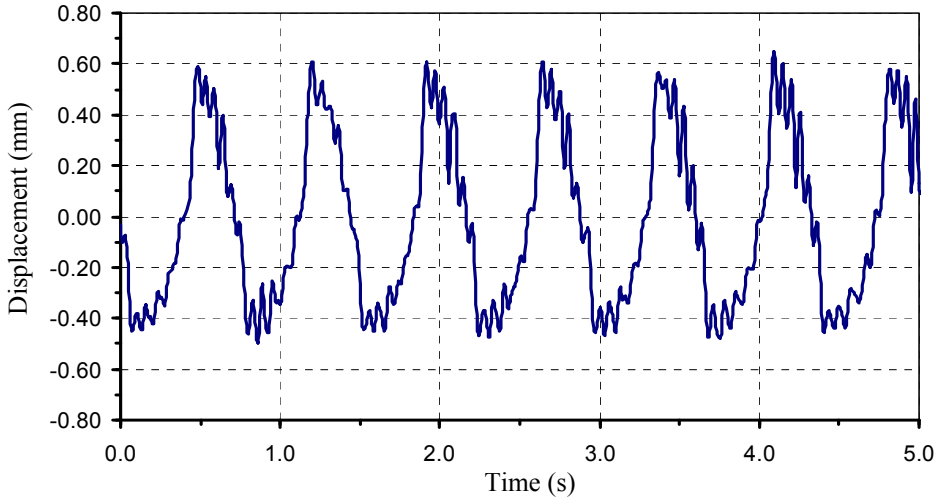

Figure 5.46 Displacement responses of two-edge-supported model Truss A with AR=2.0

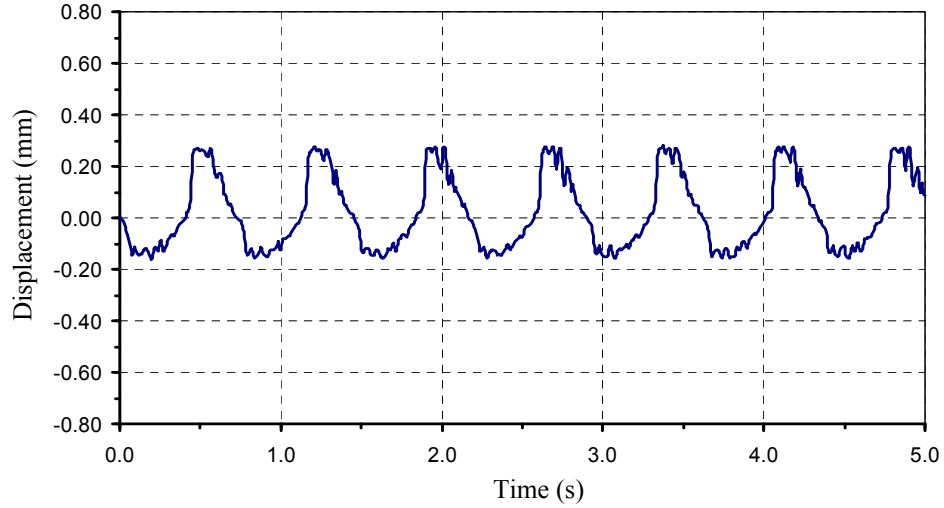

Figure 5.47 Displacement responses of two-edge-supported model Truss B with AR=2.0

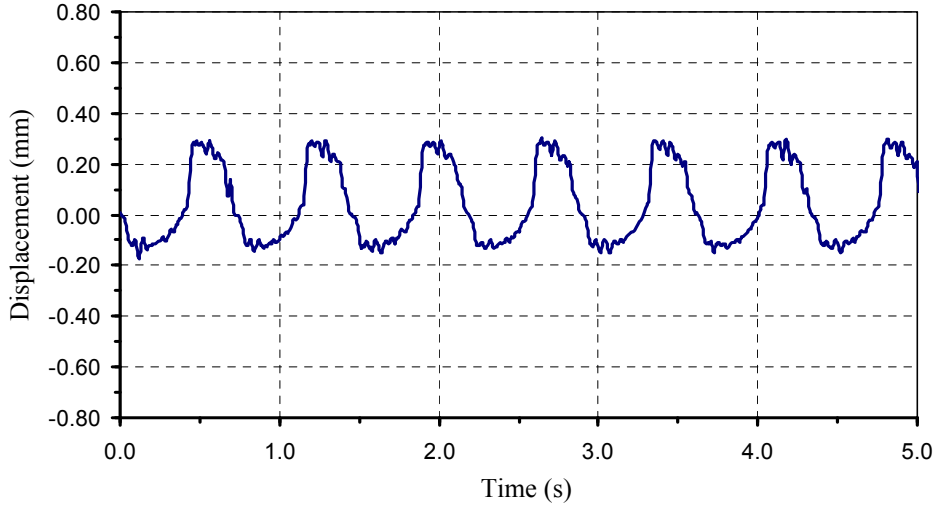

Figure 5.48 Displacement responses of two-edge-supported model Truss C with AR=2.0

Table 5.16 Maximum and minimum responses of edge-supported models with AR=2.0

	Truss A	**Truss B**	**Truss C**
Max. displacement (mm)	+0.647	+0.281	0.303
Min. displacement (mm)	-0.498	-0.161	-0.173

As can be seen from above Figures 5.46 to 5.48, there was a noticeable reduction in the lateral displacement of composite models under shaking table vibrations. This increase in the lateral resistance of models is though to be a direct result for the increase in models' stiffness by the introduction of composite action. However, the composite action resulted in increases in the diagonal member forces including those in the middle regions, while there was a reduction in forces in the lower chords perpendicular to the vibration direction (Figure 5.49).

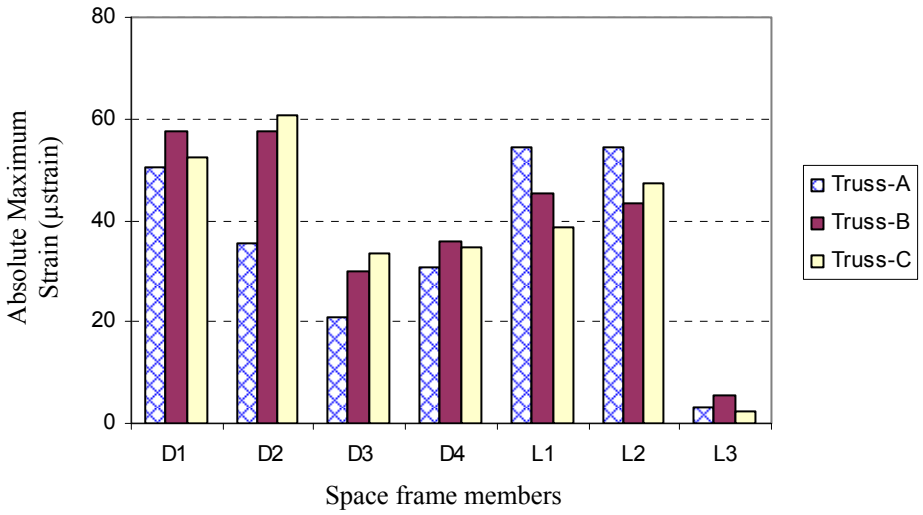

Figure 5.49 Member forces of two-edge-supported models with AR=2.0

5.5 Summary of experimental results on space frame models

Tests were repeated for the three Trusses A, B and C to consider the cases with other aspect ratios including 1.2, 1.5 and 3.0. The results of all experimental tests are summarised and presented in Tables 5.17 and 5.18 for the cases with corner and two-edge supports, respectively. Full details of results are presented in Appendix C.

5.6 Summary

The results of experimental tests carried out on composite and non-composite space frame models are presented in this chapter. The tests were divided into two groups. The first group included tests aimed at determining the changes in dynamic properties such as vibration frequency in vertical and horizontal directions caused by the application of composite action with top aluminium and timber decks. The second group measured the response of models to shaking table vibration history. The response included the lateral displacements at the models' middle upper joint and the internal forces in a number of chord and diagonal members. The results of the two commonly used aspect ratios, 1.0 and 2.0, are presented in detail in this chapter, while the experimental results for models with other aspect ratios, 1.2, 1.5 and 3.0, can be found in detail in Appendix C. Through all tests, no yield or member failure was recorded and the models continued to behave in a linear elastic manner throughout the tests.

Table 5.17 Summary of experimental results of corner-supported models

	Aspect ratio=1.0					
	Frequency (Hz)		**D. Ratio ξ %**		**Displacement Response (mm)**	
	F_V	F_H	Val	Hr	Max	Min
Truss A	18.85	20.93	2.68%	4.24%	0.543	-0.439
Truss B	20.10	29.44	0.72%	2.43%	0.276	-0.171
Truss C	19.29	28.55	1.52%	5.28%	0.281	-0.211
	Aspect ratio=1.2					
	Frequency (Hz)		**D. Ratio ξ %**		**Displacement Response (mm)**	
	F_V	F_H	Val	Hr	Max	Min
Truss A	19.89	17.13	4.56%	4.67%	0.635	-0.406
Truss B	20.50	22.74	1.34%	2.02%	0.338	-0.220
Truss C	20.50	22.28	1.61%	3.15%	0.382	-0.239
	Aspect ratio=1.5					
	Frequency (Hz)		**D. Ratio ξ %**		**Displacement Response (mm)**	
	F_V	F_H	Val	Hr	Max	Min
Truss A	21.71	17.04	2.95%	3.71%	+0.577	-0.443
Truss B	22.42	27.27	1.83%	2.56%	+0.233	-0.214
Truss C	22.31	22.86	3.39%	3.57%	+0.265	-0.223
	Aspect ratio=2.0					
	Frequency (Hz)		**D. Ratio ξ %**		**Displacement Response (mm)**	
	F_V	F_H	Val	Hr	Max	Min
Truss A	22.36	15.54	7.05%	3.87%	0.684	-0.553
Truss B	22.28	21.56	9.61%	0.76%	0.264	-0.170
Truss C	23.69	21.69	12.36%	0.78%	0.275	-0.175
	Aspect ratio=3.0					
	Frequency (Hz)		**D. Ratio ξ %**		**Displacement Response (mm)**	
	F_V	F_H	Val	Hr	Max	Min
Truss A	22.79	14.12	6.32%	5.59%	+0.820	-0.672
Truss B	25.36	23.74	5.58%	1.53%	+0.261	-0.234
Truss C	26.23	22.30	6.26%	1.48%	+0.298	-0.242

Table 5.18 Summary of experimental results of two-edge-supported models

	Aspect ratio=1.0					
	Frequency (Hz)		**D. Ratio ξ %**		**Displacement Response (mm)**	
	F_V	F_H	Val	Hr	Max	Min
Truss A	25.60	21.46	6.51%	17.99%	0.511	-0.366
Truss B	29.22	37.42	1.72%	1.95%	0.222	-0.126
Truss C	29.20	35.96	3.63%	11.75%	0.229	-0.204
	Aspect ratio=1.2					
	Frequency (Hz)		**D. Ratio ξ %**		**Displacement Response (mm)**	
	F_V	F_H	Val	Hr	Max	Min
Truss A	25.39	17.17	4.53%	7.32%	+0.580	-0.415
Truss B	27.35	26.71	1.21%	1.22%	+0.219	-0.185
Truss C	27.52	26.61	0.79%	3.71 %	0.248	-0.182
	Aspect ratio=1.5					
	Frequency (Hz)		**D. Ratio ξ %**		**Displacement Response (mm)**	
	F_V	F_H	Val	Hal	Max	Min
Truss A	26.15	16.19	6.51%	7.85%	0.581	-0.440
Truss B	27.93	25.65	1.75%	2.13%	+0.210	-0.191
Truss C	28.44	24.35	2.51%	4.71 %	0.243	-0.193
	Aspect ratio=2.0					
	Frequency (Hz)		**D. Ratio ξ %**		**Displacement Response (mm)**	
	F_V	F_H	Val	Hr	Max	Min
Truss A	25.21	17.87	5.79%	5.78%	+0.647	-0.498
Truss B	27.95	26.86	6.02%	2.75%	+0.281	-0.161
Truss C	27.69	23.15	7.59%	2.79%	0.303	-0.173
	Aspect ratio=3.0					
	Frequency (Hz)		**D. Ratio ξ %**		**Displacement Response (mm)**	
	F_V	F_H	Val	Hr	Max	Min
Truss A	23.13	14.26	6.14%	2.93%	0.647	-0.498
Truss B	26.74	26.36	7.15%	1.53%	+0.232	-0.224
Truss C	26.22	22.61	7.21%	1.56%	0.280	-0.262

CHAPTER 6

ANALYSIS AND DISCUSSION OF EXPERIMENTAL RESULTS

6.1 Introduction:

The discussion of results obtained from the experimental tests carried out on space frame Trusses A, B and C is presented in this chapter. The discussion focuses on assessing the changes in the dynamic characteristics and behaviour of space frames caused by the introduction of composite action. Assessment of changes in dynamic characteristics includes the changes in natural frequencies and damping ratios, while the evaluation of the changes in dynamic behaviour is derived from comparing the lateral displacements under shaking table vibration history.

The discussion includes an evaluation of the effect of changing the support conditions and aspect ratios of models on their natural frequencies and damping ratios in addition to the responses to shaking table vibrations including lateral displacements and forces in selected members. As mentioned in Chapter 3, two support conditions were considered, namely corner supports and supports along two parallel edges at the lower chord level. Five aspect ratios were also considered; 1.0, 1.20, 1.50, 2.0 and 3.0. Further discussion of the effect of support conditions and space frame configurations is included in Chapter 7.

The discussions in this chapter focus on the most common case of square models (AR=1.0) followed by a less detailed analysis of models with other aspect ratios.

6.2 Effect of composite action on square models

The discussion in this section covers both corner and two-edge-supported square models (AR = 1.0).

6.2.1 Changes in dynamic characteristics of corner-supported models

The experimental tests carried out on models showed the variation in their dynamic characteristics caused by the introduction of composite action. Table 6.1 and Figure 6.1 present a comparison between the vibration frequencies and damping ratios of composite and non-composite models in both the vertical and horizontal directions.

The results included in Table 6.1 for Truss A represent the case with inverted (eccentric) masses as this allowed direct comparison of results with the composite models.

Table 6.1 Results of snap tests carried out on corner-supported models

Mode of frequency	Truss A		Truss B		Truss C	
	f	ξ	f	ξ	f	ξ
Ver. mode	18.85	2.68%	20.10	0.72%	19.29	1.52%
Hor. mode	20.93	4.24%	29.44	2.43%	28.55	5.28%

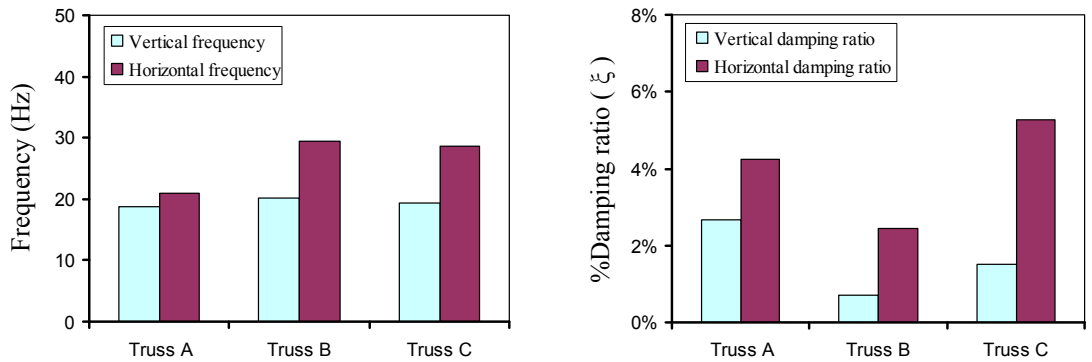

a. Natural frequencies of models

b. Damping ratios of models

Figure 6.1 Natural vibration frequencies and damping ratios for corner-supported models as obtained from the experimental tests

The results above demonstrate an overall increase in the vertical and horizontal vibration frequencies associated with the use of composite action in Trusses B and C in all test directions. However, the effect of composite action on changing the damping ratio varied according to the material used in the composite deck and the test direction.

For vibration frequencies in vertical direction, results showed little increase with 6.7% for Truss B and only 2.4 % for Truss C. This increase stems from the increase in models' vertical stiffness due to the introduction of composite action. Although there was a 6.3% increase in the mass of Trusses B and C associated with the introduction of composite deck, the increase of models' stiffness was larger, which led, according to Equation 6.1, to increases in the vibration frequency in the vertical direction.

$$\omega = \sqrt{\frac{K}{M}} \tag{6.1}$$

where ω is the natural frequency of the structure, K and M are the stiffness and mass of the structure, respectively.

There was also a 0.3% difference in mass, M, between composite Trusses B and C, which led to a small effect of mass on the values of frequency of vibrations between both models. However, the vibration frequency of composite models was dominantly affected by both the properties and the thickness of deck material.

It is worth mentioning that the vibration frequency obtained experimentally was the damped frequency, ω_d, which according to Equation 6.2 depended on both the natural frequency, ω, of the system and the damping ratio of the system, ξ as follows:

$$\omega_d = \omega\sqrt{1-\xi^2} \tag{6.2}$$

By applying Equation 6.2 on the obtained results of non-composite and composite

Trusses A and B to evaluate the effect of damping on the vertical frequency of both models, the following results are obtained;

$$\text{Damping effect on Truss A} = \frac{\omega_d}{\omega} = \sqrt{1 - 0.0268^2} = 0.99964 \cong 1.0 \qquad (6.3)$$

$$\text{Damping effect on Truss C} = \frac{\omega_d}{\omega} = \sqrt{1 - 0.0152^2} = 0.99988 \cong 1.0 \qquad (6.4)$$

The above results show clearly that the damping ratio had a little effect on the vertical vibration frequency of both composite and non-composite models and could be ignored, leaving only the changes in stiffness to affect the values of natural frequency.

The phenomenon of the increase of natural frequency for composite models was repeated when the models were excited in the horizontal direction during the horizontal snap tests since the horizontal frequencies of vibration of both composite Trusses B and C were much larger than that of non-composite Truss A. The increases in the horizontal frequency of vibration reached 40.6% and 36.4% for Trusses B and C, respectively. These increases were a result of the increase in lateral stiffness of composite models. Moreover, the increase in stiffness of composite models in horizontal direction, deduced from the increase of vibration frequencies, can be explained by the formation of a plate like behaviour caused by the high in-plane stiffness of the composite deck. At the same time, the upper joints of composite models worked as several supports for deck plate resulting in stiffness increase of deck in horizontal direction to work as a deep beam with great stiffness.

Changes in the damping ratio related to the vertical mode of vibration were evident. A reduction in damping was observed when using the aluminium deck in Truss B or timber deck in Truss C. The damping reduction can be explained by the changes brought to the stiffness and mass of the structure by the composite action. These

changes, in turn, affected the value of the critical damping, C_{cr}, which could be obtained according to Equation 6.5 as follows:

$$C_{cr} = 2M\omega = 2\sqrt{KM} \qquad (6.5)$$

where C_{cr} is the value of critical damping of the structure, M is the total mass of the structure and K is the stiffness of the structure in the assigned direction.

In both Trusses B and C, there was a slight increase in models' mass besides the large increase of models' stiffness caused by the composite action, which led, according to Equation 6.5, to the increase of the critical damping.

According to Equation 6.6, the damping ratio of structure, ξ, depends mainly on the actual damping, C, and the critical damping values, C_{cr}.

$$\xi = \frac{C}{C_{cr}} \qquad (6.6)$$

The overall damping, C, increases by the increase in energy loss due to friction, which is known as Coulomb Damping. For composite models, there were several sources of friction such as the friction between joints' components, which tend to deform and make relative movements during the tests, and friction between the deck and the top joints, which thought to have effective role in increasing the energy losses.

Although there was an increase in the overall damping, C, coming from different sources of energy loss, the increase in mass and stiffness of composite models led to a much larger increase in the critical damping, C_{cr}, resulting in an overall reduction of damping ratio in vertical mode of vibration in the case of Truss B with an aluminium deck.

Similar behaviour of the reduction in the vertical damping ratio was observed when using the timber deck in Truss C. The reduction in the damping ratio in the case of

Truss C with timber deck was lower than that of Truss B due to the nature of timber as a material with higher material damping, since the timber is known as good vibrations absorbent material, in addition to the higher friction between timber and top joints. As a result, the reduction in the vertical damping ratio reached 73.1% in the case of Model B, while it was 43.3% in the case of Model C.

On the other hand, the damping ratio, ξ, in the horizontal direction decreased by 42.7% when aluminium deck was used but increased with the use of a timber deck by 24.5% relative to Model A. The reduction in damping ratio due to the use of an aluminium deck can be explained, according to Equations 6.5 and 6.6, by the large increase in the critical damping, C_{cr}, associated with the increase in model's lateral stiffness, K. On the other hand, the increase in actual damping, C, due to friction from different sources did not gain the same increase resulting in an overall reduction in the damping ratio of Model B in the horizontal mode of vibration.

In contrast, the damping ratio, ξ, for Truss C was higher than that of non-composite Model A and this could be explained by the increase in model's lateral stiffness, which led to an increase in the value of critical damping, $C_{cr.}$. At the same time, the actual damping, C, increased enormously by the use of timber deck with high friction at joints and high material damping leading to the overall increase in damping ratio.

6.2.2 Response of corner-supported models to shaking table vibrations

The increase in lateral stiffness of space frame models caused by the introduction of composite action had large effect in decreasing the lateral displacement of models (Figure 6.2). The reduction in lateral displacements reached 49.2% in the case of Truss B, while reached 48.3% in the case of Model C.

This reduction is thought to be a direct result of the increase in lateral stiffness of

composite models, caused by the formation of a rigid top continuum (Figure 6.2).

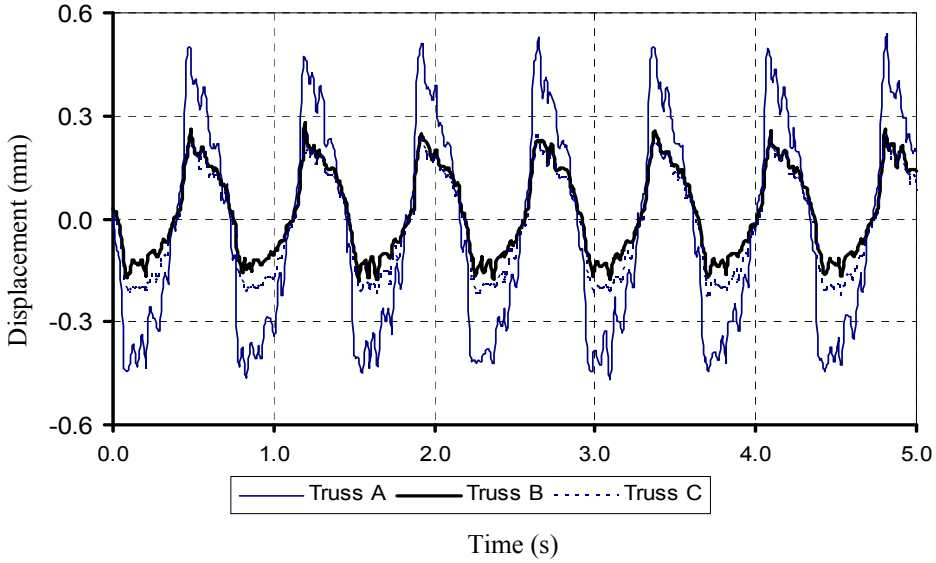

Figure 6.2 The lateral displacement of the three models under shaking table vibrations

The introduction of composite action led also to changes in the member force distribution in test models. The influenced members included diagonal and lower chord members only since the forces in the upper chord members developed due to the shaking table vibrations, were diminished by the application of composite action. Results of member forces were limited by the number of available data logging channels. A number of selected diagonal and lower chord members located at the models' edges, corners and middle regions were monitored as shown in Figures 3.15 and 5.2.

As can be seen in Figure 6.3, forces in the diagonal member D1 at a corner support stayed almost at the same level or had a slight increase with composite action, while forces in the middle diagonal members D2 and D3 decreased by 66% to 51% and 49% to 44% in Trusses B and C, respectively. In addition, the axial force in a diagonal member at an edge parallel to the direction of vibration (D4) increased by 14% in

Truss B and 30% in Truss C.

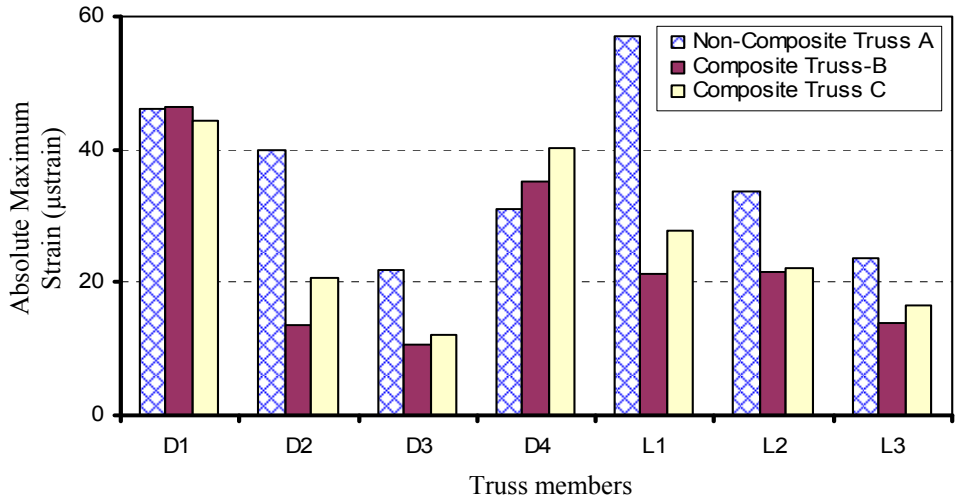

Figure 6.3 Axial force distribution in corner-supported square space frame models

According to the obtained results for selected members, there was a general reduction in axial forces in lower chord members which appeared mainly at member L1, at the middle point of the edge normal to the direction of vibration, with 63.5% in Truss B and 51.3% in Truss C. However, reduction in lower chord axial forces located at the middle region of the test models, L2 and L3, ranged from 36.6% to 41.1% and 30.2% to 34.3% for Trusses B and C, respectively.

These changes can be explained by the increase in structure stiffness caused by the introduction of composite action, which made the top continuum work with the top chord members as a stiff composite plate. This composite plate was supported along the two edges parallel to the vibration direction forming a rigid diaphragm with high stiffness in its longitudinal direction as can be seen in Figure 6.4. This structural action led to a significant reduction in the forces transmitted through the diagonal members located at the middle region, which, in turn, reduced the internal force flow into the

lower chord members.

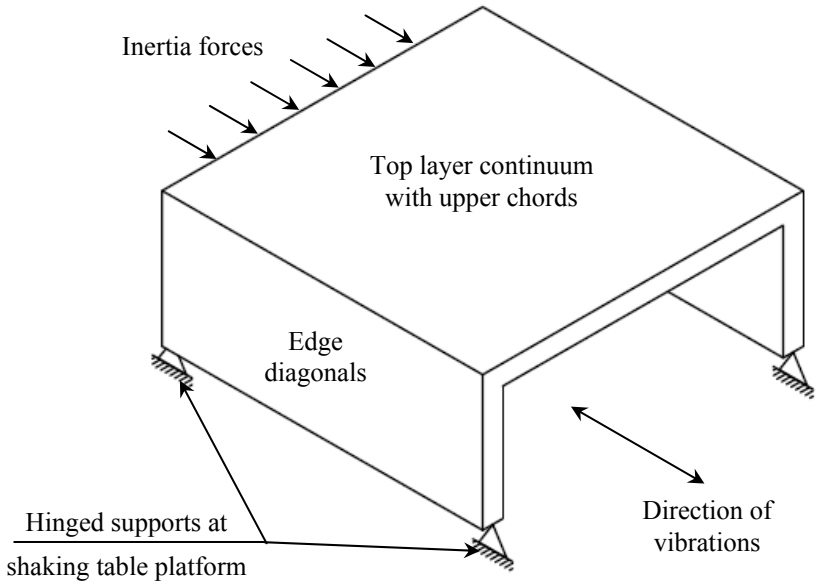

Figure 6.4 Stiff diaphragm formed by a top composite continuum and side diagonal-member panels

6.2.3 Changes in dynamic characteristics of two-edge-supported models

The following section introduces a discussion for the effect of composite action on changing frequencies of vibration, damping ratios and responses to shaking table vibrations of space frame Trusses A, B and C supported along the two lower edges parallel to the direction of shaking table vibrations.

I. Changes in vibration frequencies of space frame models

Results of vertical snap tests showed an increase in the frequency of vibration in the vertical direction of both composite Trusses B and C by 14.2 % compared to non-composite Truss A (Table 6.2). This increase is thought to be a pointer for the increase of the composite models' vertical stiffness. However, the slight increase 6.3% in the mass of composite models had a little effect compared to the stiffness gained by the application of composite action as discussed before with corner-supported models.

Moreover, increases in the horizontal frequency of vibration were observed for composite models. This increase reached 74.3% and 67.5% for Trusses B and C, respectively (Table 6.2).

Table 6.2 Results of snap tests carried out on two-edge supported models

Mode of frequency	Truss A		Truss B		Truss C	
	F	ξ	f	ξ	f	ξ
Ver. Dir.	25.60	6.51 %	29.22	1.72 %	29.20	3.63 %
Hor. Dir.	21.46	17.99 %	37.42	1.90%	35.96	11.75%

As a general observation, the values of vibration frequencies increased in all test directions for all two-edge-supported models compared to those of corner-supported models, which could be explained by the overall increase of stiffness of two-edge supported models by having more supported nodes. The increases ranged from 35.8% to 51.4% in the vertical direction and from 2.5% to 27.1% in the horizontal direction as can be seen in Figure 6.5.

It can also be observed from results that adding more supports at the two edges in case of non-composite Truss A triggered the horizontal mode of vibration to be the first mode of vibration followed by the vertical mode of vibration. This behaviour can be interpreted by the large amount of stiffness added to the non-composite model in the vertical direction compared to the stiffness gained in the horizontal direction. However, the introduction of composite action for Models B and C was associated by large increase in models' stiffness in horizontal direction, which resulted in keeping the vertical frequency of vibration in the first order followed by higher vibration frequency in horizontal direction in the second order.

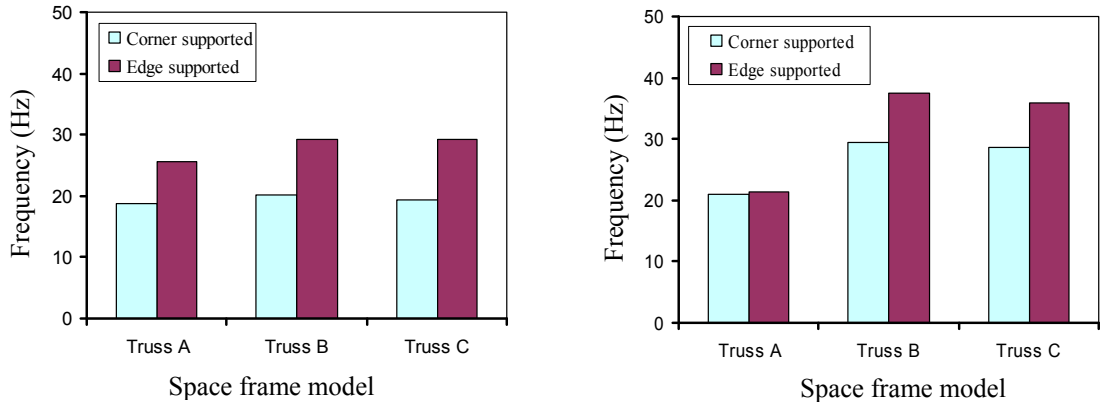

a. Frequencies in vertical direction

b. Frequencies in horizontal direction

Figure 6.5 Effect of support condition on vertical and horizontal frequencies

II. Changes to damping ratio of test models

Results of snap tests in vertical and horizontal directions showed a drop in damping ratio by using an aluminium deck to achieve the composite action (Truss B). Although the addition of deck plate should participate in increasing the model' damping, C, due to the increase of friction between the deck plate, top joints' components and added masses, the large increase of stiffness and masses had more effect in increasing the critical damping, C_{cr}, resulting in a general reduction of damping ratio, according to Equation 6.5, by 73.6% and 89.4% in vertical and horizontal directions, respectively.

The same phenomenon of the reduction of damping in the vertical and horizontal directions was observed in the case of using timber deck in building composite Truss C. Although the composite Truss C had high damping caused by the friction between the timber deck and the top joints in addition to the nature of timber as a vibration absorbent material, the increase of model's mass and stiffness caused the critical damping, C_{cr}, to have high levels leading to an overall reduction of damping ratio, ξ, in both directions. The reduction in damping ratio was 44.2% and 35.7% in vertical and horizontal directions, respectively.

Despite the increase of models' stiffness by the addition of more supports, which should be reflected as a reduction of the damping ratio, ξ, due to the increase of the critical damping, C_{cr}, the friction between the models and the supports was high enough leading to a large increase in damping, C. As a result, a general increase in damping ratios was observed for almost all models in the two test directions compared to models supported at corners (Figure 6.6). The increases in damping ratio ranged from 138.9% to 142.9% in vertical direction and from 122.5% to 324.5% in the horizontal direction. The only case of disagreement with these findings was the reduction of horizontal damping ratio of Truss B when supported at the two-edges. This disagreement is thought to be a result of the great stiffness added to the structure by the addition of more supports, which participated in a large increase of critical damping value, C_{cr}, leading to an overall reduction in the value of damping ratio, ξ by about 21%.

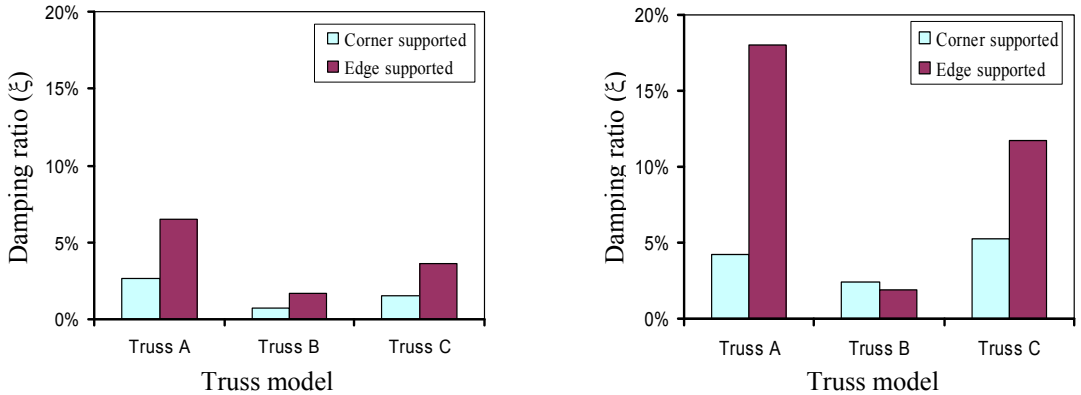

a. Damping ratios in vertical direction b. Damping ratios in horizontal direction

Figure 6.6 Effect of support condition on vertical and horizontal damping ratios

6.2.4 Response of two-edge-supported models to shaking table vibrations

I. Changes in lateral displacements

As shown in Figure 6.7, composite action proved its superiority in reducing the lateral displacements in response to shaking table vibration caused by the large increase in the

lateral stiffness of models. This reduction in lateral displacement reached 57.1% for Truss B and 55.4% for Truss C.

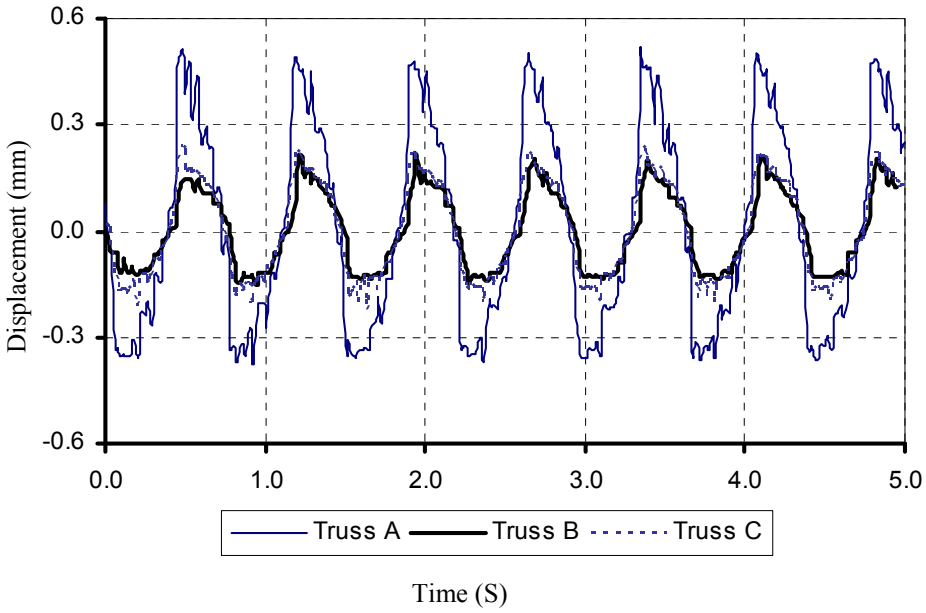

Figure 6.7 Effect of composite action on lateral displacement of two-edge supported models

II. Changes in member forces

Experimental results of monitored axial forces in selected members are presented in Figure 6.8. Axial forces in diagonal members were observed to be more concentrated at edges and around the corners, which appeared in the increase of forces in diagonal member D1 by 29.1% and D4 by 7.2%, while forces in D2 and D3 were reduced by 89.2% and 27.3%, respectively. This phenomenon was similar to the case of corner-supported models with the same behaviour of forming the stiff diaphragm shown in Figure 6.4 resulting in the concentration of forces along the supported edges and reduction of axial forces in members located at the middle region. Axial force in lower chord member located at the middle edge normal to the vibration direction, L1, were reduced due to the reduction of forces in diagonal members, while forces in middle lower chords almost had the same level of axial forces for both cases of composite and

non-composite.

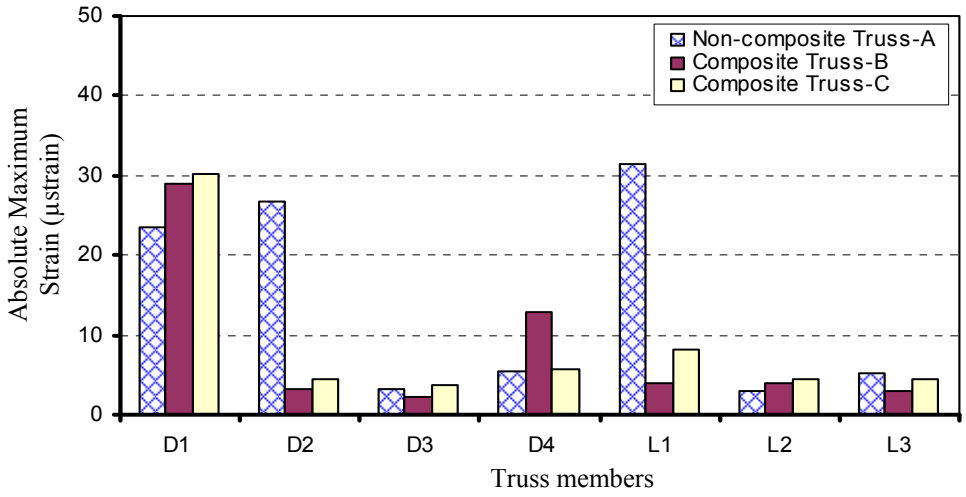

Figure 6.8 Effect of composite action on axial force distribution

6.3 Effect of models' aspect ratio on their dynamic characteristics and behaviour

The increase in models' aspect ratio was resulted from removing panels in one direction. This change in model size affected the stiffness of models in all directions and reduced their masses. In this section, the effect of changing the aspect ratio of the experimentally tested models is discussed. Furthermore, the discussion covers this effect on the dynamic characteristics and behaviour of models with both cases of corner and two-edge-supported models.

6.3.1 Corner-supported models with different aspect ratios

I. Dynamic characteristics

As can be seen in Figure 6.9, there was an increase in vibration frequencies of all models in the vertical direction associated with the increase of aspect ratio. This increase is thought to be caused by the reduction in models' mass, M, associated with the successive removal of upper joints and their masses. At the same time, the reduction in stiffness was not as rapid, leading to a general increase in vertical frequencies of vibration according to Equation 6.1.

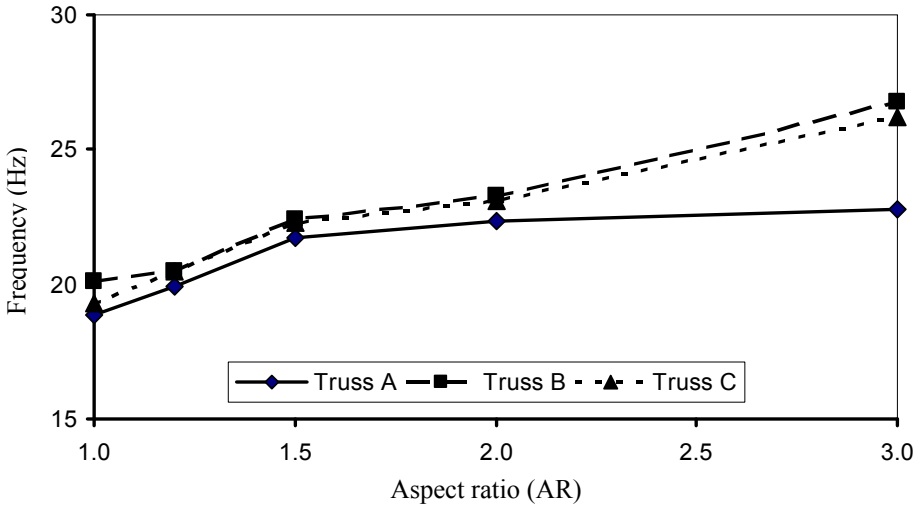

Figure 6.9 Effect of aspect ratio on vertical vibration frequency of corner-supported models

It can also be observed from Figure 6.9 that composite Trusses B and C had higher stiffness compared to non-composite Truss A, which proves the positive effect of composite action in increasing the stiffness of models with different aspect ratios.

The vibration frequencies in the horizontal direction followed a different trend since there was a large reduction in horizontal vibration frequencies in all models with the removal of the first panel (AR=1.2) (Figure 6.10). Deterioration of models stiffness accompanied by a reduction in horizontal frequencies continued for all models with the higher rate for non-composite Truss A until reaching an aspect ratio of 2.0 (AR=2.0). Beyond this aspect ratio, non-composite Truss A experienced successive reductions in horizontal frequencies with the removal of further panels, while composite Trusses B and C had an opposite trend with an increases in horizontal frequencies. According to Equation 6.1, this increase indicated the high stiffness to mass ratio of composite models, Trusses B and C, with high levels of aspect ratios compared to non-composite model Truss A.

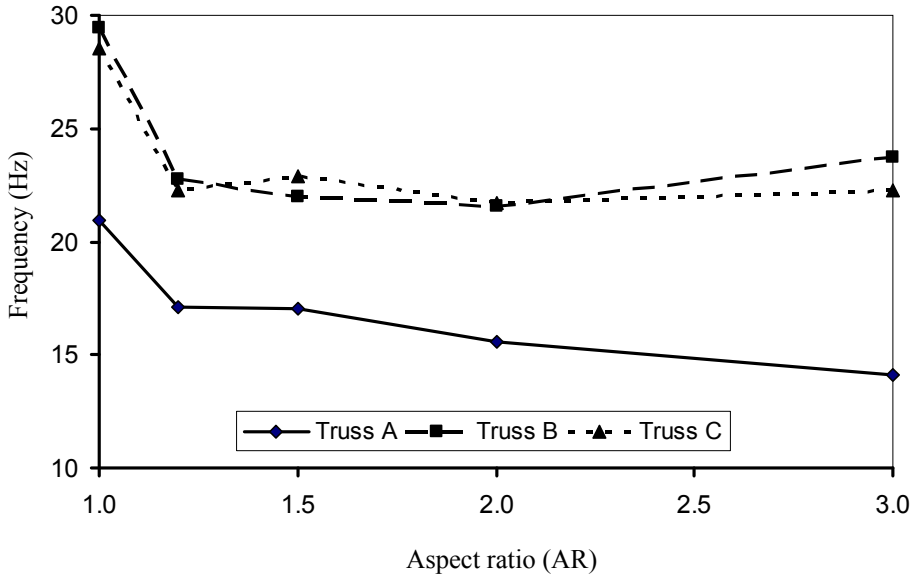

Figure 6.10 Effect of aspect ratio on horizontal vibration frequency of corner-supported models

For all cases of aspect ratios, composite Trusses B and C had higher vibration frequencies than non-composite Truss A as can be seen in Figure 6.10. This behaviour further illustrates the advantages of composite action in increasing the vibration frequencies in horizontal direction.

In addition, the effect of composite action in increasing frequencies showed higher values in horizontal direction compared to those in vertical direction, which can be seen in Figures 6.9 and 6.10 for all values of aspect ratios.

Further, there was a general increase in the damping ratio, ξ, in the vertical direction with the increase of models' aspect ratio up to 2.0 and further increases in aspect ratio led to reductions in the damping ratio (Figure 6.11). This behaviour can be explained by the considerable decrease in critical damping, C_{cr}, caused by the deterioration in models' stiffness, while the level of friction damping, C, between models components still had large values which resulted finally in increasing the damping ratios, ξ, in the

vertical direction, see Equations 6.5 and 6.6.

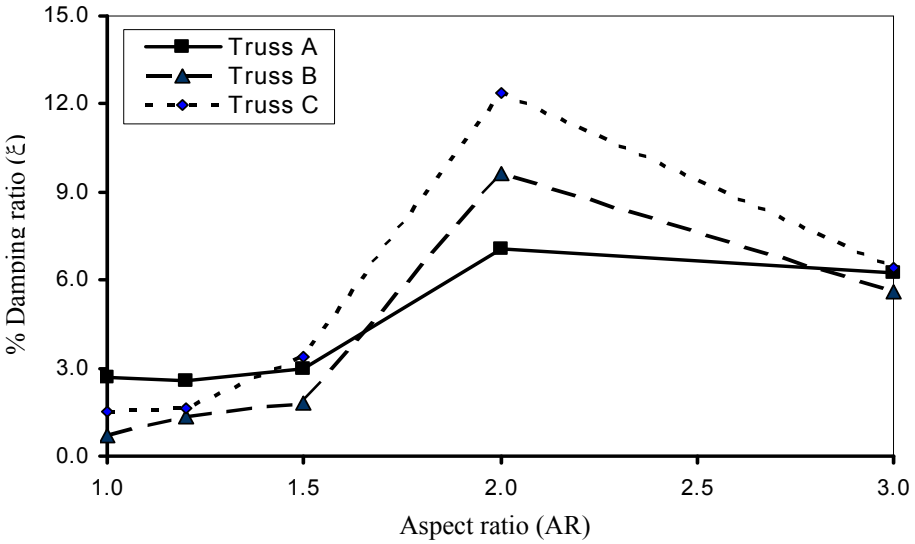

Figure 6.11 Effect of aspect ratio on vertical damping ratio of corner-supported models

As a general observation, Truss B had the lowest damping ratios for all aspect ratios compared to Truss C due to the high stiffness added by connecting the aluminium deck, in addition to the low values of friction between the deck and other model's components. On the other hand, Truss C had lower damping ratio than Truss A at low values of aspect ratios up to 1.5 (AR=1.5). Beyond this aspect ratio, damping ratios of Truss C exceeded those of Trusses A and B due to the nature of timber as a vibration absorbent material with high material damping compared to aluminium. In addition, the high friction between the timber deck with rough surface and components of the top joints led to a considerable increase in the overall model's damping, C. Moreover, the decrease in critical damping, C_{cr}, due to the deterioration in model's stiffness and mass had a large effect in boosting the damping ratio (Figure 6.11).

However, the increase of aspect ratio had a fluctuating effect on the damping ratio in the horizontal direction (Figure 6.12). For non-composite Truss A, the horizontal damping ratio saw a slight increase with low aspect ratios up to 1.2 due to the

reduction in stiffness leading to a decrease in critical damping, C_{cr}. With further increases in aspect ratio, the stiffness deteriorated successively, affecting the critical damping. At the same time, the friction between model's components was also decreased due to the removal of further elements and joints, leading to an overall reduction in the damping ratio with aspect ratio up to 1.5. By further increases in aspect ratio, by the removal of more panels, pushed further reduction in model's stiffness and mass, and consequently to the critical damping, C_{cr}, while the decrease of damping, C, due to the decrease in friction between model's components had lower rate causing an overall increase in damping ratio, ξ.

In contrast, the deterioration in horizontal stiffness in the case of composite Trusses B and C had a slower rate than Model A, and that was evident in a slower rate of reduction in the horizontal frequency of vibration, pushing the critical damping to slower deterioration as well. However, the friction between composite models' components saw rapid reduction due to the successive removal of panels, leading to an overall reduction in damping ratio, ξ, until reaching an aspect ratio of 2.0. Beyond this aspect ratio, damping ratio started to increase due to the high deterioration of horizontal stiffness with further removal of panels and reduction of mass resulting in rapid reduction in critical damping, C_{cr}, while friction damping did not have the same rate of reduction, which led to an overall increase of damping ratio (Figure 6.12).

II. Lateral displacement response

As the aspect ratio increased, the lateral stiffness of the structure deteriorated, but at the same time more masses were successively removed, leading to lower values of inertia forces. It is clear from Figure 6.13 that for non-composite Truss A, the increase in aspect ratio was accompanied by an increase in maximum displacement values. On the other hand, there were no considerable changes in the maximum displacements for

composite Trusses B and C due the proportional reduction in mass and stiffness offered by the composite action even for high values of aspect ratio.

In general, lateral displacement of composite models were excessively lower than that for the case of non-composite proving the superiority of composite action in reducing the lateral displacement responses for all cases of aspect ratios (Figure 6.13).

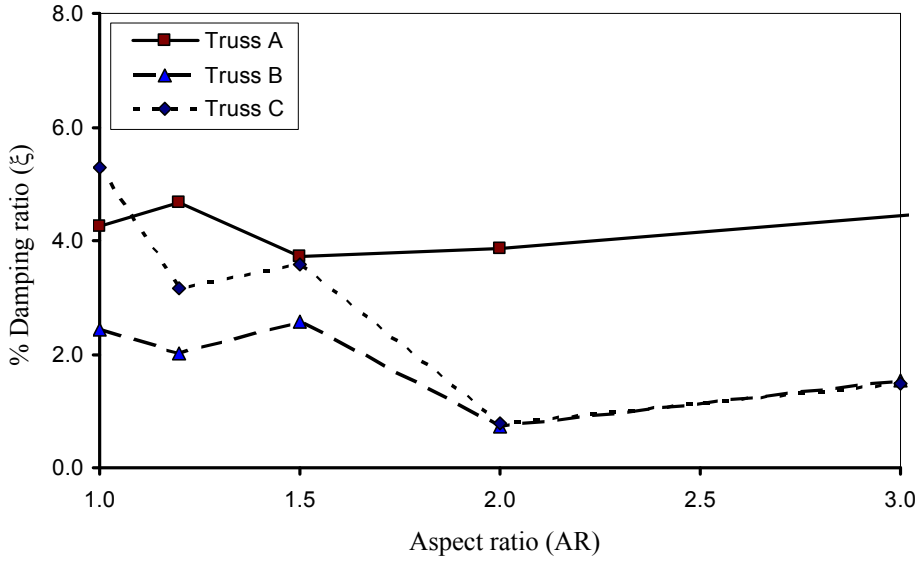

Figure 6.12 Effect of aspect ratio on horizontal damping ratio of corner-supported models

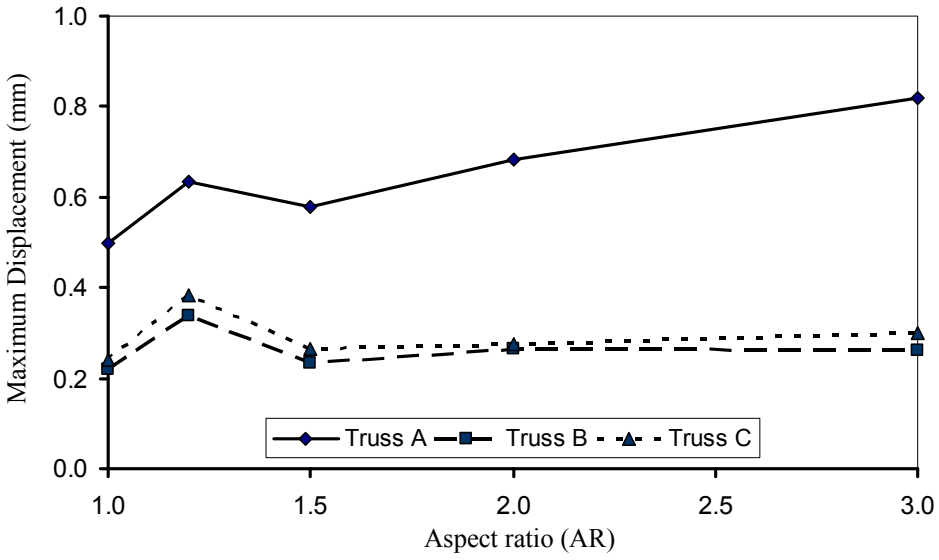

Figure 6.13 Effect of aspect ratio on maximum displacement of corner-supported models

6.3.2 Two-edge-supported models with different aspect ratios

I. Dynamic characteristics

In case of two-edge supported models, a general reduction of frequencies in vertical direction was observed for all test models by the increase of the aspect ratio (Figure 6.14). This reduction is thought to be caused by the reduction of models' stiffness in vertical direction by the successive removal of panels.

However, composite Trusses B and C had the higher frequencies with all aspect ratios compared to non-composite model Truss A (Figure 6.14).

In the horizontal direction, a general reduction in vibration frequencies was observed for all test models by the increase of aspect ratios (Figure 6.15). This reduction in horizontal frequencies is thought to be a direct result to the drop in lateral stiffness of models by the successive removal of panels from the horizontal direction.

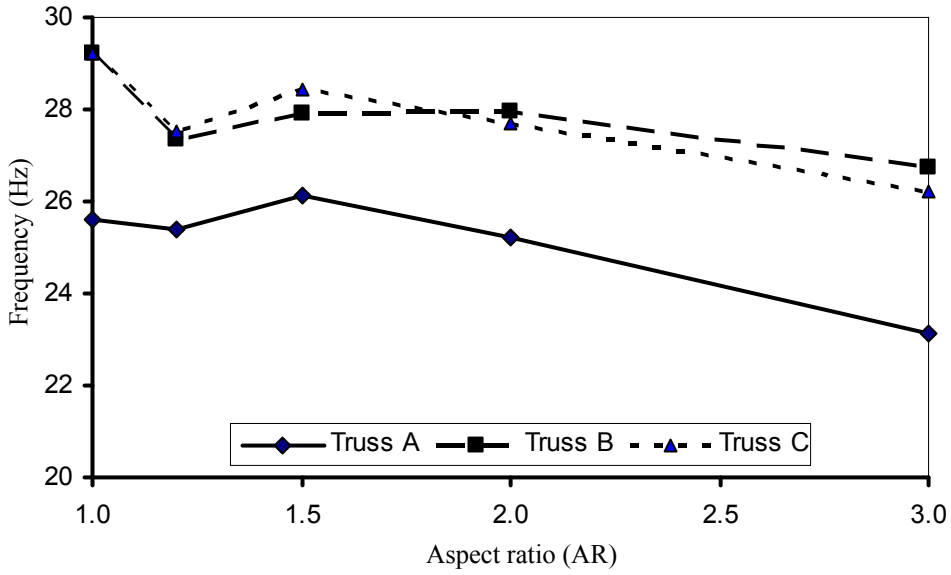

Figure 6.14 Effect of aspect ratio on vertical vibration frequency of two-edge-supported models

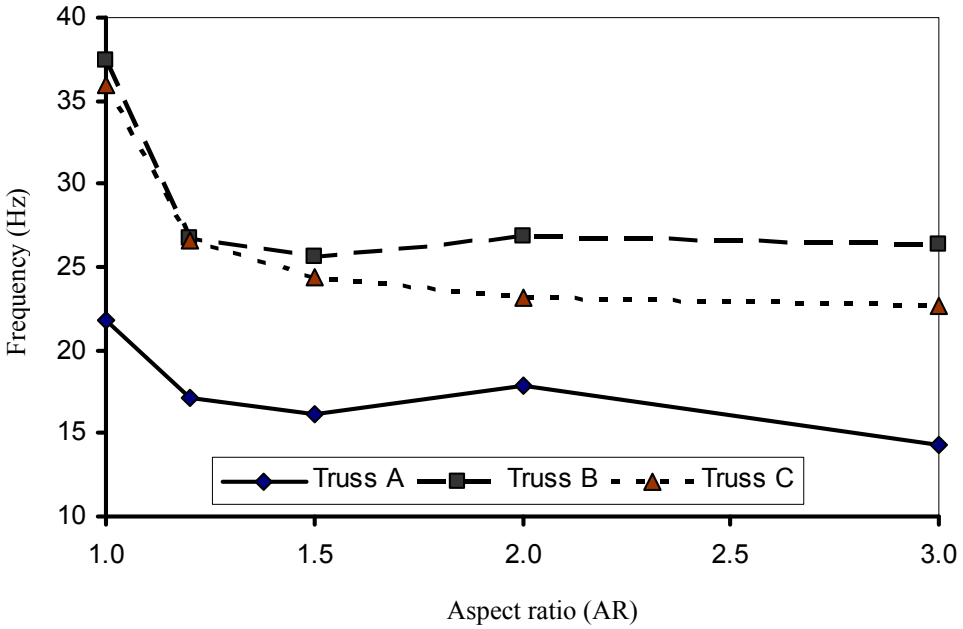

Figure 6.15 Effect of aspect ratio on horizontal vibration frequency of two-edge-supported models

It can also be noticed that composite models had higher lateral stiffness leading to higher values of vibration frequencies compared to non-composite model for all aspect ratios. Moreover, the composite action helped in reducing the loss in horizontal stiffness especially with large values of aspect ratios, beyond 2.0, as can be seen in Figure 6.15.

For damping ratio in the vertical direction, a noticeable reduction was experienced for all test models by the increase of aspect ratio up to 1.2 (Figure 6.16), which can be explained by the large reduction of damping in models compared to the reduction experienced with the critical damping. An increase in the damping ratio was observed by further increases in the aspect ratio, which continued for composite Trusses B and C with aspect ratio up to 3.0, but stopped with aspect ratio up to 1.5 for Truss A then started to decrease until AR=3.0.

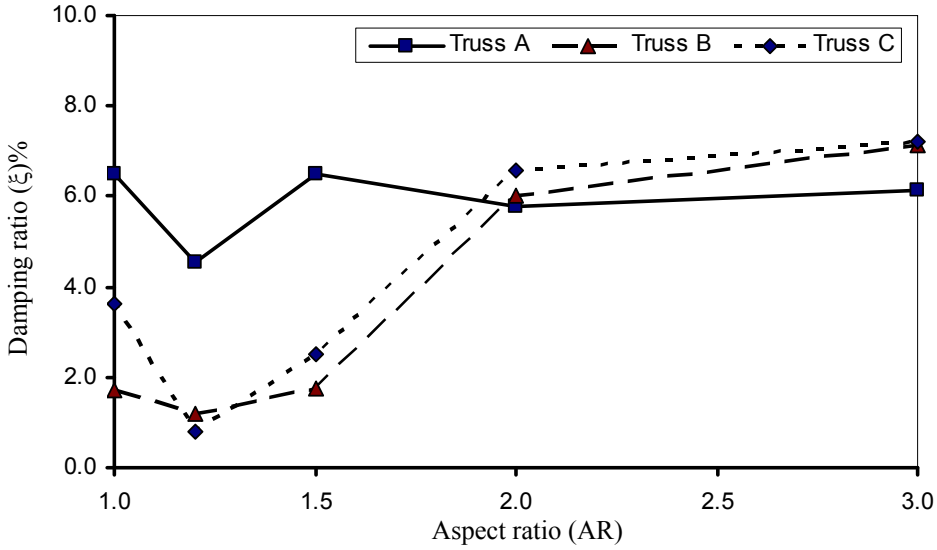

Figure 6.16 Effect of aspect ratio on vertical damping ratios of two-edge-supported models

In horizontal direction, there was a continuous decrease in the values of damping ratios for all models by the increase of aspect ratio, which can be explained by the higher reduction of friction and material damping by the successive removal of panels while the rate of deterioration in stiffness was still low (Figure 6.17).

On the other hand, the large increase in horizontal stiffness of composite Trusses B and C with different aspect ratios had a large effect in keeping higher values of critical damping, C_{cr}, compared to damping experienced by material and friction, C, leading to lower values of damping ratios compared to Truss A as can be seen from Figure 6.17.

II. Displacement responses to shaking table vibrations

As shown in Figure 6.18, the response of non-composite Truss A was proportional to the aspect ratio due to the reduction in horizontal stiffness of the model due to the removal of panels. For composite Trusses B and C, the increase in lateral displacement responses was limited compared to non-composite Truss A, which can be explained by the ability of composite models to keep their lateral stiffness by the increase of their aspect ratios. In general, the maximum displacements of composite models were lower

than those for non-composite models for all cases of aspect ratios which ranged from 53% to 64%.

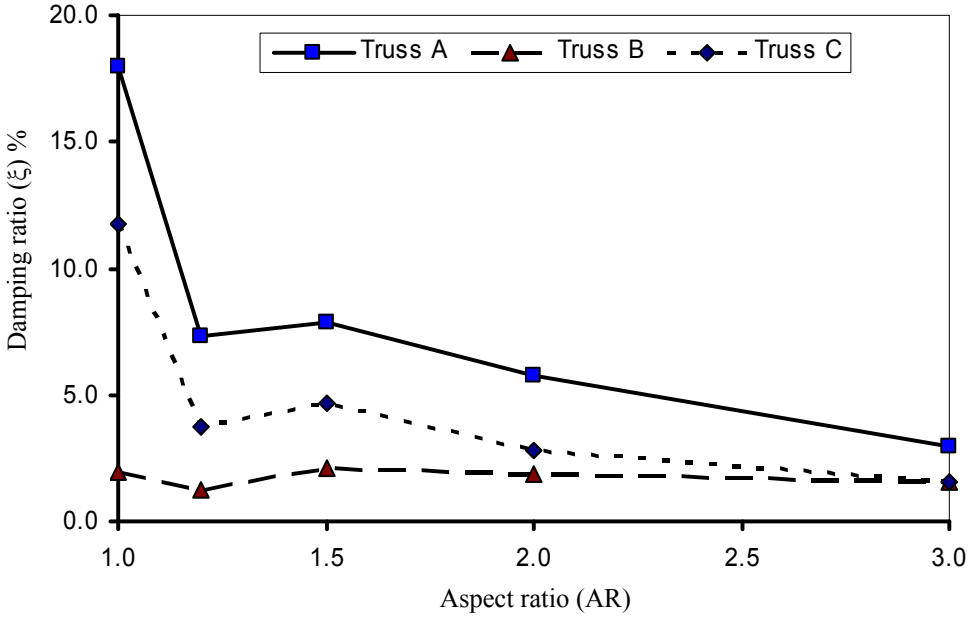

Figure 6.17 Effect of aspect ratio on horizontal damping ratio of two-edge-supported models

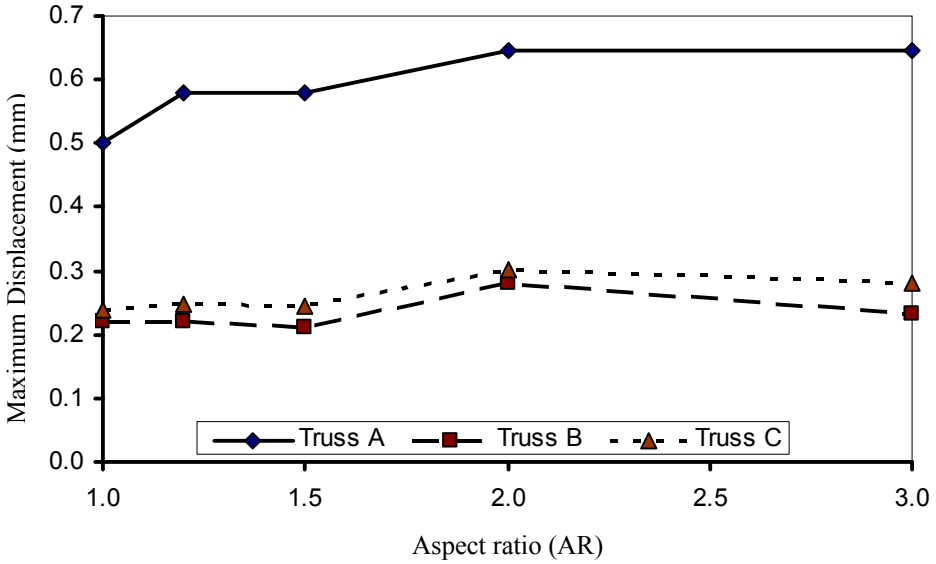

Figure 6.18 Effect of aspect ratio on maximum displacement of two-edge-supported models

6.4 Effect of support conditions

It was observed from experimental results that the dynamic characteristics and behaviour of space frame models were influenced by the support conditions. As stated before, two support conditions were considered, which involved corner supports and supports along the two lower edges parallel to the direction of shaking table vibrations.

I. Frequencies of vibrations in vertical and horizontal directions

For all space frame models, the addition of more supports at the edges resulted in higher stiffness in vertical direction, which reflected in the increase of vertical frequency of vibrations. This observation was the same for all values of aspect ratios (Figure 6.19a). The increase in frequency, which ranged from 0.1% to 51.4%, was clear for square space frame models then decreased by the increase of aspect ratio with the minimum for models with aspect ratio of 3.0.

Above observations were applicable for frequencies of vibration in the horizontal direction since the addition of more supports increased the frequencies of all tested models in this direction, which was noticeable for models with small aspect ratios then decreased with the increase of aspect ratio which can be seen in Figure 6.19b.

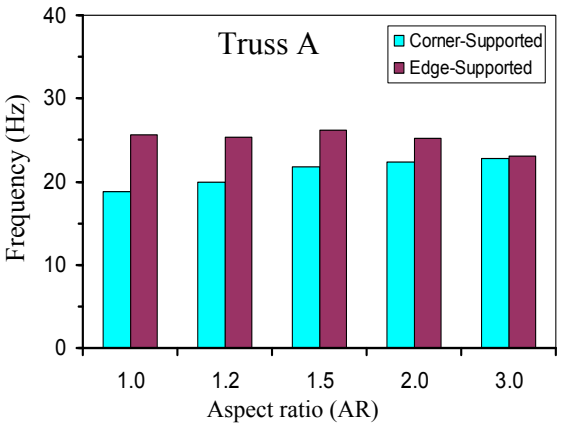

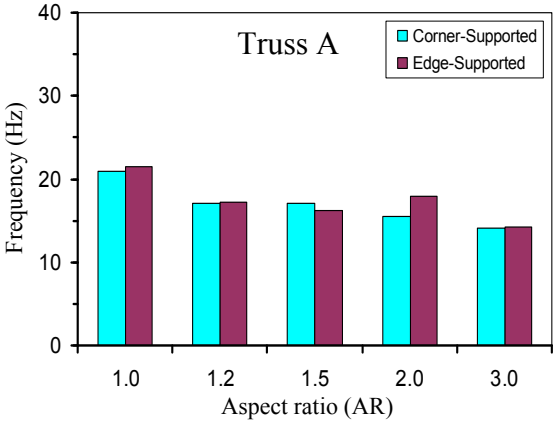

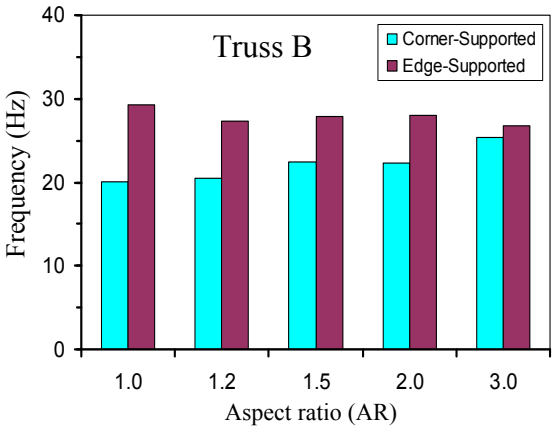

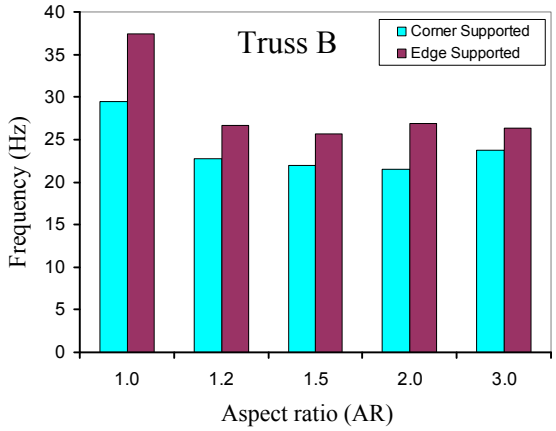

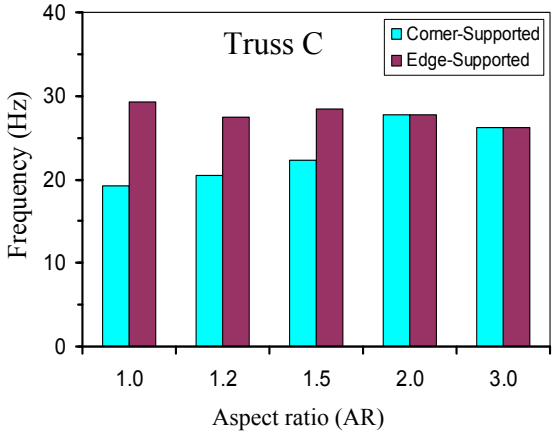

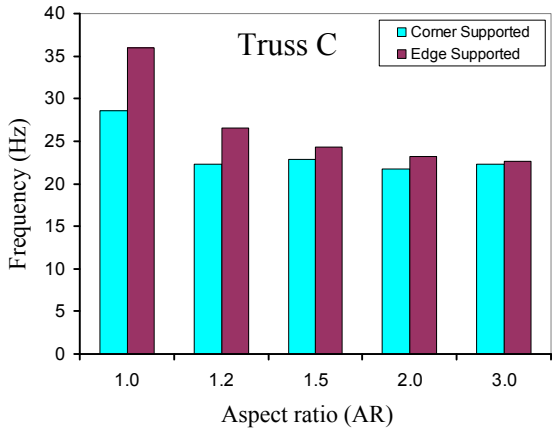

a. Vertical vibration frequencies of space frame models

b. Horizontal vibration frequencies of space frame models

Figure 6.19 Effect of support conditions on vertical and horizontal frequencies

II. Damping ratio in vertical and horizontal directions

As can be seen in Figure 6.20a for non-composite Truss A, the damping ratio in the vertical direction considerably decreased with the use of more supports, which extended to all aspect ratios. This trend can be explained by the noticeable increase in vertical stiffness, leading to an increase in the critical damping value, C_{cr}.

A fluctuating effect of adding more supports was observed on vertical damping ratio for composite Trusses B and C as shown in Figure 6.20a. This variation of the effect was a result of the dramatic changes in damping added to the structure by friction between the deck and top joints and also friction at supports besides the large increase in models' stiffness, which affected both the overall damping and the critical damping of structures. For lower values of aspect ratios, there was a considerable increase in the vertical damping ratio by using more supports due to the large damping added by the above mentioned sources. However, with further increases in the aspect ratio, a deterioration of models' stiffness was experienced leading to a reduction in critical damping, $C_{cr,}$ and consequently an increase in the damping ratios.

For the damping ratio in the horizontal direction, an increase was observed in non-composite Truss A with the use of more supports due to the increase of friction at the supports and hence the increase in damping, C, (Figure 6.20b). In the case of composite Truss B, the stiffness added to the model in the horizontal direction in addition to the limited value of friction between the aluminium deck and model components resulted in keeping higher values of critical damping, $C_{cr,}$ leading to a general reduction of damping ratio for almost all cases of aspect ratios.

For composite Truss C, the friction added to the model with use of more supports in addition to the friction and material damping already existed by the use of a timber

deck succeeded in keeping higher values of damping, C, compared to corner-supported models, which was also applicable for all aspect ratios.

III. Lateral displacement responses under shaking table vibration

Adding more supports along the two edges resulted in reducing the lateral displacements of test models in response to vibrations induced by the shaking table for the majority of cases (Figure 6.21). The reduction ranged between 5.4% to 21.1% in case of non-composite Truss A, while it ranged between 9.9% to 35.2% and 6% to 35% in case of composite Trusses B and C, respectively. This reduction in lateral displacements was thought to be a pointer for the increase of lateral stiffness of models by using more supports along the edges of the structure in the direction of induced vibrations.

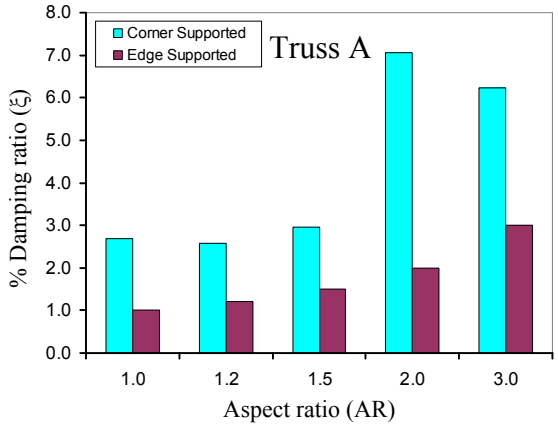

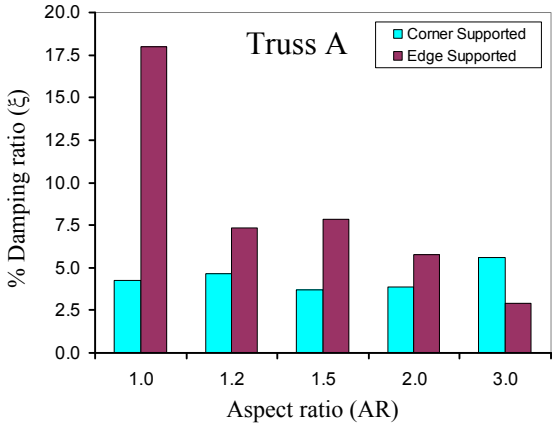

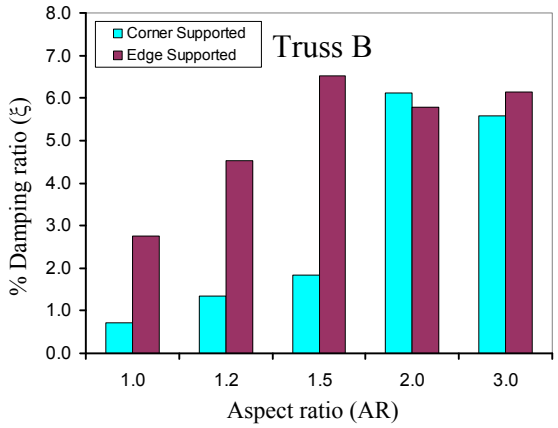

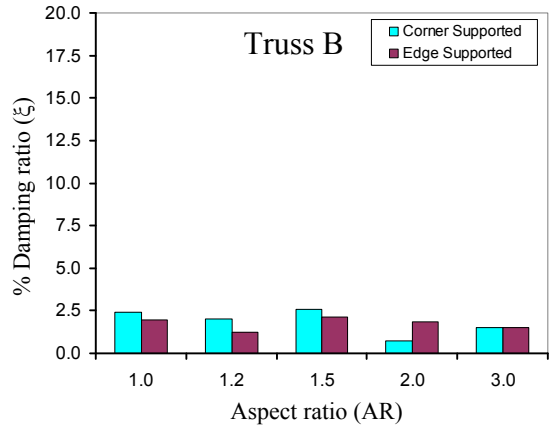

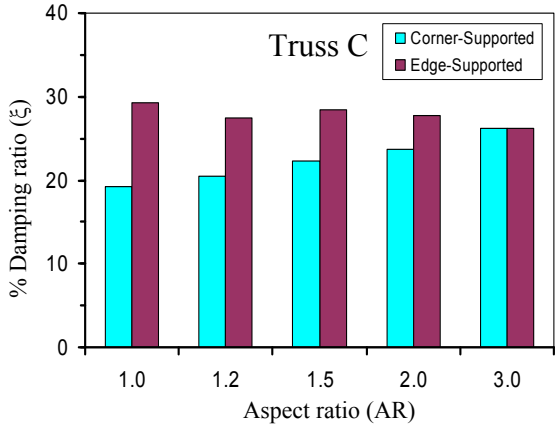

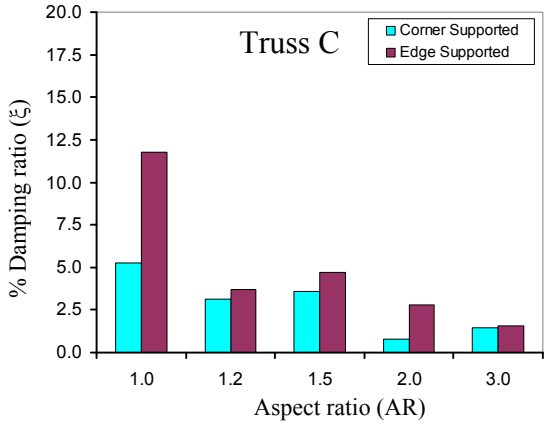

a. Vertical damping ratio of space frame models

b. Horizontal damping ratio of space frame models

Figure 6.20 Effect of support conditions on vertical and horizontal damping ratio

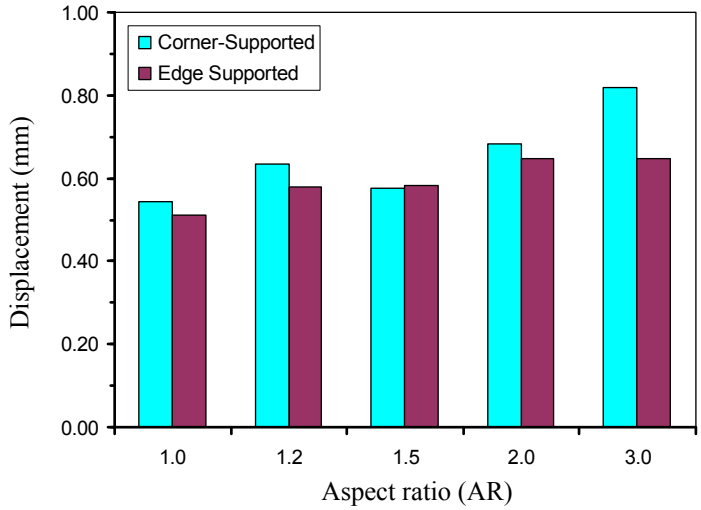

a. Displacement responses for space frame Truss A

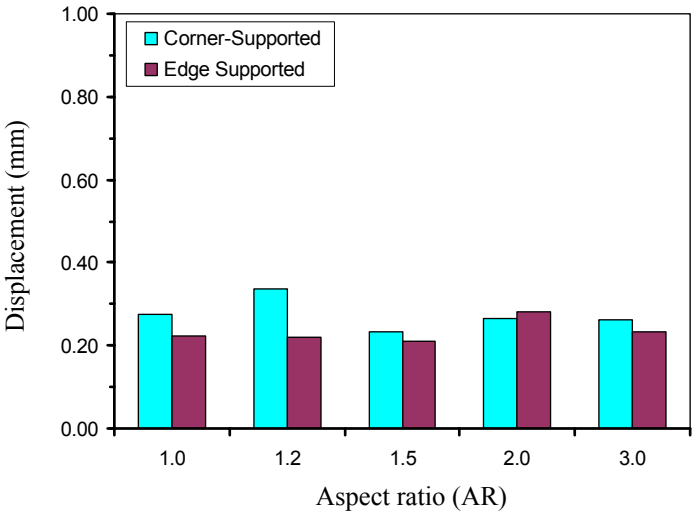

b. Displacement responses for space frame Truss B

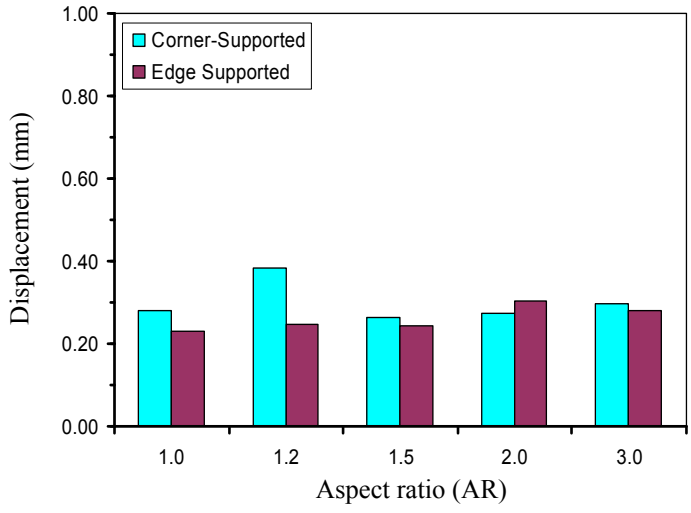

c. Displacement responses for space frame Truss C

Figure 6.21 Effect of support configuration of lateral displacement responses

6.5 General comments

This chapter presented a detailed discussion of the experimental test results carried out on composite and non-composite space frame models. The main findings of the experimental study are listed below:

1. Introducing composite action to a space frames led to large changes in the dynamic characteristics of the structure in all directions including increases in natural frequencies and a variable effect on damping ratio in test directions. The increases in vibration frequencies are thought to be a direct result of the increase in the overall stiffness of models by the application of composite action, while the increase in their masses was limited compared to non-composite models.
2. The increase in the models' aspect ratio resulted in an increase in damping ratio in the vertical direction and a reduction in horizontal direction for corner-supported models, which was the same for models supported along the two parallel edges.
3. Composite action resulted in reducing the lateral displacements under shaking table vibrations by about 50%, which could be explained by the increase in lateral stiffness of models due to the introduction of composite action.
4. Adding supports along the edges of test models resulted in higher stiffness, which led to increases in natural frequencies in addition to a considerable reduction to the lateral displacements in response to induced vibrations.
5. The material used in the composite deck affected the models' damping ratio since the use of a timber deck led to keep the damping ratio being higher than that of the composite model with an aluminium deck for the majority of cases.

CHAPTER 7

NUMERICAL ANALYSIS RESULTS

7.1 Introduction

In this chapter, results of numerical analysis carried out on non-composite space frame Truss A and composite Trusses B and C, previously described in Chapter 3, are discussed. The main aims of conducting this numerical analysis can be summarised in the following points:

1. Selecting an optimal numerical model able to simulate (reproduce) experimental results obtained under lab conditions.
2. Expanding the study to include more parameters, which were difficult to consider during the experimental study.
3. Estimate of mechanical response, which was difficult to record during lab tests.

7.2 Numerical model selection and assessment process

The assessment of accuracy of the numerical models in predicting the dynamic characteristics and behaviour of test models was carried out using the following procedure:

1. Evaluating the accuracy of nine proposed models (Models 1 to 9; previously described in Chapter 3) in predicting the dynamic properties of test models, and in particular the natural frequencies in the excitation directions.
2. Evaluating the accuracy of models in predicting the dynamic lateral displacements at a number of specific points, which were previously considered in experimental tests, under an acceleration time history similar to that produced by the shaking table.

The assessment procedure covered cases with and without composite decks, corner and edge-supports, and aspect ratios, AR = 1.0 and 2.0. The selection of the most suitable numerical model depended on the accuracy in predicting both the dynamic characteristics and the lateral response of test models. This procedure ensured that the selected model would be able to represent this type of structures correctly and with acceptable accuracy.

7.3 Modal analysis results of numerical simulations

The results of modal analysis conducted on the numerical models in chapter 3 are briefly introduced in Tables 7.1 to 7.4. For corner-supported models, the first 5 natural frequencies were presented and used in comparison with those obtained experimentally. However, only the first 3 natural frequencies of two-edge supported models were compared with experimental results. In both cases, the selected frequencies of vibration covered the directions considered in the experimental tests so they could be used in the comparisons, while the higher vibration modes were rotational or representing a duplication of fundamental modes.

Mode shapes accompanied by Mass Participation Factors (MPF) helped in depicting the modes that could be used in comparison with those excited during experimental tests. Appendix D presents the natural frequencies and MPF resulted from modal analysis.

Figure 7.1 shows the vibration mode shapes of non-composite Truss A and composite Trusses B and C. As Trusses B and C exhibited identical behaviour in all vibration modes, only the results of Truss B were presented.

The following observations were evident from the behaviour comparisons held:

1. The first vibration mode of all square corner-supported models was in the

vertical, Z, direction (Figure 7.1). The frequency underwent only a slight increase with the adoption of composite action, within 0-10%.

2. In horizontal direction, composite action increased the natural frequencies by about 30% in some of the FE simulations (Model 1 through 9), see Table 7.1. This increase was due to the large growth in the horizontal stiffness of composite models without noticeable increase in their masses.
3. For non-composite models with AR = 1.0 supported along the two edges, the first mode of vibration was in the X-direction, while it was rotational about the Y-axis in composite models (Figure 7.3). This phenomenon resulted from the large increase of stiffness in the X-direction by composite action.
4. The second mode of frequency for all square edge-supported models was in Z-direction, which can be explained by the modest changes to the models' vertical stiffness by the application of composite action (Figure 7.3).
5. For corner-supported models with AR = 2.0, the first vibration mode of non-composite Truss A, was in the X-direction, while the second was in the Z-direction. On the other hand, the first vibration mode in composite models was in the Z-direction, while the second and the third modes were in the X-direction (Figure 7.2). This behaviour was consistent with the large increase in lateral stiffness added to the structure in the X-direction by the application of composite action.
6. The mode shapes in all composite edge-supported models with AR = 2.0 were similar to those of the non-composite model (Figure 7.4), but the composite models had larger values of frequency as shown in Table 7.4.

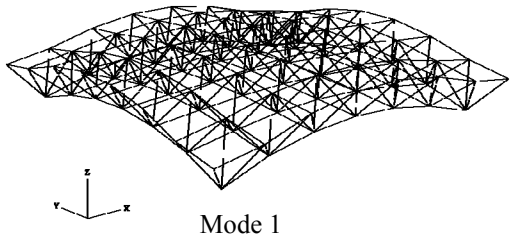

Mode 1

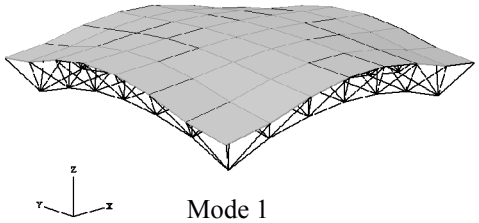

Mode 1

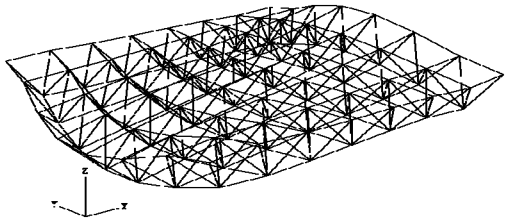

Mode 2

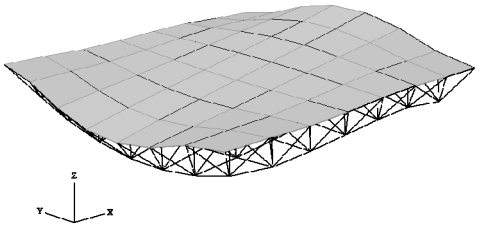

Mode 2

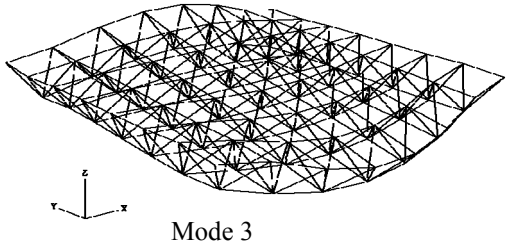

Mode 3

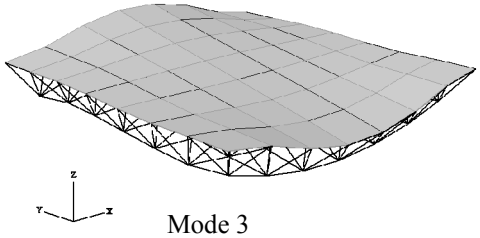

Mode 3

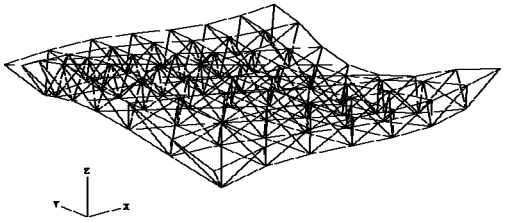

Mode 4

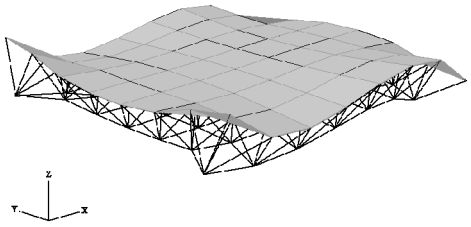

Mode 4

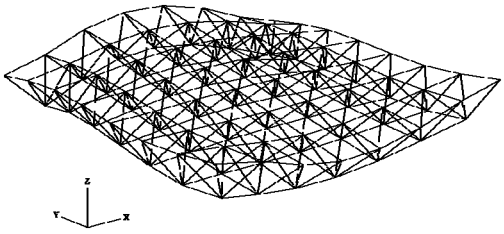

Mode 5

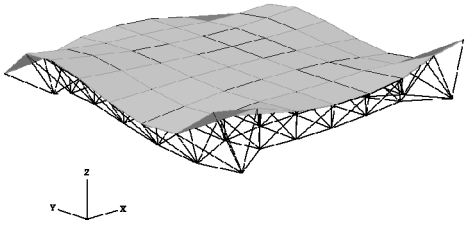

Mode 5

a. Non-composite FE model

b. Composite FE model

Figure 7.1 Vibration mode shapes for corner-supported models with AR = 1.0

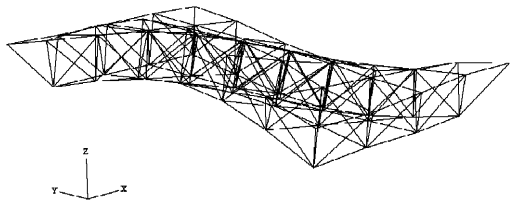

Mode 1

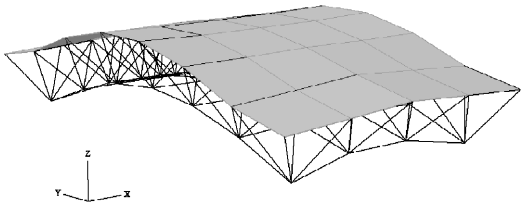

Mode 1

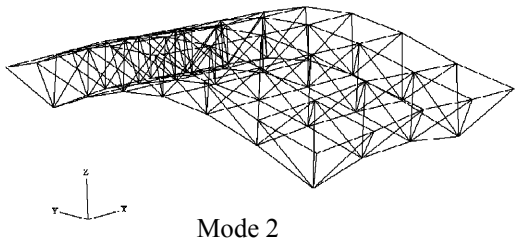

Mode 2

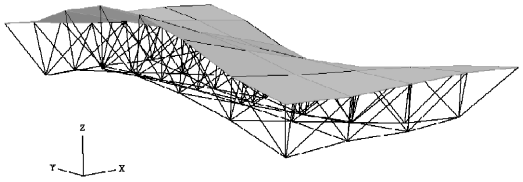

Mode 2

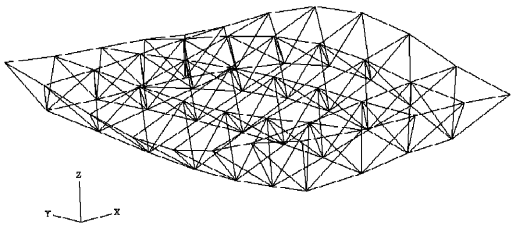

Mode 3

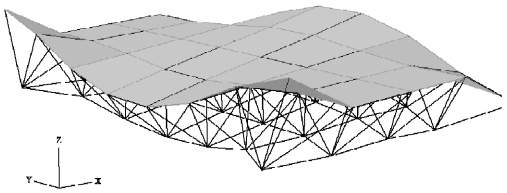

Mode 3

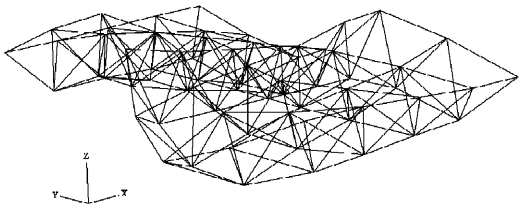

Mode 4

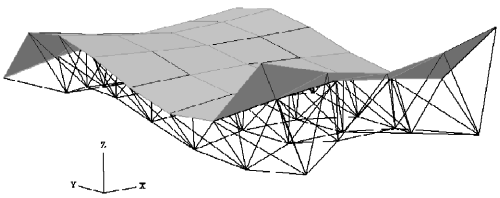

Mode 4

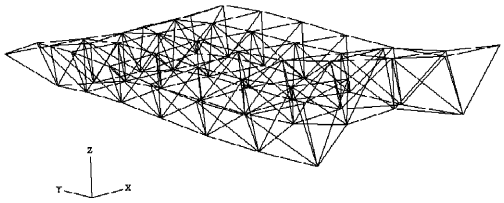

Mode 5

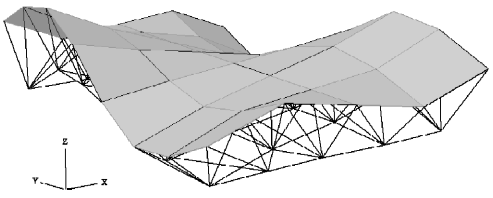

Mode 5

a. Non-composite FE model

b. Composite FE model

Figure 7.2 Vibration mode shapes of corner-supported models with AR = 2.0

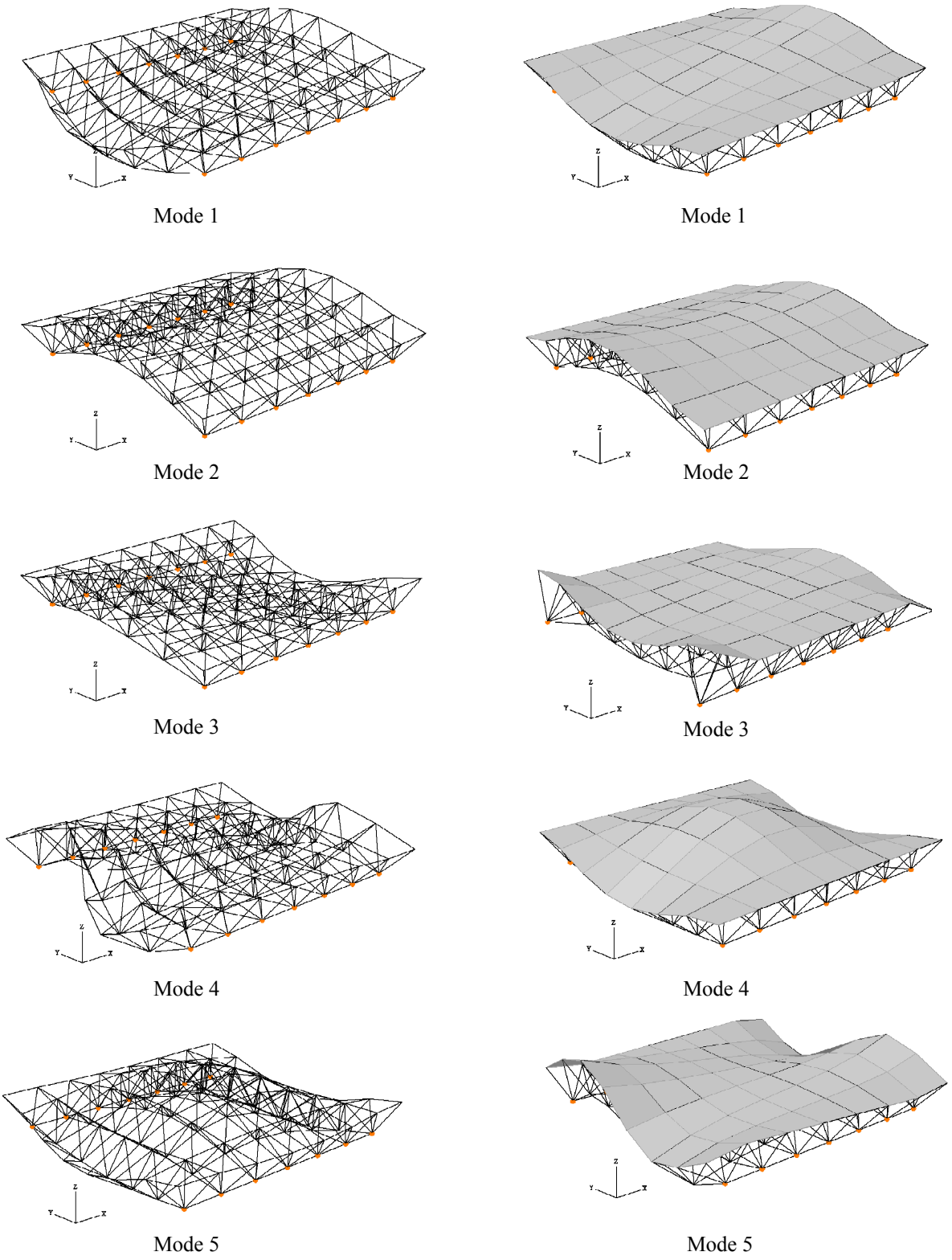

a. Non-composite FE model b. Composite FE model

Figure 7.3 Vibration mode shapes of edge-supported models with AR = 1.0

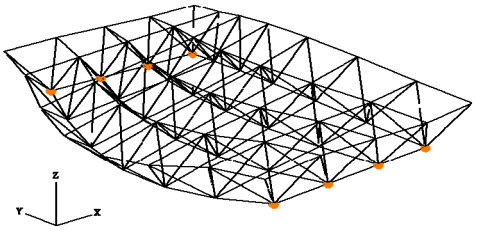

Mode 1

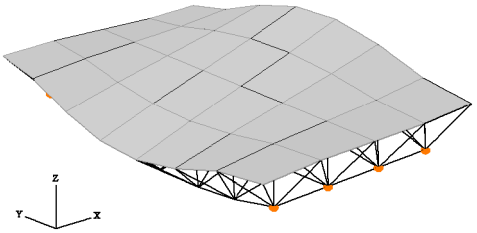

Mode 1

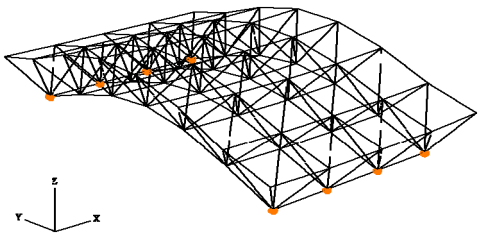

Mode 2

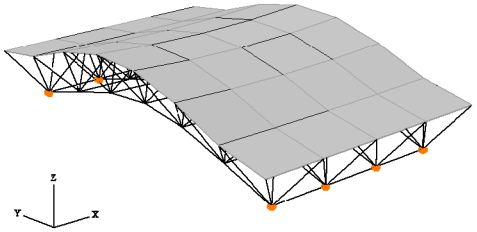

Mode 2

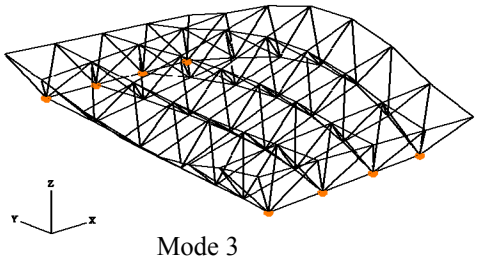

Mode 3

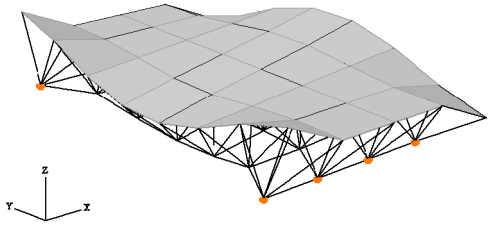

Mode 3

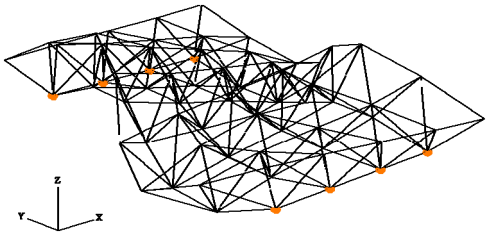

Mode 4

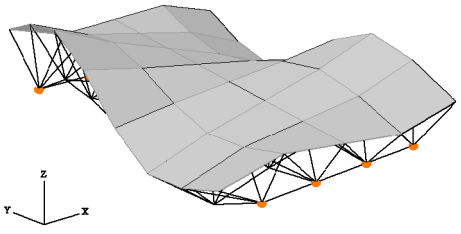

Mode 4

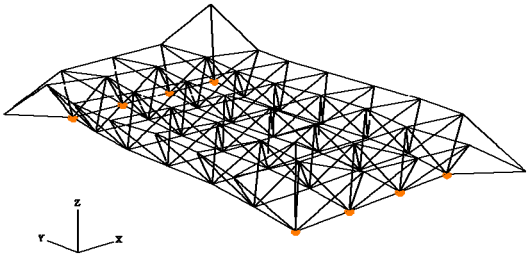

Mode 5

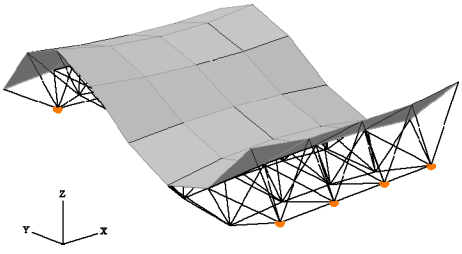

Mode 5

a. Non-composite FE model

b. Composite FE model

Figure 7.4 Vibration mode shapes for edge-supported models with AR = 2.0

Table 7.1 Experimental and numerical results of corner-supported space frame models with AR = 1.0

I- Non-Composite Truss A											
Mode	Exp.	Direct.	Model 1	Model 2	Model 3	Model 4	Model 5	Model 6	Model 7	Model 8	Model 9
1	**18.847**	Z	16.955	16.966	17.687	14.779	16.609	15.418	16.381	17.014	19.356
2	**20.929**	X	19.018	19.08	19.98	17.465	19.146	17.948	18.734	19.816	20.767
3	-------	------	19.018	19.08	19.98	17.465	19.146	17.948	18.734	19.816	20.935
4	-------	------	24.26	24.302	26.578	23.272	25.406	24.594	25.547	29.14	26.759
5	-------	------	24.26	24.302	26.578	23.272	25.406	24.594	25.547	29.14	27.418
II- Composite Truss with Aluminium Deck Truss B											
Mode	Exp.	Direct.	Model 1	Model 2	Model 3	Model 4	Model 5	Model 6	Model 7	Model 8	Model 9
1	**20.104**	Z	18.705	18.719	19.176	17.093	18.605	17.767	18.118	19.967	20.69
2	-------	------	24.782	24.816	25.433	22.867	24.723	23.71	24.144	27.379	26.992
3	-------	------	24.782	24.817	25.433	22.867	24.723	23.71	24.144	27.379	27.725
4	**29.435**	X	31.559	31.589	33.703	30.236	32.732	31.229	31.819	32.461	33.167
5	-------	------	31.559	31.592	33.703	30.236	32.732	31.229	31.819	32.461	36.531
III- Composite Truss with Timer Deck Truss C											
Mode	Exp.	Direct.	Model 1	Model 2	Model 3	Model 4	Model 5	Model 6	Model 7	Model 8	Model 9
1	**19.293**	Z	16.946	16.958	18.955	17.003	18.418	17.62	17.947	19.731	20.329
2	-------	------	22.759	22.79	25.094	22.688	24.422	23.46	23.871	26.95	26.528
3	-------	------	22.759	22.79	25.094	22.688	24.422	23.46	23.871	26.95	27.157
4	**28.553**	X	28.844	28.87	33.313	29.979	32.379	30.924	31.495	32.135	32.747
5	-------	Y	28.844	28.872	33.313	29.979	32.379	30.924	31.495	32.135	36.027

Table 7.2 Experimental and numerical results of corner-supported space frame models with AR = 2.0

I- Non-Composite Truss A											
Mode	Exp.	Direct.	Model 1	Model 2	Model 3	Model 4	Model 5	Model 6	Model 7	Model 8	Model 9
1	**15.544**	X	16.82	16.526	13.954	15.17	21.116	17.372	15.71	16.105	18.853
2	**22.355**	Z	22.195	21.202	17.157	18.666	26.462	20.457	19.799	21.323	25.504
3	-------	------	25.984	25.278	21.655	24.231	32.768	26.612	24.197	26.792	28.604
4	-------	------	32.049	31.439	25.771	28.322	39.229	32.42	28.938	29.502	28.655
5	-------	------	35.477	34.274	28.943	31.336	43.106	32.852	32.879	33.131	29.745
II- Composite Truss with Aluminium Deck Truss B											
Mode	Exp.	Direct.	Model 1	Model 2	Model 3	Model 4	Model 5	Model 6	Model 7	Model 8	Model 9
1	**21.559**	Z	24.495	23.973	20.965	21.814	29.529	25.351	22.573	23.648	27.662
2	**22.282**	X	24.786	24.505	22.641	23.573	31.476	27.661	23.821	24.38	27.688
3	-------	------	33.492	32.989	27.709	29.444	36.598	30.663	29.583	30.162	35.299
4	-------	------	37.506	35.843	32.696	32.98	48.578	42.792	37.158	36.682	43.306
5	-------	------	41.159	40.113	35.845	37.433	51.861	44.698	39.116	38.519	44.581
III- Composite Truss with Timer Deck Truss C											
Mode	Exp.	Direct.	Model 1	Model 2	Model 3	Model 4	Model 5	Model 6	Model 7	Model 8	Model 9
1	**21.687**	Z	23.99	21.782	20.76	21.481	28.869	24.98	22.344	23.334	27.011
2	**27.693**	X	24.376	22.853	22.584	23.346	30.956	27.531	23.72	24.218	27.228
3	-------	------	32.7	30.167	27.565	29.068	35.953	30.299	29.348	29.86	34.575
4	-------	------	37.405	33.539	32.769	32.956	48.428	42.7	37.133	36.657	43.129
5	-------	------	41.007	38.082	36.088	37.486	51.584	44.589	39.223	38.637	44.411

Table 7.3 Experimental and numerical results of two-edge-supported space frame models with AR = 1.0

I- Non-Composite Truss A											
Mode	Exp.	Dir.	Model 1	Model 2	Model 3	Model 4	Model 5	Model 6	Model 7	Model 8	Model 9
1	**21.462**	X	20.092	20.163	21.258	18.673	20.378	19.178	20.013	16.502	22.298
2	**25.597**	Z	25.6	25.617	26.655	22.515	25.007	23.034	24.502	18.984	29.101
3	-------	------	26.255	26.307	28.138	24.345	26.789	25.792	26.877	25.707	29.268
II- Composite Truss with Aluminium Deck Truss B											
Mode	Exp.	Dir.	Model 1	Model 2	Model 3	Model 4	Model 5	Model 6	Model 7	Model 8	Model 9
1	-------	-------	27.471	27.509	27.532	24.459	26.677	25.435	25.946	24.1	30.344
2	**29.221**	Z	30	30.024	29.563	25.785	28.526	27.004	27.607	24.802	32.865
3	**37.416**	X	41.411	41.464	39.023	33.432	37.443	35.524	36.342	30.528	42.558
III- Composite Truss with Timber Deck Truss C											
Mode	Exp.	Dir.	Model 1	Model 2	Model 3	Model 4	Model 5	Model 6	Model 7	Model 8	Model 9
1	-------	-------	26.749	25.158	27.051	24.184	26.244	25.075	25.562	23.817	29.551
2	**29.202**	Z	29.048	26.966	28.903	25.398	27.931	26.511	27.083	24.528	31.81
3	**35.955**	X	40.502	37.488	38.401	33.082	36.9	35.061	35.846	30.286	41.718

Table 7.4 Experimental and numerical results of two-edge-supported space frame models with AR = 2.0

I- Non-Composite Truss A											
Mode	Exp.		Model 1	Model 2	Model 3	Model 4	Model 5	Model 6	Model 7	Model 8	Model 9
1	**17.868**	X	17.039	16.758	14.282	15.475	21.477	17.679	15.942	16.349	19.195
2	**25.205**	Z	24.983	23.776	19.53	20.763	29.819	23.124	22.059	23.471	28.174
3	**-------**	**------**	26.319	25.65	21.983	24.753	33.271	26.919	24.354	27.013	29.13
II- Composite Truss with Aluminium Deck Truss B											
Mode	Exp.		Model 1	Model 2	Model 3	Model 4	Model 5	Model 6	Model 7	Model 8	Model 9
1	**26.864**	X	25.355	25.099	23.092	24.089	25.099	28.244	24.134	24.744	28.359
2	**27.947**	Z	29.069	28.578	24.021	25.269	28.578	28.757	25.216	26.563	31.753
3	**-------**	**------**	35.866	35.848	28.939	31.566	35.848	31.203	30.232	30.919	38.225
III- Composite Truss with Aluminium Deck Truss C											
Mode	Exp.		Model 1	Model 2	Model 3	Model 4	Model 5	Model 6	Model 7	Model 8	Model 9
1	**23.148**	X	24.891	23.37	22.961	23.795	23.37	28.004	23.983	24.535	27.825
2	**27.693**	Z	28.168	25.755	23.611	24.696	25.755	28.142	24.844	26.075	30.735
3	**-------**	**------**	34.913	32.652	28.806	31.13	32.652	30.84	29.999	30.608	37.369

7.3.1 Results of modal analysis of corner-supported models

I. Models with aspect ratio, AR = 1.0

As can be seen in Figure 7.5a, the results of modal analysis carried out on corner-supported square models show clearly that FE Model 9 was the most accurate in predicting the vertical frequency of Trusses A to C, with only 2.7% overestimate in frequencies of vibration experimentally obtained. On the other hand, FE Model 4 was the best in estimating the frequency of the horizontal vibration mode in composite Trusses B and C, while Model 9 presented excellent agreement in non-composite Truss A (Figure 7.5b). It should be noted that first group in the graphs, referred to as Exp, is the reference group showing results of the experimental tests carried out on space frame Trusses A, B and C. Dashed lines shown in figures are used as a visual guide to select the best FE model that agree with the experimental results.

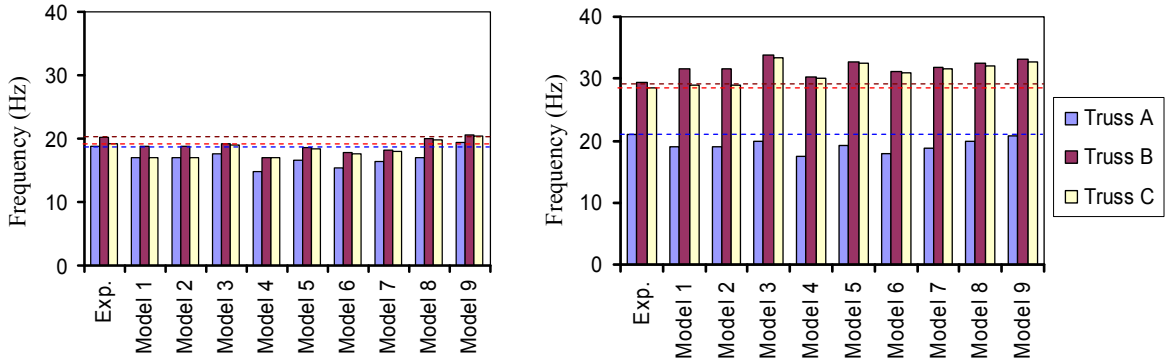

a. Vertical vibration frequency

b. Horizontal vibration frequency

Figure 7.5 Modal analysis results for corner-supported models with AR = 1.0

II. Models with aspect ratio, AR = 2.0

For models with aspect ratio of 2.0, composite action appeared to increase the horizontal stiffness of Trusses B and C more than the increase in the vertical stiffness. This effect was clear in making the vertical mode of vibration the first, with lower values, in composite Trusses B and C, and the second in Truss A (Figure 7.2).

In case of the vertical vibration mode, non-composite FE Model 1 showed an excellent agreement with experimental results of non-composite Truss A with only 0.7% overestimate (Figure 7.6a). On the other hand, composite FE Models 3 and 7 showed a good case of agreement with experimental results of Trusses B and C in the horizontal direction with 1.6% and 0.1%, respectively (Figure 7.6a). In horizontal direction Model 7 showed agreement with experimental results of Truss A, while Model 4 showed close match with composite Trusses B and C with 1.2% and 1%, respectively.

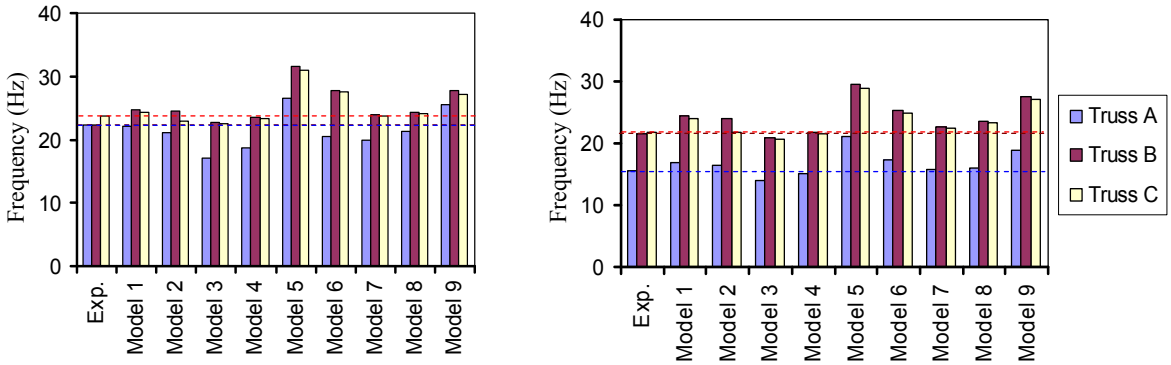

a. Vertical vibration frequency

b. Horizontal vibration frequency

Figure 7.6 Modal analysis results for corner supported models with AR = 2.0

In general, all FE models showed an increase in stiffness with the application of composite action, resulting in noticeable increases in frequency of vibration values. The effect of composite action on FE models was clear in changing the arrangement of vibration modes, which appeared in shifting the horizontal vibration mode from the first order to be the second order for composite model as shown in Figure 7.2.

7.3.2 Results of modal analysis of two-edge-supported models

I. Models with AR = 1.0

The first and second vibration modes of edge-supported models were in the horizontal and vertical directions, respectively. This observation remained valid with different aspect ratios (Figure 7.3). Numerical models presented a good agreement with the

experimental results in horizontal direction with the best achieved with FE Models 3 for Truss A with only 1.0% underestimate and Model 5 for Trusses B and C with 0.1% and 2.6% overestimate, respectively (Figure 7.7b).

All models showed good accuracy in predicting the vibration frequencies of vertical modes, with the best accuracy observed with Model 1 for Truss A with zero difference. Models 3 and 1 showed an excellent accuracy in predicting the vibration frequency in the horizontal direction for Trusses B and C, respectively, with 1.2% overestimate for Truss B and 0.5% for Truss C (Figure 7.7a).

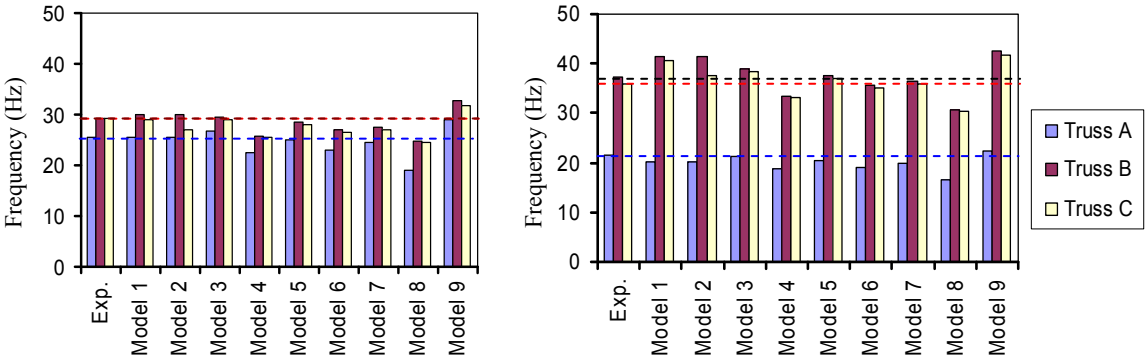

a. Vertical mode of frequency b. Horizontal mode of frequency

Figure 7.7 Vibration frequencies for two-edge supported models with AR = 1.0

II. Models with AR = 2.0

For all edge-supported models with AR = 2.0, the first mode of frequency was in the X-direction. This was compatible with the large reduction in stiffness in the horizontal direction caused by the removal of three truss panels. In case of non-composite Truss A, Model 6 had the highest accuracy in predicting the horizontal frequency with only 1.1 % underestimation. This was followed by Model 1, which had 6.6% of frequency underestimation.

For composite Trusses B and C, Models 6 and 2 offered the closest match with the experimental results, with underestimates of 5.1% and 1.0%, respectively

(Figure 7.8b).

Vibration in the vertical direction was the second mode in all composite and non-composite models. For non-composite Truss A, FE Model 1 underestimated the frequency by 0.9%, offering the highest accuracy, while Model 6 had the best agreement with the experimental results for composite Trusses B and C with only 2.9% and 1.6% overestimates, respectively (Figure 7.8a).

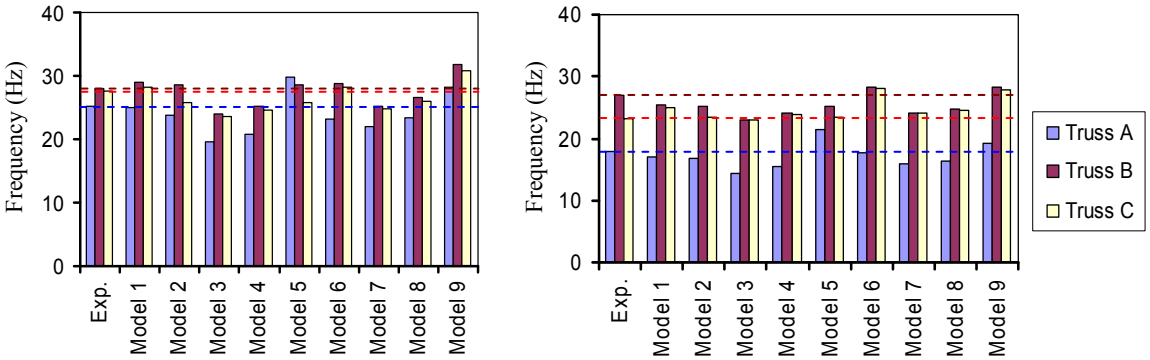

a. Vertical vibration frequency

b. Horizontal vibration frequency

Figure 7.8 Vibration frequencies for two-edge-supported models with AR = 2.0

7.4 Lateral displacements under shaking table vibrations

To check the validity of numerical models in simulating the dynamic behaviour of test models, all proposed FE models were exposed to an acceleration time-history similar to that produced by the shaking table. The lateral displacement was recorded at the middle joint of the top edge perpendicular to the shaking table movements (Figure 3.16). This joint was where the lateral displacement response of test models was measured in the laboratory.

7.4.1 Corner-supported models

Figure 7.9 shows an example of the output of numerical analysis results of Model 4 compared to the output recorded experimentally for corner-supported non-composite

Truss A with an aspect ratio, AR = 1.0. An example of the accuracy of composite Model 1 in predicting the lateral displacements of composite Truss B is shown in Figure 7.10. Both figures demonstrate the high accuracy of the numerical models in simulating actual models, which can be seen in Table 7.5.

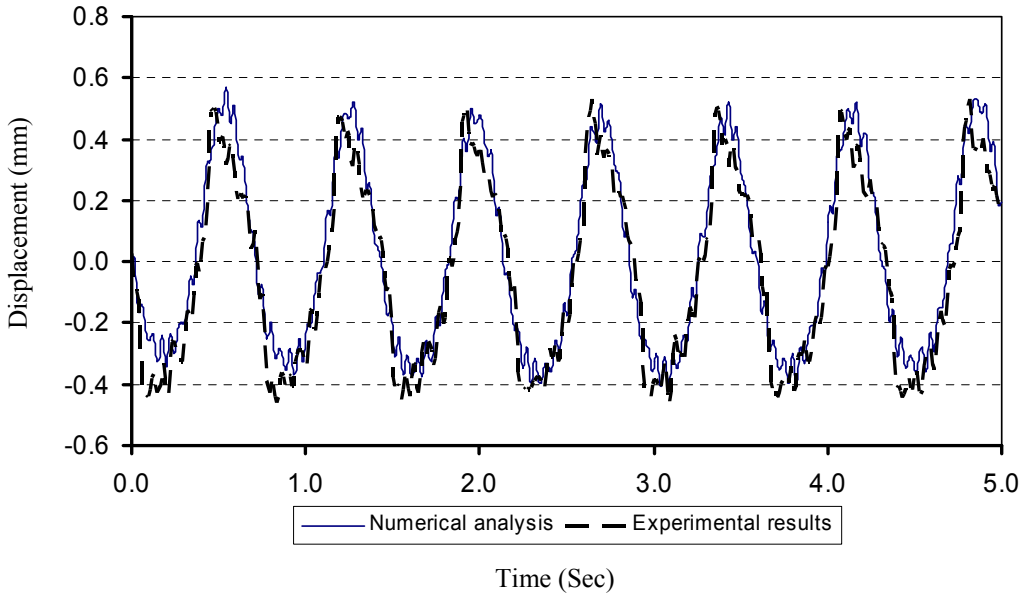

Figure 7.9 Experimental and numerical analysis results of non-composite Truss A

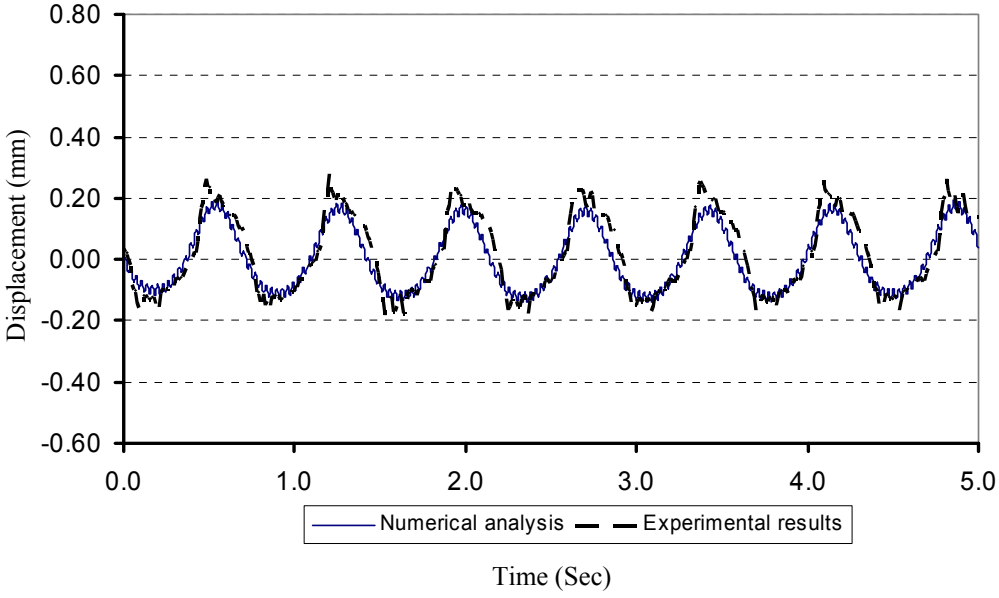

Figure 7.10 Experimental and numerical analysis results of composite Truss B

A more complete list of displacement responses to shaking table vibrations, obtained experimentally and from numerical analysis carried out on composite and non-composite corner-supported models with AR = 1.0, is shown in Table 7.5. Furthermore, the results of corner-supported models with AR = 2.0 can be found in Table 7.6.

Table 7.5 Lateral displacements of corner-supported models with AR = 1.0

I- Non-composite model Truss A										
	Exp.	Model1	Model2	Model3	Model4	Model5	Model6	Model7	Model8	Model9
Max	0.543	0.571	0.564	0.456	0.545	0.466	0.489	0.477	0.332	0.402
Min	-0.44	-0.409	-0.409	-0.333	-0.393	-0.344	0.362	0.352	-0.241	-0.288
II- Composite model with Aluminium deck Truss B										
	Exp.	Model1	Model2	Model3	Model4	Model5	Model6	Model7	Model8	Model9
Max	0.276	0.278	0.194	0.175	0.218	0.185	0.203	0.197	0.176	0.172
Min	-0.17	-0.183	-0.141	-0.127	-0.157	-0.134	-0.147	-0.142	-0.127	-0.124
III- Composite model with timber deck Truss C										
	Exp.	Model1	Model2	Model3	Model4	Model5	Model6	Model7	Model8	Model9
Max	0.245	0.240	0.240	0.184	0.226	0.195	0.211	0.206	0.185	0.181
Min	-0.21	-0.173	-0.173	-0.133	-0.162	-0.140	-0.154	-0.148	-0.133	-0.131

Table 7.6 Lateral displacements of corner-supported models with AR = 2.0

I- Non-composite model Truss A										
	Exp.	Model1	Model2	Model3	Model4	Model5	Model6	Model7	Model8	Model9
Max	0.684	0.655	0.652	0.753	0.667	0.350	0.466	0.642	0.596	0.442
Min	-0.53	-0.466	-0.481	-0.546	-0.480	-0.251	-0.333	-0.475	-0.437	-0.323
I- Composite model with Aluminium deck Truss B										
	Exp.	Model1	Model2	Model3	Model4	Model5	Model6	Model7	Model8	Model9
Max	0.264	0.175	0.179	0.258	0.227	0.139	0.193	0.226	0.209	0.156
Min	-0.17	-0.126	-0.131	-0.186	-0.166	-0.102	-0.146	-0.162	-0.146	-0.113
I- Composite model with timber deck Truss C										
	Exp.	Model1	Model2	Model3	Model4	Model5	Model6	Model7	Model8	Model9
Max	0.275	0.187	0.225	0.266	0.240	0.149	0.201	0.235	0.220	0.168
Min	-0.18	-0.134	-0.160	-0.192	-0.173	-0.108	-0.142	-0.171	-0.156	-0.119

where (Exp) in the above tables stands for Experimental.

The results shown in Tables 7.5 and 7.6 are plotted in Figures 7.11a and b, respectively, to enable quick comparison between models accuracy in predicting the maximum displacement to shaking table vibrations. Maximum values of displacement responses were considered in judging the accuracy of numerical models since the maximum response of structures exposed to dynamic loads are always the main point of interest in design procedures.

As can be seen from Figure 7.11, Models 4 and 1 demonstrated close match with physical test results on non-composite model Truss A with maximum displacement overestimation of 0.4% and 5.2%, respectively. For composite Trusses B and C, FE Model 1 was superior in simulating the composite deck models with only 0.7% displacement overestimation.

For non-composite models with aspect ratio of 2.0, Model 4 and 1 offered reasonable agreement with physical tests with 2.5% and 4.2% displacement underestimation, respectively. For composite Trusses B and C, FE Model 3 achieved the best agreement with experiments with underestimation of 2.3% followed by Models 4 and 7.

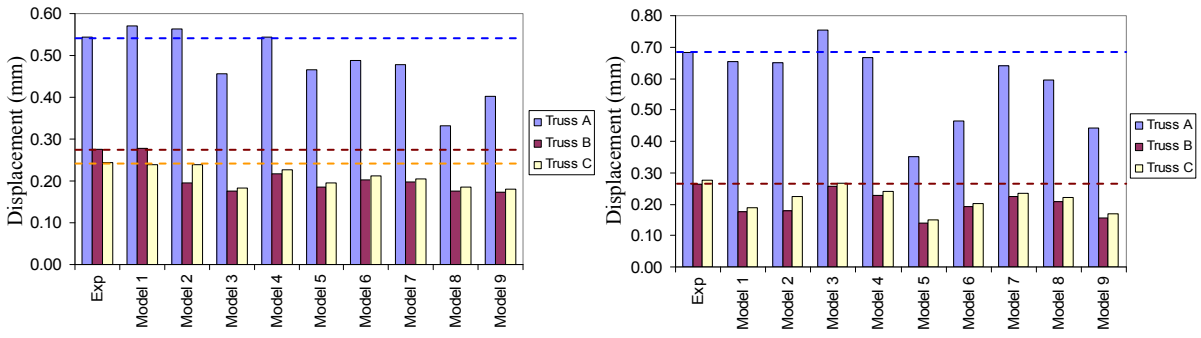

a. Models with aspect ratio of 1.0

b. Models with aspect ratio of 2.0

Figure 7.11 Response comparison for different corner supported models

7.4.2 Two-edge-supported models

Numerical analysis was carried out on FE models supported along the two lower edges parallel to the applied vibrations. The models included cases with AR = 1.0 and 2.0. All FE models were exposed to an acceleration history similar to that applied experimentally to physical models. Figure 7.12 presents an example of the results obtained by FE analysis for Model 1 demonstrating the ability of FE models in simulating the actual behaviour. The results obtained from FE analysis, in addition to those obtained from physical tests, are summarised in Tables 7.7 and 7.8 for models with AR = 1.0 and 2.0, respectively. The results are also plotted in Figure 7.13 to enable quick visual assessment of numerical models with AR=1.0 and 2.0.

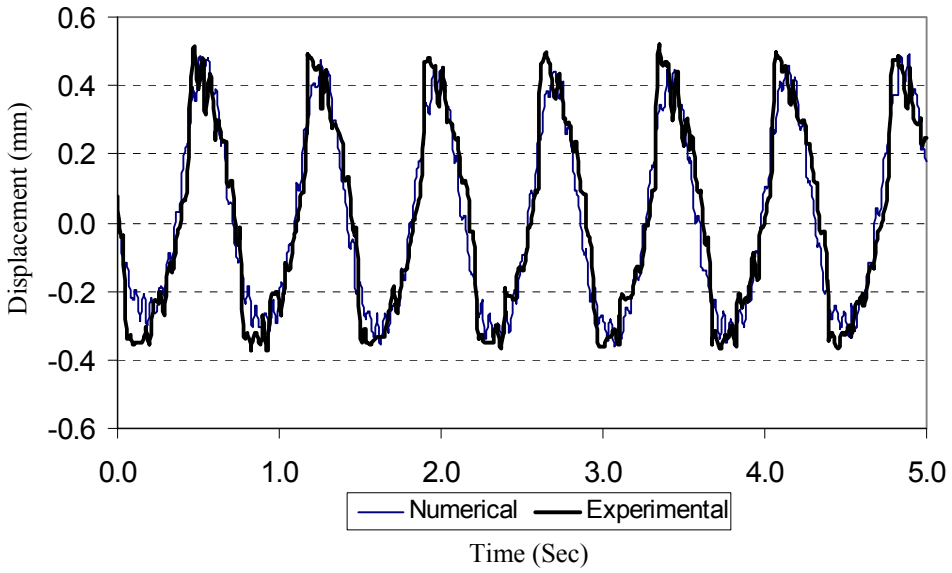

Figure 7.12 Experimental and numerical displacement behaviour of the two-edge-supported Truss A

As shown in Figure 7.13a for models with AR = 1.0, FE Model 4 underestimated the maximum displacement response of non-composite Truss A with only 1.2% followed by 4.1% for Model 1, while FE Model 8 showed the best accuracy for composite

Trusses B and C with 9.5% of underestimated displacements, followed by 20.3% for Model 5.

Table 7.7 Lateral displacements of two-edge-supported models with AR = 1.0 (mm)

I- Non-composite model Truss A										
	Exp.	Model1	Model2	Model3	Model4	Model5	Model6	Model7	Model8	Model9
Max	0.511	0.490	0.496	0.408	0.505	0.429	0.454	0.432	0.390	0.338
Min	-0.37	-0.363	-0.360	-0.305	-0.350	-0.318	-0.327	-0.319	-0.277	-0.246
I- Composite model with Aluminium deck Truss B										
	Exp.	Model1	Model2	Model3	Model4	Model5	Model6	Model7	Model8	Model9
Max	0.222	0.118	0.117	0.131	0.177	0.142	0.158	0.150	0.201	0.103
Min	-0.13	-0.084	0.085	-0.096	-0.129	-0.103	-0.114	-0.109	-0.143	-0.076
I- Composite model with timber deck Truss C										
	Exp.	Model1	Model2	Model3	Model4	Model5	Model6	Model7	Model8	Model9
Max	0.229	0.127	0.148	0.141	0.185	0.152	0.167	0.161	0.210	0.113
Min	-0.20	-0.092	-0107	-0.101	-0.133	-0.109	-0.121	-0.115	-0.149	-0.082

Table 7.8 Lateral displacements of two-edge-supported models with AR = 2.0 (mm)

I- Non-composite model Truss A										
	Exp.	Model1	Model2	Model3	Model4	Model5	Model6	Model7	Model8	Model9
Max	0.647	0.634	0.634	0.707	0.635	0.338	0.448	0.627	0.573	0.418
Min	0.498	-0.446	-0.454	-0.519	-0.448	-0.248	-0.325	-0.465	-0.412	-0.303
I- Composite model with Aluminium deck Truss B										
	Exp.	Model1	Model2	Model3	Model4	Model5	Model6	Model7	Model8	Model9
Max	0.281	0.151	0.152	0.236	0.198	0.128	0.185	0.216	0.194	0.130
Min	-0.161	-0.109	-0.110	-0.170	-0.142	-0.091	-0.139	-0.155	-0.137	-0.094
I- Composite model with timber deck Truss C										
	Exp.	Model1	Model2	Model3	Model4	Model5	Model6	Model7	Model8	Model9
Max	0.303	0.164	0.192	0.244	0.209	0.140	0.196	0.225	0.205	0.141
Min	0.173	-0.119	-0.136	0.175	-0.152	-0.101	-0.141	-0.162	-0.147	-0.102

Note that (Exp) in Tables 7.7 and 7.8 denotes to Experimental test results.

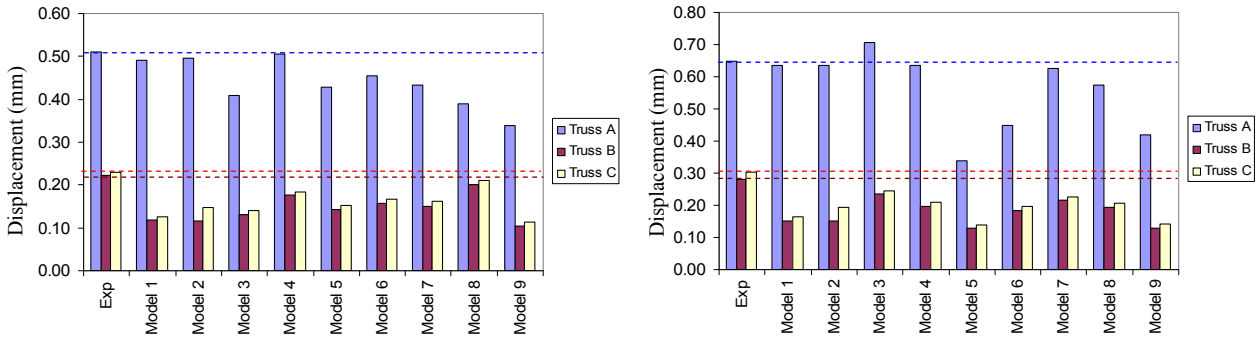

a. Edge-supported models with AR = 1.0

b. Edge-supported models with AR = 2.0

Figure 7.13 Response comparisons for edge-supported models

For models with AR = 2.0, FE Models 1 and 4 presented the best accuracy for non-composite Truss A, both with 2.0% displacement underestimation. On the other hand, Model 3 followed by Model 4 showed the best match with physical tests for composite Trusses B and C, with displacement underestimations of 16% and 29.5%, respectively.

The inaccuracies experienced with FE models in predicting the lateral response of physical models are thought to be due to the difficulties in simulating the local behaviour of joints at the connection with the top deck. In addition, the removal of the deck in physical models allowed for more local joint deformations which were difficult to simulate by FE models, leading to overestimation of lateral stiffness and consequently underestimation of lateral displacement responses. Furthermore, the friction and the slippage between joint components in addition to the friction at supports were difficult to be evaluated, leading to lower accuracy of numerical models especially for those models with higher details such as Models 8 and 9.

7.5 Model selection and general comments

The previous discussion on numerical analysis results revealed the following trends:

1. Composite action had a noticeable effect in changing the dynamic characteristics of space frames, which was evident in increasing the vibration

frequencies in all directions and changing the arrangement of vibration modes as observed in corner- supported models (Figure 7.2).

2. Composite action caused a clear reduction in the lateral deformation of models under shaking table acceleration history as a result of the increase in lateral stiffness.

3. Numerical models with concentric member-joint connections were still able to predict the changes in structural dynamic behaviour with reasonable accuracy as can be seen in the case of Model 1.

4. There was no specific numerical model that offered the highest accuracy for all cases with corner and edge supports or with different aspect ratios.

According to the above observations, the selection of an optimum numerical model was not straight forward and statistics had to facilitate this task as explained below:

1. The average (AVR) accuracy in predicting the frequency and lateral maximum displacement values were determined for each FE model.

2. Since the average does not represent a real picture on the variation of obtained results about this average, the standard division (SD) was important to achieve more confidence in the selected model.

Tables 7.9 and 7.10 show the accuracy, Numerical/Experimental, of different FE models in predicting the vibration frequencies and the maximum lateral displacement values of test models.

Table 7.9 Accuracy ratios in predicting models' frequencies of vibration in vertical and horizontal directions

Model	Model1	Model2	Model3	Model4	Model5	Model6	Model7	Model8	Model9
Corner supported model Truss A (AR = 1.0)									
X-dir	0.900	0.900	0.938	0.784	0.881	0.818	0.869	0.903	1.027
Z-dir	0.909	0.912	0.955	0.834	0.915	0.858	0.895	0.947	0.992
Corner supported model Truss B (AR = 1.0)									
X-dir	0.930	0.931	0.954	0.850	0.925	0.884	0.901	0.993	1.029
Z-dir	1.072	1.073	1.145	1.027	1.112	1.061	1.081	1.103	1.127
Corner supported model Truss C (AR = 1.0)									
X-dir	0.878	0.879	0.982	0.881	0.955	0.913	0.930	1.023	1.054
Z-dir	1.010	1.011	1.167	1.050	1.134	1.083	1.103	1.125	1.147
Corner supported model Truss A (AR = 2.0)									
X-dir	1.082	1.063	0.898	0.976	1.358	1.118	1.011	1.036	1.213
Z-dir	0.993	0.948	0.767	0.835	1.184	0.915	0.886	0.954	1.141
Corner supported model Truss B (AR = 2.0)									
X-dir	1.136	1.112	0.972	1.012	1.370	1.176	1.047	1.097	1.283
Z-dir	1.112	1.100	1.016	1.058	1.413	1.241	1.069	1.094	1.243
Corner supported model Truss C (AR = 2.0)									
X-dir	1.036	0.941	0.897	0.928	1.247	1.079	0.965	1.008	1.167
Z-dir	0.880	0.825	0.816	0.843	1.118	0.994	0.857	0.875	0.983
Two-edge supported model Truss A (AR = 1.0)									
X-dir	0.936	0.939	0.990	0.870	0.949	0.894	0.932	0.769	1.039
Z-dir	1.000	1.001	1.041	0.880	0.977	0.900	0.957	0.742	1.137
Two-edge supported model Truss B (AR = 1.0)									
X-dir	1.027	1.027	1.012	0.882	0.976	0.924	0.945	0.849	1.125
Z-dir	1.107	1.108	1.043	0.894	1.001	0.949	0.971	0.816	1.137
Two-edge supported model Truss C (AR = 1.0)									
X-dir	0.995	0.923	0.990	0.870	0.956	0.908	0.927	0.840	1.089
Z-dir	1.126	1.043	1.068	0.920	1.026	0.975	0.997	0.842	1.160
Two-edge supported model Truss A (AR = 2.0)									
X-dir	0.954	0.938	0.799	0.866	1.202	0.989	0.892	0.915	1.074
Z-dir	0.991	0.943	0.775	0.824	1.183	0.917	0.875	0.931	1.118
Two-edge supported model Truss A (AR = 2.0)									
X-dir	0.944	0.934	0.860	0.897	0.934	1.051	0.898	0.921	1.056
Z-dir	1.040	1.023	0.860	0.904	1.023	1.029	0.902	0.950	1.136
Two-edge supported model Truss A (AR = 2.0)									
X-dir	1.075	1.010	0.992	1.028	1.010	1.210	1.036	1.060	1.202
Z-dir	1.017	0.930	0.853	0.892	0.930	1.016	0.897	0.942	1.110
AVR	**1.009**	**0.980**	**0.950**	**0.909**	**1.074**	**0.996**	**0.952**	**0.947**	**1.116**
SD	**0.077**	**0.077**	**0.108**	**0.077**	**0.156**	**0.113**	**0.072**	**0.107**	**0.076**

Table 7.10 Accuracy percentages in predicting maximum displacements

Model	Model1	Model2	Model3	Model4	Model5	Model6	Model7	Model8	Model9
Corner supported models with AR = 1.0									
Truss A	1.052	1.039	0.840	1.004	0.858	0.901	0.878	0.611	0.740
Truss B	1.007	0.703	0.634	0.790	0.670	0.736	0.714	0.638	0.623
Truss C	0.980	0.980	0.751	0.922	0.796	0.861	0.841	0.755	0.739
Corner supported models with AR = 2.0									
Truss A	0.980	0.980	1.093	0.981	0.522	0.692	0.969	0.886	0.646
Truss B	0.537	0.541	0.840	0.705	0.456	0.658	0.769	0.690	0.463
Truss C	0.541	0.634	0.805	0.690	0.462	0.647	0.743	0.677	0.465
Edge supported models with AR = 1.0									
Truss A	0.959	0.971	0.798	0.988	0.840	0.888	0.845	0.763	0.661
Truss B	0.532	0.527	0.590	0.797	0.640	0.712	0.676	0.905	0.464
Truss C	0.555	0.646	0.616	0.808	0.664	0.729	0.703	0.917	0.493
Edge supported models with AR = 2.0									
Truss A	0.980	0.980	1.093	0.981	0.522	0.692	0.969	0.886	0.646
Truss B	0.537	0.541	0.840	0.705	0.456	0.658	0.769	0.690	0.463
Truss C	0.541	0.634	0.805	0.690	0.462	0.647	0.743	0.677	0.465
AVR	**0.787**	**0.789**	**0.834**	**0.866**	**0.624**	**0.747**	**0.816**	**0.775**	**0.595**
SD	**0.217**	**0.188**	**0.174**	**0.110**	**0.144**	**0.087**	**0.094**	**0.106**	**0.102**

As can be seen from Tables 7.9 and 7.10, Model 1 was the best in predicting the horizontal and vertical vibration frequencies of test models with an average of 100.9% and lowest SD of 7.7%. However, Model 1 offered a modest accuracy in predicting the maximum displacement with an average of 78.7% and SD of 21.7%.

The same trend occurred with Model 4, which offered the highest accuracy with an average of 86.6% and 11.0% of SD in predicting the maximum displacements, while it offered an average of 90.9% in predicting vibration frequencies with 7.7% SD.

From the above discussion, it was observed that Model 1 was the best in predicting the vibration frequencies, while Model 4 was the best in predicting the displacement response. These results led to the need to calculate the overall average and standard deviation of results in addition to the Coefficient of Variance (COV = SD/AVR), see Table 7.11.

Table 7.11 Overall average, standard deviation and COV of numerical models' accuracy

	Model1	Model2	Model3	Model4	Model5	Model6	Model7	Model8	Model9
AVR	0.926	0.908	0.903	0.885	0.920	0.909	0.902	0.884	0.935
SD	0.187	0.167	0.142	0.101	0.269	0.164	0.108	0.140	0.275
COV	0.202	0.184	0.158	0.114	0.292	0.180	0.120	0.159	0.294
95%Conf.	0.061	0.055	0.046	0.033	0.088	0.054	0.035	0.046	0.090

The COV (SD/AVR) and the confidence interval of 95% were used to determine the FE model with best results and less variation around the mean to increase the confidence in the obtained results.

It is clear from Table 7.11 that Model 4 had an overall average of 88.5% and a minimum standard deviation of 10.1% with the minimum COV of 11.4% and minimum confidence interval of 88.5% ± 3.3%, which means that this model was the optimum model in predicting behaviour of physical models with reasonable accuracy and minimum variation around the mean value (error ratio).

Although more sophisticated FE Models 5 to 9 attempted to represent the actual details of physical models' components, which theoretically should improve accuracy, their performance was possibly affected by the lack of knowledge on the friction between joint components and also between composite decks and upper joints. These models may give improved accuracy if the analysis was carried out at the joint level which gives more attention to internal friction between joint surfaces in addition to local deformations, but this kind of analysis was not possible with models in this study due to large number of joints and elements. However, results obtained from FE analysis on all models showed, in general, good agreement with experimental tests with the highest for Model 4.

Last discussion resulted in selecting Model 4 to represent the physical models, so it was selected to be used in the next parametric study. In this model, upper and lower

chord members acted as beam elements released to rotate about their horizontal axis (out of plan) and restrained in the other directions due to the continuity of chords at joints. Diagonal members had a circular cross section with 4 mm diameter. Both ends were simulated with horizontal flat beam elements with rectangular cross section of 6.28×2.0mm and 10 mm length (Figure 7.14). More details about Model 4 can be found in Chapter 3.

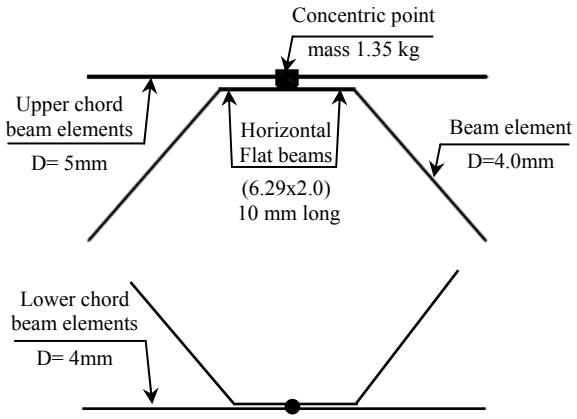

Figure 7.14 Modelling details of Model 4

7.6 Parametric study

The study included several parameters, which were difficult to be simulated in the laboratory environment due to the limitation of time and the difficulty in building several models required for the study. All models used in this study had dimensions similar to those used in the experimental models (see Chapter 3). The parameters considered and the details of the numerical study are given below:

1. Two cases of composite and non-composite models were used. Only aluminium deck with thickness of 1.20mm was used as a covering deck to achieve the composite action with top chord members. Composite action with timber board was not considered since its experimental results did not vary

much from those with an aluminium deck.

2. Three support conditions with corner, corner and mid-edge, and full-edge supports were included in the study (Figure 7.15).
3. Three common space frame configurations were considered, namely; square on square offset (SOS), square on large square (SOLS) and square on diagonal (SOD) (Figures 7.15 to 7.17).
4. Five aspect ratios were considered; 1.0, 1.20, 1.50, 2.0 and 3.0.

The total number of FE models included in the study was 90 models. Two types of analysis; namely; modal and non-linear dynamic analysis, were conducted on all models using FE program ABAQUS. The analysis results are presented and discussed in the reminder of this chapter and the detailed results can be found in Appendix E. The results include the first five frequencies of vibration in addition to the mass participation factors in X, Y and Z directions. The results also include the maximum lateral displacements due to exposing the models to shaking table time history similar to that applied during experimental tests.

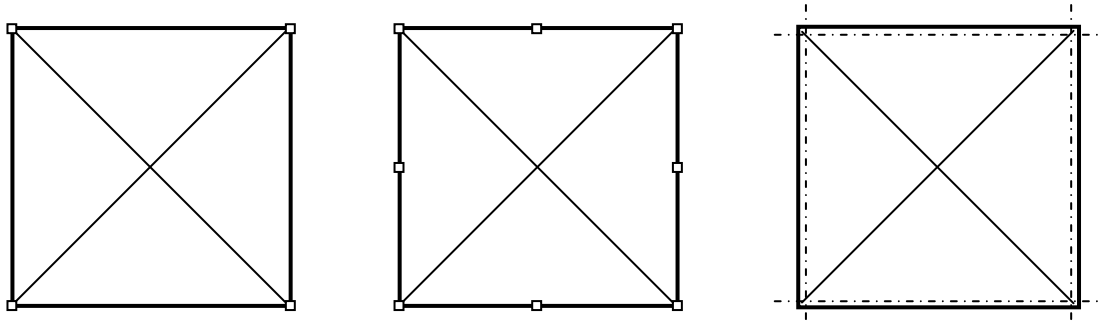

Figure 7.15 Boundary conditions considered in the parametric study

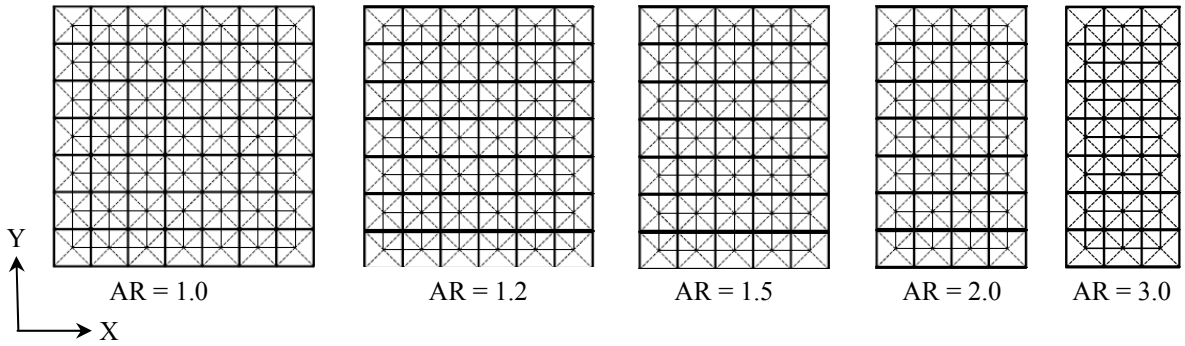

Figure 7.16 Square on square (SOS) space frame configuration with different aspect ratios

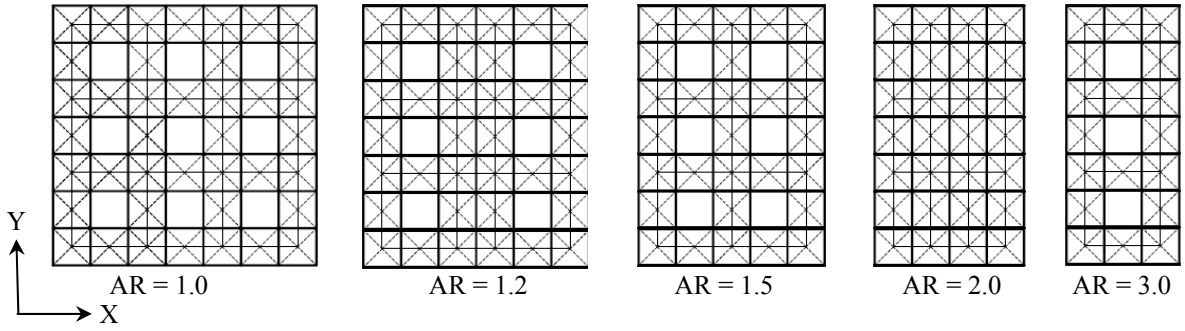

Figure 7.17 Square on large square (SOLS) space frame layouts with different aspect ratios

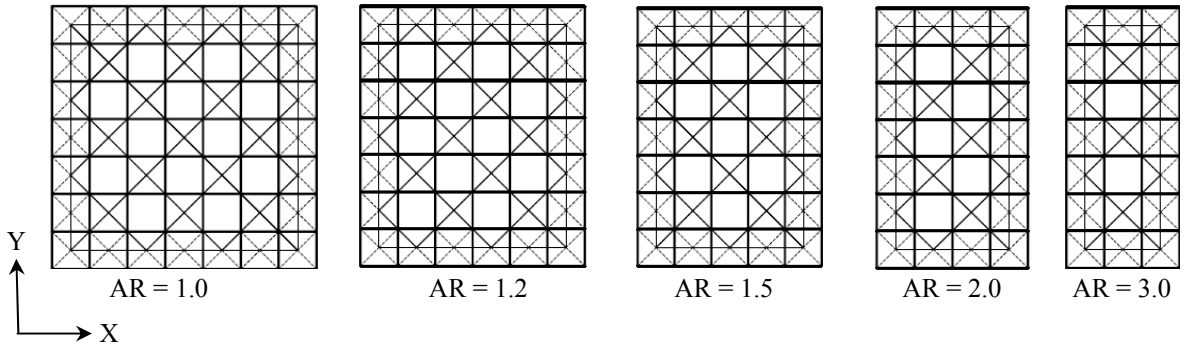

Figure 7.18 Square on diagonal (SOD) space frame configuration with different aspect ratios

7.7 Presentation and discussion of results of parametric study

7.7.1 Dynamic characteristics of models

The current study of the changes to vibration frequencies caused by the introduction of composite action, and variations in aspect ratio and boundary conditions is limited to the frequencies of vibration in the vertical (Z) and horizontal (X and Y) directions. The analysis started by determining the frequencies in the three directions by conducting modal analysis on models.

7.7.1.1 Effect of composite action

Figures 7.19 to 7.21 present the effect of composite action in changing the natural vibration frequencies of models with different aspect ratios. As a general observation, there were increases in vibration frequencies in all models due to the application of composite action. The average increases of models with different aspect ratios are listed in Table 7.12 as follows;

Table 7.12 Percentage average increases in the vibration frequencies by composite action

Direction	Corner-supported			Corner and mid-edge			Edge-supported		
	SOS	SOLS	SOD	SOS	SOLS	SOD	SOS	SOLS	SOD
X	49.5	65.1	41.2	17.0	56.9	14.1	19.1	8.1	10.5
Y	23.7	42.6	17.4	9.4	29.4	5.4	11.5	11.7	9.8
Z	10.2	8.5	7.0	6.1	3.9	2.5	14.7	11.3	6.3

As shown in Table 7.12, there was a general increase in models' frequencies in all directions. This increase was thought to be due to the stiffness added to the models by the introduction of composite action without noticeable increase in masses of tested structures. It can also be noticed that the increases in vibration frequencies in the horizontal mode of vibration were modest for all edge-supported models due to the

large horizontal stiffness of non-composite models, so little stiffness was gained by the application of composite action. However, the increases in vibration frequencies in the vertical mode of vibration were in the same range as other support conditions.

The composite action was also associated with changing the order of vibration modes that appeared clearly in the exchange of positions of vertical and horizontal modes of vibration especially in cases with high aspect ratios; see Tables E.1 to E.9 in Appendix E. It can also be observed from Table 7.12 that, the increase in lateral stiffness caused by the composite action was greater than the accompanying increase in vertical stiffness, which was reflected in the lower increases of vertical vibration frequencies compared to horizontal values.

Furthermore, the average increase in horizontal frequencies was large for models supported at corners and at corners and mid-edges, while it was small for edge-supported models. On the other hand, the above phenomenon was reversed in the case of frequency of vibration in the vertical direction.

This behaviour can be explained by the large increase of models' stiffness by have supports along the four edges, which did not have large increase by the application of composite action. However, the composite action added considerable stiffness in the vertical direction to edge-supported models, a lower value of stiffness was added in the vertical direction to models supported on corners and corners and mid-edges.

It should be noted that it was not been possible to show the stimulated modes in Figures 7.19 to 7.22, so the successive points are presenting the frequencies of vibrations in different modes.

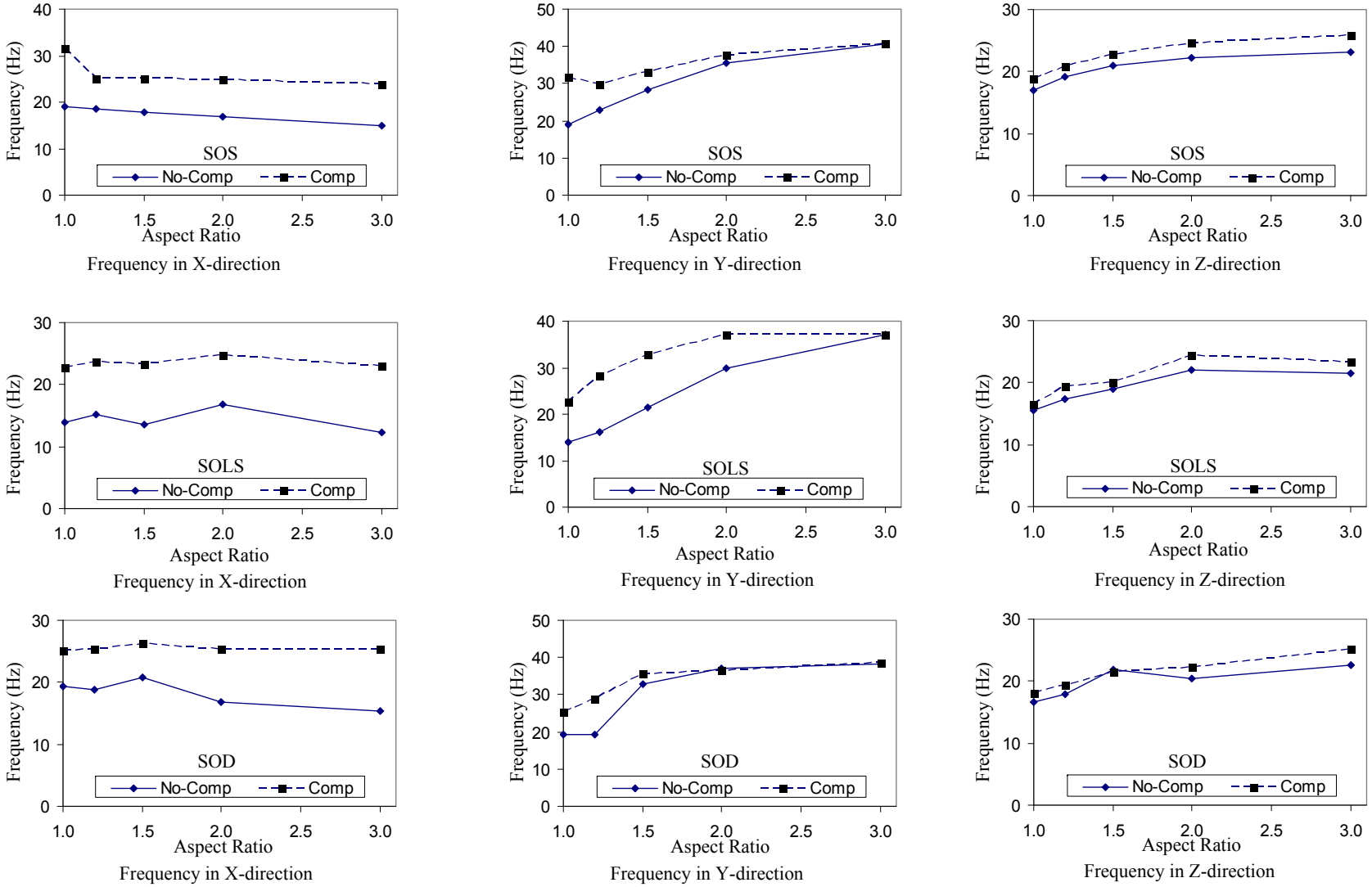

Figure 7.19 Effect of composite action on frequencies in X, Y and Z directions for corner-supported models with different aspect ratios

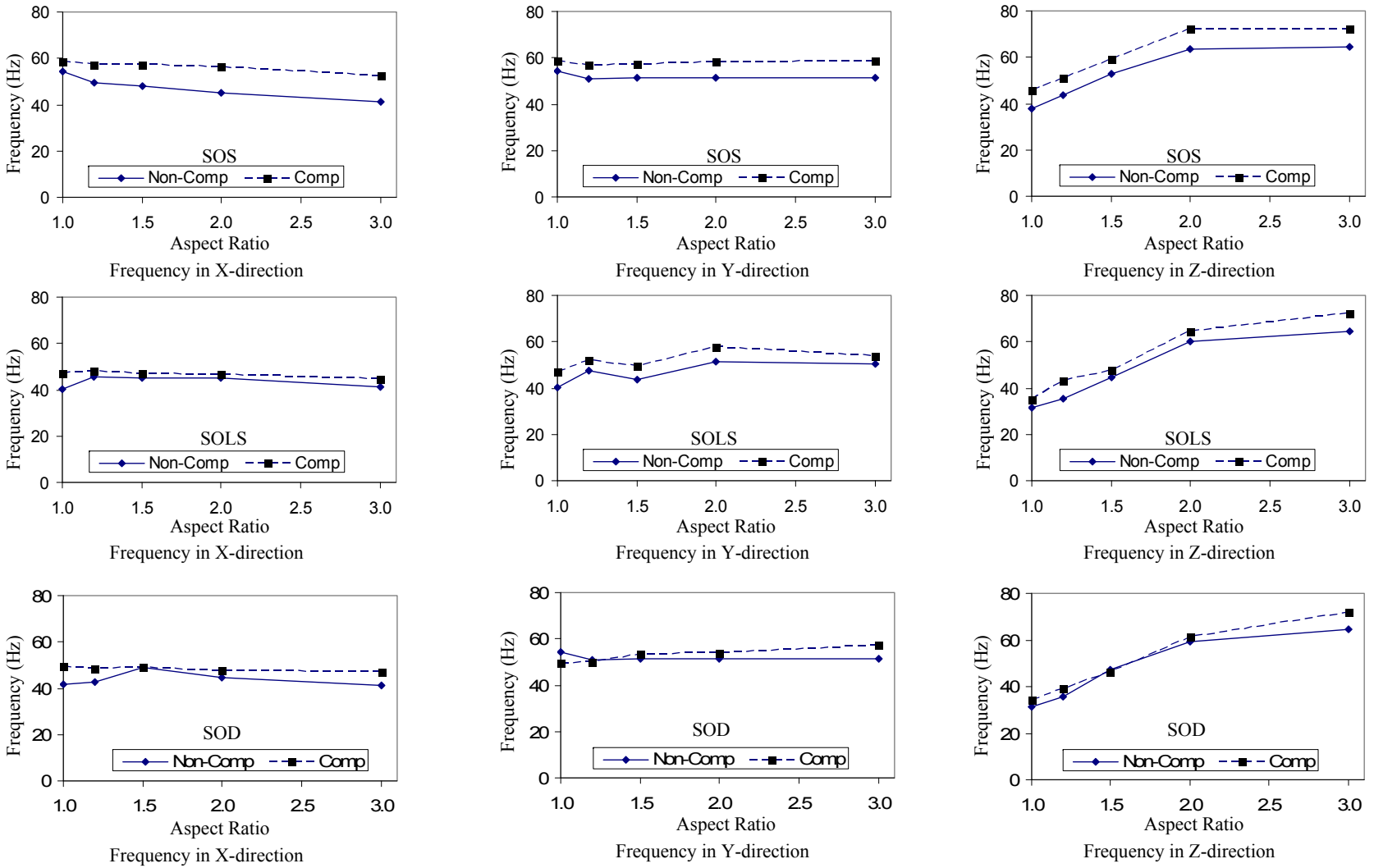

Figure 7.20 Effect of composite action on frequencies in X, Y and Z directions for edge-supported models with different aspect ratios

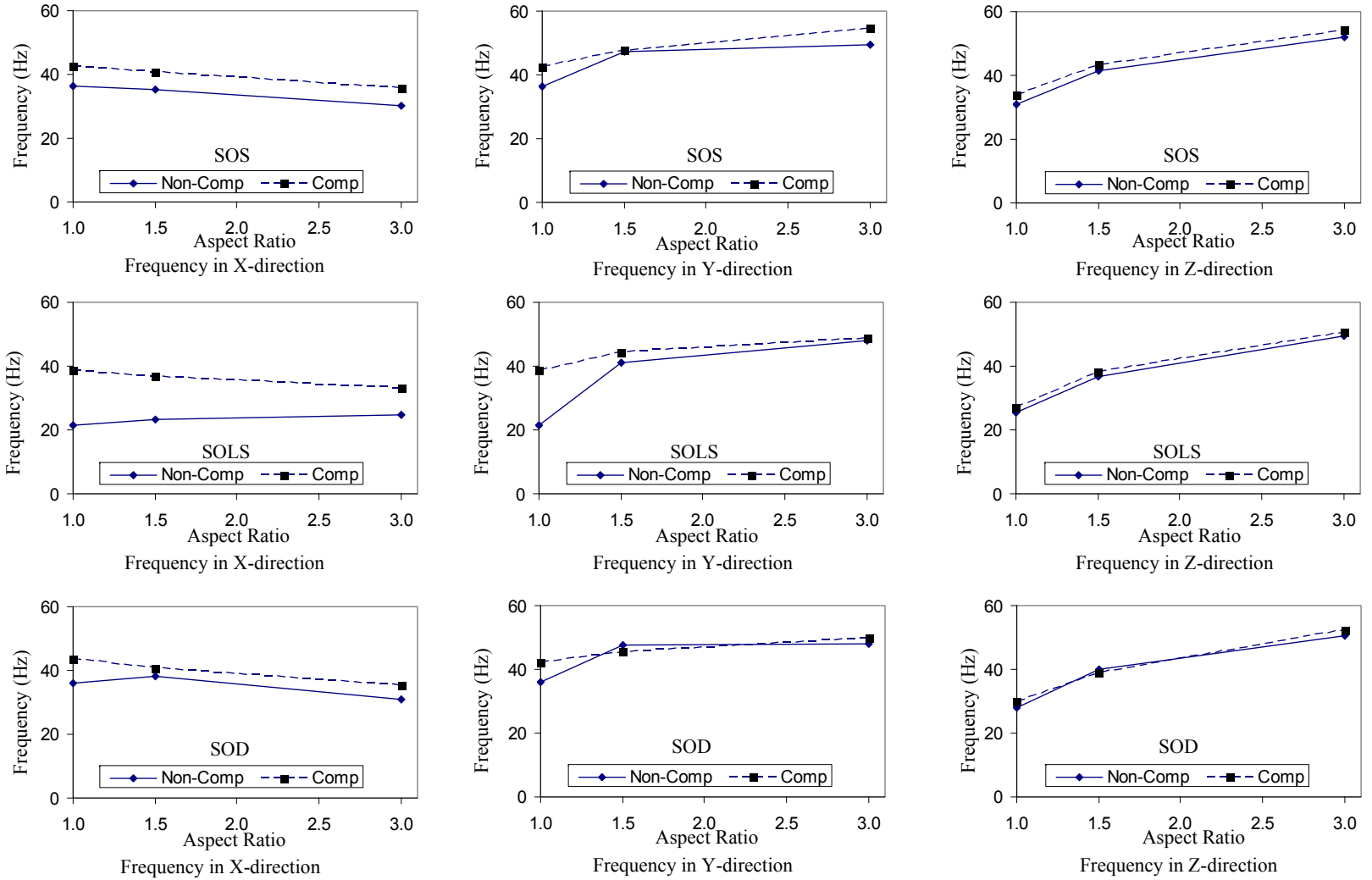

Figure 7.21 Effect of composite action on frequencies in X, Y and Z directions for models supported at corner and mid-edge points

7.7.1.2 Effect of support conditions

The change of support conditions had an effect in changing the dynamic characteristics of the numerical models as shown in Figure 7.22. The following are the main observations of this part of the study:

- For all support conditions, there was a slight reduction in frequencies of vibrations in the X-direction with the increase of aspect ratios for non-composite and composite models, which thought to be due to the reduction in model's stiffness in the X-direction due to the loss of one or more panels.

- Corner supported models had the lowest frequencies of vibration in X-direction, while edge supported models had the highest values. This trend was expected since the model's overall stiffness increased with the addition of more supports in all directions.

- For almost all cases of support conditions, there was an increase in frequencies of vibration of all models in Y-direction with the increase of aspect ratio. This trend was thought to be related to the increase in stiffness/mass ratio with the successive removal of grid panels in X-direction, leading to a general increase in the vibration frequencies in the Y-direction.

- The increase of supported points resulted in increases in vibration frequencies of all models in Z-direction with the maximum for edge-supported condition.

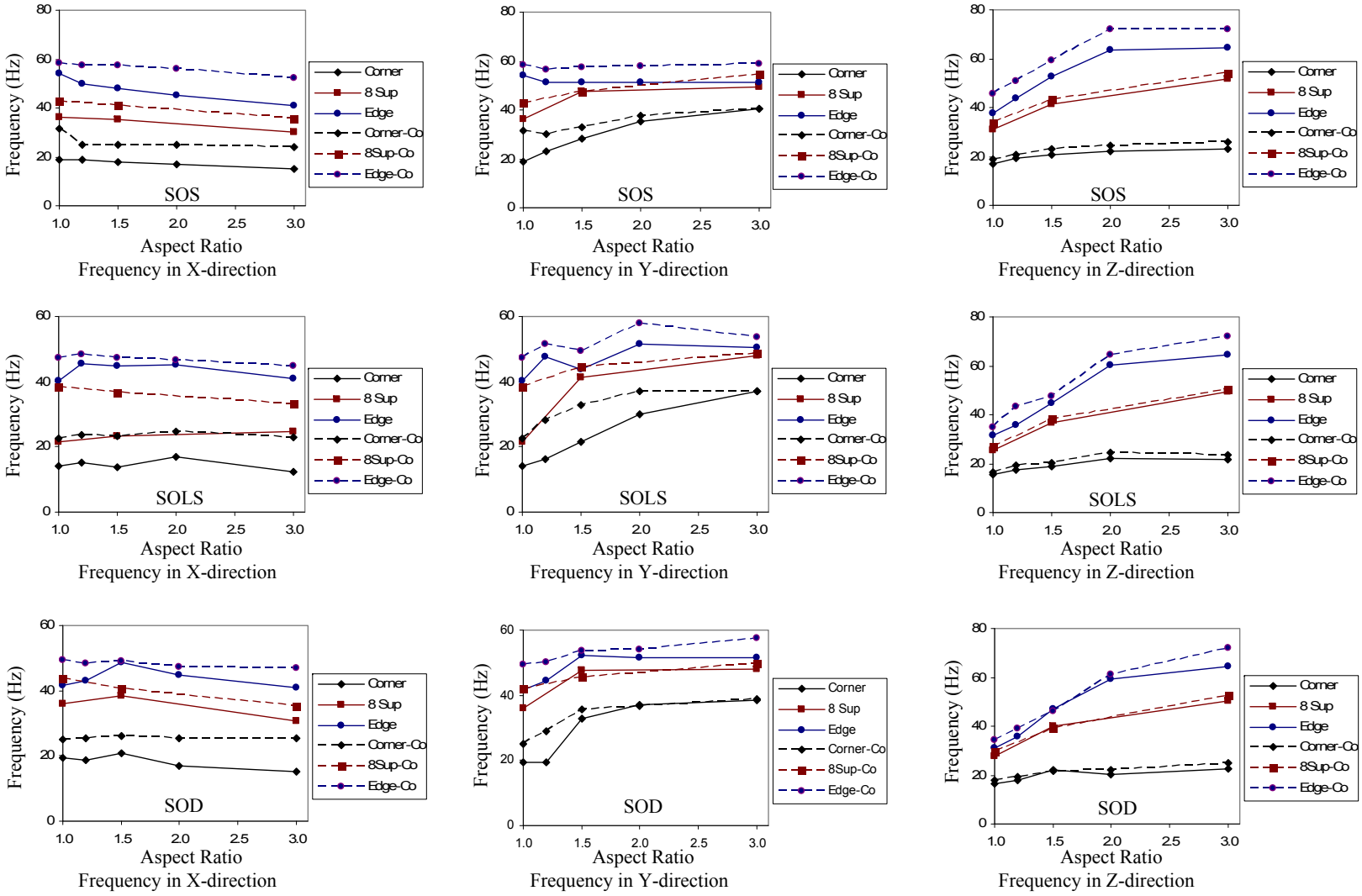

Figure 7.22 Effect of support conditions on vibration frequencies of models in X, Y and Z directions with different aspect ratios

7.7.1.3 Effect of aspect ratio

The increase of models aspect ratio resulted in a slight reduction in frequencies of vibration in X-direction with different support condition due to the noticeable reduction in stiffness to mass ratio caused by successive removal of panels (Figure 7.22). On the other hand, the increase in models' aspect ratio resulted in an increase in the vibration frequencies in Y-direction. This behaviour could be explained by the modest reduction of models' stiffness in Y-direction compared to the large reduction in mass caused by removing a panel or more in the X-direction.

A similar phenomenon occurred for frequencies of vibration in the Z-direction as there was an increase in vibration frequencies of models with the increase of aspect ratio. The increase in vibration frequencies resulted from the considerable reduction in models' masses caused by the removal of panels.

The above trends were the same for composite and non-composite models with different configurations and support conditions.

7.7.1.4 Effect of space frame configuration

Studying the effect of changing space frame configuration was one of the important parameters covered by this parametric study since the experimental study was limited to the commonly used space frames with SOS configurations. Figures 7.23 to 7.25 show the variation in frequencies of vibration in the X, Y and Z directions, respectively, associated with changes in space frame configurations. The following observations were noted from this study:

- Non-composite and composite models with SOS configuration had the highest values of vibration frequencies in the X-direction followed by SOD then SOLS configuration. On the other hand, there was a reduction in vibration frequencies

in the X-direction for composite and non-composite models with different configurations by the increase of aspect ratios. This trend extended to cover all support conditions.

- An increase in vibration frequencies was observed for all models with different configurations in Y-direction with the largest increase recorded with models supported at the corners (Figure 7.23b). Models with SOS configuration had the largest values of vibration frequencies in the Y-direction followed by SOD then SOLS. This could be explained by quick deterioration of stiffness in Y-direction in SOD and SOLS configurations by the removal of panels.

- As a general observation, all composite and non-composite models with different configurations showed an increase in frequencies of vibration in the vertical Z-direction associated with the increases in aspect ratios. SOS models had the largest frequencies in the Z-direction followed by SOD and finally SOLS models. This trend continued to include all studied cases of support conditions. This behaviour was a result of the removal of several diagonals and lower chord members in SOD and SOLS models which undoubtedly affected the vertical stiffness of the models.

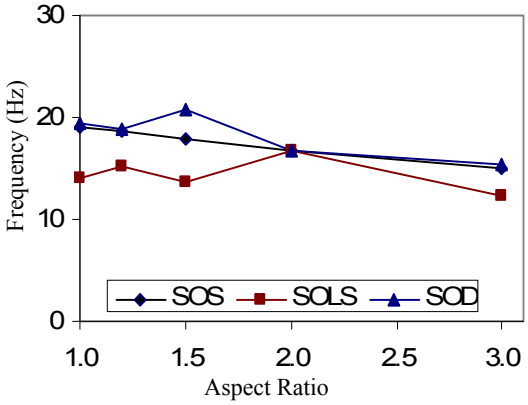

Non-composite space frame models

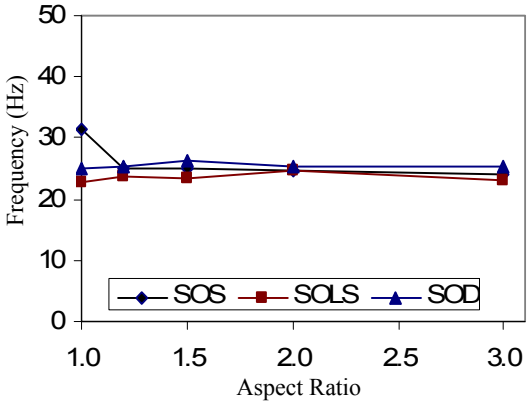

Composite space frame models

a. Frequency in X-direction

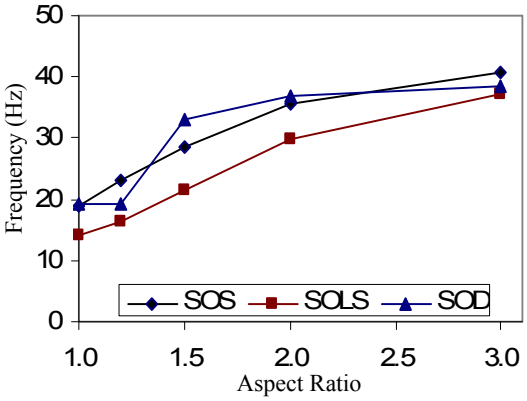

Non-Composite space frame models

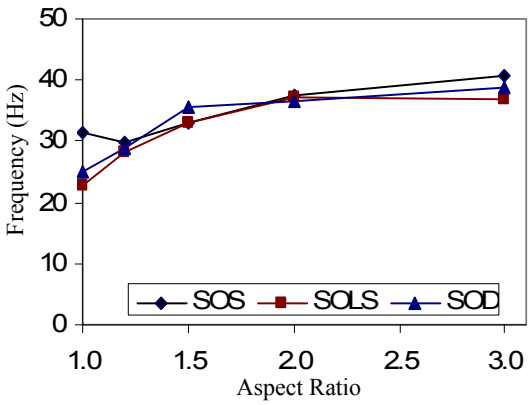

Composite space frame models

b. Frequency in Y-direction

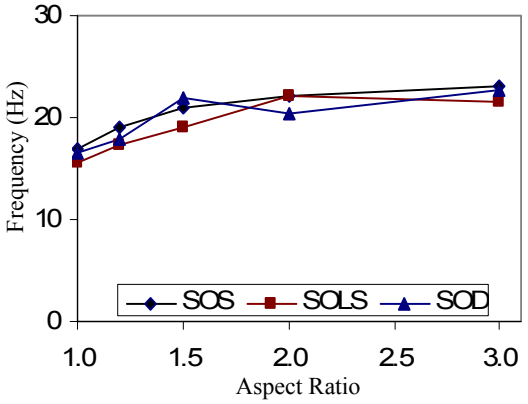

Non-composite space frame models

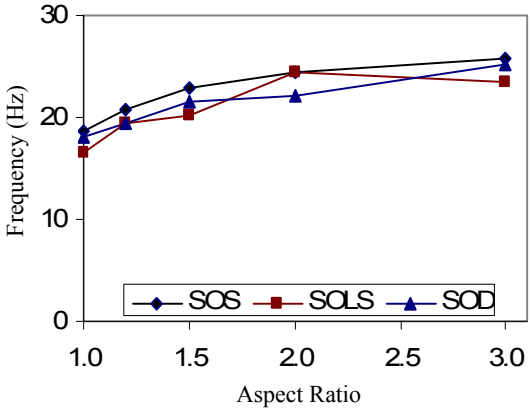

Composite space frame models

c. Frequency in Z-direction

Figure 7.23 Effect of space frame configuration on frequencies of composite and non-composite corner supported models

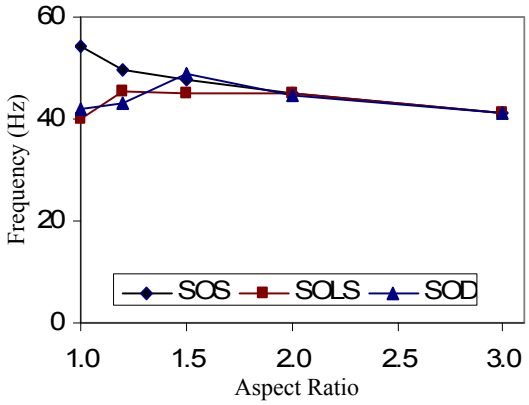

Non-Composite space frame models

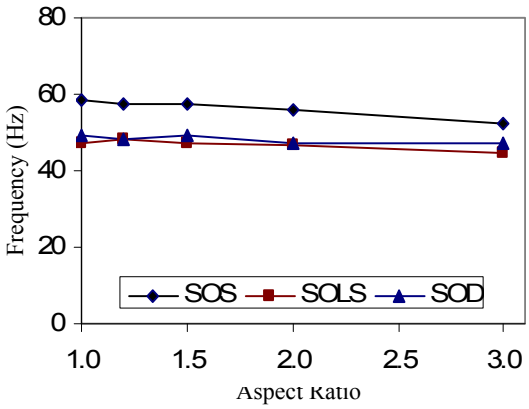

Composite space frame models

a. Frequency in X-direction

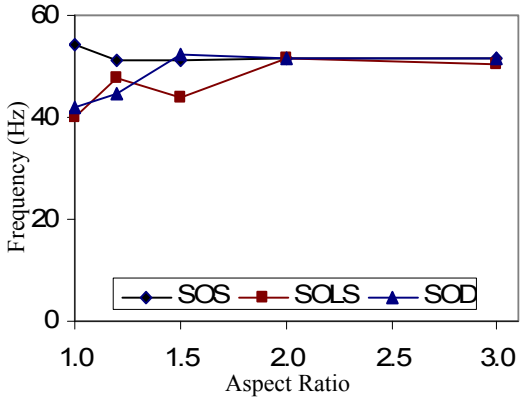

Non-Composite space frame models

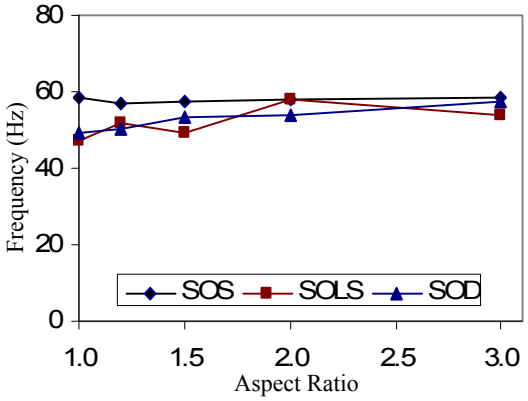

Composite space frame models

b. Frequency in Y-direction

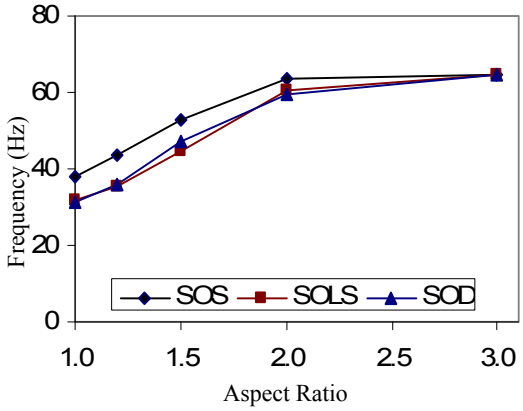

Non-Composite space frame models

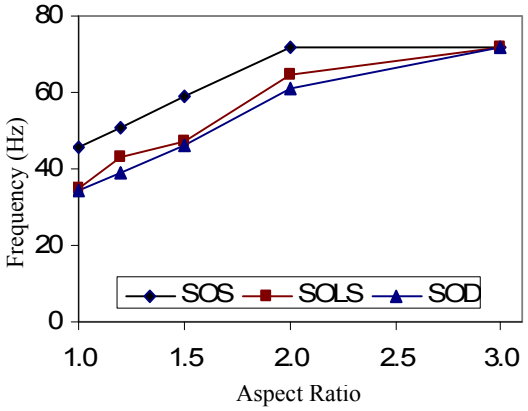

Composite space frame models

c. Frequency in Z-direction

Figure 7.24 Effect of space frame configuration on frequencies of composite and non-composite edge-supported models

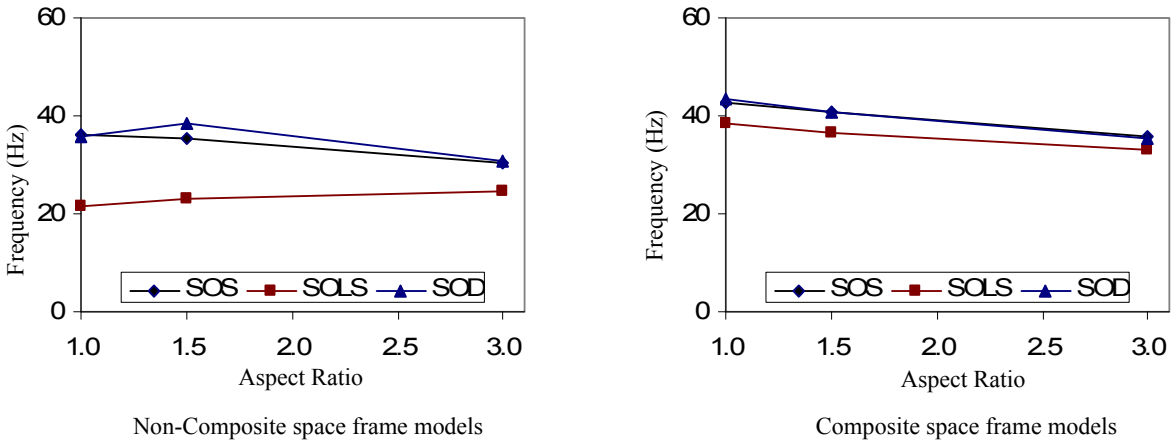

a. Frequency in X-direction

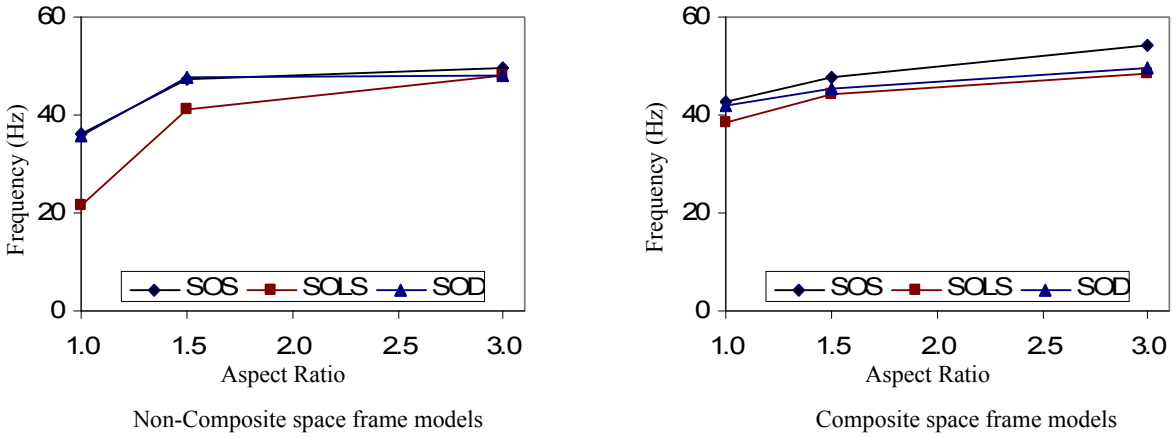

b. Frequency in Y-direction

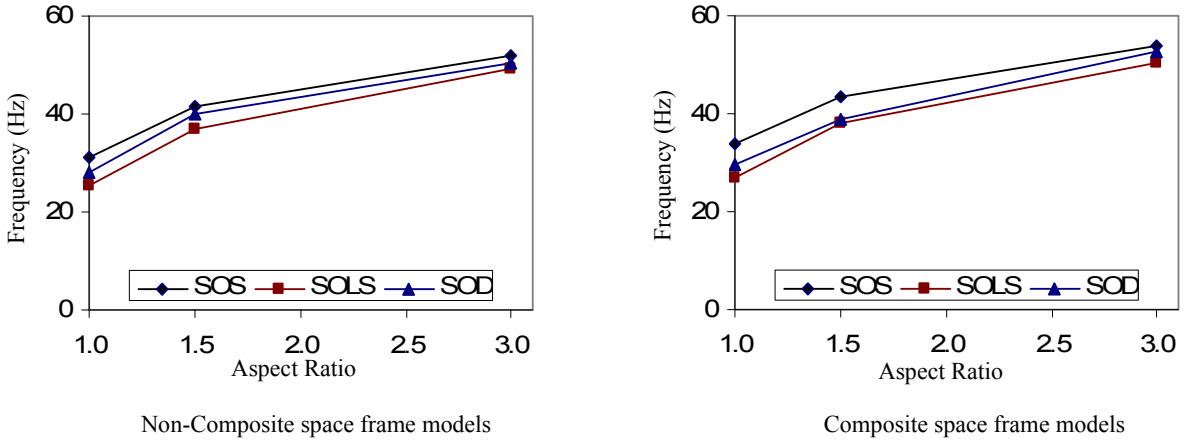

c. Frequency in Z-direction

Figure 7.25 Effect of space frame configuration on frequencies of composite and non-composite models supported at corners and mid-edges

7.7.2 Maximum responses of models

7.7.2.1 Maximum displacement responses

Figures 7.26 to 7.30 demonstrate, respectively, the effect of space frame configuration, support conditions, composite action and aspect ratio on maximum displacement response of space frame models. All models were exposed to the shaking table acceleration time history similar to that applied to physical models at the laboratory.

The following are the main observations of this part of the study:

- For all composite models, the maximum displacement responses were significantly lower than those of corresponding non-composite models with ratios that ranged between.

- Displacement responses for all edge-supported models were lower than those for models with other support conditions. This drop in lateral displacement response was expected as a result of the large increase in lateral stiffness caused by the supporting of additional points.

- The maximum displacements experienced by SOLS models were higher than thos of SOS and SOD models. This observation was valid for all cases with different aspect ratios and supporting conditions. This trend reflected the deterioration in lateral stiffness caused by the removal of some lower and diagonal members in SOLS models.

- Square on diagonal models (SOD) were superior in resisting lateral vibrations in cases with corner supports. In this case, SOD models experienced less displacements compared to SOS models, despite the former having fewer diagonal and lower chord members. This trend was reversed in edge-supported models with SOS demonstrating the least displacements.

- For all edge-supported models, the difference in maximum displacement values between models with different configurations was not as high as that of the case of corner-supported models.

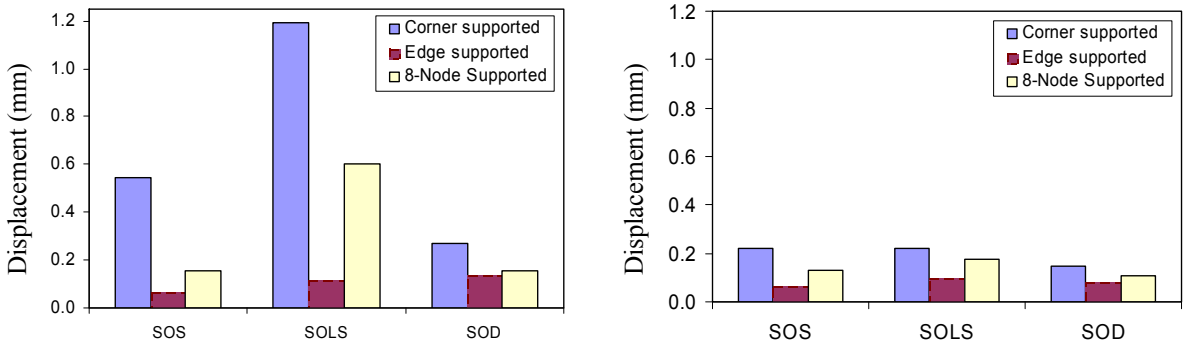

a. Non-Composite models b. Composite models

Figure 7.26 Effect of space frame configuration with different support condition on the displacement response of models with AR = 1.0

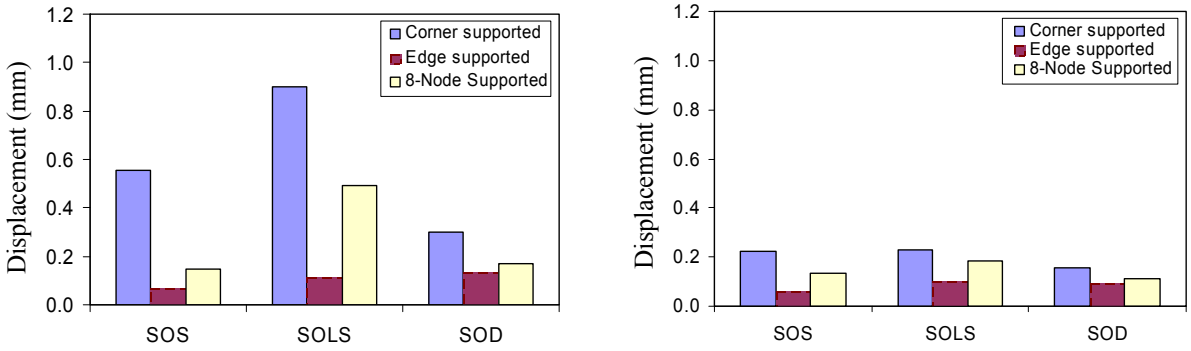

a. Non-Composite models b. Composite models

Figure 7.27 Effect of space frame configuration with different support condition on the displacement response of models with AR = 1.2

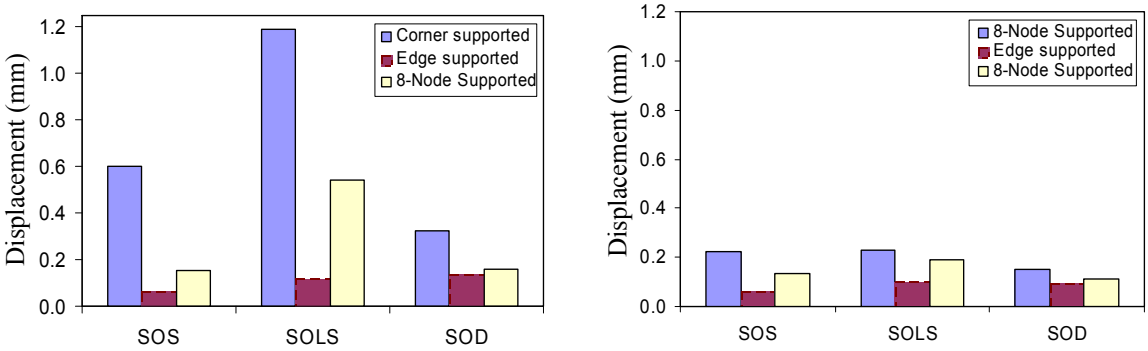

a. Non-Composite models b. Composite models

Figure 7.28 Effect of space frame configuration with different support condition on the displacement response for models with AR = 1.5

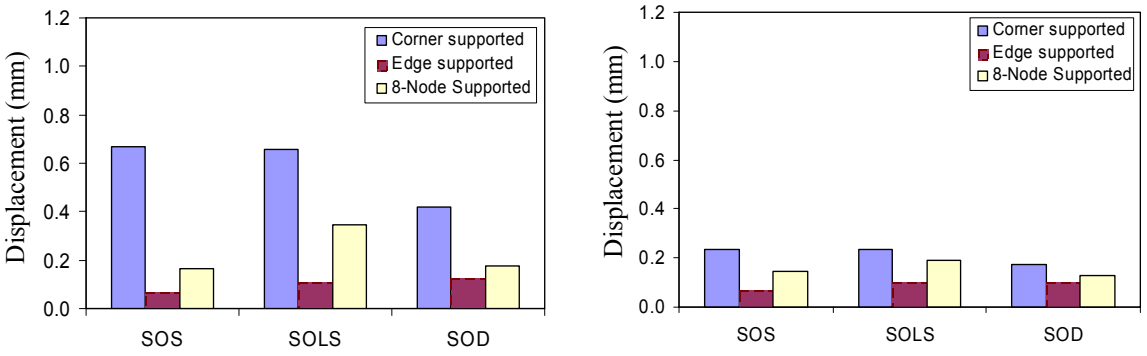

a. Non-Composite models b. Composite models

Figure 7.29 Effect of space frame configuration with different support condition on the displacement response for models with AR = 2.0

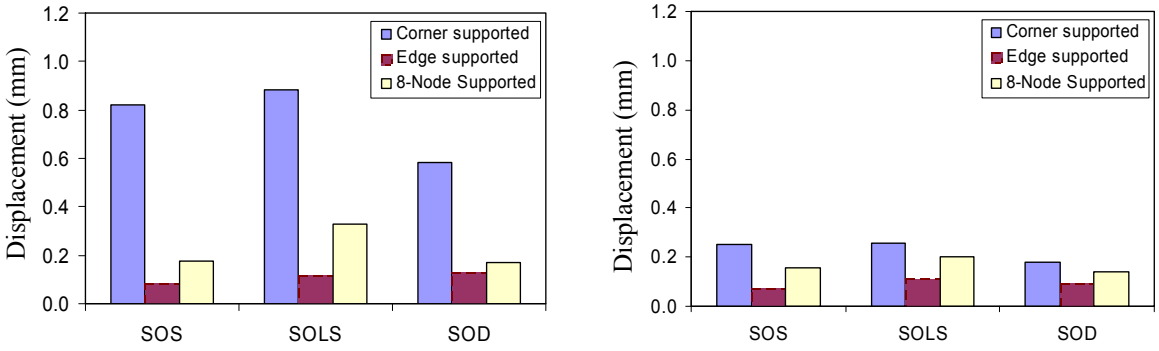

a. Non-Composite models b. Composite models

Figure 7.30 Effect of space frame configuration with different Support condition on the displacement response for models with AR = 3.0

The effect of aspect ratio on the maximum displacement of corner-supported non-composite and composite models is illustrated in Figure 7.31. The figure shows high rate of increase in lateral displacements of non-composite models with the increase of aspect ratio, while the rate of increase was slower in the case of composite models.

For non-composite models, the SOLS configuration was associated with the maximum displacement response for all aspect ratios while SOD models had the lowest displacement response, which was applicable with different aspect ratios. However, the SOS and SOLS composite models showed little difference in maximum displacement

while it was high for SOD configuration. The lower values of displacement in SOD models with different aspect ratios were related to the models' greater stiffness over other space frame configurations.

For edge-supported models, the maximum displacements had little values due to the models' large stiffness caused by the addition of several supports (Figure 7.32). In addition, it can be noticed that SOS models had the lowest displacements compared to corresponding composite and non-composite models with other configurations. In general, all composite models had smaller responses than those of non-composite models due to the large stiffness of composite models caused by composite action.

Figure 7.33 shows the variation of maximum displacements experienced by all models supported at the corners and mid-edge points with different aspect ratios. Models with the SOLS configuration had the largest displacements while SOS and SOD models had almost the same lower values. In addition, all composite models had lower values of displacements than non-composite models, which proved the role of composite action in increasing the stiffness of models.

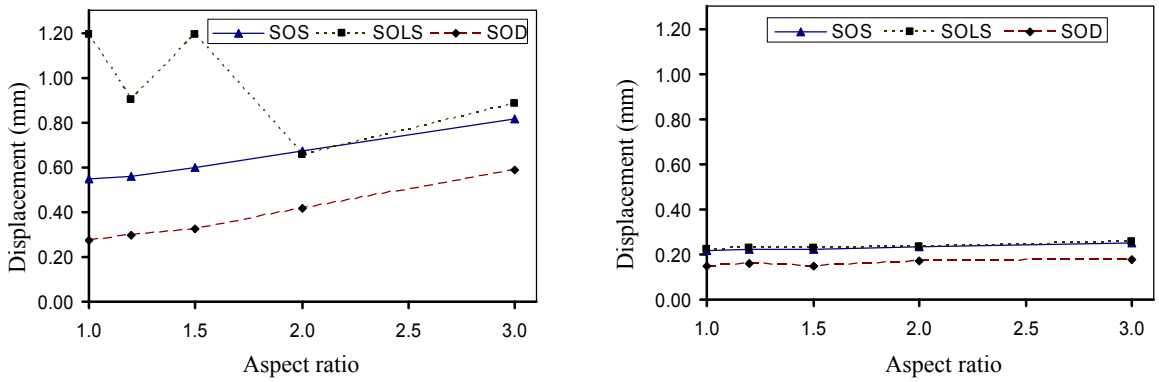

a. Non-Composite models

b. Composite models

Figure 7.31 Effect of aspect ratio on maximum response of corner-supported models

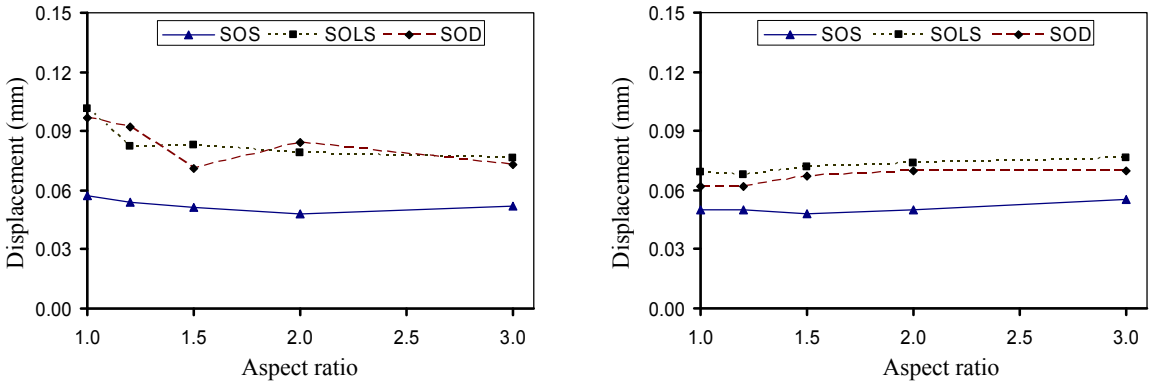

a. Non-Composite models b. Composite models

Figure 7.32 Effect of aspect ratio on maximum response of edge-supported models

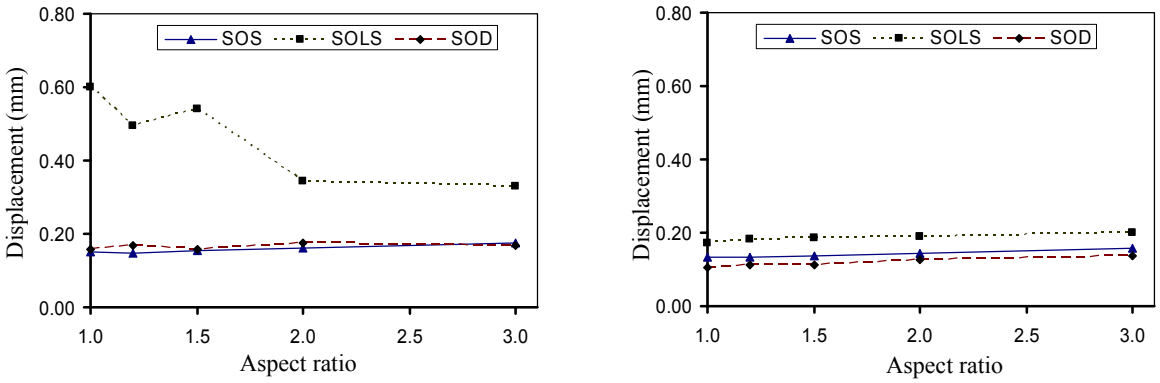

a. Non-Composite models b. Composite models

Figure 7.33 Effect of aspect ratio on maximum displacement of models supported at corners and mid-edge points

7.7.2.2 Axial force responses

Beside the effect of composite action in altering the dynamic characteristics of test models and reducing their lateral displacements, it had a great effect on the magnitude and the distribution of the internal member forces under dynamic loading. The current study focused on the diagonal and lower members only since it was found through tests that forces in upper chord members diminished by the application of composite action.

It was noticed from the analysis of several models that the changes to member forces were concentrated at the models' corners and edges, so special care was directed towards these members although a number of members at the middle regions of models were monitored to check the validity of this observation. The marked members shown in Figure 7.34 present the elements, which had been selected for axial force comparisons for SOS, SOLS and SOD models.

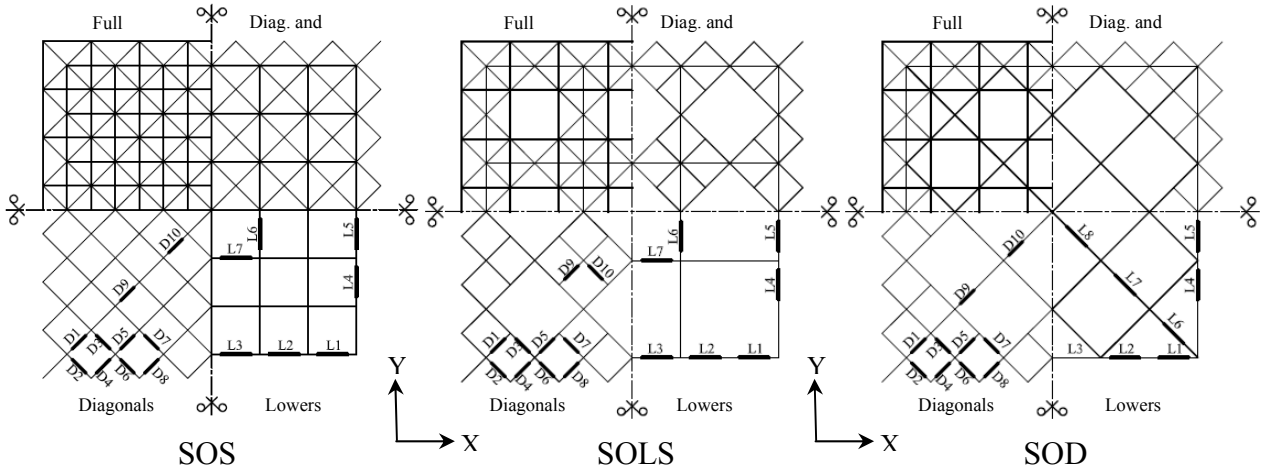

Figure 7.34 Selected members in SOS, SOLS and SOD space frame models

I. Corner-supported models

Figures 7.35 to 7.37 present the internal absolute member forces in square corner-supported composite and non-composite models.

Figure 7.35 shows that the application of composite action in SOS models increased the axial forces in the external diagonal members D2, D4, D6 and D8 and reduced the forces in internal diagonal members D1, D3, D5 and D7. In addition, forces in diagonal members at the model's middle region, D9 and D10, were clearly decreased.

For lower chord members, a reduction in forces caused by the composite action was noticed in members perpendicular to the direction of vibration (L1 to L3), while forces

in members parallel to the vibration direction (L4 and L5) were decreased. The composite action also reduced member forces in the lower chords at the middle region (Figure 7.35b).

For SOLS models, it was clear that the application of composite action had two effects on redistributing the forces in diagonal members. First, it made the distribution of forces at edge members more even which appears clearly in reducing the fluctuation of forces' values. Second, the diagonal member forces became concentrated at the two edges parallel to the vibration direction while forces in diagonal members at the model's middle region, D9 and D10, were reduced considerably (Figure 7.36a).

For the lower chords of the same model, it was clear that the composite action increased the forces in the edge members parallel to the direction of vibrations, L1, L2 and L3, while forces at the other edges were reduced (L4 and L5). Member forces at the model's middle regions, L6 and L7, were markedly reduced (Figure 7.36b).

In case of SOD models, the composite action clearly played an important role in concentrating the forces at the edge regions. This trend appeared clearly in increasing the forces in diagonal and lower members in the direction parallel to induced vibrations and in making the distribution of member forces more even. However, forces in members at model's middle region, D9, D10, L7 and L8, were decreased (Figure 7.37).

As can be noticed from the above discussion, the redistribution of forces came out as a result of the application of composite action for all space frame configurations. This behaviour can be explained by the large increase in lateral stiffness of models associated with the composite action especially at the top chord level, at which the lateral inertia forces are concentrated. The large stiffness of composite deck caused a

reduction in the flow of forces from upper chord regions to diagonal members and hence to lower chord members. In addition, the formation of stiff diaphragm between composite deck and diagonal members at the two edges parallel to the direction of vibration led the forces in members to be concentrated at diagonal and lower edge members in the direction of vibration. This phenomenon sheds the light on the importance of diagonal and lower chord members located at corner and edges in carrying higher lateral loads in composite space frames, which should be considered during the design stage.

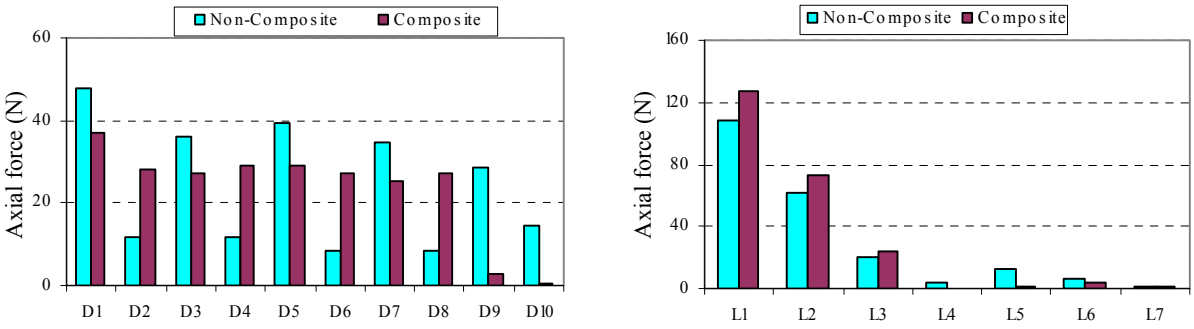

a. Diagonal members b. Lower chord members

Figure 7.35 Member forces in square corner-supported SOS model

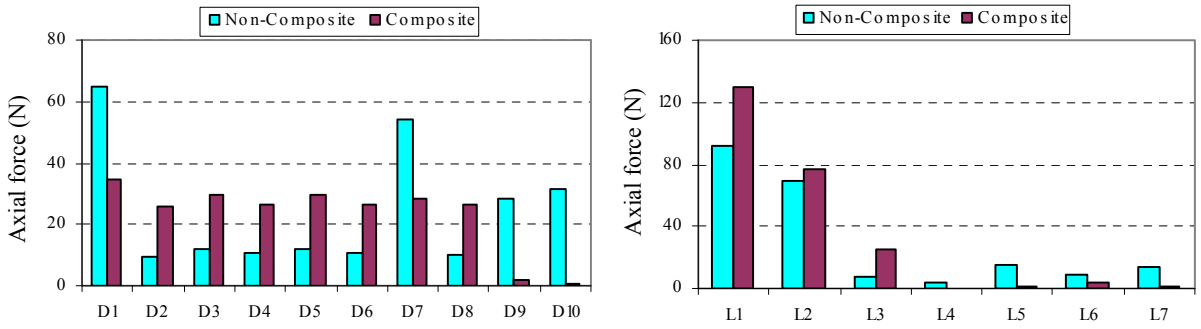

a. Diagonal members b. Lower chord members

Figure 7.36 Member forces in corner supported SOLS space frame model

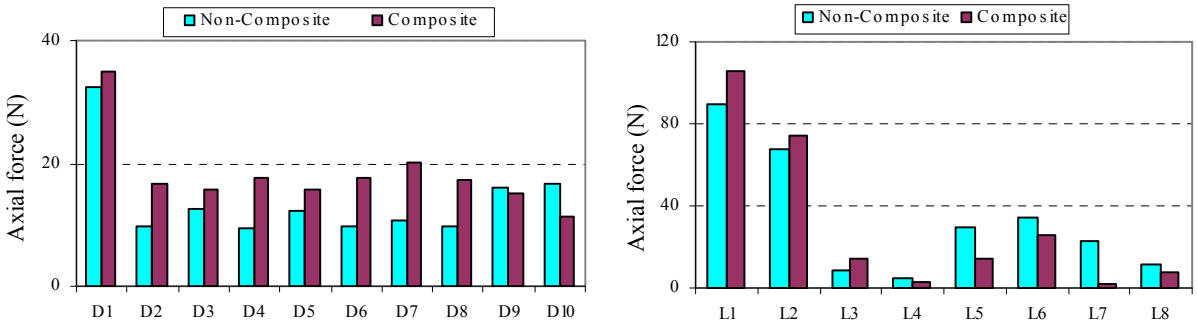

a. Diagonal members b. Lower chord members

Figure 7.37 Member forces in corner-supported SOD space frame model

II. Edge-supported models

The effect of composite action on the force distribution in the diagonal and lower members of edge-supported space frame models with different configurations (SOS, SOLS and SOD) was covered in the current parametric study (Figures 7.38 to 7.40).

For SOS configuration, the effect of composite action on edge-supported models was different from the cases with corner supports since the axial forces in internal diagonal members, D1, D3, D5 and D7, increased slightly by the application of composite action while forces in external diagonal members, D2, D4, D6 and D8, decreased or remained unchanged compared to non-composite model (Figure 7.38a). Meanwhile, the middle diagonal members, D9 and D10, saw an increase associated with the application of composite action. This was an opposite trend to that observed before with corner-supported models.

For lower chord members (Figure 7.36b), all edge members that were parallel or perpendicular to the induced vibration remained unaffected since all their nodes were restrained against displacement in all directions. Furthermore, composite action had a considerable effect in increasing the axial forces in lower chord members located at the middle region of the model, which was again the opposite trend compared to corner-

supported models.

In case of SOLS model, there was a general increase in diagonal member forces at the model's edges but forces in the middle were reduced slightly or stayed the same as for the non-composite case (Figure 7.39a). For the lower chords, a similar behaviour to that observed with the SOS model was observed as the forces in the lower chord members increased slightly at the middle region of the model (Figure 7.39b).

Forces in the diagonal members of the SOD model followed the same trends like the other two configurations with the force increases at the edges and decreases at the middle region. The SOD model did not, however, show the same trend for lower chord members since the composite action caused a reduction in member forces at the middle region, which was an opposite trend to what was observed with other configurations (Figure 7.40).

These changes in member forces came out as a result of the large increase in stiffness caused by increasing the number of supported points and the addition of composite action. The general increase in forces in diagonal members with composite action is thought to be coming from the slight increase in the mass of the structure, added by the application of composite action, leading to considerable increases in the horizontal inertia forces generated by the vibration.

The slight decrease in forces for lower chord members in SOD configuration was caused by the higher efficiency of this configuration in transferring the forces from the diagonal members to the supports, which was clear in the direct reduction of member forces at the middle region.

III. Models supported at corners and mid-edge points

The distribution of diagonal member forces in this case was similar to that of the

corner-supported models. The diagonal member forces were again more concentrated at the two edges parallel to the direction of vibration while the composite action reduced the forces in diagonal members at the middle region of the model as shown in Figures 7.41a, 7.42a and 7.43a.

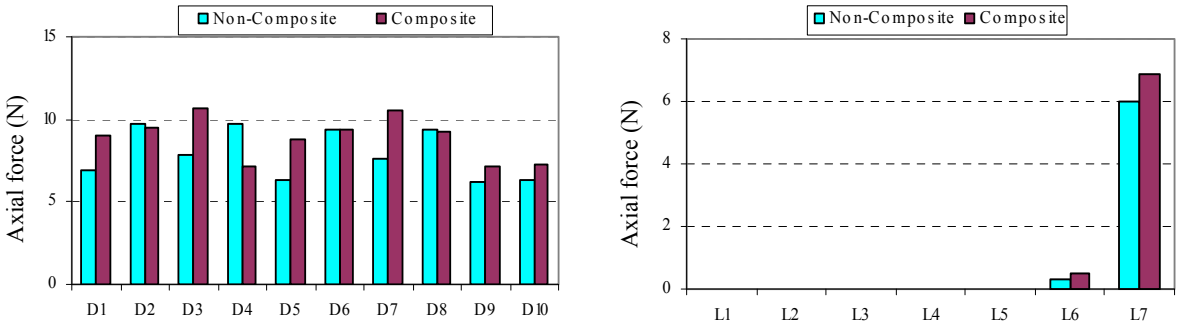

a. Diagonal members b. Lower chord members

Figure 7.38 Member forces for edge supported SOS model

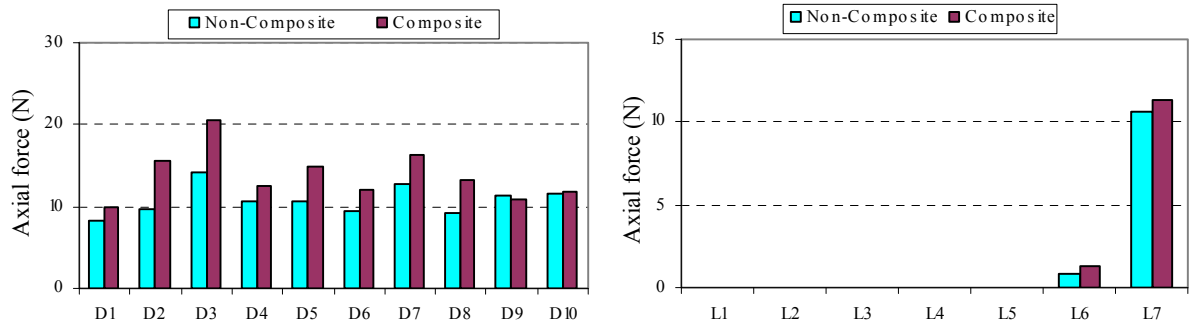

a. Diagonal members b. Lower chord members

Figure 7.39 Member forces for edge-supported SOLS model

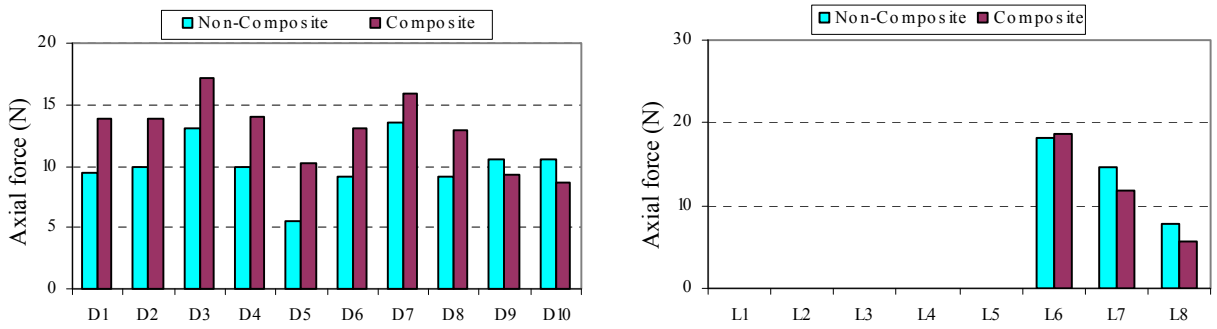

a. Diagonal members b. Lower chord members

Figure 7.40 Member forces for edge-supported supported SOD model

For the lower chord members of models supported at the corner and mid-edge points, forces increased at edge members near the supports while forces decreased in members perpendicular to the direction of vibration and the models' middle region (Figures 7.41b, 7.42b and 7.43b).

This behaviour could again be explained by the increase of model lateral stiffness at the top chords caused by the composite action which led the model to behave similar to a stiff diaphragm supported at the two edges parallel to the direction of the vibration.

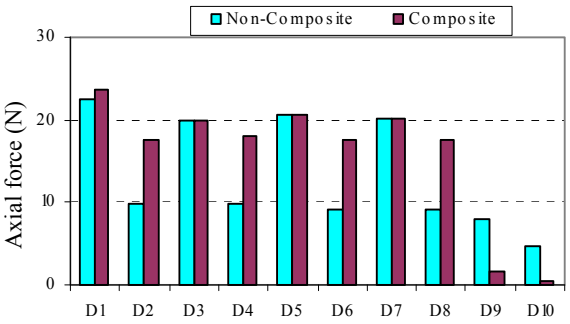

a. Diagonal members

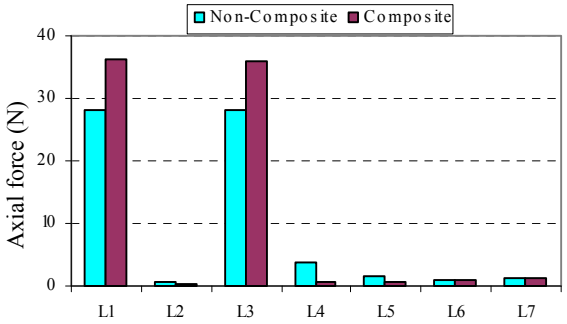

b. Lower chord members

Figure 7.41 Member forces of SOS models supported corners and mid-edges

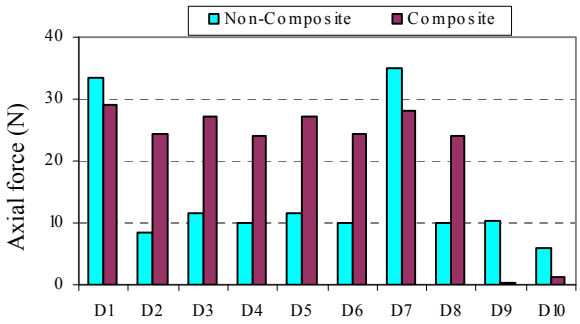

a. Diagonal members

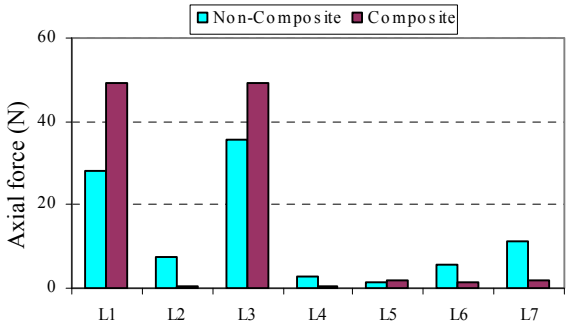

b. Lower chord members

Figure 7.42 Member forces of SOLS models supported corners and mid-edges

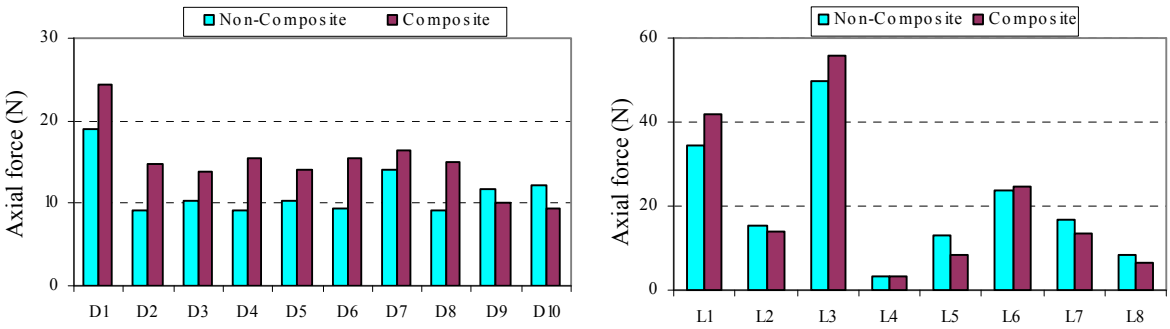

a. Diagonal members b. Lower chord members

Figure 7.43 Member forces of SOD models supported corners and mid-edges

7.8 Summary

In this chapter, the finite element method was used to construct a numerical model able to simulate the dynamic behaviour of the experimental test space frames. Numerical analysis was carried out using ABAQUS on nine proposed FE models with different detailing levels, see Chapter 3. The experimental results obtained from tests carried out on composite and non-composite space frame models were used to validate and select the optimum numerical model, which could be used to represent this type of structure. The selection process led to the selection of Model 4, which offered the highest accuracy and lowest variance in predicting the vibration frequencies and the displacement response of the experimental test structures.

Later in this chapter, Model 4 was used in a parametric study using FE package, ABAQUS, to study the effect of variables, some of which were difficult to be considered in the laboratory due to time limitations and manufacturing complexities. The study focused on several parameters such as composite action, boundary conditions, aspect ratio and space frame configuration. The results of this study showed the effect of composite action in increasing, shifting and rearranging the vibration frequencies and modes of vibrations of the models with different

configurations and support conditions.

In addition, the study discussed the changes to the maximum lateral displacements, which clearly showed the superiority of composite action in increasing the lateral stiffness of models leading to large reduction in the lateral displacement, which reached for some models more than 50%.

Furthermore, the study discussed the effect of composite action in redistributing member forces in diagonal and lower chord members revealing the formation of diaphragm like behaviour between composite deck and diagonal members at the edges parallel to the vibration direction. This behaviour led to the concentration of member forces at corners and edges for both cases of corner-supported models and those supported at corners and mid-edges, while there was a considerable reduction of forces in the middle regions. However, an opposite trend was noticed for edge-supported models for the forces in diagonal and lower chord members at located at the edges and middle regions.

CHAPTER 8

SUMMARY, CONCLUSIONS AND RECOMMENDATIONS FOR FUTURE WORK

8.1 Introduction

This chapter presents a brief summary for the research conducted in this project and covers the main conclusions drawn from the analysis and discussion of the experimental and numerical work done. At the end of this chapter, suggestions are made for future work to extend the present study.

8.2 Summary

Previous research on the construction of composite flat double-layer space frames, by adding a top deck firmly attached to the frame's top joints, proved the efficiency of composite action in enhancing the space frames' capacity and behaviour. The main findings of earlier research included:

1. The application of composite action prevented the potential progressive collapse of space frames, making the behaviour of the structure dependent mainly on the characteristics of tension lower chord members.
2. The composite action led to considerable increases in the load carrying capacity of space frames, which reached more than 200% in some studies.
3. Composite action could be applied to common types of space frames using several methods including those presented by Castello (1967), Al-Bazzaz (1976), Kuleib (1989), Sebastian and McConnel (1993), Elsheikh and

McConnel (1993) and Shabaan (1997).

4. Several deck forms could be used to achieve the composite action with space frames such as concrete slabs, timber decks and claddings.
5. The application of composite action made it more economically feasible to use space frames as internal floors instead of being limited to applications as roof structures.
6. In case of using timber deck to achieve the composite action with space frames, reduction in self weights and increased stiffness were observed compared to non-composite frames.
7. Composite space frames proved their cost competitiveness compared to non-composite frames and conventional structural systems (Shabaan, 1997).

Despite the significant advances in knowledge on effect of composite action on the static behaviour of space frames, its effects on the dynamic behaviour did not receive much attention in spite of its importance in applications subjected to earthquake, wind, explosions and serviceability vibrations. This research has been designed to address this gap in knowledge.

8.2.1 Experimental test programme

In the current research, three square on square (SOS) flat space frame models of the same dimensions were manufactured of aluminium members. The models were 1200×1200mm span and 150mm depth with 6×6 panels and 7×7 panels for bottom and top grids, respectively. An aluminium deck with 1.2mm thickness was added to one of the models and connected at the top joints to simulate composite action with a commonly used cover such as sandwich panels. Another model was covered with a timber deck of 4mm thickness to represent the case with top timber boards. The third

model presented the case of a non-composite space frame. Specially formed lead masses were added to the models at the top joints. A uni-axial mechanical shaking table was designed to generate a sine-like wave, and to apply a vibration history on the test models to determine their dynamic behaviour. The responses of models were monitored with particular attention given to the lateral displacements and strains in specific lower and diagonal members.

The dynamic characteristics in vertical and horizontal directions were determined for test models by carrying out snap (initial displacement) tests. In these tests, a load applied at a specific point was released suddenly leaving the structure to vibrate naturally. The logarithmic decrement method and the power spectrum method were used to calculate the natural frequencies and damping ratios from the recorded displacement data.

The experimental study considered the effect of deck material (aluminium and timber), support conditions (corner supports and supports along the two edges parallel to the induced vibrations), and space frames aspect ratios (1.0, 1.2, 1.5, 2.0 and 3.0).

8.2.2 Results of experimental tests

The results of the experimental tests can be summarised in the following points:

1. Composite models showed a general increase in structural stiffness, which reflected in the increases of the vibration frequency of models in all test directions associated with the introduction of composite action. This observation was valid for all cases of support conditions and aspect ratios.
2. The introduction of composite action using both types of materials, aluminium and timber, resulted in a considerable reduction in the lateral displacements to shaking table vibrations, which reached more than 50%.

3. The application of composite action using aluminium deck resulted in general reduction of the damping ratio of space frame models in test directions.
4. The first mode of vibration for composite and non-composite models supported at their corners was in the vertical Z-direction.
5. The introduction of composite action resulted in a slight increases of vibration frequencies in the vertical direction of corner supported models, which continued with all aspect ratios.
6. There was a reduction in the vertical vibration frequency of two-edge-supported composite and non-composite models associated with the increase of space frames' aspect ratios.
7. There was a slight reduction of vibration frequencies in horizontal X-direction associated with the increase of models' aspect ratios for non-composite models. A similar behaviour was experienced with composite models for cases with aspect ratios (AR<2.0) then the horizontal vibration frequency remained unchanged or experienced a slight increase with higher aspect ratios (AR>2.0). The phenomenon was valid for both cases of support conditions
8. A reduction of damping ratio in horizontal X-direction was experienced for composite models with different cases of aspect ratios, which was valid for both cases of support conditions.
9. Under vibrations induced by the shaking table, increases in the axial forces in the members located at the corners and along the edges parallel to the vibration direction were observed for all composite models, which could be explained by the formation of a stiff diaphragm composed of top composite deck and the diagonal members along the two edges parallel to the direction of vibrations.
10. An increase was experienced in lateral displacements of non-composite models

with the increase of aspect ratio, while remained unchanged or with slight increase for composite models. This behaviour can be explained by the high sensitivity of non-composite space frame by quick deterioration of its lateral stiffness by the increase of structure's aspect ratio, while composite space frames showed more resistance to the deterioration in lateral stiffness by the increase of aspect ratio.

8.2.3 Finite element study programme

Nine finite element models were suggested and the finite element program ABAQUS was used to select one of the models to represent the test models under laboratory conditions. The finite element model selected in the above study was used later to assess the effect of parameters, which could not be included in the experimental study.

The finite element programme considered the effect of space frame configuration by including three space frame configurations; i.e. square on square (SOS), square on large square (SOLS) and square on diagonal (SOD) and considered three support conditions; i.e. corner, edge supports and supports at corners and mid-edges. The study also considered the effect of space frames' aspect ratio by conducting analysis on space frames with five aspect ratios; i.e. 1.0, 1.2, 1.5, 2.0 and 3.0.

All finite element models' dimensions, materials and loading details were similar to those of the experimental test models.

8.2.4 Results of finite element study

The results of the finite element parametric study can be summarised in the following points:

1. For space frames with different configurations and support conditions, the introduction of composite action resulted in a general increase of their stiffness,

which reflected in the increase of vibration frequencies in all directions.

2. The introduction of composite action resulted in considerable reduction in the maximum displacement response for space frames with different configurations, support conditions and aspect ratios.
3. For all composite and non-composite models, there was an increase in the vertical frequency of vibration with the increase of aspect ratio, which was applicable for all considered support conditions and frames' configurations.
4. There was a slight reduction of vibration frequency in horizontal X-direction in all space frame configurations associated with the increase of aspect ratios.
5. An increase was observed in the vibration frequency in the horizontal Y-direction for the majority of space frames associated with the increase of aspect ratio, which was applicable to all configurations and support conditions.
6. Space frames with SOS and SOD configurations had the highest frequencies of vibrations in all directions compared to SOLS configuration, which was applicable to both cases of composite and non-composite models.
7. The introduction of composite action resulted making the axial forces in diagonal and lower chords to increase in members located around the supports and the two edges parallel to the direction of vibrations while it resulted in the forces to increases in the members at the middle regions of edge-supported models.

8.3 Conclusions

The following is a list of conclusions drawn from the experimental and numerical study conducted in this research:

1. The large increase in lateral stiffness of space frames due to composite action results in large reductions in lateral displacements under forced vibrations by

about 50%. This trend is valid for space frames with different aspect ratios, support conditions and configurations.

2. The introduction of composite action to space frames results in increasing the overall stiffness, leading to the increase in vibration frequencies of space frames with different configurations, support conditions and aspect ratios in all directions.
3. Non-composite and composite space frames with the square on diagonal (SOD) configuration have the lowest lateral displacements, while frames with square on large square (SOLS) configuration have the highest lateral displacements under dynamic loads. The superiority of SOD configuration in resisting the lateral displacement is thought to be a direct result of the high lateral stiffness of this configuration.
4. Composite space frames experience concentration of member forces around the supports and the edges parallel to the induced vibration, and a reduction in forces at the middle region of the structure.
5. The top chord members of composite space frames experience little axial forces due to the relatively high stiffness of the top deck.
6. The use of an aluminium deck to create composite action with a space frame results in reduced damping ratios for the majority of cases with different support conditions and aspect ratios.
7. Using a timber deck to achieve composite action with space frame results in a reduction of damping ratio in horizontal direction for the majority of cases; however, this trend is valid in the vertical direction only in cases of lower aspect ratios.
8. Increasing the number of supports of a composite or a non-composite space

frame leads to increases in all vibration frequencies due to the overall increase in stiffness.

9. Space frames with SOS and SOD configurations have higher natural frequencies in all directions compared to SOLS space frames due to the low stiffness of SOLS configuration.
10. The vertical vibration frequency of composite and non-composite space frames increases slightly with the increase of frames' aspect ratio, which is valid for all space frame configurations and support conditions.
11. The increase of aspect ratio leads to a general reduction in horizontal vibration frequency in the short X-direction of non-composite space frames as a result of the deterioration in the horizontal stiffness, while shows a slight reduction, or remains unchanged, in composite space frames.
12. The increase in aspect ratio leads to an increase in horizontal vibration frequency in the long Y-direction of non-composite and composite space frames with different configurations and support conditions.
13. The first mode of vibration of corner-supported composite and non-composite space frames is in the vertical direction. The value of vertical vibration frequency in this direction undergoes only little increase (5.6%-12.4%) with the application of composite action.
14. Composite action leads to changes in the arrangement of vibration modes due to the unequal changes in models' stiffness experienced in different directions.
15. The first mode of vibration of non-composite space frames supported along two parallel edges is in horizontal X-direction, parallel to the supports' line, due to the large increase in stiffness added to the structure in the vertical Z-direction by having supports along the edges.

8.4 Recommendations for future work

For more understanding to the effect of composite action on the dynamic characteristics and behaviour of space frames and from the findings of current study, the following suggestions are presented:

1. Due to the complicated nature of damping, experimental tests on real scale model are unavoidable.
2. An extension of the study is needed to include more covering materials such as concrete and FRP panels.
3. For more accurate conclusion about the effect of composite action in changing the dynamic response of space frames, experimental tests using large shaking tables which are able to reproduce full earthquake histories are needed.
4. Study is needed to be extended to include other types of space frames with different jointing systems.
5. Study also is recommended to be extended to study the effect of composite action on both dynamic characteristics and behaviour of curved in one and two direction space structures.

REFERENCES

Abaqus (2007), "Analysis user's manual", Version 6.7, 2007.

Al-Bazzaz, A. J. (1976), "An investigation into composite double layer space grid structures", PhD thesis, University of Strathclyde.

Carvill, J. (1993), "Mechanical engineer's data handbook", Boca Raton, Fl., CRC Press.

Castillo, H. (1967), "A space frame construction with steel and reinforced concrete-tridilosa spatial structure", In: Davies, R. M. (Ed.), Space Structures, Blackwell Scientific Publisher, Oxford: pp1089-1093.

Chan, S. L., Chui, P. P. T.(1993), "Non-linear dynamic analysis of roof trusses connected by rigid, pinned and semi-rigid joints", Space Structures 4, Proceedings of the Fourth International Conference on Space Structures, University of Surrey, Thomas Telford House, UK, 1993: pp. 406-412.

Chilton, J. (2000), "Space grid structures", Oxford, Architectural Press.

Chopra, A. K. (1995), "Dynamics of structures: theory and applications to earthquake engineering", Englewood Cliffs, N.J., Prentice Hall; London: Prentice-Hall International (UK).

Clough, R. W. and J. Penzien (1993), "Dynamics of structures", McGraw-Hill.

Codd, E. T. (1983), "A new space frame", Metal Structures Conference, Brisbane, May 1983: pp. 203-210.

Codd, E. T. (1984), "Low technology space frames", Proceedings of the Third International Conference on Space Structures, Surrey, 1984: pp. 955-960.

Collins, I. M. (1981), "Collapse analysis of double-layer grids." PhD thesis, University of Surry, UK.

Dyke, S.J., Spencer, B.F., Sain, M.K. and Carlson, J.D. (1998), "An Experimental Study of MR Dampers for Seismic Protection", Smart Material in Structures, Vol. 7, pp. 693-703.

El-Bakry, H. F. (1995), "Development of new space truss", PhD thesis, University of Dundee, UK.

El-Sheikh A. and Shaaban, H. (1999), "Experimental study of composite space trusses

with continuous chords", Advances in Structural Engineering, Vol. 2, No. (3), pp. 219-232.

El-Sheikh, A. (2000), "Approximate Dynamic Analysis of Space Trusses", Engineering Structures, Vol. 22, pp. 26-38.

El-Sheikh, A. I. (1995), "Sensitivity of space trusses to member geometric imperfections", International Journal of Space Structures, Vol. 10, No. (2): pp. 89-98.

El-Sheikh, A. I. (1996a), "Sensitivity of space trusses to sudden member loss", International Journal of Space Structures, Vol. 12, No. (1): pp. 31-41.

El-Sheikh, A. I. (1996b), "Sensitivity of space trusses to uneven support settlement", International Journal of Space Structures, Vol. 11, No. (4): pp 393-400.

El-Sheikh, A. I. and McContvd, R. E. (1993), "Experimental study of behaviour of composite space trusses", Journal of Structural Engineering, ASCE, Vol.119, No. (3) :pp. 747-766.

Fulop, A. and M. Ivanyi (2004), "Experimentally analyzed stability and ductility behaviour of a space-truss roof system", Thin-Walled Structures, Vol. 42, No. (2): pp 309-320.

Gebhardt, D. H. (1984), "The power-strut space frame system", Third International Conference on Space Structures, University of Surrey, Ed. H. Nooshin, Elsevier Applied Science Publishers, UK: pp. 53-58.

Hanaor, A. and Levy, R. (1985), "Imposed lack of fit as a means of enhancing space truss design", International Journal of Space Structures, Vol. 1, No. (3): pp. 147-154.

Hanaor, A. and Ong, A. (1988), "On structural redundancy in space trusses", International Journal of Space Structures, Vol. 3, No. (4): pp. 237-241.

Hong, S. C. (1984), "Analysis and Experiment of Composite Space Slab-Grid Structure.", Third International Conference on Space Structures, University of Surrey, UK, Ed. H. Nooshin, Elsevier Applied Science Publishers, UK: pp.192-195.

Imai, K., T. Morita, et al. (1993), "The KT space truss system", Space Structures 4, Proceedings of the Fourth International Conference on Space Structures, University of Surrey, Thomas Telford House, UK, Vol. 2 :pp. 1374-1382.

Kato, S., Nakazawa, S., Matsushita, F., Ohya, T and Okamoto, T. (2002), "A new system of intermediate isolation for space structures against earthquakes", 5th International Conference on Space Structures, pp.1053-1062, August 19-21, 2002.

Kato, S., Kim, Y. B., et al. (2005). "Simulation of the cyclic behaviour of J-shaped steel

hysteresis devices and study on the efficiency for reducing earthquake responses of space structures" Journal of Constructional Steel Research, Vol. 61, No. 10: 1457-1473.

Kuleib, M. M. A. (1989), "The analysis and behaviour of composite space frames with profiled steel sheet floors", PhD thesis, University of Salford, UK.

Levy, R., Hanaor, A. and Rizzuto, N. (1994), "Experimental investigation of prestressing in double-layer grids", International Journal of Space Structures, Vol. 9, No. 1, 1994, pp. 21-26.

Madden G. J., Symans M. D. and Wongprasert N., (2000), "Adaptive seismic isolation systems for structures subjected to disparate earthquake ground motions", 14th Analysis and computational specialty conference, Proceedings of the 2000 structures congress and exposition, May 8-10, Philadelphia, Pennsylvania:167-176.

Malla, R., Wang, B.(1993), "A Method to determine dynamic response of truss structures during sudden consecutive member failure", Space Structures 4, Proceedings of the Forth International Conference on Space Structures, University of Surrey, Thomas Telford House, UK, 1993: pp. 413-422.

Marsh, C. and Fard, M. R. (1984), "Optimisation of Space Trusses Using Non-Linear Behaviour of Eccentric Diagonals", Third International Conference on Space Structures, University of Surrey, Ed. H. Nooshin, Elsevier Applied Science Publishers, UK, 1984: pp. 669-671.

Moghaddam, H. A. (2000), "Seismic behaviour of space structures", International Journal of Space Structures, Vol. 15, No. (2), 2000.

Muhlenkamp (1997), "Analysis, design, and construction of a shaking table facility", MSc. Thesis, Rice University, Houston, Texas.

Noor, A. K., Peters, J. M. (1980), "Nonlinear dynamic analysis of space trusses", Computer Methods in Applied Mechanics and Engineering, Vol. 21: pp. 131-151.

Oh, H. and Onoda, J. (2002), “An experimental study of a semi-active magneto-rheological fluid variable damper for vibration suppression of truss structures”, Smart Material in Structures, Vol. 11, 2002: pp. 156-162.

Parke, G. A. R. (1993), "A novel soft member for space trusses", Fourth International Conference of Space Structures, Surrey, UK, Thomas Telford Services Ltd. Vol. 1: pp.116-126.

Parke, G. A. R. and Walker, H. B. (1984) "A limit state design of double-layer grids", Third International Conference on Space Structures, University of Surrey, Ed. H. Nooshin, Elsevier Applied Science Publishers, UK, 1984, pp. 528-532.

Pashaei, M. H., Davoodi, M. R., Nooshin, H. (2006), "Effects of tightness of bolts on the damping of a MERO-type double-layer Grid", International Journal of Space Structures, Vol. 21, No. 2: pp. 103-110.

Schmidt, L. C, Morgan, P. R. and Hanaor, A. (1982), "Ultimate load testing of space trusses", Journal of the Structural Division, ASCE, Vol. 108, No. (ST6), June 1982: pp. 1324-1335.

Schmidt, L. C, Morgan, P. R, O'Meagher, A. J. and Cogan, K. (1980), "Ultimate load behaviour of a full-scale space truss", Proceedings of the Institution of Civil Engineers, Vol. 69, Part (2), March 1980: pp. 97-109.

Schmidt, L. C, Morgan, P. R. and Clarkson, J. A. (1976), "Space trusses with brittle-type strut buckling", Journal of the Structural Division, ASCE, Vol. 102, No. ST7, July 1976: pp. 1479-1492.

Schmidt, L. C, Morgan, P. R. and Coulthard, B. R. (1977), "The influence of eccentricity and continuity on the inelastic behaviour of a space truss", Sixth Australasian Conference on the Mechanics of Structures and Materials, University of Canterbury, Christchurch, New Zealand, August 1977: pp. 274-281

Schmidt, L. C, Morgan, P. R. and Phang, P. W. (1981), "Influence of joint eccentricity and rigidity on the load capacity of a space truss sub-assemblage", Journal of Constructional Steel Research, Vol. 1, No. (4), September 1981: pp. 16-22.

Schmidt, L. C, Morgan, P. R. and Stevens, L. K. (1975), "The influence of imperfections on the behaviour of a space truss", Second International Conference on Space Structures, University of Surrey, Billing & Sons Limited, UK, September 1975: pp 55-64.

Schmidt, L. C. (1976), "Member buckling characteristics and space truss behaviour", lASS World Congress on Space Enclosures, Building Research Centre, Concordia University Montreal, July 1976: pp 849-857

Schmidt, L. C. and Hanaor, A. (1979), "Force limiting devices in space trusses", Journal of the Structural Division, ASCE, Vol. 105, No. ST5, May 1979: pp. 939-951.

Sebastian, W. M. and McConnel, R. E. (1993), "An investigation into the possibility of a composite space truss bridge", Fourth International Conference of Space Structures, Surrey, UK, Thomas Telford Services Ltd. Vol. 2: 1640-1649.

Shaaban, H. F. (1997), "Effect of composite action on a space truss system with continuous chord members", PhD thesis, University of Dundee, UK.

Smith, E. A. (1984), "Ductility in double layer grid space trusses", Third International

Conference on Space Structures, Surrey, UK, 510-515.

Smith, E. A. and Epstine, H. I. (1980), "Hartford Coliseum Roof Collapse: Structural Collapse and Lessons Learned", Civil Engineering ASCE, 1980, pp. 59-62.

Smith, E. M. (1988), "Alternate path analysis of space trusses for progressive collapse", Journal of Structural Engineering, ASCE, Vol. 114, No. 9:pp. 1978-1999.

Smith, J. W. (1988), "Vibration of Structures, Application- in Civil Engineering Design", Chapman and Hall Ltd.

Song, G., Vlattas, J., Johnson, S. E. and Agrawal, B. N.(2001), "Active vibration control of a space truss using a lead zirconate-titanate stack actuator", Proceedings of the I MECH E Part G Journal of Aerospace Engineering, Vol. 215, No. (6), 21 December 2001: pp. 355-361.

Souza, A. S. C., R. M. Gonçelves, et al. (2008) "A strategy of numerical analysis of space truss connections with stamped bar ends", International Journal of Space Structures, Vol. 23, No. (3): pp. 143-152.

Suzuki, T. (2005), "Development of W-Truss system", Japan, Nippon Steel Technical Report, No. 92, July 2005.

Tabatabaei, M. and Marsh, C. (1993), "Strengthening space trusses by diagonal removal", International Journal of Space Structures, Vol. 8, No. (4), 1993:pp. 231-239.

Tada, M. and Wakiyama, K. (1993), "Load-carrying capacity of space trusses under the influence of imperfections", Space Structures 4, Proceedings of the Fourth International Conference on Space Structures, University of Surrey, Thomas Telford House, UK, 1993: pp. 205-212.

Walker, H., B. (1981), "The NODUS system for the design and construction of space frames.", Analysis, Design and Construction of Double-Layer Grids, Ed. Z. S. Makowski, Applied Science Publishers Ltd., London, 1981: pp. 331-354.

Wang, C. Y., R. Z. Wang, *et al.* (2006). "Nonlinear dynamic analysis of reticulated space truss structures", Journal of Mechanics, Vol. 22, No. (3): pp. 199-212.

Zhu, K., Al-Bermani, F. G. A. and Kitipornchai, S. (1994), "Nonlinear dynamic analysis of lattice structures", Computers & structures, Vol. 52, No. (1): pp. 9-15.

Appendix A

SHAKING TABLE DETAILS AND INTSTRUMENTATION

A.1 Introduction

This appendix presents the manufacturing drawing details of the shaking table. It presents information about mechanical components such as linear guide bearings and rod end specifications and electric components like electric motor and servomotor. Details of instruments used will be also introduced.

A.2 Shaking table description and layout

The following sheets 1 through 5 give full manufacturing details for shaking table.

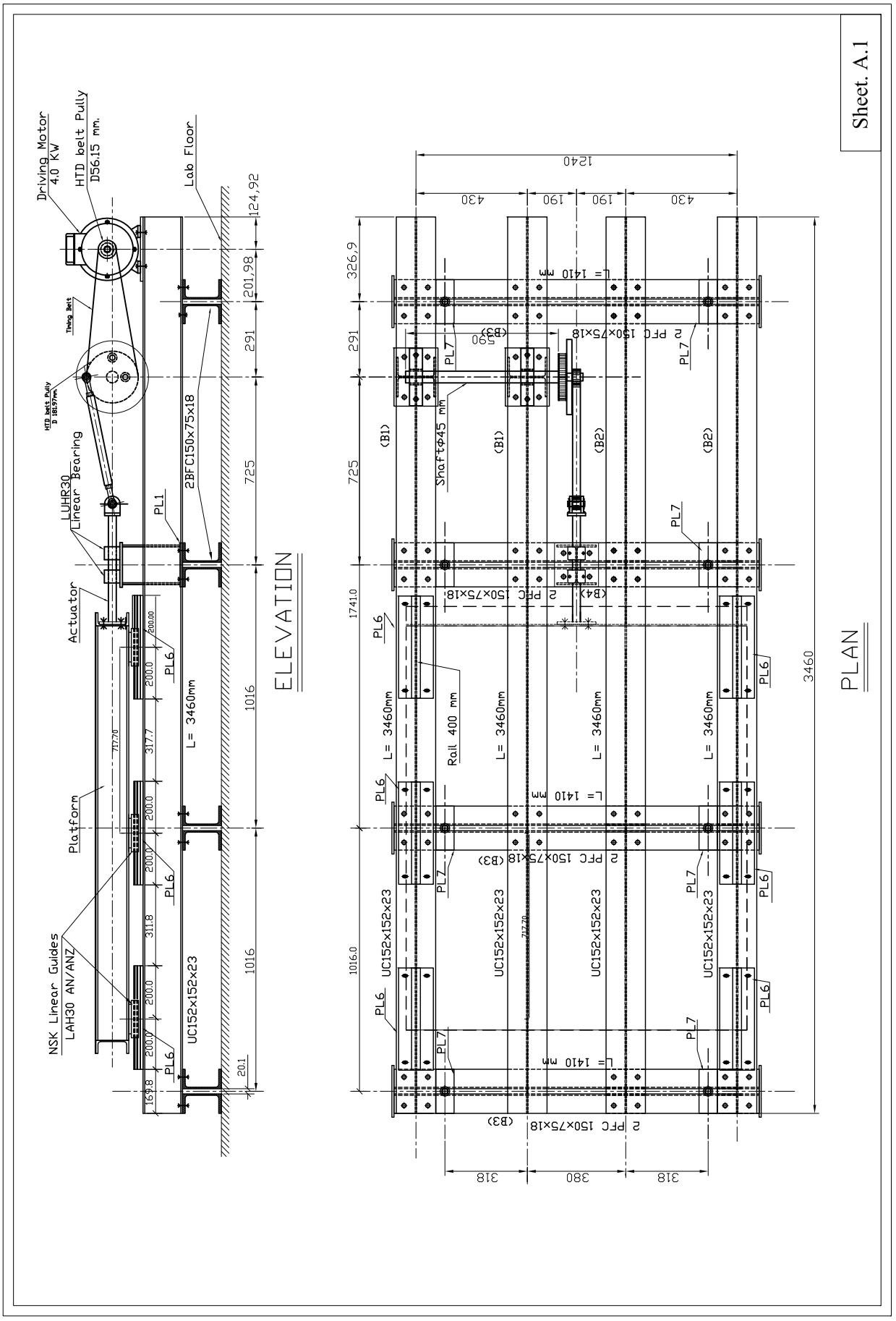
Sheet. A.1
ELEVATION
PLAN
Driving Motor
4.0 KW
HTD belt Pully
D56.15 mm.
Lab Floor
Timing Belt
LUHR30
Linear Bearing
Actuator
Platform
NSK Linear Guides
LAH30 AN/ANZ
PL1
PL6
PL7
2BFC150x75x18
UC152x152x23
L= 3460mm
Rail 400 mm
Shaft Φ45 mm
2 PFC 150x75x18
L= 1410 mm
124,92
201,98
291
725
1016
326,9
1741.0
1016.0
3460
1240
430
190
318
380

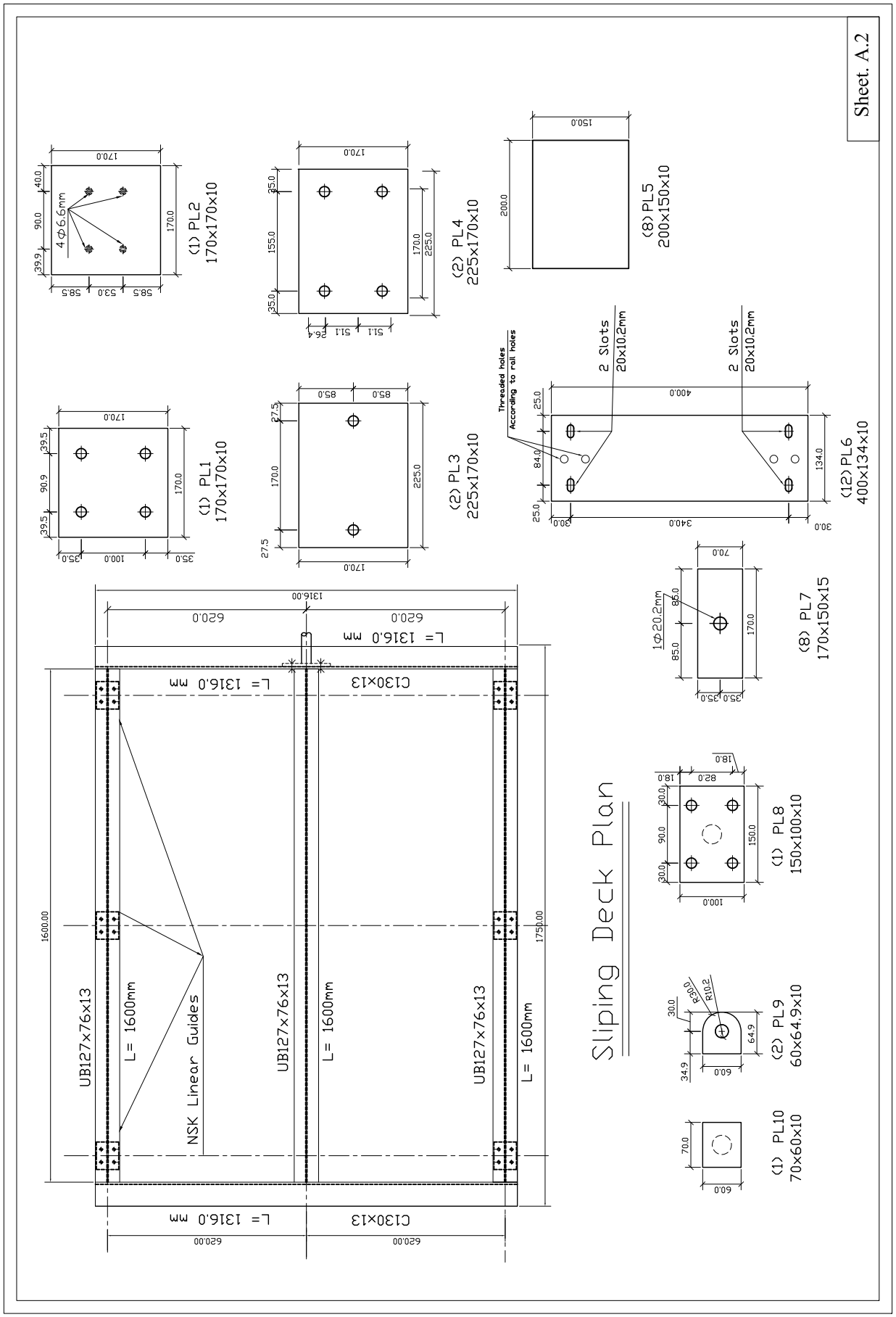
Sheet. A.2
Sliping Deck Plan
UB127×76×13
L= 1600mm
NSK Linear Guides
C130×13
L= 1316.0 mm
1600.00
1750.00
620.0
1316.00
(1) PL2
170×170×10
(2) PL4
225×170×10
(8) PL5
200×150×10
(1) PL1
170×170×10
(2) PL3
225×170×10
(12) PL6
400×134×10
2 Slots
20×10.2mm
Threaded holes
According to rail holes
(8) PL7
170×150×15
(1) PL8
150×100×10
(2) PL9
60×64.9×10
(1) PL10
70×60×10

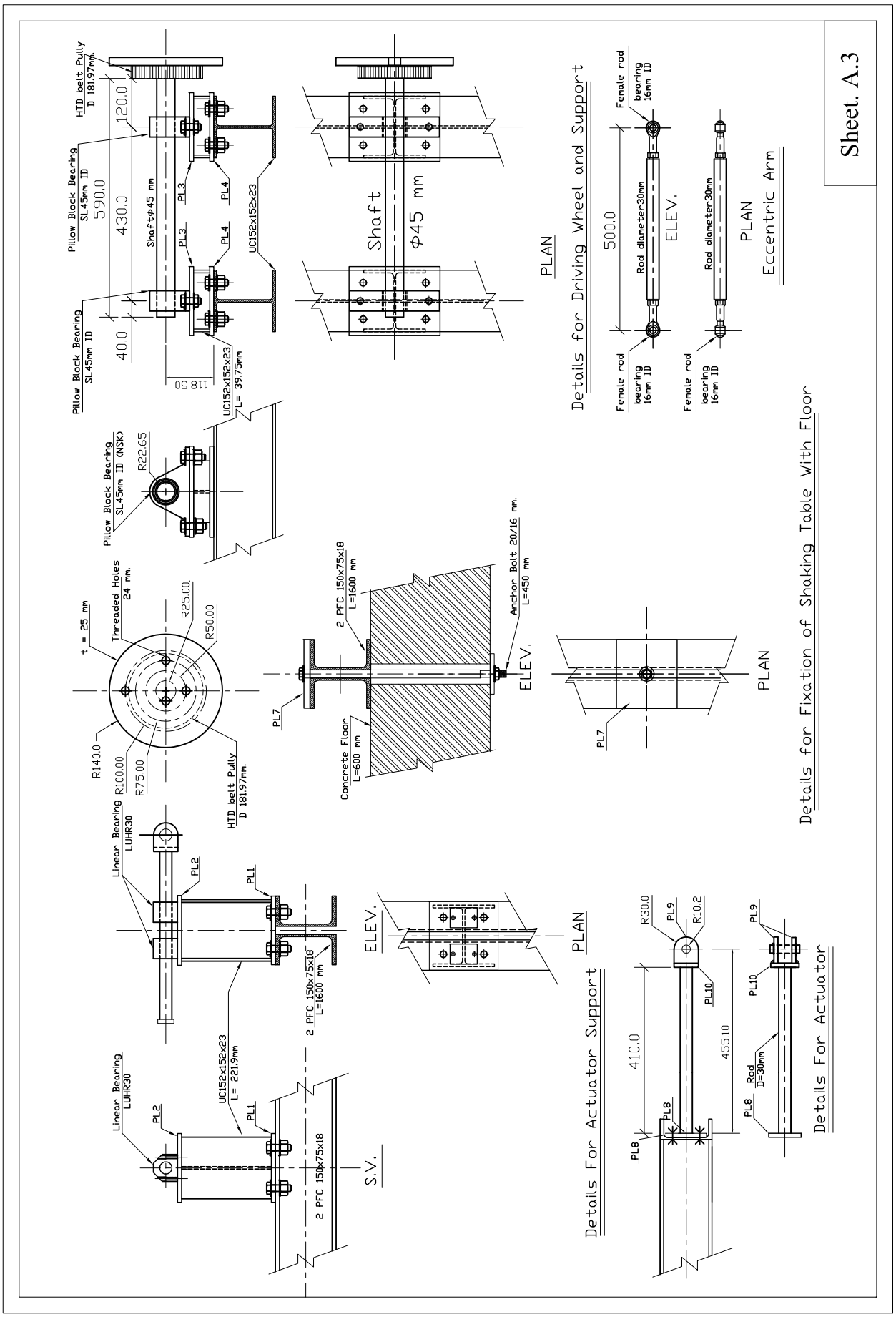
Sheet. A.3
Details for Fixation of Shaking Table with Floor
Details for Driving Wheel and Support
Eccentric Arm
Details For Actuator Support
Details For Actuator
HTD belt Pully D 181.97mm.
Pillow Block Bearing SL45mm ID
Shaft φ45 mm
UC152x152x23
PL3
PL4
590.0
430.0
120.0
40.0
118.50
Shaft
φ45 mm
PLAN
500.0
Female rod bearing 16mm ID
Rod diameter30mm
ELEV.
PLAN
Pillow Block Bearing SL45mm ID (NSK)
R22.65
UC152x152x23 L= 39.75mm
t = 25 mm
Threaded Holes 24 mm.
R25.00
R50.00
R140.0
R100.00
R75.00
2 PFC 150x75x18 L=1600 mm
Anchor Bolt 20/16 mm. L=450 mm
Concrete Floor L=600 mm
PL7
ELEV.
PLAN
Linear Bearing LUHR30
PL2
PL1
UC152x152x23 L= 221.9mm
2 PFC 150x75x18
S.V.
ELEV.
PLAN
R30.0
R10.2
PL9
PL10
PL8
410.0
455.10
Rod D=30mm

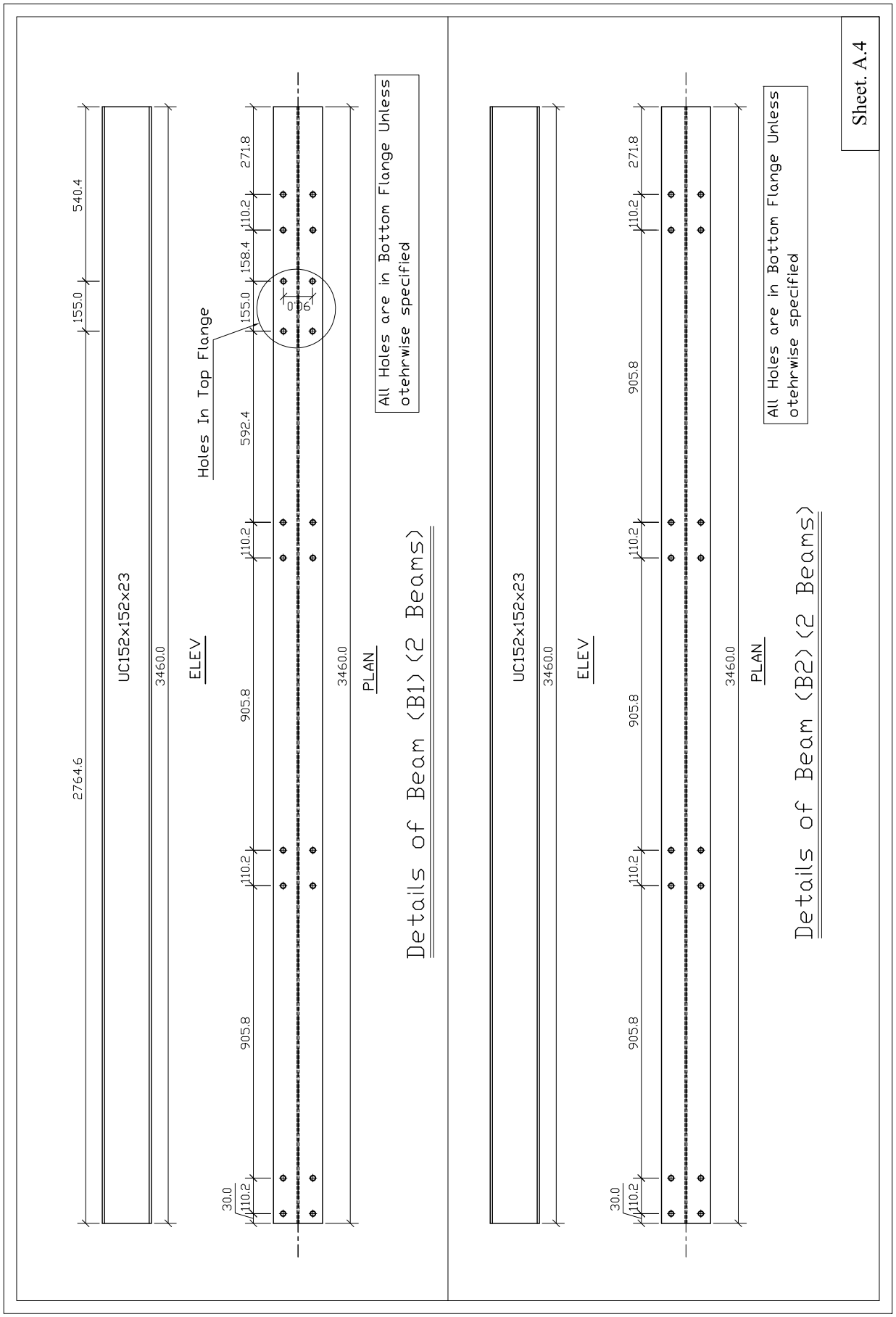
Sheet. A.4
Details of Beam (B1) (2 Beams)
ELEV
UC152x152x23
3460.0
2764.6
155.0
540.4
PLAN
Holes In Top Flange
All Holes are in Bottom Flange Unless otehrwise specified
30.0
110.2
905.8
592.4
158.4
271.8
Details of Beam (B2) (2 Beams)

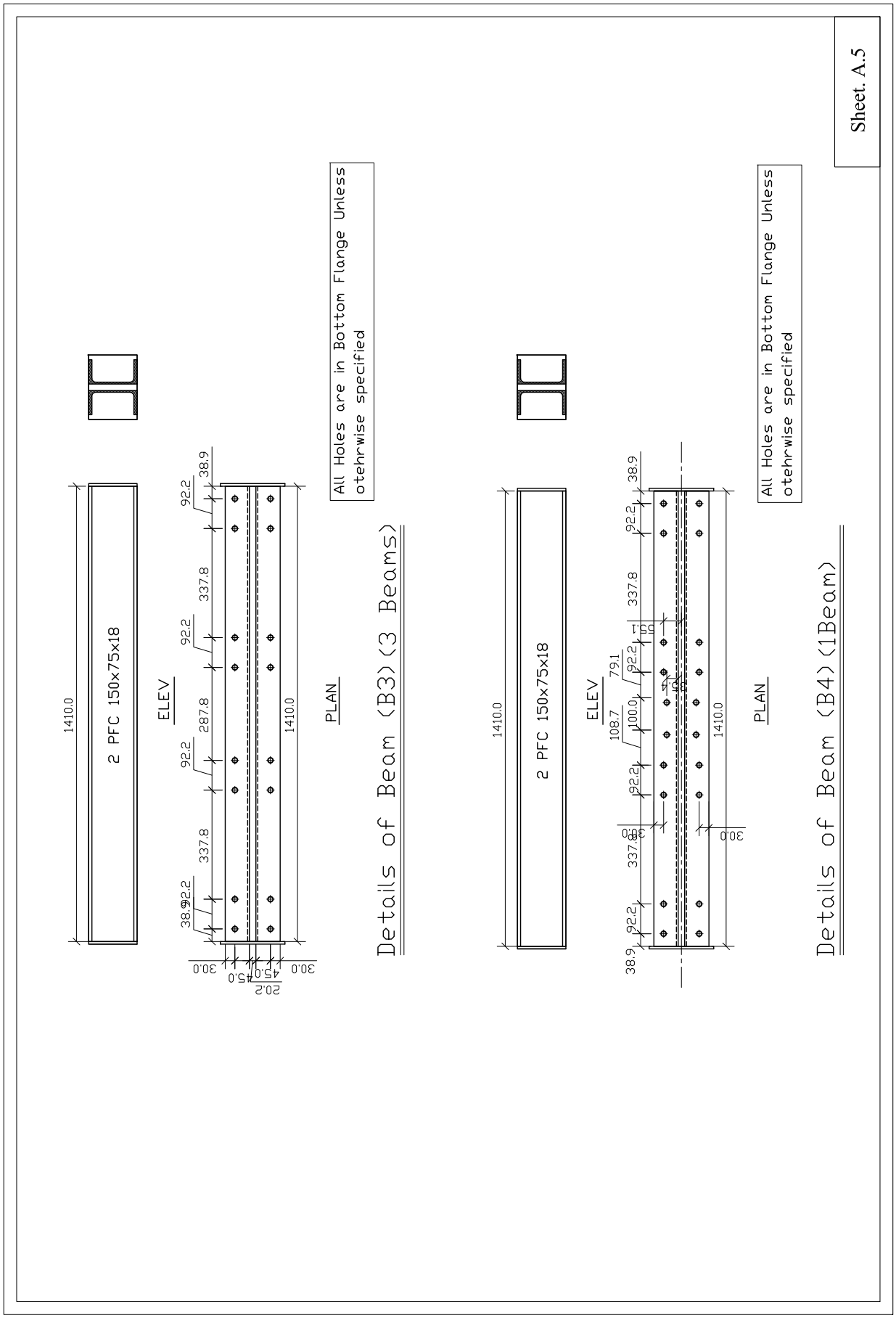
Sheet. A.5
Details of Beam (B3)(3 Beams)
All Holes are in Bottom Flange Unless otehrwise specified
2 PFC 150x75x18
1410.0
ELEV
PLAN
92.2
38.9
337.8
287.8
30.0
45.0
20.2
Details of Beam (B4)(1Beam)
All Holes are in Bottom Flange Unless otehrwise specified
2 PFC 150x75x18
1410.0
ELEV
PLAN
108.7
79.1
100.0
92.2
38.9
337.8
30.0

A.3 Electric motor design for shaking table

In the following page the sheet used for designing the motor needed for the shaking table.

WHEN BUYING OR INSTALLING ELECTRIC MOTORS TO MAKE OBJECTS MOVE WE TEND TO THINK OF THE MOTOR'S POWER AND SPEED, HOWEVER, TORQUE IS ACTUALLY ONE OF THE FIRST THINGS WE SHOULD BE THINKING ABOUT.

Torque is basically force applied to a radius, or a rotational force, which means that every time we turn something, torque is generated. Knowing what torque is required to turn a load helps to make the right motor choice.

UNDERSTANDING TORQUE

Electric motors produce a rated motor torque which can be calculated from the power of the motor and its speed.

$$\text{Motor Torque (Nm)} = \frac{9500 \times \text{Power (kW)}}{\text{Speed (rpm)}} \quad (1)$$

However, the other important factor which needs to be considered when selecting a motor for a job, is the "load" torque. This is the torque required to overcome the friction and inertia of the load and moving parts to be moved.

For example; a crane needs to lift a box to a certain height at a certain speed. In practice the motor torque needs to be greater than the load torque in order to get it to move. If the motor torque only just matches the load torque the box won't move. If the motor is too small it may not be able to lift the container or it might even drop the container completely.

IMPACT OF FORCE

Before we calculate the load torque we need to understand force, or the effort required to move a body. Force is proportional to the mass or weight of the object and the acceleration at which it is moving.

$$\text{Force} = \text{mass of object to be moved (in kg)} \times \text{acceleration (in m/s}^2\text{)} \quad (2)$$

In lifting applications where the body to be lifted is stationary the acceleration is due to gravity (roughly 10m/s^2).

LOAD TORQUE

The force required to move a body with a motor is rotational and acts through a pulley or sprocket, where the actual force is applied at the outer edge of the pulley. So the "load" torque is the force or effort required to move a load through the turning action of a pulley or sprocket, and is calculated as;

$$\text{Load Torque} = \text{Force} \times \text{Radius} \quad (3)$$

With torque expressed in Nm (Newton metres), force is expressed in Newtons and radius is expressed in metres.

By calculating the motor torque, and ensuring it is more than the load torque we can select the right motor for the task in hand.

RS stocks a wide range of motors including:

- ac synchronous
- brushed dc
- brushless dc
- ironcore dc
- ironless dc
- ac induction
- steppers
- ac servos

See BOOK 1 Section 21 or visit rswww.com

WILL THE MOTOR LIFT A BOX?

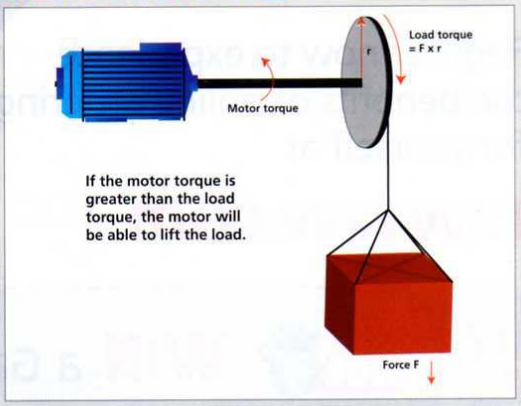

A box weighing 10kg is to be lifted using a rope wound round a 20cm diameter pulley driven by a 2.2kW 4 pole motor.

Based on the load torque equation: (3)

mass (10kg) x gravity (10m/s^2) x radius (0.1m) = 10Nm

So the motor must produce at least 10Nm to hold the box still, and more to lift it.

And, the motor torque (1) produced by the 2.2kW 4 pole (1450rpm) motor is

(9550 x 2.2kW) / 1450 = 14.5Nm

The motor torque 14.5Nm is greater than the load torque 10Nm, and is therefore enough to lift the box. In the real world a gearbox would be connected to the motor to reduce the speed of the pulley, and this would have the effect of increasing the torque. The output torque of a motor-gearbox combination is the motor torque times the gearbox ratio times the efficiency of the gearbox.

For more information and an engineering guide to motor selection visit **rswww.com/automation**

A.4 Instruments used in tests

I- Microlink 770 Data Acquisition system

1- Microlink 770 DAQ card

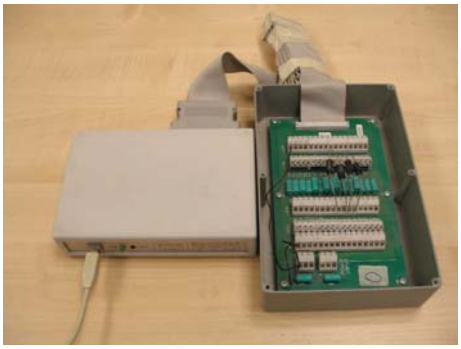

2- DAQ card with connection box

Figure A. 1 Microlink 770 DAQ

Listed below are main features of the DAQ system used during experimental work, (http://www.windmillsoft.com/acatalog/A000_1.html)

- Measures temperature, strain, pressure, voltage or current through 16 analogue input channels.
- A 16-bit analogue-to-digital converter gives high resolution readings.
- Independent input ranges let you mix different types of measurements - thermocouples and 4-20 mA process signals for example - without losing resolution.
- For more accurate timing than your computer's clock allows, you can connect an external crystal-controlled clock.
- Save data both before and after an event (pre- and post-trigger data). Useful for seeing, for example, what happened immediately before a fault occurred.
- Use the 770 to start other equipment simultaneously with data capture.
- A digital input into the Microlink lets other equipment trigger data capture.

- Alternatively wait until 1 or 2 readings cross a threshold before automatically starting to collect data. For example, when the temperature goes above or below your set points.
- Exclude channels from a scan if necessary. This lets you use the 770 with different set-ups without having to rewire.
- Set both the interval between reading each channel (thermocouple, strain gauge, etc), and how often all channels are read. For example, you may choose to wait a millisecond between reading each channel, but after the last channel has been read pause for 10 seconds before starting again.
- To work as a strain gauge reader it needs a Microlink 594 connection box with built in bridge style.

II- LVDT transducers

Two types of LVDT transducers were used. The first type used was small transducers with self rebound features and 10 mm stroke length. This one was used to measure vibrations during snap tests and responses due to shaking table vibrations. The short stroke of this transducer allowed for very high accuracy in measuring minute displacement responses in tested models, see Figure A.2.

The other LVDT transducer was of long stroke type (300mm) without a rebound feature, see Figure A.3. This one was connected to the shaking table platform to measure the displacement output resulted from platform movements during tests.

Both transducers were of ± 10 volts type. Which allowed very high accuracy in measuring responses especially for the first one which combined with the above mentioned DAQ was able to measure responses within ± 0.003 mm.

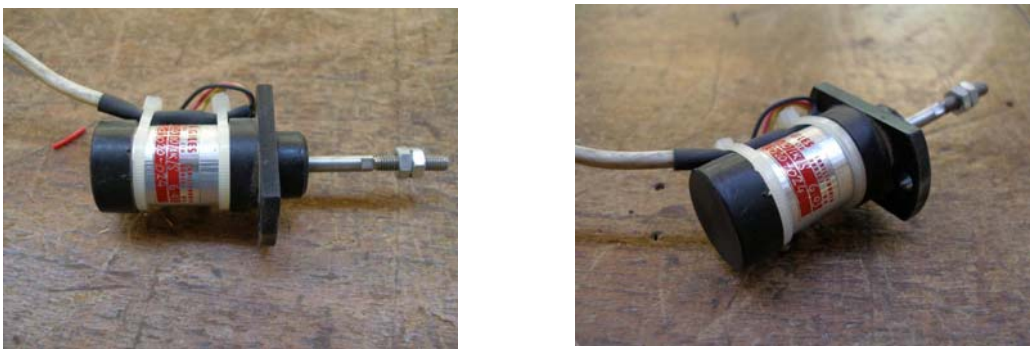

Figure A. 2 Short stroke LVDT transducer used during experiments to measure models' displacements

Figure A. 3 Long stroke LVDT transducer used during experiments to measure shaking table platform output

A.5 Shaking table and test rig in pictures

Figure A. 4 Shaking table with one of test models

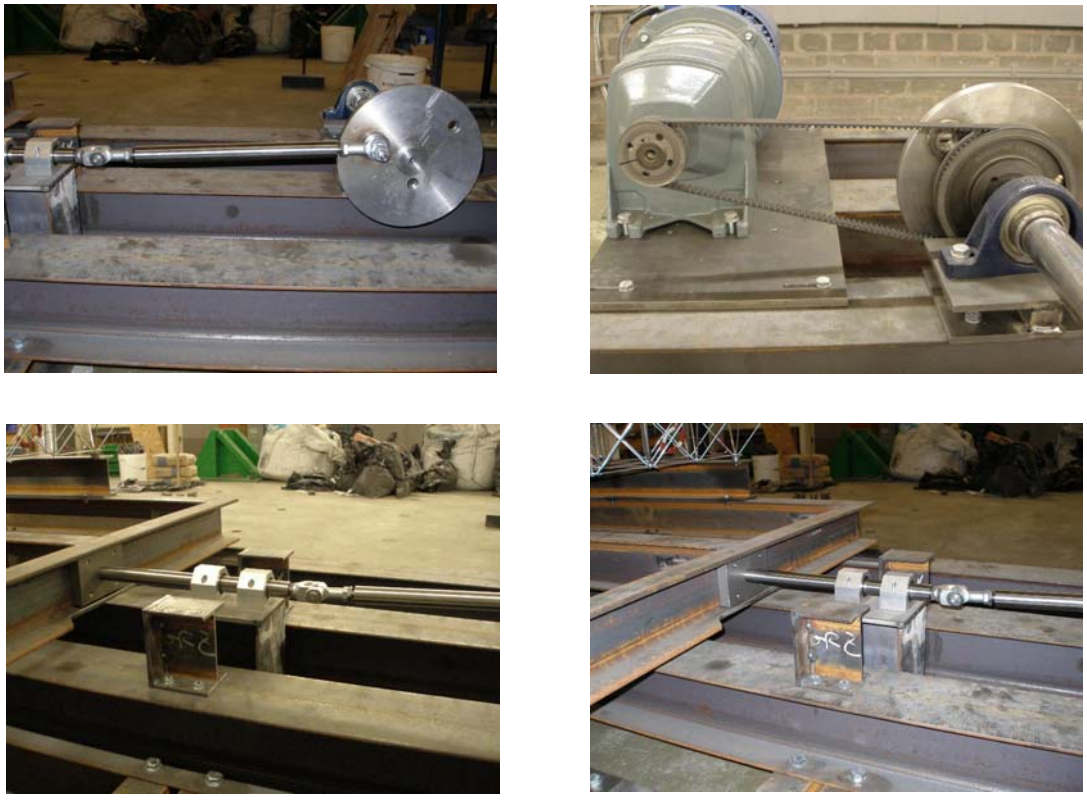

Figure A. 5 Circular to linear motion conversion

a. Compression test for pinned upper chord

b. Tension test for timber material sample

c. Compression test for continuous upper chord

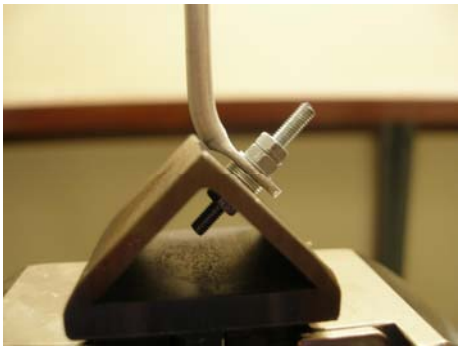

d. Diagonal member support during test

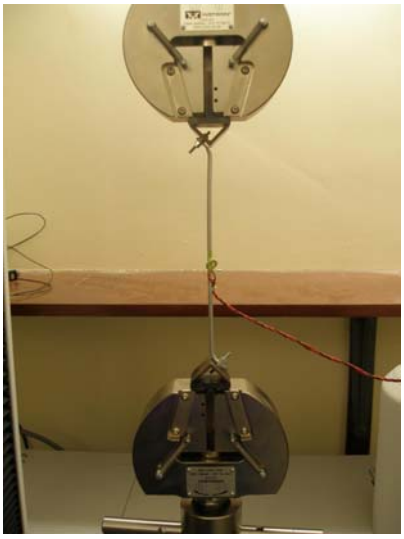

e. Diagonal member test

f. Diagonal member during compression test

Figure A. 6 Testing of material samples and elements of space truss models

a. Non-Composite space frme Truss-A

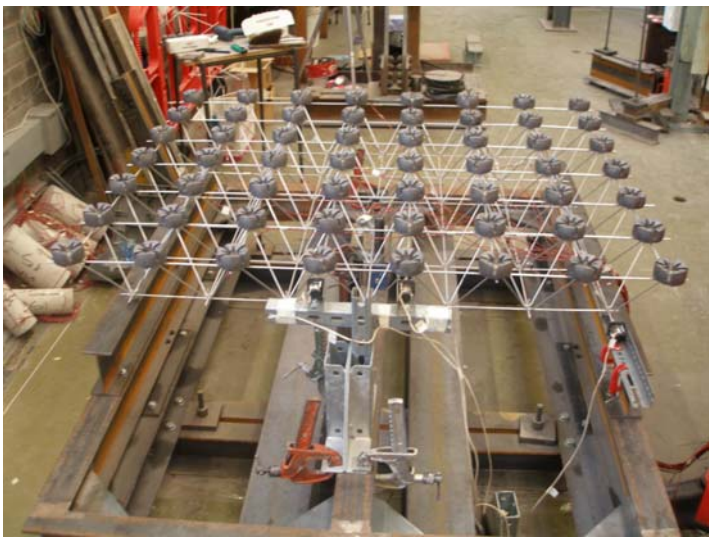

Composite space frame with aluminum deck, Truss B

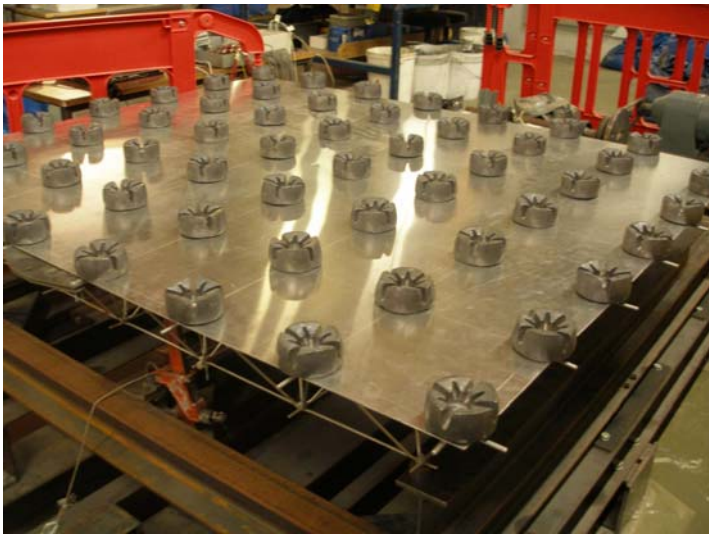

Composite space frame with timber deck Truss C

Figure A. 7 Experimental space frame models

Appendix B

DATA FILTRATION USING FAST FOURIER TRANSFORMATION

B.1 MATLAB program for data filtration using FFT

```
%*********************************************************************
% This File is to Filter the Frequencies within a specific data range
% This file targeted to filter the output for only 12 channels in Time-Domain
% Data should be 13 columns by which the left one is the time
% By:
% Maher Elabd
% Dundee University
% *********************************************************************
% Reading the original data from File and Plotting it [Time-Domain]
%*********************************************************************
clc
clear all
File=input('Enter Data File Name     :','s')
data=load (File);                % Copy Data from file to a temp. Matrix data
time=data(:,1);                  % Reading time vector data
T=time(5)-time(4);               % Periodic Time
strs=data(:,[2:end]);            % Response vector (Strain [Data from 10 strain Gauges])
)
[r c]=size(strs)                 % Finding Data matrix size [rows columns]
%D=length(time)                  % Finding the length of data vector
hold on
subplot(2,1,1);
plot(2,1,time,strs(:,1),'r');    % Plotting original data
Ulimit=max(strs(:,1))+5
Mlimit=-1*max(strs(:,1))-5
axis([0 time(r) Mlimit Ulimit])
grid
title('Vibration Test Strains')
xlabel('Time')
ylabel('Mico-Strain')

%% ***************************************************************
% Carry out FFT for Data Obtained from Input File
%** ***************************************************************
Z=2^nextpow2(r)                  % Next power of 2 from length of DATA
Y = fft(strs,Z);                 % Carry out FFT for a Z number of vector [delta]
%spx=abs(Y).^2                   % Power spectrum of the data
%freq=(0:(Z-1))/(T*Z)             % Frequency Domain
%plot(freq(1:Z/2),spx((1:Z/2),1))  % Plotting power spectrum output
```

```
%axis([0 20 0 2e11])            % Axis limits for spectrum
%Y(1,1:end)=0                   % Removed because it is just the summation of data

%% ***************************************************************
% Selecting the unwanted noise frequencies to be filtered [Frequency-Domain]
%***************************************************************
rmin= input('Enter lower range of frequencies to be Omitted     :')
rmax=input('Enter upper range of frequencies to be Omitted      :')
R=zeros(Z,c);
xmin=floor(rmin*Z*T+1.5);
xmax=floor(rmax*Z*T);
for i=1:(Z/2 )
for j=1:c
   if i< xmin || i> xmax
      R(i,j)=Y(i,j);
   else
      R(i,j)=0;
   end
end
end
%Second part of Data (inversed as it is the second half (negative part)
xmin2=floor(Z-(rmin*Z*T+1.5)+2);
for i=((Z/2)+1 ):Z;
   for j=1:c
      if i<xmin2;
      R(i,j)=0;
      else
      R(i,j)=Y(i,j);
      end
   end
end

%% ***************************************************************
% Carrying out Inverse FFT on the rest of filtered frequencies (Frequency-->Time
Domain)
%***************************************************************
FR=ifft(R);             %Inverse on filtered(R)
fin=real(FR);           %find the real values of inversed(R) at it is in imaginary case
%%***************************************************************
% Plotting the final results Time-Domain.
%***************************************************************
hold on
subplot(2,1,2);plot(2,2,time(1:r),fin(1:r))
%plot(time(1:D),fin(1:D))
axis([0 time(r) Mlimit Ulimit])
grid
title('Filtered Vibration Test Strains ')
xlabel('Time')
ylabel('Mico-Strain')
dd=[time(1:r),fin(1:r,1:c)];
%%
```

```
g=13-(c+1);
if g>0;
   df=zeros(r,g);
   ds=[dd df];
else
   ds=dd;
end;

%% ***************************************************************
% Saving output results to file (Time-Domain).
%***************************************************************
Outf=input('Enter Output File Name   :','s')
fid = fopen(Outf, 'wt');
fprintf(fid,'%6.4f  %12.4f %12.4f %12.4f %12.4f %12.4f %12.4f %12.4f
%12.4f %12.4f %12.4f %12.4f\n',ds');
fclose(fid);
hold off
```

B.2 MATLAB program to determine the frequency using power spectrum method

```
%****************************************************************
% Finding the maximum frequency using power spectrum method
%% Reading Data From File and Plotting it
%****************************************************************
clc
clear all
File=input('Enter Data File Name     :','s')
data=load (File);                                   % Copy Data from file to a temp. Matrix
                                                    data
time=data(:,1);
T=time(2)-time(1)
delta=data(:,2);
D=length(delta)
title('Vertical Snap Test')
grid
hold on
plot(time,delta,'b');
pause
%% Carry out FFT for Data Obtained from Input File
Z=2^nextpow2(D)                      % Next power of 2 from length of y
Y = fft(delta,Z);
Y(1)=[];                  % Removed because it is just the summation of data

% Obtaining the No of Elements in Y Matrix (vector) to use get (n/2)
%% positve frequency values only
n=length(Y)                          % it should be the same value as (Z-1) as there is
                                     one element removed
power = abs(Y(1:floor(n/2))).^2;    %Floor= Round to the lower value (Power
                                                 Sepctrum)
%nyquist = 1/2;
%ss=(0:(n/2)-1);
freq = (0:(n/2)-1)/(n*T);
plot(freq,power)
xlabel('Samples/Second')
title('Periodogram')
plot(freq(1:200),power(1:200))
xlabel('cycles/year')
%period=1./freq;
period=freq;
semilogx(freq,power);
%axis([0 200 0 2e+4]);
ylabel('Power');
xlabel('Period (Years/Cycle)');
hold on;

%% Finding the index of the Max frequency and Plotting the Value
index=find(power==max(power))
mainPeriodStr=num2str(period(index));
```

```
plot(period(index),power(index),'r.', 'MarkerSize',20);
text(period(index)+2,power(index),['Period = ',mainPeriodStr]);
hold off;
```

Appendix C

EXPERIMENTAL RESULTS OF MODELS WITH ASPECT RATIOS OF 1.2, 1.5 AND 3.0

C. 1 Introduction

This Appendix presents detailed results of the experimental tests carried out on Trusses A, B and C, with aspect ratios of 1.2, 1.5 and 3.0.

C. 2 Results for space frame models with aspect ratio of 1.2

Results of snap and shaking table tests on Trusses A, B and C with AR = 1.2 are summarised in the following section.

C. 3.1 Results of corner-supported models

Results of vertical snap tests on models with AR = 1.2 are presented in Table C.1, while results of horizontal snap tests are presented in Table C.2. For non-composite Truss A, the case of eccentric mass was considered as it was the nearest simulation for the position of the mass. Figures C.1, C.2 and C.3 present the displacement of Trusses A, B and C during the vertical snap tests.

Table C.1 Results of the vertical snap tests on corner-supported models with AR = 1.2

	Truss A		**Truss B**		**Truss C**	
	Freq. (f) Hz	Damping ratio (ζ)	Freq. (f) Hz	Damping ratio (ζ)	Freq. (f) Hz	Damping ratio (ζ)
Test 1	19.93	4.57%	20.55	1.33%	20.48	1.70%
Test 2	19.80	4.41%	20.55	1.33%	20.55	1.70%
Test 3	19.93	4.69%	20.41	1.35%	20.48	1.44%
Average	**19.89**	**4.56%**	**20.50**	**1.34%**	**20.50**	**1.61%**

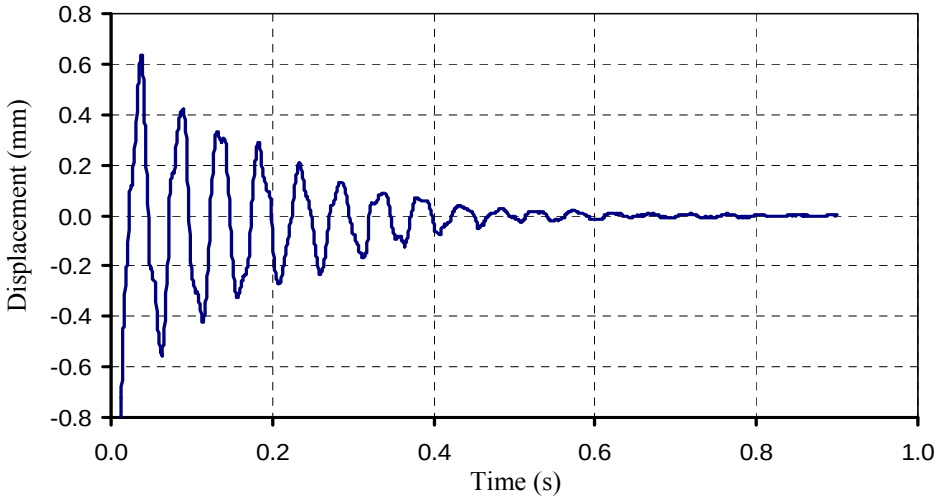

Figure C.1 Vertical displacement of Truss A with AR = 1.2 during the vertical snap test

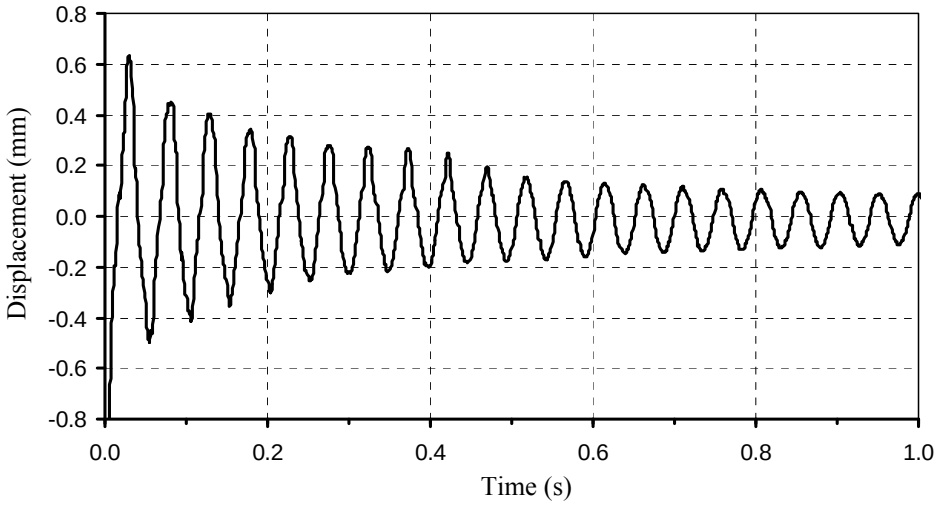

Figure C.2 Vertical displacement of Truss B with AR = 1.2 during the vertical snap test

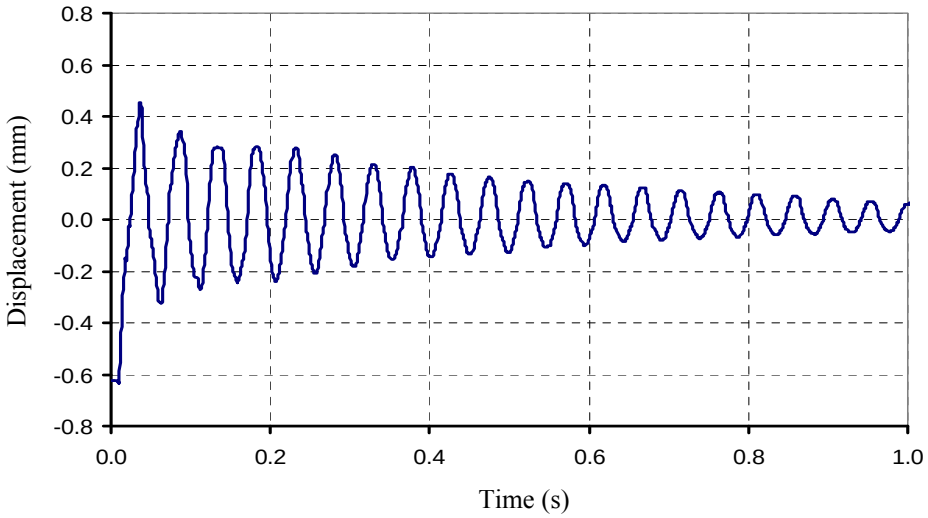

Figure C.3 Vertical displacement of Truss C with AR = 1.2 during the vertical snap test

Results of horizontal snap tests on models with AR = 1.2 are presented in Table C.2. The horizontal displacements of Trusses A, B and C during horizontal snap tests are shown in Figure C.4, C.5 and C.6, respectively.

Table C.2 Results of the horizontal snap tests on corner-supported models with AR=1.2

	Truss A		**Truss B**		**Truss C**	
	Freq. (f) Hz	Damping ratio (ζ)	Freq. (f) Hz	Damping ratio (ζ)	Freq. (f) Hz	Damping ratio (ζ)
Test 1	17.24	4.41%	22.47	1.91%	22.10	3.79%
Test 2	17.00	4.89%	23.39	1.69%	22.39	2.95%
Test 3	17.14	4.71%	22.35	2.47%	22.35	2.71%
Average	**17.13**	**4.67%**	**22.74**	**2.02%**	**22.28**	**3.15%**

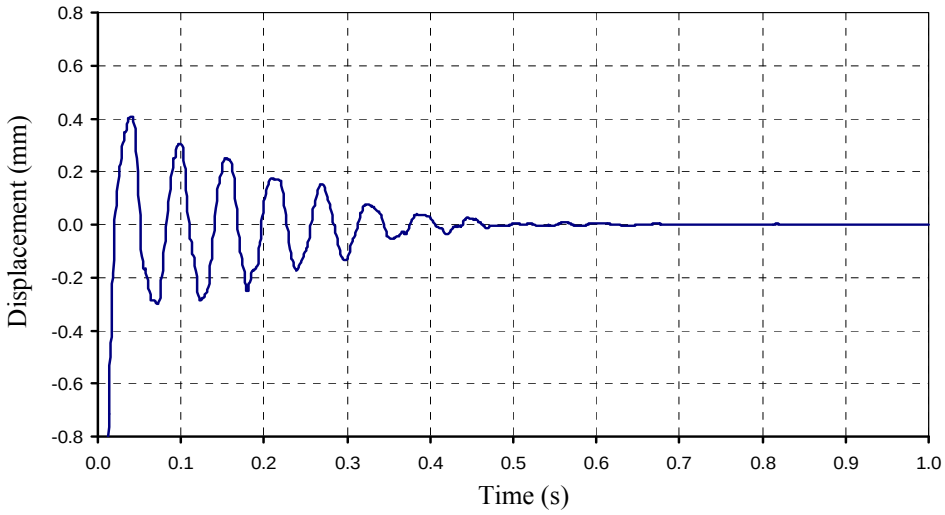

Figure C.4 Horizontal displacement of corner-supported Truss A with AR = 1.2 during the horizontal snap test

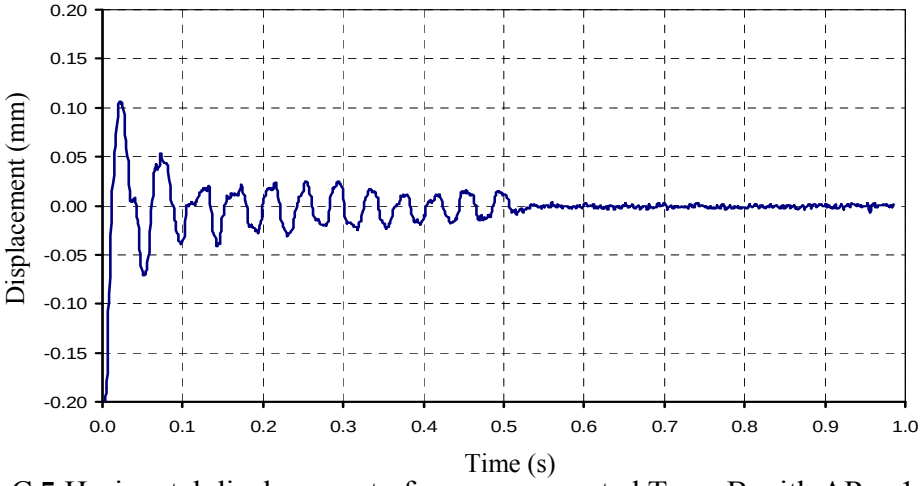

Figure C.**5** Horizontal displacement of corner-supported Truss B with AR = 1.2 during the horizontal snap test

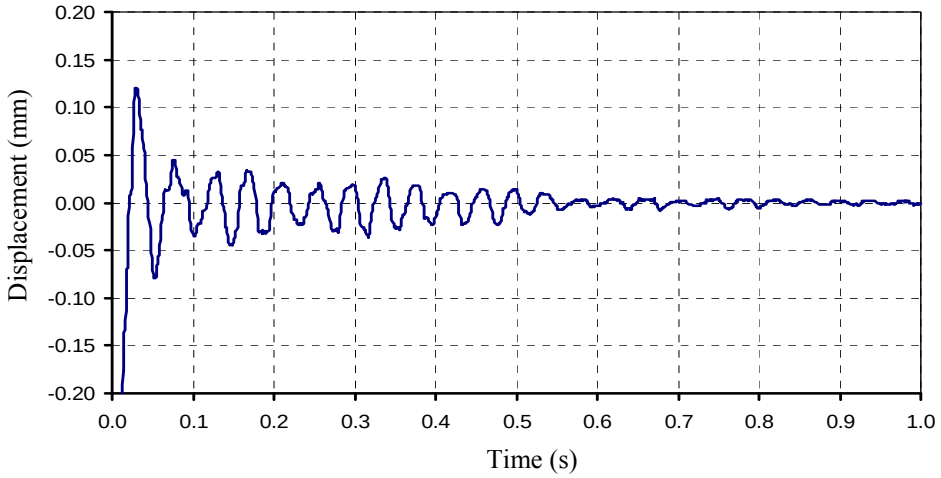

Figure C.6 Horizontal displacement of corner-supported Truss C with AR = 1.2 during the horizontal snap test

The maximum and minimum lateral displacement of space frame models subjected to shaking table vibrations are presented in Table C.3, while Figure C.7 presents the lateral displacement history of Trusses A, B and C.

Table C.3 Maximum and minimum responses for space frame models

	Truss A	Truss B	Truss C
Max. response	+0.635	+0.338	+0.382
Min. response	-0.406	-0.220	-0.239

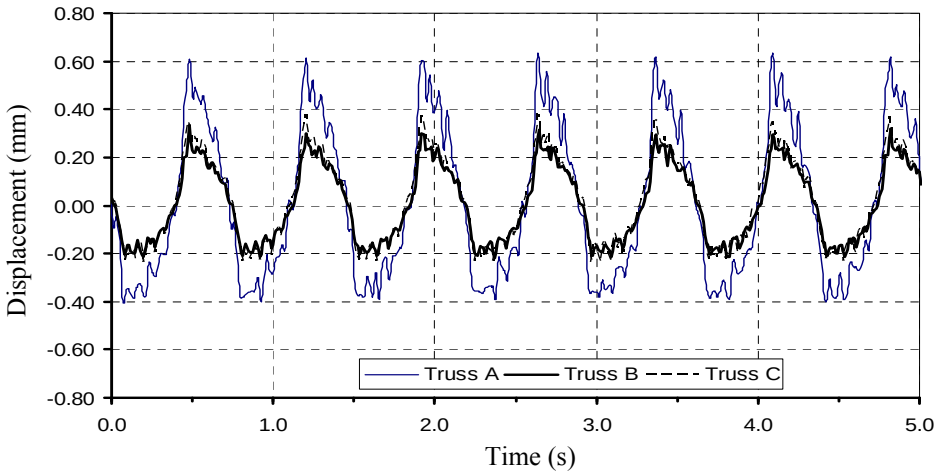

Figure C.7 Critical response for corner supported frame model Truss A

C.2.2 Results of two-edge-supported models

Results of the vertical snap tests conducted on Trusses A, B and C supported along the

two edges parallel to X-direction are listed in Table C.4. The vertical displacements of models during the vertical snap test are shown in Figures C.8, C.9 and C.10.

Table C.4 Results of the vertical snap tests on edge-supported models with AR = 1.2

	Truss A		**Truss B**		**Truss C**	
	Freq. (f) Hz	Damping ratio (ζ)	Freq. (f) Hz	Damping ratio (ζ)	Freq. (f) Hz	Damping ratio (ζ)
Test 1	25.32	4.63%	27.03	1.26%	27.52	0.82%
Test 2	25.53	4.44%	27.62	1.22%	27.52	0.86%
Test 3	25.32	4.53%	27.40	1.14%	27.52	0.70%
Average	**25.39**	**4.53%**	**27.35**	**1.21%**	**27.52**	**0.79%**

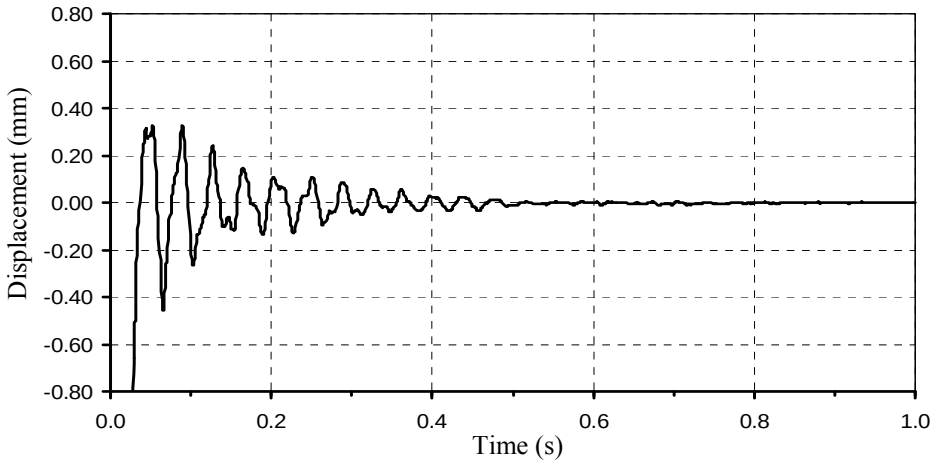

Figure C.8 Vertical displacement of edge-supported Truss A with AR = 1.2 during the vertical snap test

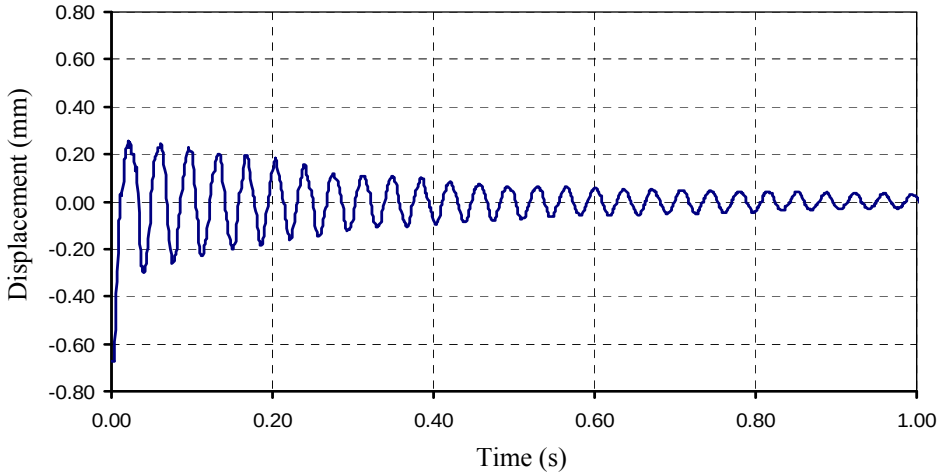

Figure C.9 Vertical displacement of edge-supported Truss B with AR = 1.2 during the vertical snap test

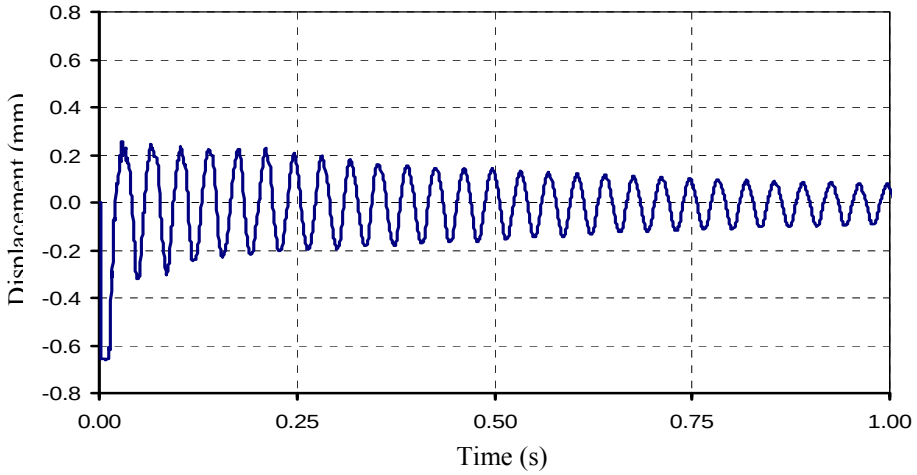

Figure **C.**10 Vertical displacement of edge-supported Truss C with AR = 1.2 during the vertical snap test

Horizontal frequencies of vibration and damping ratios resulted from horizontal snap tests are presented in Table C.5. Figures C.11, C.12 and C.13 present the displacements during the horizontal snap test.

Table C.5 Results of the horizontal snap tests on edge-supported models with AR=1.2

	Truss A		Truss B		Truss C	
	Freq. (f) Hz	Damping ratio (ζ)	Freq. (f) Hz	Damping ratio (ζ)	Freq. (f) Hz	Damping ratio (ζ)
Test 1	17.12329	7.02%	26.667	1.15%	26.490	3.98%
Test 2	17.06485	7.47%	26.786	1.25%	26.667	3.53%
Test 3	17.31602	7.47%	26.667	1.27%	26.667	3.62%
Average	17.16805	7.32%	26.70667	1.22%	26.608	3.71%

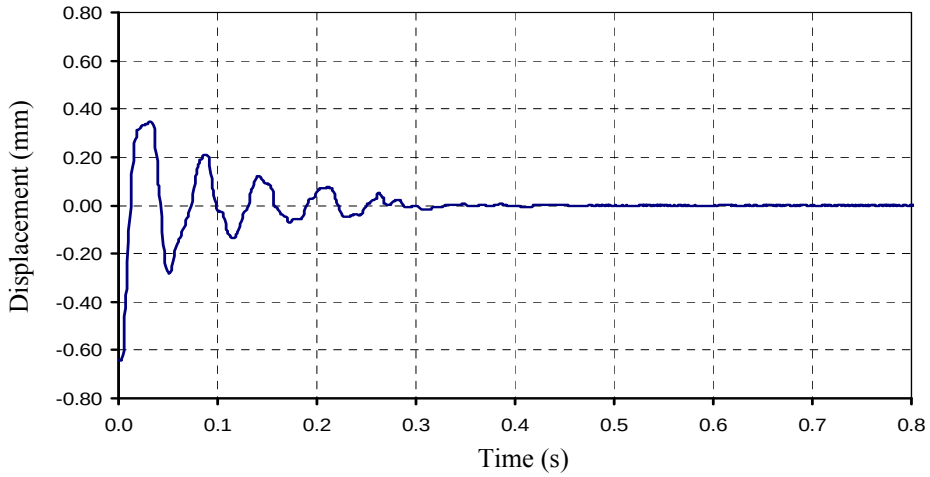

Figure C.11 Horizontal displacement of edge-supported Truss A with AR = 1.2 during the horizontal snap test

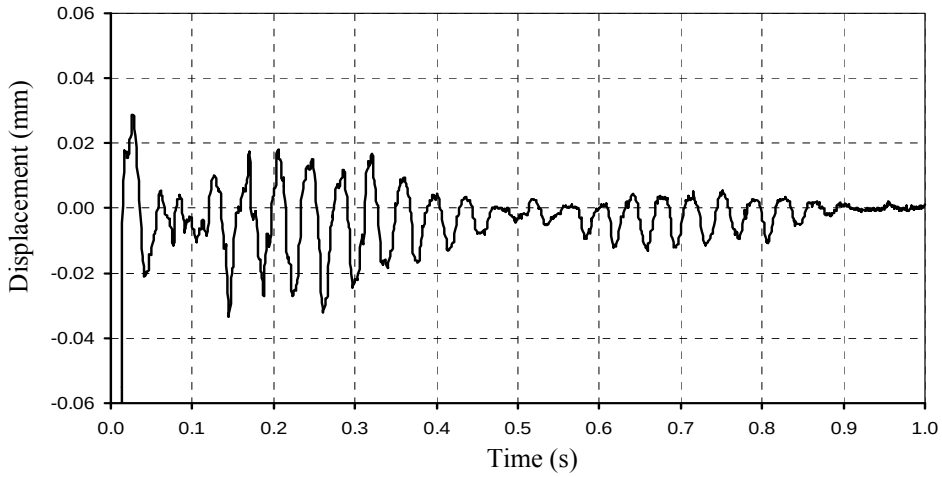

Figure C.12 Horizontal displacement of edge-supported Truss B with AR = 1.2 during horizontal snap test

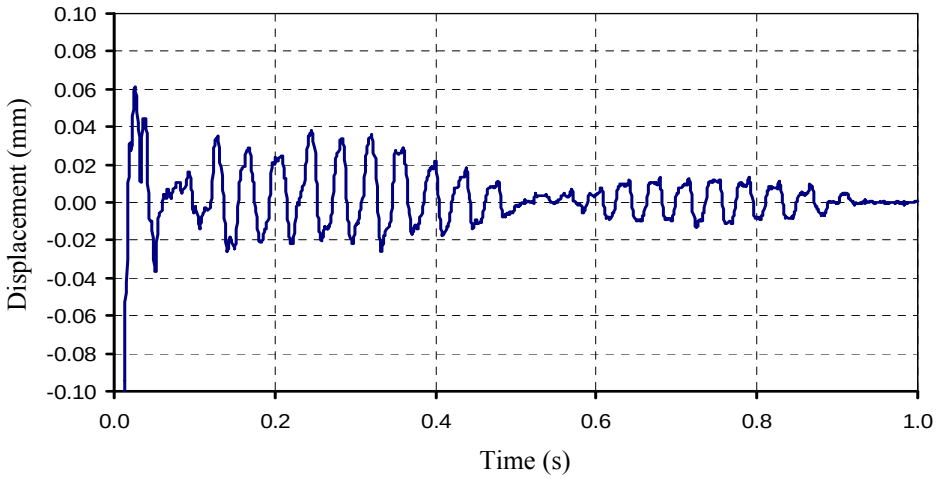

Figure C.13 Horizontal displacement of edge-supported Truss C with AR = 1.2 during horizontal snap test

The maximum and minimum displacement of Trusses A, B and C during shaking table tests can be found in Table C.6, and the net displacement results are shown in Figure C.13.

Table C.6 Maximum and minimum displacements of models during shaking table tests

	Truss A	**Truss B**	**Truss C**
Max. displacement	+0.580	+0.219	0.248
Min. displacement	-0.415	-0.185	-0.182

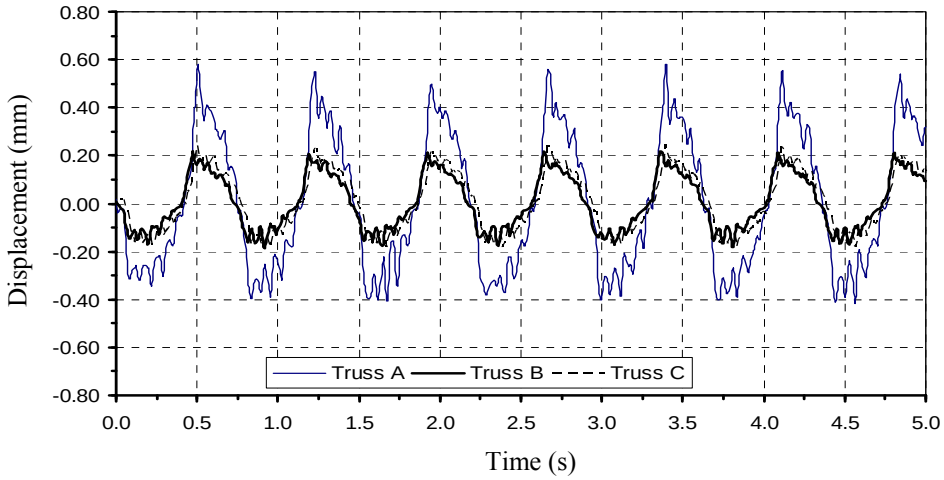

Figure C.14 Critical response for edge-supported models with AR = 1.2 during shaking table vibrations

C.3 Space frames with aspect ratio of 1.5

By removing two panels from one side of all models associated with cutting the decks, the aspect ratio of structure is changed to be 1.50. Results of tests carried on models with AR = 1.5 are presented in the following section.

C.3.1 Results of corner-supported models with AR=1.5

Values of vibration frequencies and damping ratios resulted from the vertical snap tests conducted on Trusses A, B and C are listed in Table C.7. The vertical displacements of models during the vertical snap test are shown in Figures C.15, C.16 and C.17.

Table C.7 Results of the vertical snap tests on corner-supported models with AR = 1.5

	Truss A		**Truss B**		**Truss C**	
	Freq. (f) Hz	Damping ratio (ζ)	Freq. (f) Hz	Damping ratio (ζ)	Freq. (f) Hz	Damping ratio (ζ)
Test 1	21.58	2.96%	22.389	1.75%	22.22	3.55%
Test 2	21.74	3.12%	22.39	1.82%	22.39	3.30%
Test 3	21.82	2.78%	22.47	1.92%	22.30	3.33%
Average	**21.71**	**2.95%**	**22.41**	**1.83%**	**22.31**	**3.39%**

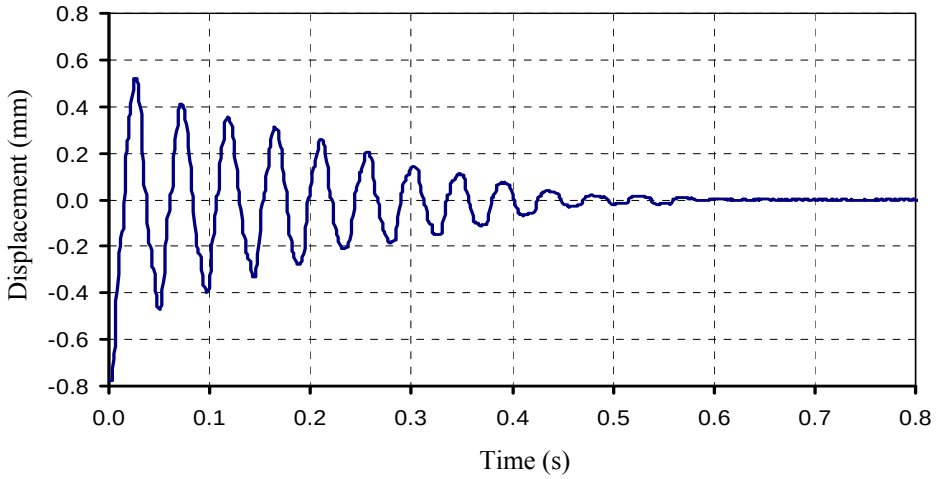

Figure C.15 Vertical displacements of corner-supported Truss A with AR = 1.5 during the vertical snap test

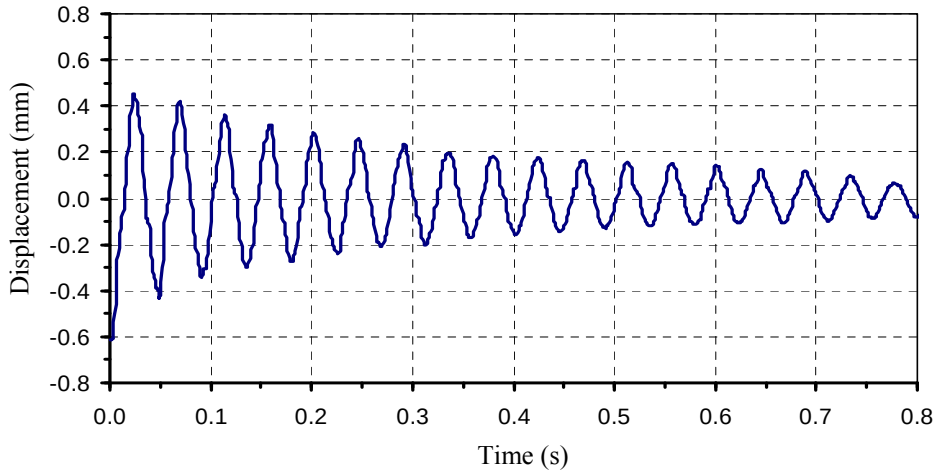

Figure C.16 Vertical displacements of corner-supported Truss B with AR = 1.5 during the vertical snap test

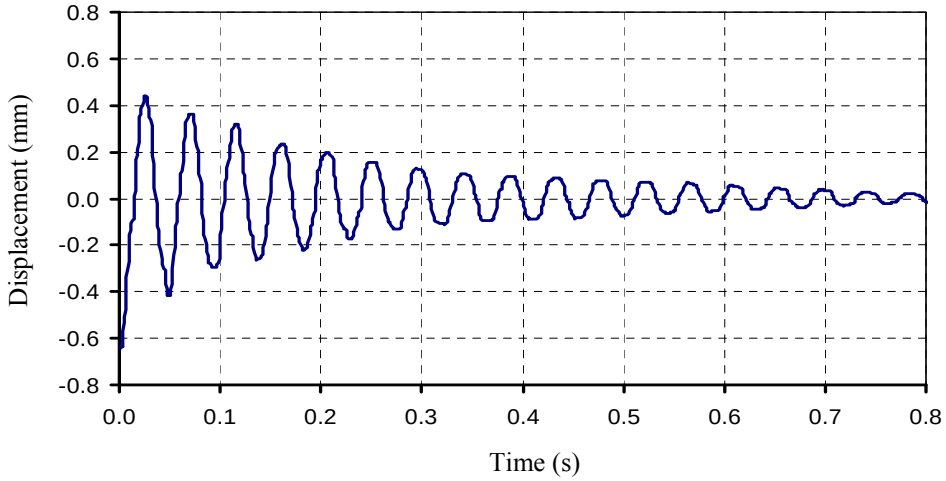

Figure C.17 Vertical displacements of corner-supported Truss C with AR = 1.5 during the vertical snap test

Horizontal snap tests were carried out on the three corner-supported models with AR = 1.5 to determine the dynamic properties of the structure in the longitudinal X-direction. Values of vibration frequencies and damping ratios obtained by tests are presented in Table C.8. However, Figures C.22 presents the snap test results for non-composite model Truss A while Figures C.23 and C.24 present the results for composite frame models Truss B and C, respectively.

Table C.8 9 Results of the horizontal snap tests on corner-supported models with AR=1.5

	Truss A		**Truss B**		**Truss C**	
	Freq. (f) Hz	Damping ratio (ζ)	Freq. (f) Hz	Damping ratio (ζ)	Freq. (f) Hz	Damping ratio (ζ)
Test 1	17.007	3.922 %	27.523	2.705 %	22.857	3.503 %
Test 2	16.949	3.795 %	27.149	2.832 %	22.989	3.209 %
Test 3	17.167	3.404 %	27.149	2.139 %	22.727	3.929 %
Average	17.041	3.707 %	27.27367	2.559 %	22.85767	3.547 %

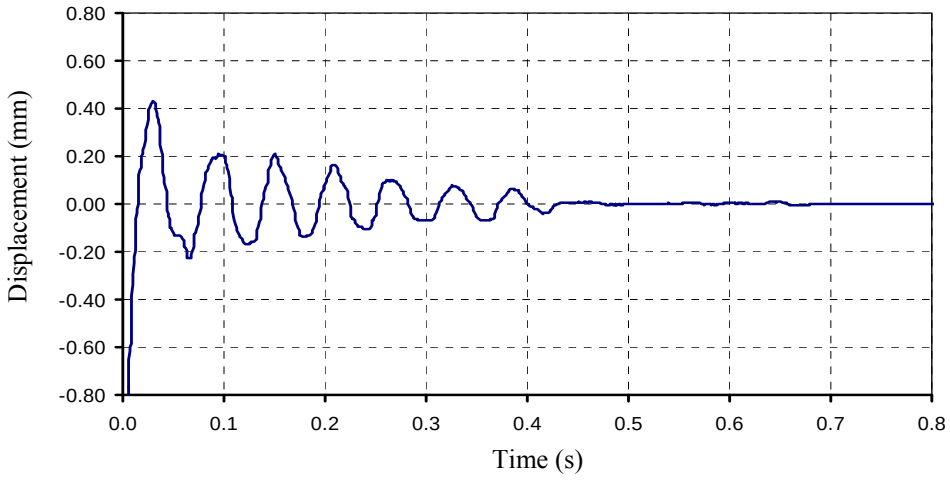

Figure C.18 Horizontal displacement of corner-supported Truss A with AR = 1.5 during horizontal snap test

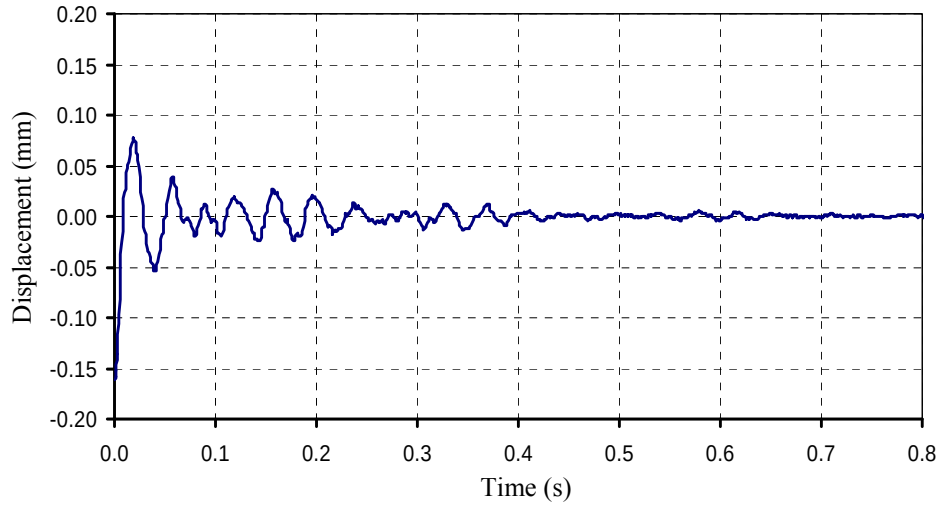

Figure C.19 Horizontal displacement of corner-supported Truss B with AR = 1.5 during the horizontal snap test

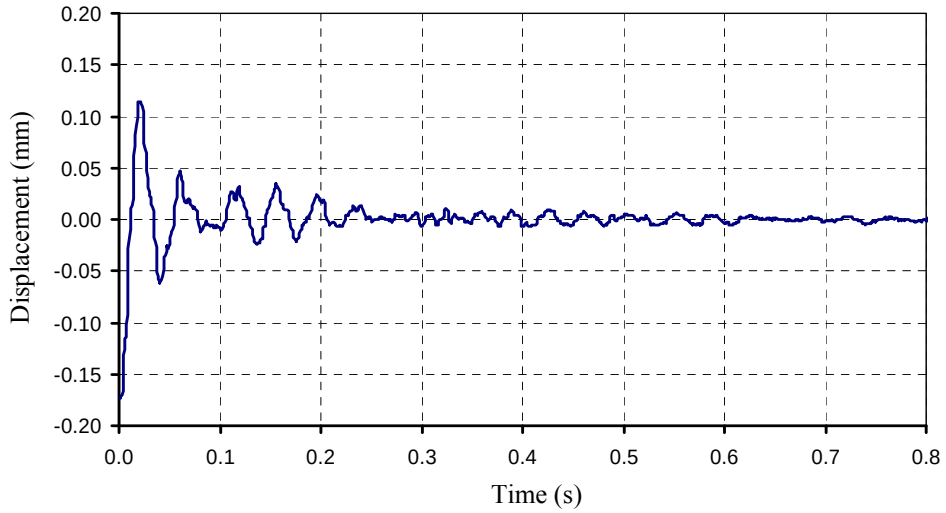

Figure C.20 Horizontal displacement of corner-supported Truss C with AR = 1.5 during the horizontal snap test

Table C.9 presents the maximum and minimum displacement responses of the test models subjected to shaking table vibrations, while Figure C. 21 shows the behaviour during the test.

Table C.10 Maximum and minimum responses for space frame models

	Truss A	**Truss B**	**Truss C**
Max. displacement	+0.577	+0.233	+0.265
Min. displacement	-0.443	-0.214	-0.223

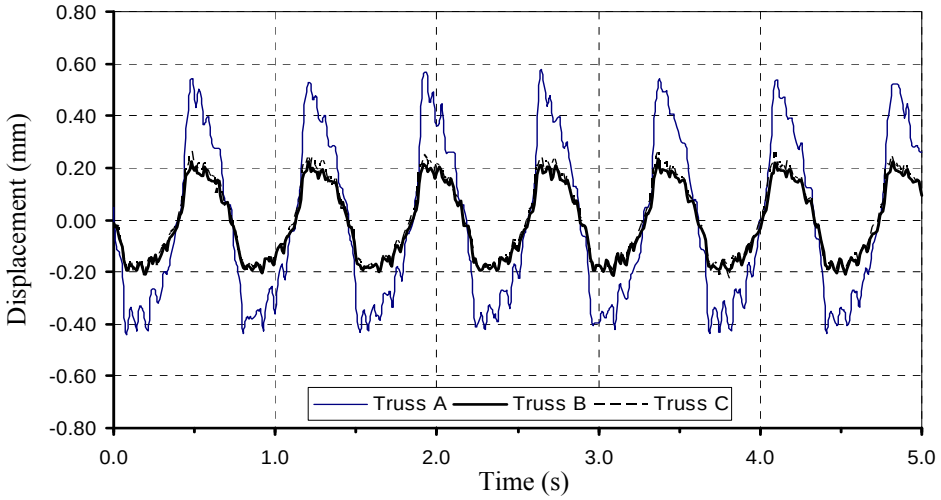

Figure C.21 Lateral displacements of corner-supported models with AR = 1.5 under the shaking table vibrations

5.5.2. Results of two-edge-supported models with aspect ratio of 1.5

The vibration frequencies and damping ratios of test models are presented in Table C.10. Furthermore, Figures C.22, C.23 and C.24 present vertical displacements during the vertical snap tests

Table C.11 Results of the vertical snap tests on edge-supported models with AR=1.5

	Truss A		**Truss B**		**Truss C**	
	Freq. (f) Hz	Damping ratio (ζ)	Freq. (f) Hz	Damping ratio (ζ)	Freq. (f) Hz	Damping ratio (ζ)
Test 1	26.14379	6.34%	27.93296	1.79%	28.57143	2.41%
Test 2	25.80645	6.51%	27.93296	1.71%	28.36879	2.51%
Test 3	26.49007	6.68%	27.93296	1.76%	28.36879	2.60%
Average	26.14677	6.51%	27.93296	1.75%	28.43634	2.51%

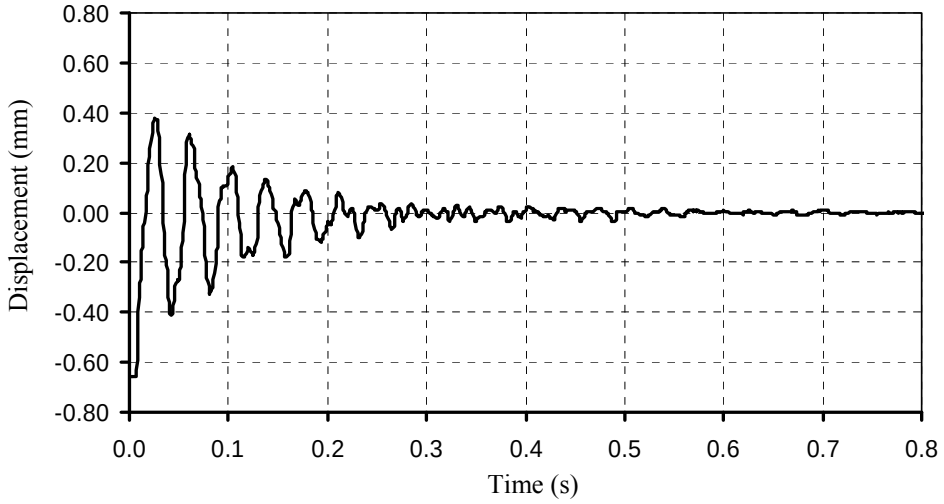

Figure C.22 Vertical displacement of two-edge-supported Truss A with AR = 1.5 during the vertical snap test

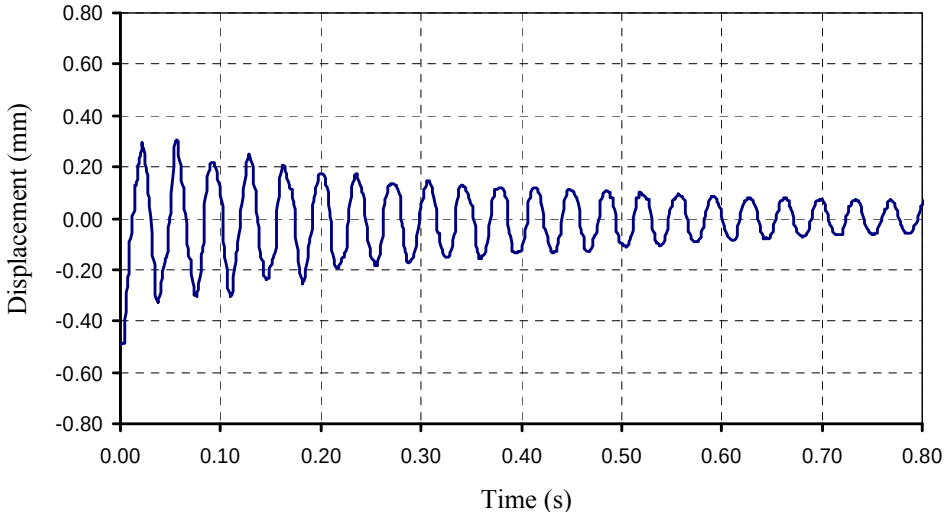

Figure C.23 Vertical displacement of two-edge-supported Truss B with AR = 1.5 during the vertical snap test

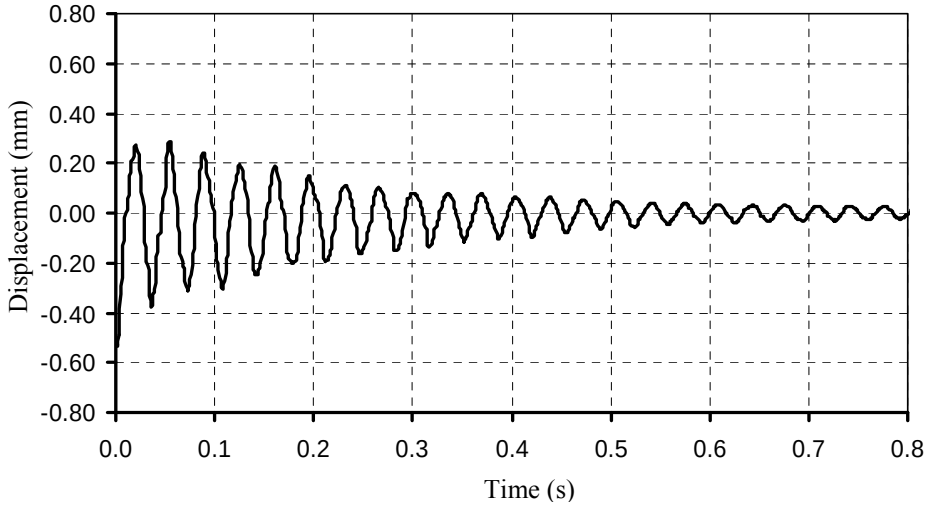

Figure C.24 Vertical displacement of Truss C with AR = 1.5 during the vertical snap test

Results of horizontal snap tests on the edge-supported models with AR = 1.50 to determine the dynamic properties of the structure in the horizontal X-direction are shown in Table c.11. Figures C.25, C.26 and C.27 show the horizontal displacements of Trusses A, B and C during the horizontal snap test.

Table C.12 Results of the horizontal snap tests on edge-supported models with AR=1.5

	Truss A		**Truss B**		**Truss C**	
	Freq. (f) Hz	Damping ratio (ζ)	Freq. (f) Hz	Damping ratio (ζ)	Freq. (f) Hz	Damping ratio (ζ)
Test 1	16.13	16.17 %	26.32	2.63 %	26.10	3.92%
Test 2	16.58	7.00 %	25.00	1.82 %	23.80	5.16%
Test 3	15.87	15.32 %	25.64	1.94 %	23.15	5.05%
Average	16.19	12.83%	25.65	2.13%	24.35	4.71%

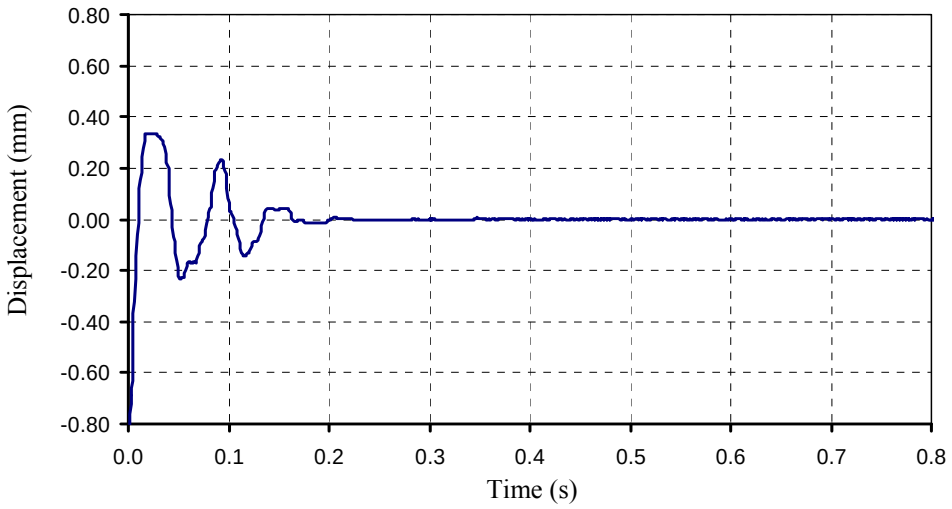

Figure C.25 Horizontal displacement of the two-edge-supported Truss A with AR=1.5 during the horizontal snap test

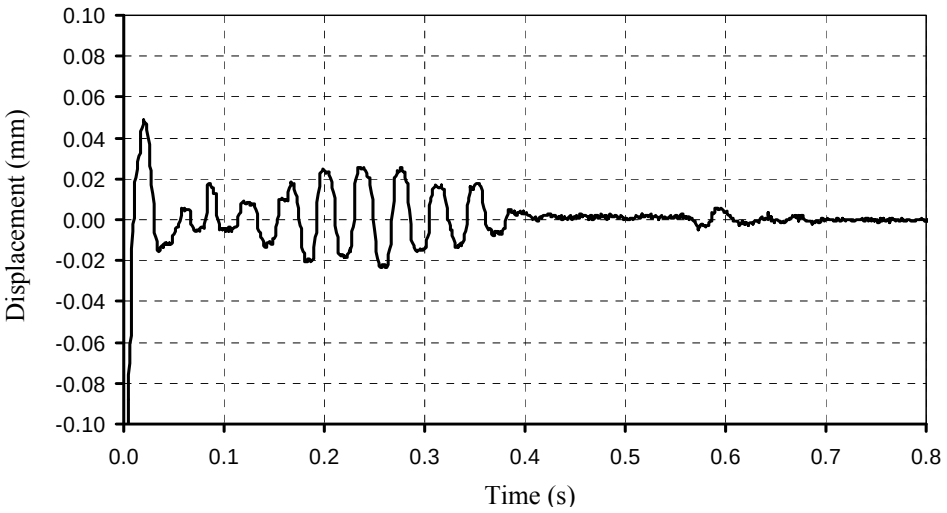

Figure C.26 Horizontal displacement of the two-edge-supported Truss B with AR = 1.5 during the horizontal snap test

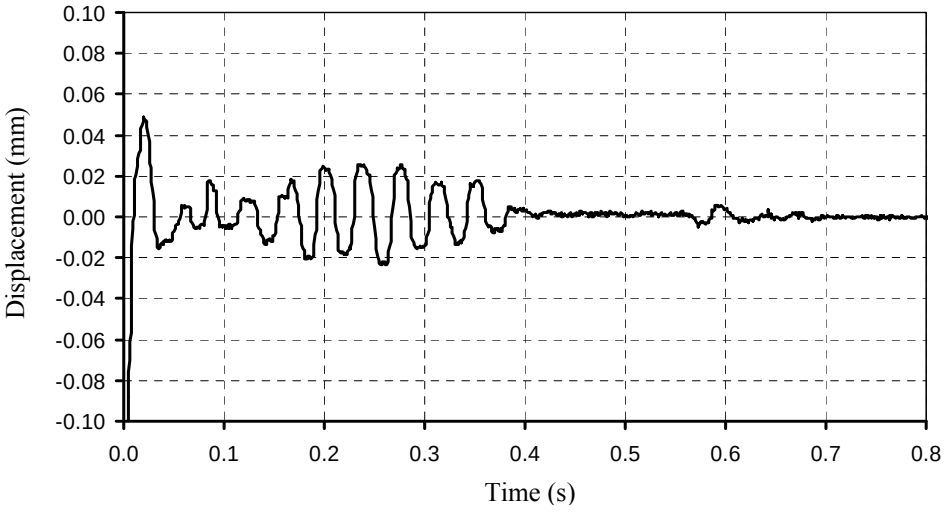

Figure C.27 Horizontal displacement of the two-edge-supported Truss C with AR = 1.5 during the horizontal snap test

The displacement response behaviour of Trusses A, B and C subjected to shaking table vibrations are shown in FigureC.28, while Table C.12 presents the maximum and minimum displacements of the test models.

Table C.13 Maximum and minimum responses for space frame models

	Truss A	**Truss B**	**Truss C**
Max. displacement (mm)	0.581	+0.210	0.243
Min. displacement (mm)	-0.440	-0.191	-0.193

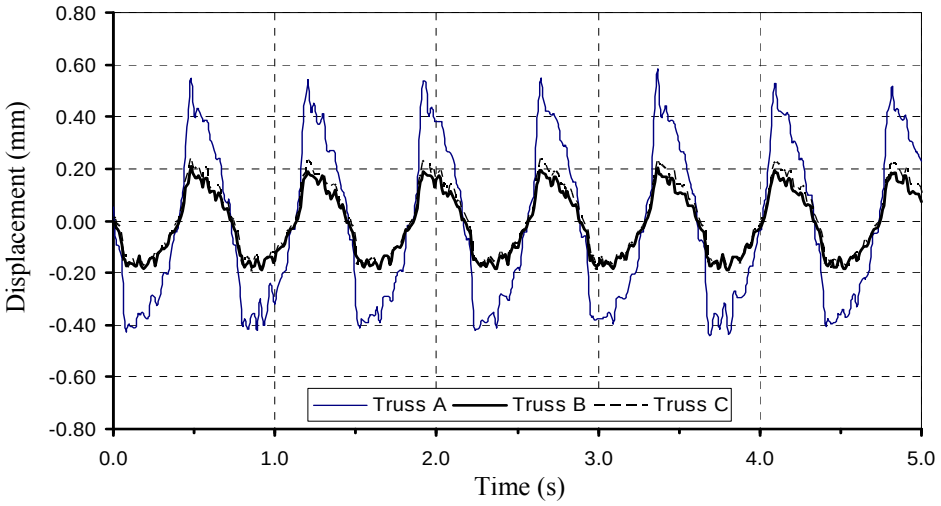

Figure C.28 Lateral displacement of the two-edge- models with AR = 1.5 under shaking table vibrations

C. 5 Results of experimental tests on models with aspect ratio of 3.0

By the removal of 4 panels in the X-direction and keeping the number of panels as 6, the aspect ratio of models was changed to be 3.0. Results of tests carried out on all models are presented in the following sections.

C.5.1 Results of corner-supported models

The summary of the vertical snap test results conducted on Trusses A, B and C is shown in Table C.13. Figures C.29, C.30 and C.31 show the displacement behaviour of test Trusses A, B and C, respectively, during the vertical snap tests.

Table C.14 Results of the vertical snap tests on corner-supported models with AR=3.0

	Truss A		**Truss B**		**Truss C**	
	Freq. (f) Hz	Damping ratio (ζ)	Freq. (f) Hz	Damping ratio (ζ)	Freq. (f) Hz	Damping ratio (ζ)
Test 1	22.90	6.40%	25.32	6.58%	26.04	6.02%
Test 2	22.52	6.55%	25.38	5.60%	26.18	6.46%
Test 3	22.94	6.02%	25.38	4.57%	26.46	6.29%
Average	**22.79**	**6.32%**	**25.36**	**5.58%**	**26.22**	**6.26%**

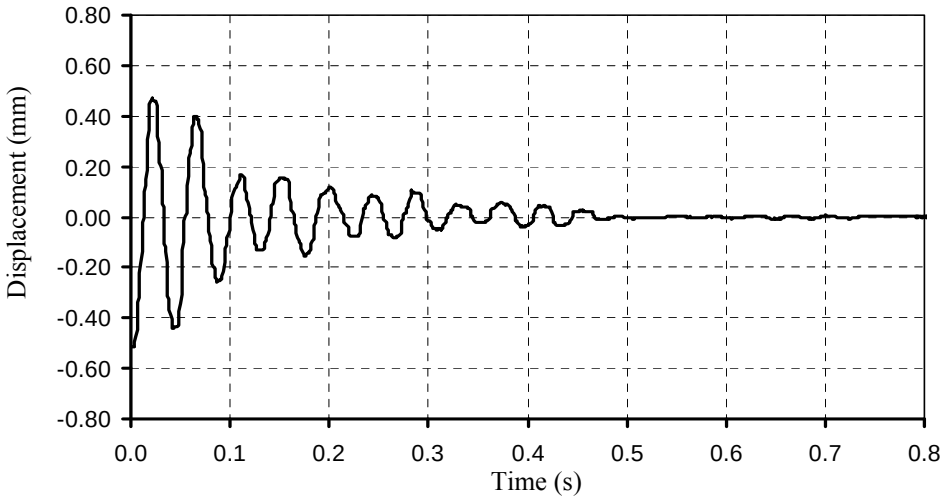

Figure C.29 Vertical displacement of the corner-supported Truss A with AR = 3.0 during the vertical snap test

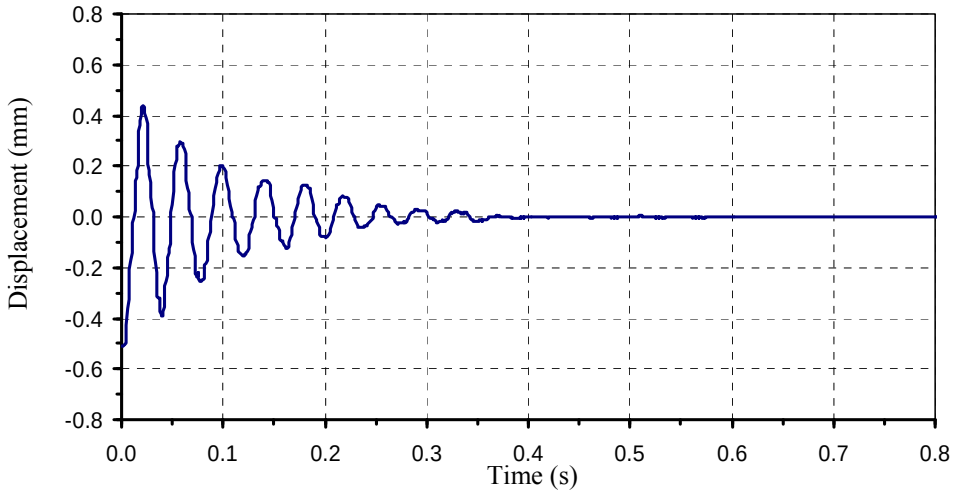

Figure C.30 Vertical displacement of the corner-supported Truss B with AR = 3.0 during the vertical snap test

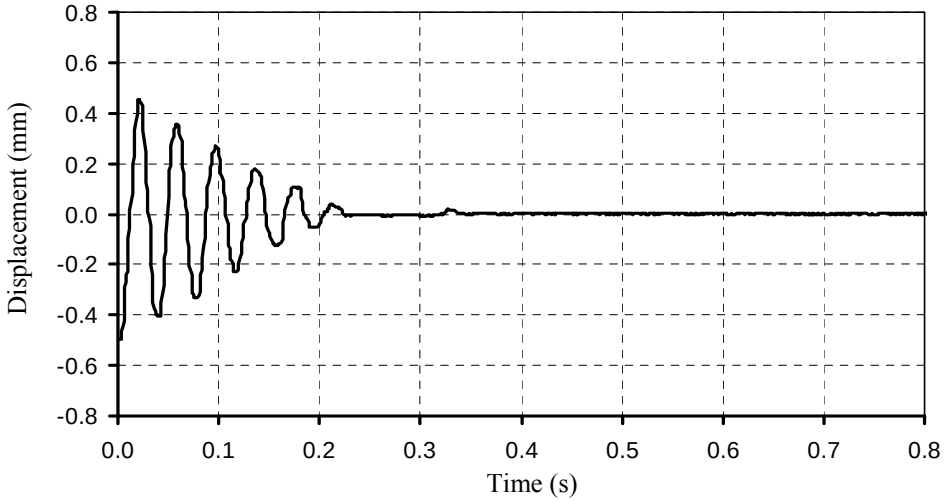

Figure C.31 Vertical displacement of the corner-supported Truss C with AR = 3.0 during the vertical snap test

To determine the horizontal frequencies and damping ratios of models, horizontal snap tests were carried out. Table C.14 presents the results of these tests, while Figures C.32, C.33 and C34 show the displacement behaviour of test models during the tests.

Table C.15 Results of the horizontal snap tests on corner-supported models with AR=3.0

	Truss A		**Truss B**		**Truss C**	
	Freq. (f) Hz	Damping ratio (ζ)	Freq. (f) Hz	Damping ratio (ζ)	Freq. (f) Hz	Damping ratio (ζ)
Test 1	14.25	6.09 %	22.14	1.783 %	21.90	1.43 %
Test 2	14.22	5.06 %	22.39	1.603 %	21.37	1.79 %
Test 3	13.89	5.62 %	26.67	1.200 %	23.62	1.22 %
Average	**14.12**	**5.59%**	**23.73**	**1.53%**	**22.30**	**1.48%**

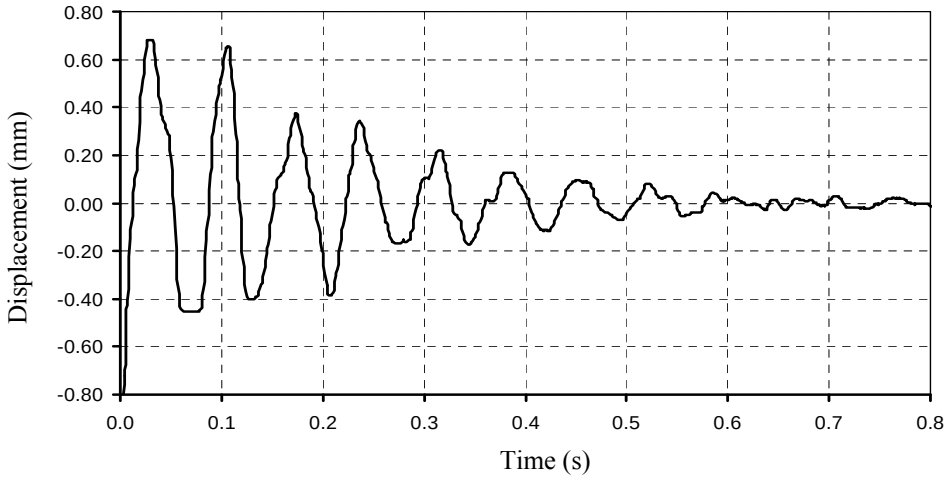

Figure C.32 Horizontal displacement of the corner-supported Truss A with AR = 3.0 during the horizontal snap test

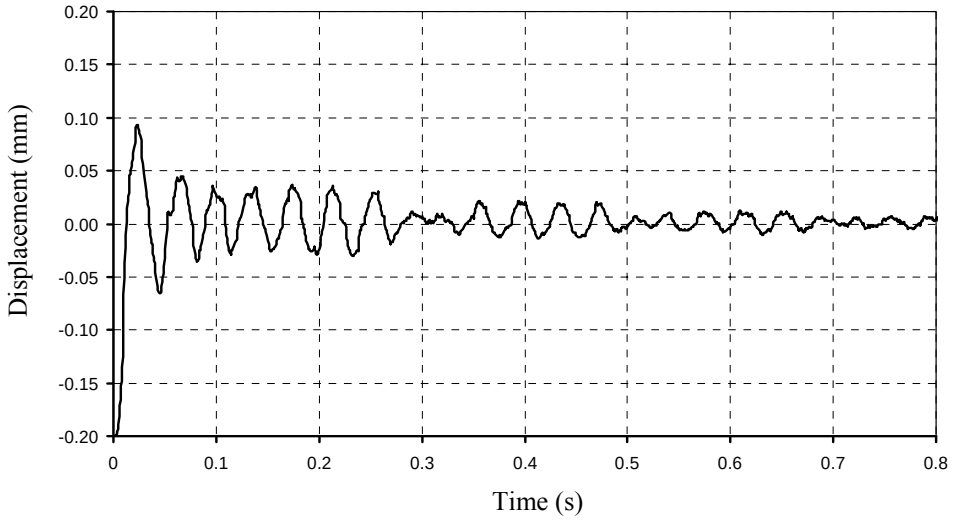

Figure C.33 Horizontal displacement of the corner-supported Truss B with AR = 3.0 during the horizontal snap test

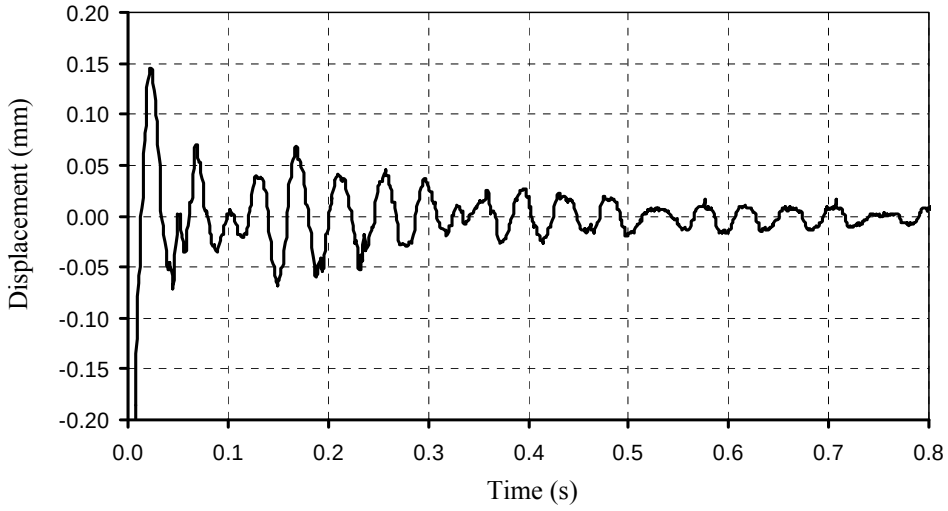

Figure C.34 Horizontal displacement of the corner-supported Truss C with AR = 3.0 during the horizontal snap test

Shaking table tests were conducted on the three Trusses A, B and C, and the maximum and minimum displacements are shown in Table. C.15. The displacement response behaviour of models can be seen in Figure C.35.

Table C.16 Maximum and minimum responses for space frame models

	Truss A	**Truss B**	**Truss C**
Max. response (mm)	+0.820	+0.261	+0.298
Min. response (mm)	-0.672	-0.234	-0.242

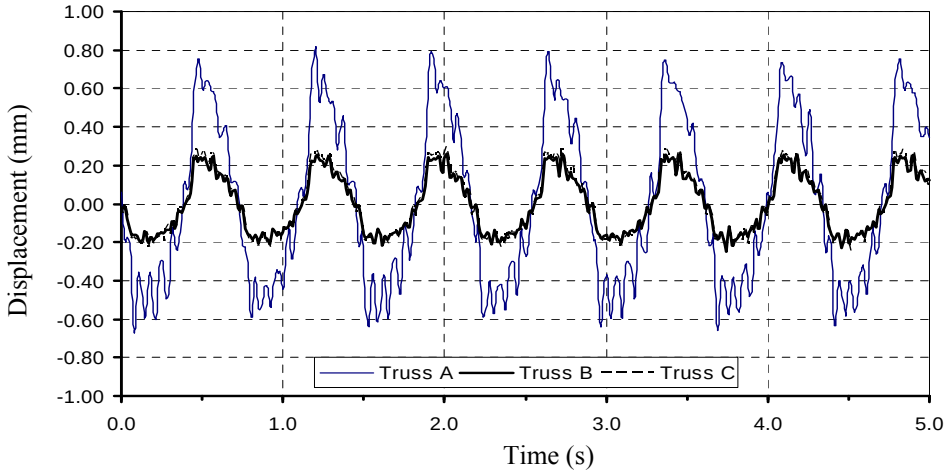

Figure C.35 Lateral displacements of corner-supported models during shaking table test

C.5.2 Results for two-edge supported space frame models with AR=3.0.

Table C.16 presents the results of the vertical snap tests conducted on the two-edge supported models. However, Figures C.36 to C.37 present the displacement behaviour of Trusses A, B and C, respectively.

Table C.17 Results of the vertical snap tests on edge-supported models with AR=3.0

	Truss A		**Truss B**		**Truss C**	
	Freq. (f) Hz	Damping ratio (ζ)	Freq. (f) Hz	Damping ratio (ζ)	Freq. (f) Hz	Damping ratio (ζ)
Test 1	23.39	7.37%	26.74	6.99%	25.81	4.28%
Test 2	23.53	5.81%	26.46	7.01%	26.88	4.22%
Test 3	22.47	5.23%	27.03	7.45%	25.97	4.29%
Average	**23.13**	**6.14%**	**26.74**	**7.15%**	**26.22**	**4.26%**

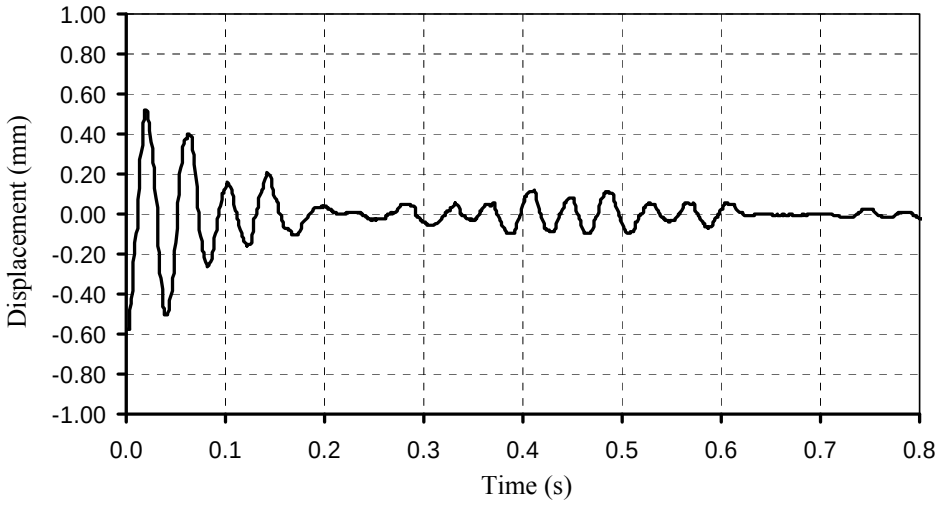

Figure C.36 Vertical displacement of two-edge supported Truss A with AR = 3.0 during the vertical snap test

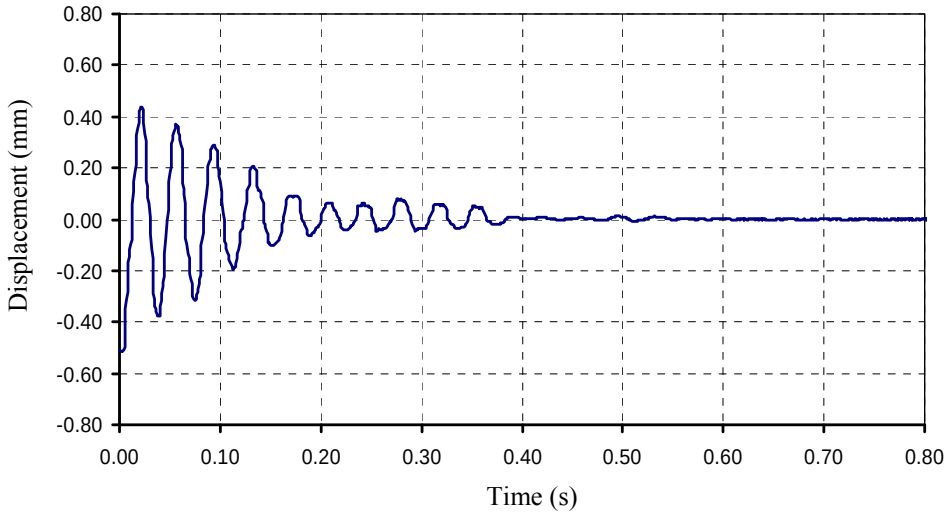

Figure C.37 Vertical displacement of two-edge supported Truss B with AR = 3.0 during the vertical snap test

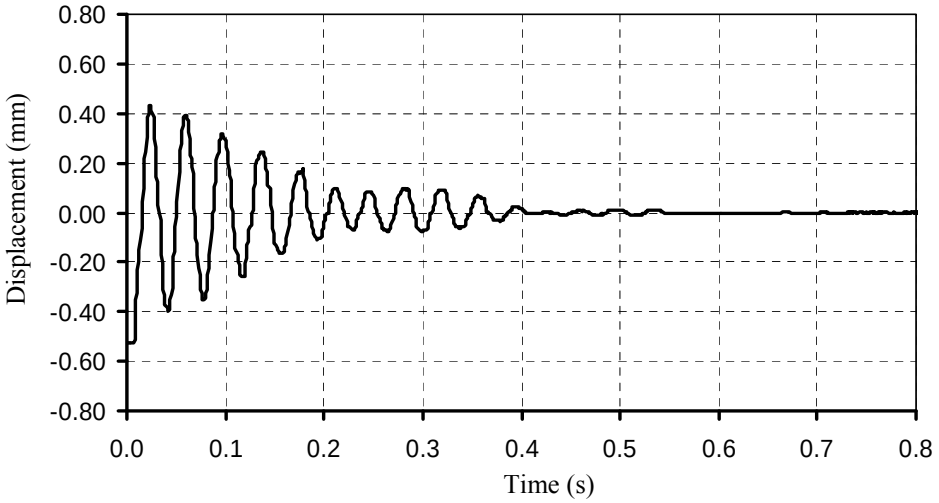

Figure C.38 Vertical displacement of two-edge supported Truss C with AR = 3.0 during the vertical snap test

5.7.2.2. Horizontal snap test results for edge-supported space frame models.

In the following Table C.17, results of the horizontal snap tests on Trusses A, B and C are presented. The displacement behaviour of the models during the tests is shown in Figures C .39 to C41.

Table C.18 Results of the horizontal snap tests on edge-supported models with AR=3.0

	Truss A		**Truss B**		**Truss C**	
	Freq. (f) Hz	Damping ratio (ζ)	Freq. (f) Hz	Damping ratio (ζ)	Freq. (f) Hz	Damping ratio (ζ)
Test 1	14.29	2.976 %	25.00	1.55 %	23.67	1.72%
Test 2	14.29	2.934 %	27.40	1.51 %	22.14	1.53%
Test 3	14.21	2.889 %	26.67	1.53 %	22.03	1.43%
Average	14.26	2.93%	26.36	1.53%	22.61	1.56%

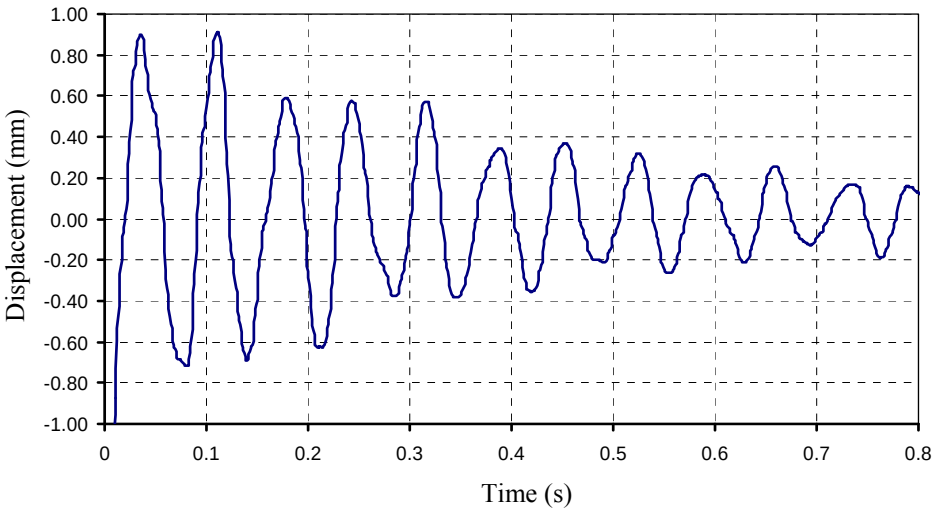

Figure C.39 Horizontal displacement of two-edge supported Truss A with AR = 3.0 during horizontal snap test

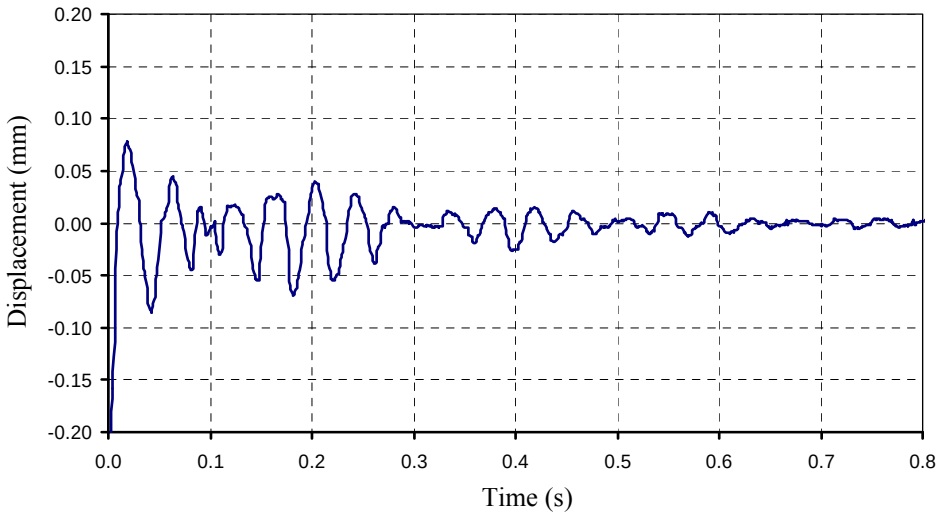

Figure C.40 Horizontal displacement of two-edge supported Truss B with AR = 3.0 during horizontal snap test

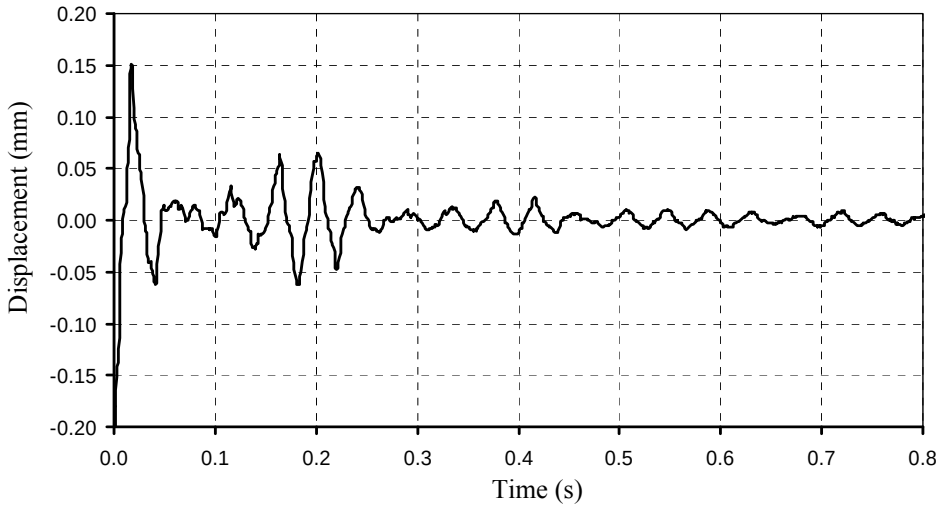

Figure C.41 Horizontal displacement of two-edge supported Truss C with AR = 3.0 during horizontal snap test

The displacement results of space frame models subjected to the shaking table time history are listed in Table C.18. The lateral response behaviour of models during the test is shown in Figure C.42

Table C.19 Maximum and minimum responses for space frame models

	Truss A	**Truss B**	**Truss C**
Max. response (mm)	0.647	+0.232	0.280
Min. response (mm)	-0.498	-0.224	-0.262

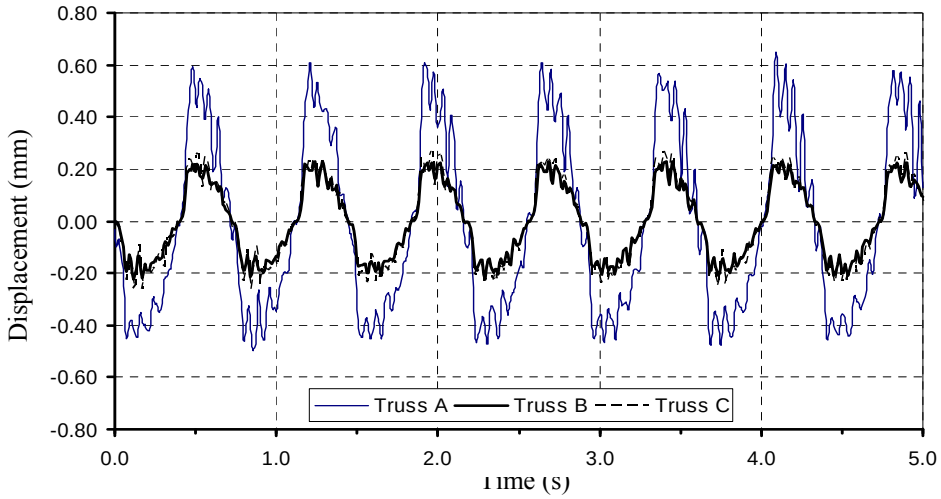

Figure C.42 Critical response for corner supported frame model Truss A

APPENDIX D

FREQUENCIES AND MASS PARTICIPATION FACTORS FOR FE VERIFICATION STUDY

D.1 Introduction

In the following tables D.1 to D.4, frequencies and mass participation factors for proposed finite element models are presented. These results are used in the selection process of a repetitive finite element model which was used later in expanding the study to include more parameters.

Table D. 1 .Summary of modal analysis results for proposed corner supported finite element models with aspect ratio of 1.0

Model 1

Mode	Truss A				Truss B				Truss C			
	Freq.	Mass participation factor			Freq.	Mass participation factor			Freq.	Mass participation factor		
	(f)Hz	x-comp	y-comp	z-comp	(f)Hz	x-comp	y-comp	z-comp	(f)Hz	x-comp	y-comp	z-comp
1	16.955	2.79E-15	6.55E-03	1.29E+00	18.705	-3.43E-15	6.09E-05	1.3156	16.946	1.52E-15	6.48E-05	1.3235
2	19.018	-1.01E+00	-1.20E-11	1.42E-13	24.782	-0.2067	5.17E-10	1.27E-12	22.759	0.16425	5.92E-10	2.24E-12
3	19.018	1.21E-11	-1.02E+00	1.15E-02	24.782	-5.17E-10	-0.20687	-5.28E-04	22.759	5.93E-10	-0.1644	-6.33E-04
4	24.26	-1.01E+00	-3.47E-11	-4.02E-14	31.559	1.0073	-5.68E-09	4.21E-13	28.844	1.031	1.34E-09	-8.33E-14
5	24.26	-3.47E-11	1.01E+00	1.07E-03	31.559	5.68E-09	1.0073	-7.44E-05	28.844	-1.34E-09	1.031	-6.49E-05

Model 2

Mode	Truss A				Truss B				Truss C			
	Freq.	Mass participation factor			Freq.	Mass participation factor			Freq.	Mass participation factor		
	(f)Hz	x-comp	y-comp	z-comp	(f)Hz	x-comp	y-comp	z-comp	(f)Hz	x-comp	y-comp	z-comp
1	16.966	1.50E-10	1.08E-02	1.295	18.719	2.50E-12	1.33E-03	1.3161	16.958	2.29E-12	1.28E-03	1.3239
2	19.08	-1.0169	-5.09E-07	9.25E-09	24.816	0.20775	5.04E-08	-4.66E-10	22.79	0.16537	4.12E-08	-3.90E-10
3	19.08	5.12E-07	-1.0235	1.80E-02	24.817	5.03E-08	-0.20827	1.69E-03	22.79	4.10E-08	-0.1658	1.36E-03
4	24.302	1.0082	-2.40E-06	-2.13E-09	31.589	1.13E-07	1.0079	-7.02E-04	28.87	1.16E-07	1.0316	-6.95E-04
5	24.302	2.40E-06	1.0084	9.30E-04	31.592	1.0079	-1.13E-07	8.02E-11	28.872	1.0316	-1.16E-07	7.91E-11

Model 3

Mode	Truss A				Truss B				Truss C			
	Freq.	Mass participation factor			Freq.	Mass participation factor			Freq.	Mass participation factor		
	(f)Hz	x-comp	y-comp	z-comp	(f)Hz	x-comp	y-comp	z-comp	(f)Hz	x-comp	y-comp	z-comp
1	17.687	3.73E-08	-2.99E-09	1.271	19.176	-5.46E-09	-8.26E-09	1.2869	18.955	-5.26E-09	-7.95E-09	1.2895
2	19.98	-0.45243	-0.76526	8.12E-08	25.433	0.16812	7.30E-02	1.56E-08	25.094	-9.39E-02	9.22E-02	3.79E-08
3	19.98	-0.76526	0.45243	9.18E-08	25.433	-7.30E-02	0.16812	5.99E-08	25.094	-9.22E-02	-9.39E-02	-2.8E-08
4	26.578	0.49531	0.73086	3.04E-08	33.703	0.224	0.99036	3.49E-09	33.313	1.0631	-3.47E-02	3.17E-09
5	26.578	-0.73086	0.49531	-1.49E-08	33.703	0.99036	-0.224	2.60E-09	33.313	3.47E-02	1.0631	3.12E-09

Model 4

Mode	Truss A				Truss B				Truss C			
	Freq.	Mass participation factor			Freq.	Mass participation factor			Freq.	Mass participation factor		
	(f)Hz	x-comp	y-comp	z-comp	(f)Hz	x-comp	y-comp	z-comp	(f)Hz	x-comp	y-comp	z-comp
1	14.779	-1.15E-08	-1.15E-08	1.2672	17.093	-6.85E-09	-6.85E-09	1.305	17.003	-6.61E-09	-6.6E-09	1.3064
2	17.465	0.35335	0.76107	3.26E-08	22.867	0.10925	-7.54E-02	5.05E-09	22.688	-1.45E-02	0.15007	2.03E-08
3	17.465	0.76107	-0.35335	1.19E-08	22.867	7.54E-02	0.10925	2.76E-08	22.688	0.15007	1.45E-02	2.47E-08
4	23.272	1.0632	0.14951	2.13E-09	30.236	-4.70E-02	1.0278	3.09E-09	29.979	0.40926	0.85309	3.83E-09
5	23.272	-0.14951	1.0632	1.60E-09	30.236	1.0278	4.70E-02	3.38E-09	29.979	0.85309	-0.40926	1.35E-09

Model 5

Mode	Truss A				Truss B				Truss C			
	Freq.	Mass participation factor			Freq.	Mass participation factor			Freq.	Mass participation factor		
	(f)Hz	x-comp	y-comp	z-comp	(f)Hz	x-comp	y-comp	z-comp	(f)Hz	x-comp	y-comp	z-comp
1	16.609	-8.55E-09	8.55E-09	1.2708	18.605	4.79E-10	-4.79E-10	1.2917	18.418	4.45E-10	-4.5E-10	1.2942
2	19.146	-0.18178	-0.97044	2.86E-08	24.723	3.78E-02	0.18428	6.17E-09	24.422	-0.17346	1.42E-03	7.91E-09
3	19.146	0.97044	-0.18178	4.18E-08	24.723	-0.18428	3.78E-02	9.36E-09	24.422	1.42E-03	0.17346	7.78E-09
4	25.406	0.82722	0.43304	-2.69E-09	32.732	1.30E-02	1.0388	8.95E-11	32.379	0.8409	0.43128	-3.50E-11
5	25.406	-0.43304	0.82722	8.60E-09	32.732	1.0388	-1.30E-02	-9.17E-11	32.379	-0.43128	0.8409	1.09E-10

Model 6

Mode	Truss A				Truss B				Truss C			
	Freq.	Mass participation factor			Freq.	Mass participation factor			Freq.	Mass participation factor		
	(f)Hz	x-comp	y-comp	z-comp	(f)Hz	x-comp	y-comp	z-comp	(f)Hz	x-comp	y-comp	z-comp
1	15.418	6.48E-09	-6.48E-09	1.2733	17.767	8.28E-10	-8.29E-10	1.2927	17.62	7.74E-10	-7.7E-10	1.2953
2	17.948	0.4248	0.7238	7.49E-09	23.71	-8.44E-02	-0.16802	-4.47E-09	23.46	-9.82E-02	0.10184	1.16E-08
3	17.948	-0.7238	0.4248	2.88E-08	23.71	-0.16802	8.44E-02	1.35E-08	23.46	0.10184	9.82E-02	-2.11E-10
4	24.594	-0.49922	0.80714	-2.68E-09	31.229	0.48584	0.86016	7.16E-11	30.924	0.205	1.0458	1.43E-10
5	24.594	0.80714	0.49922	6.32E-10	31.229	0.86016	-0.48584	-2.57E-10	30.924	1.0458	-0.205	-2.13E-10

Model 7

Mode	Truss A				Truss B				Truss C			
	Freq.	Mass participation factor			Freq.	Mass participation factor			Freq.	Mass participation factor		
	(f)Hz	x-comp	y-comp	z-comp	(f)Hz	x-comp	y-comp	z-comp	(f)Hz	x-comp	y-comp	z-comp
1	16.381	8.94E-09	-8.94E-09	1.2743	18.118	8.60E-10	-8.60E-10	1.2919	17.947	8.06E-10	-8. 6E-10	1.2944
2	18.734	8.84E-02	0.99646	2.66E-08	24.144	-9.10E-02	-0.16158	-3.95E-09	23.871	-0.17737	5.71E-02	1.43E-08
3	18.734	-0.99646	8.84E-02	3.18E-08	24.144	-0.16158	9.10E-02	1.41E-08	23.871	5.71E-02	0.17737	7.31E-09
4	25.547	1.08E-02	1.0302	-3.19E-09	31.819	1.0388	-0.13582	-2.21E-10	31.495	1.0688	4.47E-02	-1.71E-10
5	25.547	-1.0302	1.08E-02	-3.26E-09	31.819	0.13582	1.0388	1.70E-10	31.495	-4.47E-02	1.0688	1.86E-10

Model 8

Mode	Truss A				Truss B				Truss C			
	Freq.	Mass participation factor			Freq.	Mass participation factor			Freq.	Mass participation factor		
	(f)Hz	x-comp	y-comp	z-comp	(f)Hz	x-comp	y-comp	z-comp	(f)Hz	x-comp	y-comp	z-comp
1	17.014	7.23E-09	-7.28E-09	1.2746	19.967	7.62E-10	-7.68E-10	1.3425	19.731	7.11E-10	-7.5E-10	1.3418
2	19.816	-0.87774	5.10E-02	3.27E-08	27.379	-0.32976	7.74E-02	7.34E-09	26.95	-0.10237	-0.31983	-3.88E-09
3	19.816	5.10E-02	0.87774	2.93E-08	27.379	-7.74E-02	-0.32976	-4.59E-09	26.95	-0.31983	0.10237	7.74E-09
4	29.14	1.087	-7.58E-02	1.89E-09	32.461	-0.21136	0.96616	1.18E-10	32.135	0.73108	-0.52023	-4.74E-11
5	29.14	7.58E-02	1.087	-1.66E-09	32.461	0.96616	0.21136	-7.50E-11	32.135	0.52023	0.73108	1.20E-11

Model 9

Mode	Truss A				Truss B				Truss C			
	Freq. (f)Hz	Mass participation factor			Freq. (f)Hz	Mass participation factor			Freq. (f)Hz	Mass participation factor		
		x-comp	y-comp	z-comp		x-comp	y-comp	z-comp		x-comp	y-comp	z-comp
1	19.356	-5.14E-12	-2.03E-11	1.2692	20.69	-3.75E-13	-1.21E-12	1.2903	20.329	4.92E-13	-5.2E-13	1.2934
2	20.767	2.75E-06	1.0229	3.87E-11	26.992	1.66E-06	0.33149	2.12E-11	26.528	1.54E-06	0.30958	1.48E-11
3	20.935	0.97875	-2.18E-06	7.79E-12	27.725	-0.4702	2.65E-07	5.04E-13	27.157	0.40946	-2.3E-07	-1.80E-12
4	26.759	1.053	-1.34E-06	-3.50E-12	33.167	1.0378	-1.44E-08	3.01E-13	32.747	1.0369	2.49E-08	-1.90E-13
5	27.418	1.10E-06	1.1145	-1.25E-11	36.531	-6.91E-08	1.003	-7.43E-13	36.027	-1.00E-07	1.0302	-7.66E-13

Table D. 2 .Summary of modal analysis results for proposed corner supported finite element models with aspect ratio of 2.0

Model 1

Mode	Truss A				Truss B				Truss C			
	Freq.	Mass participation factor			Freq.	Mass participation factor			Freq.	Mass participation factor		
	(f)Hz	x-comp	y-comp	z-comp	(f)Hz	x-comp	y-comp	z-comp	(f)Hz	x-comp	y-comp	z-comp
1	16.82	0.89688	-8.68E-16	8.51E-16	24.495	-6.04E-13	-1.19E-04	1.3049	23.99	4.28E-14	-1.35E-04	1.3011
2	22.195	-3.77E-15	-1.35E-04	1.2456	24.786	0.56519	1.71E-14	2.82E-12	24.376	-0.49928	3.35E-15	2.58E-13
3	25.984	0.91363	9.89E-16	5.25E-15	33.492	1.1277	5.58E-14	-2.20E-14	32.7	1.1609	1.11E-14	4.88E-15
4	32.049	1.69E-03	-5.90E-16	5.97E-16	37.506	-4.55E-14	0.86273	2.45E-04	37.405	-8.1E-15	0.8709	2.65E-04
5	35.477	1.61E-15	1.3226	5.37E-04	41.159	6.61E-04	2.31E-14	1.07E-15	41.007	-7.0E-04	-3.04E-14	-5.42E-15

Model 2

Mode	Truss A				Truss B				Truss C			
	Freq.	Mass participation factor			Freq.	Mass participation factor			Freq.	Mass participation factor		
	(f)Hz	x-comp	y-comp	z-comp	(f)Hz	x-comp	y-comp	z-comp	(f)Hz	x-comp	y-comp	z-comp
1	16.526	-0.90979	-2.49E-11	1.64E-11	23.973	-8.19E-12	1.29E-03	1.3002	21.782	-5.05E-12	1.12E-03	1.2941
2	21.202	3.18E-11	7.96E-04	1.2283	24.505	0.5649	5.28E-11	2.51E-11	22.853	0.52904	5.30E-11	1.51E-11
3	25.278	-0.92338	2.90E-11	3.41E-11	32.989	1.1283	8.98E-11	6.17E-13	30.167	1.1782	7.23E-11	2.42E-13
4	31.439	1.89E-03	-6.64E-11	3.29E-11	35.843	-7.44E-11	0.86394	-3.47E-04	33.539	-5.97E-11	0.87847	-2.67E-04
5	34.274	2.72E-11	1.2906	9.15E-05	40.113	1.37E-03	-1.43E-11	2.50E-11	38.082	1.31E-03	-1.26E-11	2.32E-11

Model 3

Mode	Truss A				Truss B				Truss C			
	Freq.	Mass participation factor			Freq.	Mass participation factor			Freq.	Mass participation factor		
	(f)Hz	x-comp	y-comp	z-comp	(f)Hz	x-comp	y-comp	z-comp	(f)Hz	x-comp	y-comp	z-comp
1	13.954	-0.90651	4.49E-07	6.45E-04	20.965	-2.75E-04	2.94E-10	1.28	20.76	-2.14E-04	2.34E-10	1.2648
2	17.157	5.10E-04	2.27E-10	1.3561	22.641	-0.58643	6.22E-07	-1.50E-03	22.584	-0.51357	5.61E-07	-1.36E-03
3	21.655	1.2178	6.47E-07	-2.29E-04	27.709	1.1502	-4.46E-07	-6.81E-05	27.565	1.1694	-4.28E-07	-5.88E-05
4	25.771	1.59E-09	-3.12E-04	-3.56E-07	32.696	3.87E-07	0.94092	7.87E-11	32.769	3.44E-07	0.90542	6.94E-11
5	28.943	1.07E-08	-1.32E-02	3.29E-08	35.845	-6.01E-11	-4.12E-04	1.76E-07	36.088	7.54E-11	3.93E-04	-1.60E-07

Model 4

Mode	Truss A				Truss B				Truss C			
	Freq.	Mass participation factor			Freq.	Mass participation factor			Freq.	Mass participation factor		
	(f)Hz	x-comp	y-comp	z-comp	(f)Hz	x-comp	y-comp	z-comp	(f)Hz	x-comp	y-comp	z-comp
1	15.17	-0.92812	1.89E-07	5.38E-04	21.814	-2.54E-04	8.08E-11	1.2674	21.481	-2.04E-04	5.30E-11	1.258
2	18.666	4.64E-04	-6.20E-10	1.2706	23.573	-0.54044	3.31E-07	-1.49E-03	23.346	-0.47097	2.98E-07	-1.39E-03
3	24.231	1.1701	-5.05E-08	-1.91E-04	29.444	1.1424	-5.24E-07	-6.08E-05	29.068	1.1654	-4.67E-07	-5.33E-05
4	28.322	3.93E-09	3.68E-04	2.82E-07	32.98	4.11E-07	0.89946	4.55E-11	32.956	3.58E-07	0.89627	4.40E-11
5	31.336	4.62E-08	1.1973	1.40E-09	37.433	2.87E-10	3.03E-04	-1.10E-07	37.486	4.75E-10	3.01E-04	-1.00E-07

Model 5

Mode	Truss A				Truss B				Truss C			
	Freq.	Mass participation factor			Freq.	Mass participation factor			Freq.	Mass participation factor		
	(f)Hz	x-comp	y-comp	z-comp	(f)Hz	x-comp	y-comp	z-comp	(f)Hz	x-comp	y-comp	z-comp
1	21.116	0.93833	5.96E-08	7.67E-08	29.529	2.02E-07	9.19E-02	1.2721	28.869	1.73E-07	8.63E-02	1.2624
2	26.462	-2.2E-09	8.17E-02	1.2625	31.476	-0.76659	-5.61E-08	3.03E+00	30.956	-0.70968	-5.51E-08	2.54E-07
3	32.768	-1.0563	-3.19E-08	6.42E-08	36.598	1.087	7.72E-08	-8.66E+00	35.953	1.1253	7.34E-08	-7.84E-08
4	39.229	0.1984	-8.17E-08	1.06E-07	48.578	-6.28E-08	0.91305	-1.11E+00	48.428	-6.07E-08	0.91724	-6.20E-03
5	43.106	-0.26413	3.82E-07	-2.31E-08	51.861	0.37222	2.13E-10	3.36E+00	51.584	0.34128	1.11E-08	2.88E-08

Model 6

Mode	Truss A				Truss B				Truss C			
	Freq.	Mass participation factor			Freq.	Mass participation factor			Freq.	Mass participation factor		
	(f) z	x-comp	y-comp	z-comp	(f)Hz	x-comp	y-comp	z-comp	(f)Hz	x-comp	y-comp	z-comp
1	17.372	-0.89906	-7.89E-09	1.78E-07	25.351	1.98E-07	8.82E-02	1.2408	24.98	1.90E-07	8.49E-02	1.2281
2	20.457	-7.8E-08	9.20E-02	1.2713	27.661	-1.0063	-1.43E-07	2.74E-07	27.531	-0.99083	-1.52E-07	2.55E-07
3	26.612	1.1247	-1.01E-07	1.19E-07	30.663	1.0243	4.14E-08	-6.81E-08	30.299	1.0651	5.55E-08	-7.86E-08
4	32.42	-0.17253	1.34E-07	-2.92E-09	42.792	-8.94E-08	0.9831	-1.33E-02	42.7	-9.25E-08	0.9916	-1.02E-02
5	32.852	0.22125	1.28E-07	8.81E-09	44.698	0.42291	1.15E-07	7.48E-08	44.589	0.40418	1.00E-07	8.02E-08

Model 7

Mode	Truss A				Truss B				Truss C			
	Freq. (f) Hz	Mass participation factor			Freq. (f) Hz	Mass participation factor			Freq. (f) Hz	Mass participation factor		
		x-comp	y-comp	z-comp		x-comp	y-comp	z-comp		x-comp	y-comp	z-comp
1	15.71	0.91114	2.63E-07	6.04E-12	22.573	-3.12E-11	-1.42E-13	1.2744	22.344	-2.58E-12	-3.48E-13	1.2627
2	19.799	-9.6E-12	4.10E-13	1.2967	23.821	0.53143	3.95E-07	1.01E-10	23.72	-0.4959	-3.74E-07	5.28E-11
3	24.197	1.0969	-7.19E-08	7.85E-12	29.583	1.1449	1.90E-07	1.99E-11	29.348	1.1663	1.86E-07	1.89E-11
4	28.938	5.91E-12	6.42E-13	5.62E-07	37.158	-1.70E-07	0.91711	3.71E-14	37.133	-1.58E-07	0.9141	-5.17E-13
5	32.879	-1.3E-07	-1.3377	-9.57E-14	39.116	3.60E-13	1.64E-10	1.14E-07	39.223	-3.74E-13	-1.26E-10	-1.09E-07

Model 8

Mode	Truss A				Truss B				Truss C			
	Freq.	Mass participation factor			Freq.	Mass participation factor			Freq.	Mass participation factor		
	(f)Hz	x-comp	y-comp	z-comp	(f)Hz	x-comp	y-comp	z-comp	(f)Hz	x-comp	y-comp	z-comp
1	16.105	0.93364	4.11E-08	2.37E-09	23.648	7.18E-09	-5.04E-11	1.2802	23.334	5.61E-09	-4.67E-11	1.2694
2	21.323	-3.5E-09	-1.03E-10	1.2656	24.38	-0.73853	-1.12E-07	2.39E-08	24.218	-0.69693	-1.09E-07	2.03E-08
3	26.792	1.0663	-5.55E-08	1.70E-09	30.162	1.1027	2.19E-08	2.66E-10	29.86	1.1321	3.01E-08	2.80E-10
4	29.502	-7.7E-10	-3.01E-10	-1.76E-08	36.682	-3.24E-08	1.0279	8.96E-12	36.657	-3.56E-08	1.0261	4.31E-12
5	33.131	2.02E-08	1.3019	-1.19E-11	38.519	1.96E-09	6.89E-09	3.46E-08	38.637	1.89E-09	6.05E-09	3.56E-08

Model 9

Mode	Truss A				Truss B				Truss C			
	Freq.	Mass participation factor			Freq.	Mass participation factor			Freq.	Mass participation factor		
	(f)Hz	x-comp	y-comp	z-comp	(f)Hz	x-comp	y-comp	z-comp	(f)Hz	x-comp	y-comp	z-comp
1	18.853	0.91352	5.98E-09	-1.47E-12	27.662	2.43E-10	-5.23E-09	1.3018	27.011	-2.00E-11	-4.97E-09	1.296
2	25.504	-4.8E-12	-2.97E-09	1.2103	27.688	-0.79995	-8.27E-09	6.93E-10	27.228	-0.7483	-6.45E-09	-5.16E-11
3	28.604	1.0804	-1.89E-06	1.23E-11	35.299	1.0959	2.29E-08	2.81E-12	34.575	1.1382	1.91E-08	2.27E-12
4	28.655	1.61E-06	1.6178	-8.63E-09	43.306	-2.21E-08	0.97529	1.59E-09	43.129	-1.89E-08	0.99203	1.22E-09
5	29.745	1.53E-08	2.21E-12	-3.97E-08	44.581	1.26E-08	-1.97E-12	-8.07E-09	44.411	1.14E-08	1.01E-11	-5.69E-09

Table D. 3 .Summary of modal analysis results for proposed edge supported finite element models with aspect ratio of 1.0

Model 1

Mode	Truss A				Truss B				Truss C			
	Freq.	Mass participation factor			Freq.	Mass participation factor			Freq.	Mass participation factor		
	(f)Hz	x-comp	y-comp	z-comp	(f)Hz	x-comp	y-comp	z-comp	(f)Hz	x-comp	y-comp	z-comp
1	20.092	-0.98596	-4.50E-16	1.12E-15	27.471	-0.26402	-1.04E-14	6.13E-13	26.749	0.21586	3.97E-15	4.89E-14
2	25.6	3.35E-14	-1.75E-04	1.3923	30	9.83E-14	-8.89E-05	1.5237	29.048	-6.9E-15	-1.07E-04	1.5138
3	26.255	-0.94393	-1.74E-16	4.78E-14	41.411	1.0717	-6.16E-15	-2.16E-14	40.502	1.1048	-2.09E-15	1.88E-15
4	37.784	6.78E-04	3.77E-16	-4.29E-15	45.117	2.80E-14	1.14E-05	0.26395	44.523	-1.7E-14	2.25E-05	0.26306
5	38.499	2.02E-15	3.34E-05	0.16746	47.483	1.01E-03	-6.93E-14	-9.78E-15	47.16	-9.5E-04	-4.58E-14	-1.07E-14

Model 2

Mode	Truss A				Truss B				Truss C			
	Freq.	Mass participation factor			Freq.	Mass participation factor			Freq.	Mass participation factor		
	(f)Hz	x-comp	y-comp	z-comp	(f)Hz	x-comp	y-comp	z-comp	(f)Hz	x-comp	y-comp	z-comp
1	20.163	-0.98893	-7.61E-13	4.53E-12	27.509	-0.2651	5.83E-13	4.74E-11	25.158	-0.22889	5.48E-13	5.71E-11
2	25.617	3.58E-11	7.91E-05	1.3922	30.024	6.16E-12	3.11E-04	1.5236	26.966	5.62E-12	2.48E-04	1.4947
3	26.307	-0.94648	-1.40E-12	4.75E-11	41.464	1.0725	2.63E-12	-1.00E-12	37.488	1.1057	2.55E-12	-6.92E-13
4	37.95	-7.3E-04	-2.70E-12	-5.12E-12	45.176	4.53E-12	4.68E-04	0.26294	41.774	-2.31E-12	-3.62E-04	-0.22455
5	38.561	4.20E-13	-5.74E-05	0.16663	47.561	1.86E-03	-4.72E-12	6.22E-13	44.66	1.54E-03	-1.34E-12	1.23E-12

Model 3

Mode	Truss A				Truss B				Truss C			
	Freq.	Mass participation factor			Freq.	Mass participation factor			Freq.	Mass participation factor		
	(f)Hz	x-comp	y-comp	z-comp	(f)Hz	x-comp	y-comp	z-comp	(f)Hz	x-comp	y-comp	z-comp
1	21.258	1.0415	-3.53E-08	3.10E-09	27.532	-0.19362	3.75E-08	7.91E-08	27.051	-0.17329	3.48E-08	8.21E-08
2	26.655	-7.9E-09	-7.32E-09	1.3828	29.563	9.09E-09	-7.71E-09	1.4132	28.903	8.23E-09	-7.17E-09	1.4104
3	28.138	1.0367	-1.53E-08	6.44E-09	39.023	1.0563	-4.64E-08	-1.26E-09	38.401	1.0871	-4.51E-08	-1.06E-09
4	39.263	4.07E-09	3.19E-09	8.00E-08	49.144	5.38E-10	-6.83E-09	0.16773	48.516	6.87E-11	-6.22E-09	0.17074
5	44.033	3.61E-10	-2.52E-09	0.14845	49.942	1.49E-08	3.99E-08	1.85E-08	49.68	1.38E-08	4.00E-08	2.19E-08

Model 4

Mode	Truss A				Truss B				Truss C			
	Freq.	Mass participation factor			Freq.	Mass participation factor			Freq.	Mass participation factor		
	(*f*)Hz	x-comp	y-comp	z-comp	(*f*)Hz	x-comp	y-comp	z-comp	(*f*)Hz	x-comp	y-comp	z-comp
1	18.673	0.99176	-1.48E-07	-2.04E-09	23617	-0.17669	1.47E-07	7.24E-08	24.184	-0.16785	1.40E-07	7.63E-08
2	22.515	7.26E-09	-9.72E-09	1.4042	26247	7.68E-09	-7.97E-09	1.383	25.398	7.52E-09	-7.47E-09	1.3784
3	24.345	1.0195	-5.32E-08	-5.20E-09	44125	1.0479	-1.23E-07	-9.27E-10	33.082	1.0717	-1.23E-07	-8.49E-10
4	34.061	3.07E-09	1.28E-09	3.33E-07	78079	-6.59E-12	-8.09E-09	0.1395	44.046	-1.84E-10	-7.25E-09	0.14227
5	38.859	3.14E-09	-3.53E-09	0.15922	78094	1.00E-08	3.69E-08	-2.16E-05	44.324	9.43E-09	3.67E-08	-1.64E-07

Model 5

Mode	Truss A				Truss B				Truss C			
	Freq.	Mass participation factor			Freq.	Mass participation factor			Freq.	Mass participation factor		
	(*f*)Hz	x-comp	y-comp	z-comp	(*f*)Hz	x-comp	y-comp	z-comp	(*f*)Hz	x-comp	y-comp	z-comp
1	20.378	-1.0463	-6.14E-08	3.46E-09	26.677	-0.19133	-5.53E-08	1.62E-09	26.244	-0.17171	-5.16E-08	2.11E-09
2	25.007	1.08E-08	5.31E-14	1.4206	28.526	1.33E-10	1.86E-13	1.4275	27.931	1.70E-10	2.63E-14	1.4197
3	26.789	-1.066	-2.69E-08	8.65E-09	37.443	1.0542	6.12E-08	-5.20E-12	36.9	1.0828	5.95E-08	-1.19E-11
4	37.413	1.31E-10	-4.85E-10	-1.27E-07	47.839	-1.49E-12	-1.64E-11	0.16206	47.261	3.56E-12	-1.02E-11	0.16528
5	41.822	6.48E-10	1.33E-10	0.14944	48.498	3.17E-12	-1.72E-10	1.33E-08	48.258	4.19E-12	-3.11E-10	2.53E-08

Model 6

Mode	Truss A				Truss B				Truss C			
	Freq.	Mass participation factor			Freq.	Mass participation factor			Freq.	Mass participation factor		
	(*f*) z	x-comp	y-comp	z-comp	(*f*)Hz	x-comp	y-comp	z-comp	(*f*)Hz	x-comp	y-comp	z-comp
1	19.178	-1.0109	1.09E-09	9.89E-10	25.435	-0.18727	-3.06E-08	2.01E-09	25.075	-0.17052	-2.97E-08	2.19E-09
2	23.034	1.34E-09	-1.84E-13	1.4051	27.004	1.47E-10	1.75E-13	1.4105	26.511	1.52E-10	2.56E-14	1.4034
3	25.792	1.0472	-7.36E-09	-6.75E-10	35.524	1.0562	2.26E-08	-1.01E-12	35.061	1.0821	2.55E-08	-3.01E-12
4	35.464	-5.8E-12	-1.51E-11	-4.26E-09	45.757	-9.48E-12	-5.65E-12	0.15012	45.262	-8.35E-12	-7.19E-12	0.1532
5	38.939	5.29E-11	-1.08E-11	0.13129	46.48	-9.74E-13	-6.20E-11	1.29E-08	46.272	-1.65E-12	-7.85E-11	1.99E-08

Model 7

Mode	Truss A				Truss B				Truss C			
	Freq. (f) Hz	Mass participation factor			Freq. (f) Hz	Mass participation factor			Freq. (f) Hz	Mass participation factor		
		x-comp	y-comp	z-comp		x-comp	y-comp	z-comp		x-comp	y-comp	z-comp
1	20.013	-1.0436	-3.33E-09	8.70E-10	25.946	-0.18984	-2.72E-08	2.10E-09	25.562	-0.17339	-2.64E-08	2.28E-09
2	24.502	1.67E-09	3.60E-14	1.399	27.607	1.57E-10	-4.26E-14	1.4148	27.083	1.61E-10	1.23E-13	1.4084
3	26.877	-1.0626	3.83E-09	1.07E-09	36.342	1.0571	2.03E-08	-1.86E-12	35.846	1.0842	2.26E-08	-3.92E-12
4	37.05	-4.3E-12	-2.06E-11	-1.52E-08	46.542	-9.18E-12	-8.20E-12	0.15358	46.02	-8.88E-12	-7.21E-12	0.15663
5	41.017	6.84E-11	-1.71E-11	0.13466	47.319	-1.52E-12	-9.75E-11	1.34E-08	47.1	-1.65E-12	-1.16E-10	1.89E-08

Model 8

Mode	Truss A				Truss B				Truss C			
	Freq.	Mass participation factor			Freq.	Mass participation factor			Freq.	Mass participation factor		
	(f)Hz	x-comp	y-comp	z-comp	(f)Hz	x-comp	y-comp	z-comp	(f)Hz	x-comp	y-comp	z-comp
1	16.502	-0.70101	2.43E-08	8.96E-11	24.1	-4.78E-11	-3.31E-12	1.3337	23.817	7.42E-11	1.08E-14	1.324
2	18.984	4.27E-11	-3.32E-12	1.3211	24.802	0.30687	1.59E-07	4.29E-10	24.528	-0.32153	-1.59E-07	6.25E-10
3	25.707	1.2317	-1.26E-07	-1.04E-11	30.528	1.0209	1.18E-07	-1.78E-12	30.286	1.026	1.24E-07	3.20E-12
4	29.62	-4.9E-11	2.57E-12	1.34E-08	42.246	2.47E-12	2.25E-10	-1.02E-07	42.062	-2.18E-12	-1.32E-10	-1.03E-07
5	31.636	7.51E-12	-1.53E-11	0.13024	42.655	5.94E-08	-0.92761	-1.11E-11	42.532	-6.31E-08	0.92592	-5.57E-12

Model 9

Mode	Truss A				Truss B				Truss C			
	Freq.	Mass participation factor			Freq.	Mass participation factor			Freq.	Mass participation factor		
	(f)Hz	x-comp	y-comp	z-comp	(f)Hz	x-comp	y-comp	z-comp	(f)Hz	x-comp	y-comp	z-comp
1	22.298	0.95222	8.53E-09	2.84E-12	30.344	-0.37748	8.18E-10	5.54E-12	29.551	-0.33119	7.19E-10	2.95E-11
2	29.101	-0.98804	1.06E-08	3.03E-10	32.865	9.79E-13	1.33E-13	1.4539	31.81	4.78E-12	1.98E-13	1.4467
3	29.268	1.59E-10	4.65E-13	1.2953	42.558	1.0192	-1.56E-09	-6.92E-14	41.718	1.0514	-1.41E-09	-4.05E-13
4	34.826	-1.0E-11	-2.11E-11	-1.58E-08	52.296	-5.61E-13	7.64E-13	0.1968	51.425	-5.06E-13	5.70E-13	0.2002
5	36.111	1.19E-08	1.7428	-2.81E-10	53.209	-2.32E-12	-1.71E-12	-8.90E-09	52.739	-2.08E-12	2.63E-12	-7.22E-09

Table D. 4 .Summary of modal analysis results for proposed edge supported finite element models with aspect ratio of 2.0

Model 1

Mode	Truss A				Truss B				Truss C			
	Freq.	Mass participation factor			Freq.	Mass participation factor			Freq.	Mass participation factor		
	(f)Hz	x-comp	y-comp	z-comp	(f)Hz	x-comp	y-comp	z-comp	(f)Hz	x-comp	y-comp	z-comp
1	17.039	0.88753	-5.05E-16	4.16E-15	25.355	-0.49581	1.10E-15	2.28E-13	24.891	-0.43036	4.71E-15	-8.99E-15
2	24.983	-2.66E-14	-1.31E-04	1.2173	29.069	7.26E-14	-5.13E-05	1.3295	28.168	-1.7E-15	-6.78E-05	1.3181
3	26.319	0.88561	1.28E-15	3.28E-14	35.866	1.1205	-9.59E-15	-1.19E-14	34.913	1.1556	-3.71E-16	-2.64E-16
4	32.321	1.44E-03	-2.61E-15	3.32E-15	42.663	1.14E-03	-1.22E-13	-5.97E-15	42.478	-1.1E-03	-2.98E-14	-2.39E-15
5	42.318	-1.88E-03	-1.10E-13	2.60E-15	46.201	1.16E-14	0.80297	5.86E-05	45.942	7.56E-16	0.81254	6.61E-05

Model 2

Mode	Truss A				Truss B				Truss C			
	Freq.	Mass participation factor			Freq.	Mass participation factor			Freq.	Mass participation factor		
	(f)Hz	x-comp	y-comp	z-comp	(f)Hz	x-comp	y-comp	z-comp	(f)Hz	x-comp	y-comp	z-comp
1	16.758	-0.89816	-1.56E-12	1.85E-12	25.099	-0.47798	1.54E-12	5.10E-11	23.37	-0.43683	1.68E-12	6.08E-11
2	23.776	-4.3E-12	2.04E-04	1.1996	28.578	1.48E-11	5.57E-04	1.3326	25.755	1.27E-11	4.50E-04	1.3222
3	25.65	0.90052	3.01E-12	8.59E-12	35.848	1.1188	8.86E-12	-3.00E-12	32.652	1.1722	8.27E-12	-1.53E-12
4	31.762	-1.7E-03	-1.47E-11	-2.74E-12	41.919	2.24E-03	2.35E-11	5.80E-12	39.776	-1.93E-03	-2.69E-11	-5.25E-12
5	41.211	-2.0E-11	-0.83546	1.40E-05	43.836	8.20E-12	-0.79073	2.09E-04	41.058	7.69E-12	-0.80514	1.61E-04

Model 3

Mode	Truss A				Truss B				Truss C			
	Freq.	Mass participation factor			Freq.	Mass participation factor			Freq.	Mass participation factor		
	(f)Hz	x-comp	y-comp	z-comp	(f)Hz	x-comp	y-comp	z-comp	(f)Hz	x-comp	y-comp	z-comp
1	14.282	-0.90578	1.55E-07	4.39E-04	23.092	-0.47955	3.12E-07	3.36E-03	22.961	-0.41227	2.95E-07	4.69E-03
2	19.53	7.24E-04	9.93E-11	1.3469	24.021	8.12E-04	-5.11E-10	1.2889	23.611	9.24E-04	-6.47E-10	1.2712
3	21.983	1.2079	2.00E-07	-4.56E-04	28.939	1.1352	-1.11E-07	-8.18E-05	28.806	1.1556	-1.17E-07	-6.61E-05
4	26.037	-9.7E-10	2.32E-04	4.93E-07	37.239	7.63E-11	4.64E-04	1.46E-07	37.493	6.84E-11	5.29E-04	1.28E-07
5	29.49	4.09E-10	-7.13E-04	1.22E-07	40.04	6.65E-08	0.8213	-3.34E-11	39.937	-6.98E-08	-0.82125	4.13E-11

Model 4

Mode	Truss A				Truss B				Truss C			
	Freq.	Mass participation factor			Freq.	Mass participation factor			Freq.	Mass participation factor		
	(f)Hz	x-comp	y-comp	z-comp	(f)Hz	x-comp	y-comp	z-comp	(f)Hz	x-comp	y-comp	z-comp
1	15.475	-0.9166	9.58E-08	4.03E-04	24.089	1.83E-03	3.13E-16	8.83E-08	23.795	-0.34747	1.61E-07	3.62E-03
2	20.763	5.21E-04	-5.14E-11	1.259	25.269	6.60E-09	1.56E-21	3.30E-02	24.696	6.01E-04	-2.80E-10	1.2798
3	24.753	1.1626	-1.06E-08	-2.85E-04	31.566	5.48E-02	4.70E-16	1.76E-10	31.13	1.1479	-1.02E-07	-5.30E-05
4	28.633	4.79E-09	1.87E-04	2.38E-07	39.449	9.25E-22	1.04E-07	3.27E-16	39.491	1.89E-10	2.07E-03	7.97E-08
5	37.142	2.36E-08	-0.86129	-1.70E-10	40.385	2.42E-16	2.96E-02	9.67E-22	40.237	-6.85E-08	-0.79594	1.55E-10

Model 5

Mode	Truss A				Truss B				Truss C			
	Freq.	Mass participation factor			Freq.	Mass participation factor			Freq.	Mass participation factor		
	(f)Hz	x-comp	y-comp	z-comp	(f)Hz	x-comp	y-comp	z-comp	(f)Hz	x-comp	y-comp	z-comp
1	21.477	0.93521	2.94E-08	3.64E-08	25.099	-0.47798	1.54E-12	5.10E-11	23.37	-0.43683	1.68E-12	6.08E-11
2	29.819	4.14E-08	4.74E-02	1.2485	28.578	1.48E-11	5.57E-04	1.3326	25.755	1.27E-11	4.50E-04	1.3222
3	33.271	-1.0516	-1.20E-08	7.82E-08	35.848	1.1188	8.86E-12	-3.00E-12	32.652	1.1722	8.27E-12	-1.53E-12
4	39.539	0.21134	-1.33E-08	9.34E-08	41.919	2.24E-03	2.35E-11	5.80E-12	39.776	-1.93E-03	-2.69E-11	-5.25E-12
5	43.755	0.32995	1.33E-08	1.20E-09	43.836	8.20E-12	-0.79073	2.09E-04	41.058	7.69E-12	-0.80514	1.61E-04

Model 6

Mode	Truss A				Truss B				Truss C			
	Freq.	Mass participation factor			Freq.	Mass participation factor			Freq.	Mass participation factor		
	(f) z	x-comp	y-comp	z-comp	(f)Hz	x-comp	y-comp	z-comp	(f)Hz	x-comp	y-comp	z-comp
1	17.679	-0.90064	1.21E-08	2.78E-09	28.244	0.96611	1.36E-07	1.23E-06	28.004	0.93092	2.79E-07	4.40E-06
2	23.124	-4.9E-08	6.20E-02	1.2454	28.757	-5.35E-07	5.67E-02	1.2333	28.142	-2.23E-06	5.42E-02	1.218
3	26.919	1.1359	-3.31E-08	3.48E-08	31.203	1.0592	1.11E-08	-1.94E-07	30.84	1.1037	1.82E-08	-1.82E-07
4	32.831	0.1103	1.72E-08	2.53E-08	46.079	0.42764	-8.30E-09	5.39E-08	45.964	0.40732	-6.93E-09	5.20E-08
5	33.159	0.23526	-2.12E-08	2.56E-09	51.006	2.18E-08	0.6338	0.113	50.705	1.99E-08	0.63077	0.10669

Model 7

Mode	Truss A				Truss B				Truss C			
	Freq. (f) Hz	Mass participation factor			Freq. (f) Hz	Mass participation factor			Freq. (f) Hz	Mass participation factor		
		x-comp	y-comp	z-comp		x-comp	y-comp	z-comp		x-comp	y-comp	z-comp
1	15.942	0.91249	1.66E-07	2.45E-12	24.134	0.47889	2.47E-07	6.56E-12	23.983	0.4465	2.38E-07	1.46E-10
2	22.059	-1.1E-13	-1.11E-13	1.2763	25.216	-8.83E-12	-3.07E-13	1.2653	24.844	-4.23E-11	3.15E-13	1.2534
3	24.354	1.0849	-2.30E-08	-1.88E-12	30.232	1.1367	8.54E-08	8.42E-12	29.999	1.1602	8.74E-08	9.70E-12
4	29.157	-1.7E-12	4.63E-13	6.49E-07	39.982	6.47E-13	-2.21E-11	1.19E-07	40.088	2.66E-12	-2.17E-11	1.08E-07
5	35.059	-1.2E-11	-1.99E-12	6.33E-08	44.853	-1.69E-08	0.79404	1.93E-13	44.672	-2.03E-08	0.78766	-1.22E-13

Model 8

Mode	Truss A				Truss B				Truss C			
	Freq.	Mass participation factor			Freq.	Mass participation factor			Freq.	Mass participation factor		
	(f)Hz	x-comp	y-comp	z-comp	(f)Hz	x-comp	y-comp	z-comp	(f)Hz	x-comp	y-comp	z-comp
1	16.349	-0.93377	-1.19E-08	5.40E-10	24.744	-0.67091	-5.33E-08	1.04E-09	24.535	-0.6306	-5.35E-08	1.25E-09
2	23.471	1.42E-09	4.77E-13	1.2396	26.563	4.18E-10	8.14E-14	1.2762	26.075	4.59E-10	3.96E-13	1.2618
3	27.013	-1.0584	1.87E-08	1.07E-09	30.919	1.0957	4.81E-09	-4.25E-11	30.608	1.1264	8.28E-09	-4.35E-11
4	29.722	-5.9E-11	6.04E-11	-2.38E-08	39.475	4.92E-12	2.28E-10	3.45E-08	39.584	6.89E-12	2.25E-10	3.22E-08
5	36.634	-3.9E-10	7.02E-10	6.24E-09	45.253	3.67E-10	0.76751	-6.08E-14	45.07	-3.73E-10	0.77408	-4.65E-13

Model 9

Mode	Truss A				Truss B				Truss C			
	Freq.	Mass participation factor			Freq.	Mass participation factor			Freq.	Mass participation factor		
	(f)Hz	x-comp	y-comp	z-comp	(f)Hz	x-comp	y-comp	z-comp	(f)Hz	x-comp	y-comp	z-comp
1	19.195	0.90647	2.24E-03	2.35E-03	28.359	0.65927	5.64E-03	2.11E-02	27.825	0.60686	5.43E-03	2.32E-02
2	28.174	-1.8E-02	3.54E-02	1.0448	31.753	-1.02E-02	1.39E-02	1.3264	30.735	-9.33E-03	1.27E-02	1.3158
3	29.13	1.0222	-2.25E-02	2.17E-02	38.225	1.0963	-1.74E-03	2.20E-03	37.369	1.1378	-1.49E-03	1.66E-03
4	29.608	2.33E-02	1.512	-3.68E-02	47.056	1.94E-02	1.02E-02	-2.61E-03	46.843	-1.69E-02	-9.54E-03	2.09E-03
5	30.289	-1.9E-02	3.90E-04	7.36E-03	52.859	-4.21E-04	-0.7725	6.45E-03	52.393	-3.83E-04	-0.7728	5.83E-03

Appendix E

FREQUENCIES AND MASS PARTCIPATION FACTORS FOR FE NUMERICAL MODELS

E.1. Modal Analysis Results

This appendix presents results for modal analysis conduction on space truss models as a part of the FE parametric study on space truss models in Chapter 7. Tables E.1 to E.9 present the results of modal analysis carried out on different space truss models, SOS, SOLS and SOD, for different values of aspect ratios and both cases of composite and non-composite cases. Presented results also include the three cases of support configurations; i.e. corner supported, 8-node supported and fully edge supported models.

Table E. 1Corner supported SOS models with different aspect ratio

AR=1.0

Mode	Non-Composite					Composite				
	Freq. (f)Hz	Mass participation factor			Max. Resp. (mm)	Freq. (f)Hz	Mass participation factor			Max. Resp. (mm)
		x-comp	y-comp	z-comp			x-comp	y-comp	z-comp	
1	14.779	-1.14E-08	-1.14E-08	1.2672	0.547	17.093	-6.82E-09	-6.82E-09	1.305	0.218
2	17.465	-0.36074	0.75278	1.14E-08		22.867	0.1417	5.01E-02	2.86E-08	
3	17.465	0.75278	0.36074	3.25E-08		22.867	-5.01E-02	0.1417	1.36E-08	
4	23.272	0.7231	0.51378	2.16E-09		30.236	0.9704	-0.24034	2.29E-09	
5	23.272	-0.51378	0.7231	3.66E-10		30.236	0.24034	0.9704	3.79E-09	

AR=1.2

Mode	Non-Composite					Composite				
	Freq. (f)Hz	Mass participation factor			Max. Resp. (mm)	Freq. (f)Hz	Mass participation factor			Max. Resp. (mm)
		x-comp	y-comp	z-comp			x-comp	y-comp	z-comp	
1	16.502	-2.43E-10	-1.16E-08	1.2631	0.557	19.096	1.38E-09	-8.84E-09	1.2906	0.222
2	17.159	0.93755	-3.60E-07	3.00E-09		23.191	0.26905	-4.40E-07	1.20E-08	
3	20.967	3.90E-07	1.0334	2.18E-08		27.712	1.20E-07	-0.34877	-1.84E-08	
4	23.523	1.0936	-5.69E-08	-7.23E-10		29.515	1.0431	-4.48E-07	-1.32E-09	
5	26.937	3.73E-08	1.0119	2.13E-09		31.311	4.60E-07	1.0028	4.11E-09	

AR=1.5

Mode	Non-Composite					Composite				
	Freq. (f)Hz	Mass participation factor			Max. Resp. (mm)	Freq. (f)Hz	Mass participation factor			Max. Resp. (mm)
		x-comp	y-comp	z-comp			x-comp	y-comp	z-comp	
1	16.547	0.93533	-3.08E-07	1.42E-09	0.599	20.789	5.13E-10	-9.57E-09	1.2735	0.223
2	18.166	-4.50E-10	-1.13E-08	1.2785		23.517	0.34636	-4.27E-07	-2.30E-09	
3	23.762	1.0908	8.54E-08	-1.20E-10		29.676	1.0784	-3.02E-07	-6.79E-11	
4	25.763	5.38E-08	1.0685	1.45E-08		33.401	-4.54E-07	-1.1623	-7.96E-09	
5	30.613	-4.12E-09	3.58E-09	-4.41E-07		34.444	3.43E-08	0.94977	-3.83E-10	

AR=2.0

Mode	Non-Composite					Composite				
	Freq. (f)Hz	Mass participation factor			Max. Resp. (mm)	Freq. (f)Hz	Mass participation factor			Max. Resp. (mm)
		x-comp	y-comp	z-comp			x-comp	y-comp	z-comp	
1	15.492	0.90813	-2.64E-07	4.81E-10	0.670	22.258	1.21E-09	-1.00E-08	1.2726	0.233
2	19.473	-4.42E-11	-1.11E-08	1.2939		23.562	0.53115	-4.53E-07	-4.39E-09	
3	23.899	1.1048	7.34E-08	-1.40E-10		29.174	1.1454	-2.31E-07	-3.28E-11	
4	28.515	3.10E-09	3.55E-10	5.63E-07		36.716	2.04E-07	0.91518	2.87E-09	
5	32.422	1.65E-07	-1.3443	-7.18E-09		38.639	9.34E-09	1.40E-09	1.32E-07	

AR=3.0

Mode	Non-Composite					Composite				
	Freq. (f)Hz	Mass participation factor			Max. Resp. (mm)	Freq. (f)Hz	Mass participation factor			Max. Resp. (mm)
		x-comp	y-comp	z-comp			x-comp	y-comp	z-comp	
1	13.707	0.85204	-2.31E-07	2.40E-10	0.818	22.852	2.96E-09	-8.92E-09	1.2418	0.250
2	20.141	-3.82E-12	-1.04E-08	1.2569		23.624	-0.75784	4.64E-07	6.83E-09	
3	23.948	1.1502	1.22E-07	-9.09E-11		28.535	1.2519	-1.05E-07	9.60E-11	
4	25.148	-2.22E-09	3.12E-11	1.11E-06		36.994	1.33E-08	-7.46E-10	1.95E-07	
5	31.472	-7.57E-08	4.78E-12	1.84E-08		39.902	8.99E-08	0.79448	2.80E-10	

Table E. 2 Corner supported SOLS models with different aspect ratio

AR=1.0

Mode	Non-Composite					Composite				
	Freq. (f)Hz	Mass participation factor			Max. Resp. (mm)	Freq. (f)Hz	Mass participation factor			Max. Resp. (mm)
		x-comp	y-comp	z-comp			x-comp	y-comp	z-comp	
1	13.18	0.94704	-7.04E-02	-2.27E-07	1.19	14.625	-5.75E-09	-5.75E-09	1.4018	0.221
2	13.18	7.04E-02	0.94704	-2.63E-07		19.983	-4.72E-02	0.1432	9.89E-09	
3	13.288	2.16E-07	2.16E-07	1.3681		19.983	-0.1432	-4.72E-02	-1.96E-08	
4	18.166	0.634	0.12647	-6.39E-09		26.64	-3.17E-08	3.17E-08	-1.50E-13	
5	18.166	0.12647	-0.634	4.26E-09		29.559	1.0484	7.11E-02	5.79E-10	

AR=1.2

Mode	Non-Composite					Composite				
	Freq. (f)Hz	Mass participation factor			Max. Resp. (mm)	Freq. (f)Hz	Mass participation factor			Max. Resp. (mm)
		x-comp	y-comp	z-comp			x-comp	y-comp	z-comp	
1	14.337	0.89917	-1.97E-07	1.64E-09	0.902	16.55	7.20E-10	-7.30E-09	1.3435	0.229
2	14.971	-3.51E-10	-4.57E-08	1.3322		20.472	0.23585	-7.34E-07	1.09E-08	
3	15.625	-6.10E-09	1.0085	5.38E-08		24.175	-2.06E-07	-0.26962	-1.33E-08	
4	19.401	-0.90025	-5.45E-07	1.52E-09		28.983	1.0918	-3.19E-07	-1.12E-09	
5	21.897	-4.62E-07	0.62566	-5.44E-09		29.912	-1.17E-08	-1.27E-07	-0.1023	

AR=1.5

Mode	Non-Composite					Composite				
	Freq. (f)Hz	Mass participation factor			Max. Resp. (mm)	Freq. (f)Hz	Mass participation factor			Max. Resp. (mm)
		x-comp	y-comp	z-comp			x-comp	y-comp	z-comp	
1	12.7	0.92156	-1.41E-07	3.48E-10	1.19	17.763	3.11E-10	-8.25E-09	1.3288	0.228
2	16.188	-3.45E-10	-1.67E-08	1.3305		20.907	0.32263	-9.28E-07	-1.54E-09	
3	18.928	-1.02E-06	1.06	1.67E-08		29.128	1.135	-1.18E-06	1.66E-10	
4	19.016	-0.69062	-3.06E-06	-2.82E-10		29.833	-7.16E-06	-0.42858	-3.05E-09	
5	22.471	3.82E-09	-2.27E-10	6.74E-07		32.348	1.24E-07	0.95769	3.19E-09	

AR=2.0

Mode	Non-Composite					Composite				
	Freq. (f)Hz	Mass participation factor			Max. Resp. (mm)	Freq. (f)Hz	Mass participation factor			Max. Resp. (mm)
		x-comp	y-comp	z-comp			x-comp	y-comp	z-comp	
1	15.37	0.91511	-2.70E-07	4.79E-10	0.658	22.062	1.35E-09	-9.58E-09	1.2716	0.236
2	19.388	-3.59E-11	-1.11E-08	1.3092		23.331	-0.56546	5.25E-07	4.77E-09	
3	23.895	1.1117	2.41E-08	-1.40E-10		28.955	1.1655	-3.50E-07	-3.04E-11	
4	28.058	2.31E-09	3.71E-10	7.08E-07		36.358	3.38E-07	0.90663	3.15E-09	
5	31.566	1.77E-07	-1.3299	-7.46E-09		38.08	8.77E-09	9.88E-10	1.81E-07	

AR=3.0

Mode	Non-Composite					Composite				
	Freq. (f)Hz	Mass participation factor			Max. Resp. (mm)	Freq. (f)Hz	Mass participation factor			Max. Resp. (mm)
		x-comp	y-comp	z-comp			x-comp	y-comp	z-comp	
1	13.561	0.85294	-2.37E-07	2.32E-10	0.882	22.809	4.94E-09	-9.12E-09	1.2694	0.254
2	20.105	-1.17E-11	-1.06E-08	1.2807		23.279	-0.7763	5.24E-07	1.08E-08	
3	23.951	1.1586	1.06E-07	-7.06E-11		28.382	1.2585	-1.71E-07	1.02E-10	
4	24.777	-6.29E-09	3.23E-11	1.29E-06		36.479	1.25E-08	-6.10E-10	2.43E-07	
5	31.396	-7.17E-08	1.49E-11	4.02E-08		39.66	1.58E-07	0.80788	3.48E-10	

Table E. 3 Corner supported SOD models with different aspect ratio

AR=1.0

Mode	Non-Composite					Composite				
	Freq. (f)Hz	Mass participation factor			Max. Resp. (mm)	Freq. (f)Hz	Mass participation factor			Max. Resp. (mm)
		x-comp	y-comp	z-comp			x-comp	y-comp	z-comp	
1	13.929	-7.45E-09	-7.46E-09	1.4324	0.271	15.638	-6.06E-09	-6.05E-09	1.4656	0.146
2	16.444	1.01E-02	0.68037	2.16E-08		20.139	-4.23E-09	4.25E-09	-1.21E-10	
3	16.444	0.68037	-1.01E-02	2.09E-08		22.469	-9.54E-02	0.52455	1.20E-08	
4	18.018	-4.83E-09	4.75E-09	-1.38E-10		22.469	0.52455	9.54E-02	1.74E-08	
5	26.127	-1.54E-09	8.63E-10	-1.39E-07		35.444	0.81108	1.60E-02	-3.65E-09	

AR=1.2

Mode	Non-Composite					Composite				
	Freq. (f)Hz	Mass participation factor			Max. Resp. (mm)	Freq. (f)Hz	Mass participation factor			Max. Resp. (mm)
		x-comp	y-comp	z-comp			x-comp	y-comp	z-comp	
1	15.022	-0.12526	9.44E-08	1.5657	0.298	16.765	-6.29E-02	5.29E-08	1.343	0.158
2	16.126	0.80556	-1.49E-07	0.36104		22.641	0.82951	-2.11E-07	6.69E-02	
3	19.497	2.41E-07	-0.73868	7.76E-07		23.654	9.02E-02	-8.36E-07	0.47269	
4	21.338	4.26E-03	6.28E-07	0.51671		26.009	-6.78E-07	0.73235	3.62E-07	
5	27.195	-2.96E-07	-4.24E-02	2.02E-07		35.195	1.83E-08	-0.8488	4.10E-08	

AR=1.5

Mode	Non-Composite					Composite				
	Freq. (f)Hz	Mass participation factor			Max. Resp. (mm)	Freq. (f)Hz	Mass participation factor			Max. Resp. (mm)
		x-comp	y-comp	z-comp			x-comp	y-comp	z-comp	
1	15.869	0.77333	-2.88E-07	2.01E-09	0.326	18.596	3.72E-10	-6.79E-09	1.2813	0.148
2	16.639	-5.97E-10	-8.00E-09	1.3223		23.766	0.8328	-3.84E-07	-7.79E-10	
3	24.804	4.02E-07	-0.76172	-1.60E-09		30.484	6.21E-10	-1.58E-08	0.52431	
4	27.084	-5.07E-09	2.94E-10	-2.47E-06		32.322	-1.00E-06	0.82484	2.14E-08	
5	28.212	9.54E-10	1.23E-08	0.59617		35.894	-1.02E-07	-0.68124	2.27E-09	

AR=2.0

Mode	Non-Composite					Composite				
	Freq. (f)Hz	Mass participation factor			Max. Resp. (mm)	Freq. (f)Hz	Mass participation factor			Max. Resp. (mm)
		x-comp	y-comp	z-comp			x-comp	y-comp	z-comp	
1	14.799	-0.85451	3.23E-07	0.10265	0.419	19.695	-0.14096	5.33E-08	1.3814	0.172
2	17.697	1.94E-02	2.69E-08	1.396		23.468	1.0341	-5.08E-07	0.17678	
3	25.777	1.58E-07	-0.25458	9.94E-07		35.379	-7.43E-07	0.84676	8.66E-09	
4	29.058	-4.40E-07	0.50782	4.22E-07		37.828	6.55E-07	-0.30965	4.01E-07	
5	32.865	-2.66E-07	-0.727	-1.22E-08		39.777	-1.08E-05	0.73472	9.62E-07	

AR=3.0

Mode	Non-Composite					Composite				
	Freq. (f)Hz	Mass participation factor			Max. Resp. (mm)	Freq. (f)Hz	Mass participation factor			Max. Resp. (mm)
		x-comp	y-comp	z-comp			x-comp	y-comp	z-comp	
1	13.5	0.81047	-2.89E-07	1.64E-10	0.585	21.603	1.11E-09	-6.62E-09	1.234	0.179
2	19.153	-6.86E-11	-8.67E-09	1.2506		24.171	0.96916	-4.76E-07	-1.34E-09	
3	24.856	5.30E-09	-1.02E-10	1.33E-06		36.803	-3.04E-07	0.74666	-4.15E-09	
4	30.689	-0.11344	9.21E-07	-6.33E-11		37.72	4.73E-09	-1.51E-09	-2.27E-07	
5	31.578	-2.30E-07	5.85E-10	5.18E-08		43.688	1.1263	-1.01E-06	2.48E-10	

Table E. 4 Fully edge supported SOS models with different aspect ratios

AR=1.0

Mode	Non-Composite					Composite				
	Freq. (f)Hz	Mass participation factor			Max. Resp. (mm)	Freq. (f)Hz	Mass participation factor			Max. Resp. (mm)
		x-comp	y-comp	z-comp			x-comp	y-comp	z-comp	
1	34.989	-1.58E-08	-1.58E-08	1.4754	0.0656	39.907	-1.36E-08	-1.36E-08	1.4518	0.0598
2	49.438	0.54549	-0.73381	4.79E-10		54.075	0.73974	-0.88821	-5.57E-12	
3	49.438	0.73381	0.54549	-3.25E-09		54.075	0.88821	0.73974	6.36E-11	
4	49.751	-5.22E-08	5.22E-08	-3.32E-08		54.775	1.16E-07	-1.16E-07	1.37E-08	
5	52.09	-2.43E-08	-2.43E-08	-2.79E-14		63.471	-0.99976	0.26866	-5.29E-09	

AR=1.2

Mode	Non-Composite					Composite				
	Freq. (f)Hz	Mass participation factor			Max. Resp. (mm)	Freq. (f)Hz	Mass participation factor			Max. Resp. (mm)
		x-comp	y-comp	z-comp			x-comp	y-comp	z-comp	
1	37.585	-6.42E-08	-3.06E-08	1.19E-08	0.0661	44.537	2.71E-09	-2.18E-08	1.4009	0.0637
2	39.082	-1.1253	4.14E-08	8.41E-09		50.346	4.63E-08	-1.69E-08	-2.61E-08	
3	39.409	-1.17E-10	-2.42E-08	1.44		51.952	-1.0971	-1.04E-06	5.12E-09	
4	40.203	-6.36E-08	-1.229	6.98E-09		52.185	9.49E-07	-1.0148	3.57E-11	
5	43.841	2.40E-09	6.82E-09	-6.46E-08		65.529	4.75E-07	1.74E-07	7.75E-08	

AR=1.5

Mode	Non-Composite					Composite				
	Freq. (f)Hz	Mass participation factor			Max. Resp. (mm)	Freq. (f)Hz	Mass participation factor			Max. Resp. (mm)
		x-comp	y-comp	z-comp			x-comp	y-comp	z-comp	
1	36.576	-8.65E-08	1.02E-09	1.17E-08	0.0643	49.394	3.78E-08	1.20E-09	3.85E-08	0.0634
2	37.58	1.016	-2.65E-08	5.07E-10		51.623	4.21E-08	-2.38E-07	1.2245	
3	40.203	-6.12E-08	-1.2203	1.30E-08		51.76	-0.98834	-7.95E-07	9.92E-09	
4	43.292	4.65E-09	-8.32E-10	-3.76E-08		52.068	8.65E-07	-1.08	-5.69E-08	
5	46.548	4.16E-09	-3.33E-08	1.3493		64.699	-1.07E-08	2.45E-07	1.1139	

AR=2.0

Mode	Non-Composite					Composite				
	Freq. (f)Hz	Mass participation factor			Max. Resp. (mm)	Freq. (f)Hz	Mass participation factor			Max. Resp. (mm)
		x-comp	y-comp	z-comp			x-comp	y-comp	z-comp	
1	34.872	-1.30E-07	4.56E-10	1.57E-08	0.0683	47.013	3.22E-08	6.07E-10	2.34E-10	0.0673
2	35.43	0.89995	-1.80E-08	3.80E-10		49.499	0.94912	8.11E-08	3.73E-10	
3	40.166	-5.80E-08	-1.2027	1.23E-08		51.942	8.01E-08	-1.0135	5.22E-09	
4	42.782	6.96E-09	-1.23E-09	-4.83E-08		63.569	4.18E-09	-5.76E-08	0.41984	
5	47.54	0.86745	5.66E-08	9.32E-10		65.912	5.38E-07	-1.36E-08	5.42E-08	

AR=3.0

Mode	Non-Composite					Composite				
	Freq. (f)Hz	Mass participation factor			Max. Resp. (mm)	Freq. (f)Hz	Mass participation factor			Max. Resp. (mm)
		x-comp	y-comp	z-comp			x-comp	y-comp	z-comp	
1	31.854	-2.45E-07	1.38E-10	1.80E-08	0.0855	44.454	3.37E-08	4.43E-10	-8.35E-10	0.0731
2	32.078	0.77058	-1.31E-08	2.61E-10		47.494	0.78001	-1.18E-08	2.22E-10	
3	40.03	-7.83E-08	-1.1674	1.21E-08		51.14	-1.63E-08	-1.0417	4.66E-09	
4	42.263	1.46E-08	-1.38E-09	-3.98E-08		63.218	-4.64E-09	1.69E-07	0.91192	
5	43.912	0.84432	-2.15E-08	5.68E-10		66.571	7.63E-09	-1.0805	9.43E-08	

Table E. 5 Fully edge supported SOLS models with different aspect ratio

AR=1.0

Mode	Non-Composite					Composite				
	Freq. (f)Hz	Mass participation factor			Max. Resp. (mm)	Freq. (f)Hz	Mass participation factor			Max. Resp. (mm)
		x-comp	y-comp	z-comp			x-comp	y-comp	z-comp	
1	27.689	-1.47E-08	-1.47E-08	1.4459	0.117	30.211	-9.43E-09	-9.42E-09	1.4399	0.0936
2	37.598	0.94637	-0.10051	7.86E-10		42.114	1.0659	0.72522	-1.81E-10	
3	37.598	0.10051	0.94637	9.63E-10		42.114	0.72522	-1.0659	3.69E-11	
4	40.457	2.77E-09	2.76E-09	1.01E-13		48.256	-1.98E-06	1.98E-06	2.69E-08	
5	41.338	9.38E-09	-9.38E-09	4.68E-08		48.26	-1.082	0.41674	-2.69E-09	

AR=1.2

Mode	Non-Composite					Composite				
	Freq. (f)Hz	Mass participation factor			Max. Resp. (mm)	Freq. (f)Hz	Mass participation factor			Max. Resp. (mm)
		x-comp	y-comp	z-comp			x-comp	y-comp	z-comp	
1	32.901	1.50E-09	-1.94E-08	1.4874	0.112	35.86	1.09E-09	-1.82E-08	1.4272	0.0999
2	36.636	-6.52E-08	-2.66E-08	1.84E-08		41.012	0.9952	1.24E-10	-1.50E-09	
3	37.719	1.3633	1.94E-07	-6.46E-09		44.013	-3.14E-09	-0.78615	-1.20E-09	
4	38.993	-2.38E-07	-1.4483	6.29E-09		44.75	1.95E-08	-5.10E-08	3.27E-08	
5	39.559	0.40018	-1.11E-06	1.35E-09			2.70E-07	-0.55834	-4.18E-09	

AR=1.5

Mode	Non-Composite					Composite				
	Freq. (f)Hz	Mass participation factor			Max. Resp. (mm)	Freq. (f)Hz	Mass participation factor			Max. Resp. (mm)
		x-comp	y-comp	z-comp			x-comp	y-comp	z-comp	
1	35.577	-6.54E-08	8.73E-10	3.00E-08	0.115	39.814	4.36E-09	-3.64E-08	1.3291	0.101
2	36.532	1.3234	-2.36E-08	2.09E-09		40.527	0.91415	7.02E-08	-7.66E-10	
3	37.163	-7.52E-11	-9.04E-08	1.4521		42.264	-5.71E-08	0.81288	4.78E-09	
4	38.23	0.56211	3.26E-06	-1.87E-09		44.107	2.40E-08	2.11E-09	5.18E-08	
5	38.427	1.76E-06	-1.1888	-1.71E-08		54.424	-8.28E-08	0.38295	4.08E-09	

AR=2.0

Mode	Non-Composite					Composite				
	Freq. (f)Hz	Mass participation factor			Max. Resp. (mm)	Freq. (f)Hz	Mass participation factor			Max. Resp. (mm)
		x-comp	y-comp	z-comp			x-comp	y-comp	z-comp	
1	34.691	-1.85E-07	4.11E-10	1.59E-08	0.107	39.843	0.99507	3.27E-08	1.92E-10	0.103
2	35.083	1.1241	1.51E-08	4.20E-10		43.239	2.44E-08	-3.37E-10	-2.91E-09	
3	39.029	0.81405	2.98E-07	3.99E-10		51.88	2.92E-08	-0.99558	9.48E-09	
4	40.12	4.02E-07	-1.1999	1.25E-08		55.731	1.27E-10	2.42E-08	1.4645	
5	40.731	1.52E-08	2.27E-09	1.29E-08		65.364	-2.06E-08	2.13E-07	1.0062	

AR=3.0

Mode	Non-Composite					Composite				
	Freq. (f)Hz	Mass participation factor			Max. Resp. (mm)	Freq. (f)Hz	Mass participation factor			Max. Resp. (mm)
		x-comp	y-comp	z-comp			x-comp	y-comp	z-comp	
1	31.728	-2.81E-07	1.29E-10	1.79E-08	0.12	38.229	1.1933	-5.04E-09	2.10E-10	0.109
2	31.92	0.89211	-3.82E-09	2.87E-10		40.37	4.31E-08	-2.65E-10	8.03E-10	
3	36.842	1.0023	1.13E-07	3.77E-10		51.127	-4.37E-09	-1.0411	4.64E-09	
4	38.298	2.60E-08	-5.14E-10	9.94E-09		63.219	-4.10E-09	1.69E-07	0.91232	
5	39.99	8.62E-08	-1.1659	1.19E-08		66.57	6.37E-09	-1.0799	9.44E-08	

Table E. 6 Fully edge supported SOD models with different aspect ratio

AR=1.0

Mode	Non-Composite					Composite				
	Freq. (f)Hz	Mass participation factor			Max. Resp. (mm)	Freq. (f)Hz	Mass participation factor			Max. Resp. (mm)
		x-comp	y-comp	z-comp			x-comp	y-comp	z-comp	
1	26.484	-1.44E-08	-1.43E-08	1.5715	0.136	29.725				0.082
2	28.596	-1.07E-09	1.08E-09	4.95E-08		43.347				
3	35.555	-0.17968	-0.97141	-1.35E-09		43.347				
4	35.555	0.97141	-0.17968	9.51E-10		50.013				
5	40.533	2.96E-09	2.69E-09	3.84E-12		50.013				

AR=1.2

Mode	Non-Composite					Composite				
	Freq. (f)Hz	Mass participation factor			Max. Resp. (mm)	Freq. (f)Hz	Mass participation factor			Max. Resp. (mm)
		x-comp	y-comp	z-comp			x-comp	y-comp	z-comp	
1	29.257	6.62E-08	9.45E-02	3.65E-08	0.134	-7.55E-09	-3.96E-03	-4.87E-08	1.501	0.0966
2	30.152	-3.60E-03	-4.84E-08	1.5608		1.2686	-0.80592	-2.48E-07	1.15E-02	
3	35.771	1.0032	4.45E-07	-4.26E-05		0.10356	-3.04E-07	0.91729	1.57E-08	
4	37.003	5.26E-07	-0.94241	-6.55E-10		-1.3504	4.34E-08	-0.1705	2.24E-08	
5	37.097	-6.36E-07	1.094	1.17E-08		0.16076	-1.76E-07	-0.95139	9.51E-09	

AR=1.5

Mode	Non-Composite					Composite				
	Freq. (f)Hz	Mass participation factor			Max. Resp. (mm)	Freq. (f)Hz	Mass participation factor			Max. Resp. (mm)
		x-comp	y-comp	z-comp			x-comp	y-comp	z-comp	
1	30.061	1.81E-09	1.60E-10	7.75E-09	0.133	40.347	1.18E-09	-1.59E-08	1.3062	0.0926
2	35.736	1.0813	3.74E-07	4.29E-09		42.568	0.79748	1.17E-07	-7.70E-11	
3	36.203	-1.22E-08	-3.97E-08	1.4109		45.873	-1.22E-07	0.83894	7.89E-10	
4	36.241	3.71E-09	-7.82E-10	2.75E-06		47.575	2.17E-08	2.08E-09	2.19E-08	
5	37.434	-0.64792	6.12E-07	-9.87E-10		56.448	-3.76E-08	-0.66675	-2.22E-10	

AR=2.0

Mode	Non-Composite					Composite				
	Freq. (f)Hz	Mass participation factor			Max. Resp. (mm)	Freq. (f)Hz	Mass participation factor			Max. Resp. (mm)
		x-comp	y-comp	z-comp			x-comp	y-comp	z-comp	
1	31.044	4.27E-08	0.12619	1.67E-09	0.125	40.2	0.77905	5.52E-08	-2.03E-02	0.101
2	34.548	-3.11E-07	-1.71E-02	1.88E-08		43.84	1.68E-08	-0.35283	4.19E-09	
3	34.897	-1.1893	-8.84E-08	6.13E-03		46.576	-6.90E-08	1.0186	-5.15E-09	
4	35.673	0.34736	1.93E-07	8.52E-03		52.922	7.79E-02	3.25E-08	1.3843	
5	38.271	1.40E-07	-0.21178	1.62E-09		65.266	0.23315	2.57E-07	1.1631	

AR=3.0

Mode	Non-Composite					Composite				
	Freq. (f)Hz	Mass participation factor			Max. Resp. (mm)	Freq. (f)Hz	Mass participation factor			Max. Resp. (mm)
		x-comp	y-comp	z-comp			x-comp	y-comp	z-comp	
1	31.799	-2.50E-07	1.36E-10	1.81E-08	0.13	41.561	0.78474	-5.76E-09	1.53E-10	0.0945
2	32.029	0.83265	-1.29E-08	2.89E-10		43.281	5.96E-08	-5.34E-10	9.10E-10	
3	35.609	0.90465	9.00E-08	3.93E-10		49.519	-7.05E-09	-0.9557	2.76E-09	
4	36.046	5.59E-09	8.10E-11	1.15E-08		63.248	-3.89E-09	1.68E-07	0.91005	
5	38.945	0.38497	1.55E-07	1.65E-10		66.182	6.93E-09	-0.99364	1.13E-07	

Table E. 7 8-supported SOS models with different aspect ratio

AR=1.0

Mode	Non-Composite					Composite				
	Freq. (f)Hz	Mass participation factor			Max. Resp. (mm)	Freq. (f)Hz	Mass participation factor			Max. Resp. (mm)
		x-comp	y-comp	z-comp			x-comp	y-comp	z-comp	
1	19.107	1.51E-07	0.58167	1.7082	0.152	23.195	7.03E-08	0.36454	1.7707	0.133
2	30.353	-7.39E-07	-0.78685	1.0115		36.208	-2.52E-07	-0.47638	0.96888	
3	32.449	1.3085	1.24E-06	7.00E-07		37.47	2.21E-06	0.97403	-2.16E-03	
4	32.982	0.10503	-1.91E-07	-1.34E-07		38.057	1.0654	-2.38E-06	4.49E-08	
5	33.517	1.38E-06	-1.1359	-0.14045		43.548	0.24589	-2.12E-07	6.80E-09	

AR=1.2

Mode	Non-Composite					Composite				
	Freq. (f)Hz	Mass participation factor			Max. Resp. (mm)	Freq. (f)Hz	Mass participation factor			Max. Resp. (mm)
		x-comp	y-comp	z-comp			x-comp	y-comp	z-comp	
1	32.355	1.1627	-4.59E-08	-6.69E-10	0.149	37.712	0.9232	-1.73E-09	9.88E-09	0.133
2	33.16	-1.43E-07	-1.69E-09	1.83E-06		38.553	-2.95E-08	-2.98E-08	1.5428	
3	33.522	2.06E-09	-3.26E-08	1.6234		42.641	-1.26E-08	-2.19E-08	-4.15E-08	
4	37.108	-4.02E-08	-3.79E-08	2.08E-08		44.39	1.33E-08	-0.92803	-2.74E-09	
5	38.352	1.0392	1.10E-07	-6.90E-09		47.564	6.78E-08	-8.24E-08	2.19E-08	

AR=1.5

Mode	Non-Composite					Composite				
	Freq. (f)Hz	Mass participation factor			Max. Resp. (mm)	Freq. (f)Hz	Mass participation factor			Max. Resp. (mm)
		x-comp	y-comp	z-comp			x-comp	y-comp	z-comp	
1	31.246	1.1113	-4.01E-08	1.12E-09	0.153	37.032	0.91388	-1.29E-08	7.06E-10	0.136
2	31.554	-3.27E-07	4.19E-11	9.32E-08		41.554	-1.83E-09	-9.25E-08	1.406	
3	36.084	7.22E-08	-9.48E-10	-5.34E-07		41.917	1.48E-08	-3.44E-09	6.00E-07	
4	36.295	-1.48E-09	-6.18E-08	1.5075		42.899	5.57E-09	0.82638	2.73E-08	
5	36.978	0.94943	4.74E-08	7.42E-10		47.763	-4.18E-08	-5.34E-08	-1.60E-08	

AR=2.0

Mode	Non-Composite					Composite				
	Freq. (f)Hz	Mass participation factor			Max. Resp. (mm)	Freq. (f)Hz	Mass participation factor			Max. Resp. (mm)
		x-comp	y-comp	z-comp			x-comp	y-comp	z-comp	
1	29.393	4.58E-07	6.07E-11	4.32E-08	0.162	35.589	0.88112	-1.08E-08	2.58E-10	0.143
2	29.58	-1.0352	3.07E-08	-4.53E-10		40.826	1.34E-08	-3.53E-10	-3.07E-08	
3	34.655	-1.26E-07	4.61E-10	7.48E-08		46.063	7.96E-10	0.7263	5.96E-08	
4	35.166	0.8669	-4.47E-09	1.49E-10		47.722	-1.55E-09	-1.00E-07	1.1718	
5	39.561	3.69E-08	-1.1845	7.53E-08		48.41	5.39E-08	3.64E-09	2.09E-07	

AR=3.0

Mode	Non-Composite					Composite				
	Freq. (f)Hz	Mass participation factor			Max. Resp. (mm)	Freq. (f)Hz	Mass participation factor			Max. Resp. (mm)
		x-comp	y-comp	z-comp			x-comp	y-comp	z-comp	
1	25.886	1.04E-07	4.20E-11	9.95E-09	0.177	33.632	0.86962	-1.99E-08	2.16E-10	0.159
2	26.524	-0.92393	3.01E-08	-2.87E-10		38.188	2.08E-08	-2.69E-10	-1.39E-08	
3	31.687	-3.13E-07	1.36E-10	6.10E-08		45.15	2.96E-08	0.64491	2.28E-08	
4	31.861	0.8056	-6.49E-09	1.91E-10		49.1	-5.35E-08	-4.43E-09	1.52E-08	
5	39.34	7.31E-08	-1.109	3.12E-08		49.281	-2.78E-09	-1.47E-07	1.2397	

Table E. 8 8-Supported SOLS models with different aspect ratio

AR=1.0

Mode	Non-Composite					Composite				
	Freq. (f)Hz	Mass participation factor			Max. Resp. (mm)	Freq. (f)Hz	Mass participation factor			Max. Resp. (mm)
		x-comp	y-comp	z-comp			x-comp	y-comp	z-comp	
1	18.259	1.0349	0.11849	-7.01E-09	0.6	25.761	-9.97E-09	-9.97E-09	1.5849	0.173
2	18.259	-0.11849	1.0349	-5.57E-09		32.748	0.36396	0.89891	-8.11E-10	
3	23.03	7.59E-09	7.59E-09	1.6677		32.748	0.89891	-0.36396	-3.46E-10	
4	23.719	3.60E-09	3.60E-09	-3.13E-12		37.097	-0.22352	0.38693	-5.83E-10	
5	23.797	-3.62E-09	3.62E-09	1.79E-09		37.097	-0.38693	-0.22352	2.11E-09	

AR=1.5

Mode	Non-Composite					Composite				
	Freq. (f)Hz	Mass participation factor			Max. Resp. (mm)	Freq. (f)Hz	Mass participation factor			Max. Resp. (mm)
		x-comp	y-comp	z-comp			x-comp	y-comp	z-comp	
1	19.091	1.0415	8.14E-09	1.54E-10	0.541	31.156	1.0105	-4.80E-08	4.34E-10	0.187
2	22.773	1.03E-08	-1.87E-11	4.44E-08		34.285	-1.03E-09	-1.21E-08	1.3907	
3	30.806	-2.29E-10	-2.51E-08	1.5676		37.063	1.07E-08	-0.64226	2.03E-08	
4	34.847	-3.33E-08	5.77E-09	-4.47E-08		39.693	-1.26E-08	-1.35E-09	-7.29E-08	
5	35.178	5.50E-08	-0.61691	1.30E-08		42.525	-1.22E-07	-0.90199	-5.11E-09	

AR=3.0

Mode	Non-Composite					Composite				
	Freq. (f)Hz	Mass participation factor			Max. Resp. (mm)	Freq. (f)Hz	Mass participation factor			Max. Resp. (mm)
		x-comp	y-comp	z-comp			x-comp	y-comp	z-comp	
1	23.13	1.0688	-2.83E-08	1.94E-10	0.329	29.669	1.1496	-1.95E-08	1.69E-10	0.201
2	25.474	-3.09E-08	3.78E-11	1.27E-08		37.6	1.12E-08	-2.42E-10	-7.23E-09	
3	31.623	-3.22E-07	1.47E-10	6.21E-08		44.793	2.18E-08	0.63732	2.92E-08	
4	31.783	0.74328	1.16E-09	1.42E-10		48.615	-5.49E-08	-5.17E-09	2.90E-06	
5	35.392	8.94E-02	-2.82E-08	-3.71E-10		48.675	-3.60E-09	-1.45E-07	1.3681	

Table E. 9 8-Supported SOD models with different aspect ratios

AR=1.0

Mode	Non-Composite					Composite				
	Freq.	Mass participation factor			Max. Resp.	Freq.	Mass participation factor			Max. Resp.
	(f)Hz	x-comp	y-comp	z-comp	(mm)	(f)Hz	x-comp	y-comp	z-comp	(mm)
1	24.201	-1.71E-08	-1.72E-08	1.8166	0.157	26.9	-1.01E-08	-1.00E-08	1.6975	0.105
2	26.906	4.14E-09	-5.10E-09	-5.96E-09		37.711	-0.69048	1.89E-02	1.17E-09	
3	31.304	5.62E-07	5.71E-07	-6.80E-11		37.711	1.89E-02	0.69048	-1.24E-09	
4	31.423	-4.44E-02	-1.2542	-6.50E-09		39.69	1.0615	-0.31743	-5.01E-09	
5	31.423	1.2542	-4.44E-02	5.88E-09		39.69	-0.31743	-1.0615	9.26E-09	

AR=1.5

Mode	Non-Composite					Composite				
	Freq.	Mass participation factor			Max. Resp.	Freq.	Mass participation factor			Max. Resp.
	(f)Hz	x-comp	y-comp	z-comp	(mm)	(f)Hz	x-comp	y-comp	z-comp	(mm)
1	27.767	2.63E-08	3.65E-10	1.14E-07	0.159	34.73	2.12E-09	-8.00E-09	1.4334	0.114
2	29.857	-1.1129	8.54E-08	-3.18E-09		37.356	1.125	-1.30E-07	-6.81E-10	
3	31.247	3.45E-08	1.43E-10	4.85E-07		38.121	-2.57E-08	-0.67796	1.42E-08	
4	31.323	-3.46E-09	-2.16E-08	1.6414		41.075	-2.74E-08	-1.13E-09	-3.79E-08	
5	35.16	8.15E-08	-0.81026	8.07E-09		45.767	7.26E-08	1.0275	-2.32E-09	

AR=3.0

Mode	Non-Composite					Composite				
	Freq.	Mass participation factor			Max. Resp.	Freq.	Mass participation factor			Max. Resp.
	(f)Hz	x-comp	y-comp	z-comp	(mm)	(f)Hz	x-comp	y-comp	z-comp	(mm)
1	25.349	8.33E-08	1.06E-10	1.59E-08	0.168	33.985	-0.89695	7.63E-08	-3.00E-10	0.137
2	26.26	-0.93174	8.03E-08	-3.02E-10		38.578	1.91E-08	-8.13E-10	-1.32E-08	
3	31.75	-2.62E-07	1.79E-10	6.78E-08		41.041	8.31E-08	0.77048	1.14E-08	
4	31.97	0.81426	-4.10E-08	2.43E-10		47.225	-1.56E-09	-1.26E-07	1.3224	
5	34.686	0.34197	-3.95E-07	2.32E-10		50.031	7.85E-08	0.9815	6.19E-08	